Augusto Emmel Selke

VARIATIONAL MODELS OF THERMO-VISCOELASTIC DAMAGE IN FINITE STRAINS: LOCAL AND NONLOCAL APPROACHES APPLIED TO POLYMER BEHAVIOR

Tese submetida à École Doctorale SPIGA para a obtenção do Grau de Docteur en Mécanique.
Orientador
École Centrale de Nantes: Prof. Laurent Stainier, D.Sc.
Coorientador
Universidade Federal de Santa Catarina: Prof. Eduardo Alberto Fancello, D.Sc.

Nantes, France

2016

Ficha de identificação da obra elaborada pelo autor,
através do Programa de Geração Automática da Biblioteca Universitária da UFSC.

Selke, Augusto Emmel
Variational models of thermo-viscoelastic damage in finite strains : Local and nonlocal approaches applied to polymer behavior / Augusto Emmel Selke ; orientador, Laurent STAINIER ; coorientador, Eduardo Alberto FANCELLO. - Florianópolis, SC, 2016.
315 p.

Tese (doutorado) - Universidade Federal de Santa Catarina, Centro Tecnológico. Programa de Pós-Graduação em Engenharia Mecânica.

Inclui referências

1. Engenharia Mecânica. 2. Modelamento constitutivo. 3. Comportamento dos polímeros. 4. Termo-viscoelasticidade. 5. Dano viscoelástico. I. STAINIER, Laurent. II. FANCELLO, Eduardo Alberto. III. Universidade Federal de Santa Catarina. Programa de Pós-Graduação em Engenharia Mecânica. IV. Título.

RAPPORT de SOUTENANCE de THESE de

DOCTORAT délivré conjointement par l'ECOLE CENTRALE de NANTES
Cotutelle avec **Universidade federal de Santa Catarina**

présenté par : **Monsieur EMMEL SELKE Augusto**

le : **14/03/2016**

The topic tackled by the thesis, i.e. the modelling of polymer behaviour using a thermo-viscoelastic variational model, is challenging in several ways. It requires a good understanding of the underlying theoretical concepts, but also on the involved physics of the studied complex materials. The quality of the presentation reflected a strong understanding by the candidate of the theoretical concepts behind the variational modelling. The complex work was presented in a clear way through a well organised and synthetic presentation. It also confirmed that the work achieved is of remarkable quantity and quality and had been developed in a rigorous way. The candidate managed to synthesize a large amount of work in 45 minutes.

Through his confident answer to questions from the jury, both on numerical and modelling aspects, the candidate has demonstrated his deep understanding of the topic, as well as his maturity.

En fonction de ces éléments, le jury lui a décerné le grade de :

Docteur délivré par l'Ecole Centrale de Nantes

Spécialité : Mécanique des solides, des matériaux des structures et des surfaces

Le Président du Jury

M. NOELS LUDOVIC

Le Rapporteur

M.

Les Membres du Jury : *(nom et signature)*

M. STAINIER L.
M. ETCHERAMENDY. D.
M. EDUARDO DE SOUZA NETO
M. EDUARDO A. FANCELLO
M.
M.
M.
M.

To Romara

ACKNOWLEDGMENTS

I would like to start by thanking my thesis advisors, Professeur Laurent Stainier and Professor Eduardo Alberto Fancello, who took on the task of guiding and motivating my works and faithfully fulfilled it beyond all expectations, ever since my master's dissertation, and throughout the last five years. On the technical side, their contributions greatly helped advance my understanding of computational mechanics. On the personal side, I thank them for their friendship, which I hope will continue for many years. On all sides, they were constantly willing, able and available to lend a helping hand. I am honored to have been their student.

I thank the European Commission for funding the French phase of this thesis within the Marie Curie Initial Training Network (ITN) in Advanced Techniques in Computational Mechanics (ATCoMe).

Other members of the ATCoMe ITN are also gratefully recognized. Network meetings, courses and other events were places of very interesting and valuable discussions. I especially thank my co-fellows Aleksandar, César, Clément, Miquel, Omid, Sudhakar, Sudhar and Vladimir, for the bonds that were created. I thank Professors Wolfgang Wall (TUM), Eduardo de Souza Neto and Antonio Gil (Swansea University) for hosting me during short stays at their universities.

While in France, I had the honor of working at the Ecole Centrale de Nantes in a team filled with great researchers and amazing people. It was a humbling and enriching experience. It was, is and shall remain a welcoming and exciting place due to people such as Professors Laurent Stainier, Nicolas Moës, Antony Nouy and Patrice Cartraud, and their phalanx of talented PhD and post-docs: Raphaël, Jean-Charles, Shaopu and Mathieu (with whom I shared an office), Thibault, Florent, Kévin, Mathieu, Andrés, Ophélie, Charbel, Olivier, Loïc, Amuthan and many others with whom I had the opportunity to cross paths.

The Brazilian phase of this thesis was funded by the Conselho Nacional de Desenvolvimento Científico e Tecnológico (CNPq) and by the Coordenação de Aperfeiçoamento de Pessoal de Nível Superior (CAPES). I sincerely thank the support of both institutions.

While in Brazil, I had the opportunity of returning to the Univesidade Federal de Santa Catarina (UFSC). There, I spent gratifying time with old acquaintances such as Professors Fancello, Paulo de Tarso and Barcellos, Armin, Dr. Diego and Paulo and developed bonds with newer faces such as Hélio, Thiago, Jan, Otávio, Rafael and Henrique. Their dedication was a source of inspiration for the stretch run of this

thesis. Our Friday morning meetings contributed greatly toward this thesis.

I also thank my employer, the Instituto Federal de São Paulo, for granting me the time to prepare and travel for my thesis defense.

Without the support of friends and family, however, all the funding and technical discussions would have been for naught. Warmth and laughter in personal contexts are indispensable during such a long journey. I take the time to thank, in no particular order: Daniel, Duca and Thadeu, my brothers from other mothers; Júlia, Adão, Jorge, Cláudia, Pedro, Valentin, Bete, Cláudia, Lion and Jordana, my in law family, close to my heart; my uncles and cousins, too many to name here; my soccer and basketball colleagues, on both sides of the Atlantic.

It is impossible not to think of my late father, Professor Carlos Alberto de Campos Selke, at the conclusion of my doctoral studies. I would like to think that this document would have brought a smile to the face of the father and planted the seed of plenty of interesting discussions with the engineer. Both the smile and the conversations shall live on in my imagination.

To my mother, Ina, my earliest and deepest supporter in all undertakings, I have nothing but the deepest gratitude. She has been a rock at difficult times, and a cheerful companion in good times. I hope this thesis will also bring a smile to her face, the only currency children can pay back their eternal debts in.

Last, but not least, I would like to gratefully acknowledge the unflinching support, companionship and love of my wife, Romara, throughout my doctoral studies. This document only exists because I was able to lean on her. She challenged me to become better everyday, and although I have often disappointed her, I have never failed to try. All my love goes out to her.

La science, mon garçon, est faite d'erreurs, mais d'erreurs qu'il est bon de commettre, car elles mènent peu à peu à la vérité.
(Jules Verne, 1864)

ABSTRACT

The development of material models dedicated to the description of polymer behavior has long been and remains a subject of interest, as their use grows in many realms of application. Their microstructural features are responsible for challenges that must be addressed for accurate constitutive modeling, including thermomechanical coupling, large strain phenomena, viscosity effects and particular degradation behavior, among others.

This thesis aims to tackle this problem within the framework of variationally-formulated constitutive modeling of dissipative phenomena. This type of energy-based approach allows for an efficient treatment of multiphysics coupling, while accounting for dissipation in a thermodynamically sound manner.

Formulations for a wide range of thermo-viscoelasticity phenomena in finite strains are presented, with an emphasis on the coupling mechanisms and on the chosen parametrization of all dissipation sources.

Similar variational approaches can be extended to the problem of degrading material properties, an essentially dissipative issue. With the microstructural features of polymers in mind, a formulation for a class of coupled thermo-viscoelastic damage is then proposed. The model hinges on hypotheses relating all physical phenomena to the same damaging function, leading to a naturally separable structure between an equivalent undamaged state where thermo-viscoelasticity is solved and a damage evolution problem.

Although capable of encompassing various aspects of polymer-like material behavior, the proposed models remain subject to the limitations of local damage modeling, namely, spurious localization. The recent Thick Level Set approach to nonlocal damage, providing an efficient level-set based bridge between damage and fracture, is explored as a way to circumvent this issue.

Keywords: Variational constitutive model. Polymer-like material behavior. Thermo-viscoelasticity. Viscoelastic damage. Nonlocal damage. Thick Level Set.

RESUMO

O desenvolvimento de modelos materiais dedicados ao comportamento dos polímeros tem sido um tema de interesse há décadas, na medida em que cresce seu uso em diversos ramos de aplicação. Aspectos da microestrutura dos polímeros são responsáveis por desafios que devem ser abordados para uma modelisação constitutiva eficaz, incluindo acoplamento termomecânico, fenômenos de grandes deformações, efeitos viscosos e comportamento de degradação particular, entre outros.

Nesta tese, propõe-se atacar este problema dentro do contexto dos modelos constitutivos variacionais para problemas dissipativos. Este tipo de abordagem energética permite um tratamento eficiente de acoplamentos multi-físicas, onde a dissipação é computada de maneira termodinamicamente coerente.

Formulações para diversos fenômenos de termo-viscoelasticidade em grandes deformações são apresentadas. Os mecanismos de acoplamento e a parametrização escolhida para as fontes de dissipação são discutidos em detalhes.

Abordagens variacionais similares podem ser estendidas ao problema de degradação das propriedades materiais, em sua essência dissipativo. Levando em conta as particularidades microestruturais dos polímeros, uma formulação para uma classe de dano termo-viscoelástico acoplado é proposta. O modelo depende de hipóteses relacionando todos os fenômenos físicos à mesma função de danificação, o que leva a uma estrutura naturalmente separável entre um estado não-danificado equivalente para o qual se resolve o problema de termo-viscoelascidade, e um problema de evolução de dano.

Embora capazes de descrever diversos aspectos do comportamento dos polímeros, os modelos propostos permanecem sujeitos às limitações da descrição local de dano, em especial a localização espúria. O método recente *Thick Level Set*, baseado em funções de nível e oferecendo uma transição natural entre os modelos de dano e de fratura, é explorado como forma de contornar estas limitações.

Palavras-chave: Modelos constitutivos variacionais. Comportamento dos polímeros. Termo-viscoelasticidade. Dano viscoelástico. Dano não-local. Thick Level Set.

RÉSUMÉ

Le developpement de modèles matériau dédiés au comportement des polymères reste depuis longtemps un sujet d'intérêt, avec leur emploi croissant dans divers domaines d'application. Des aspects microstructuraux donnent origine à des défis qui doivent être relevés pour une modélisation constitutive éfficace, y compris le couplage thermomécanique, les effets de vitesse et des comportements caractéristiques de dégradation, entre autres.
Cette thèse propose d'aborder ce problème dans le cadre des modèles constitutifs variationnels pour des phenomènes dissipatifs. Ce type d'approche énergétique offre un traitement efficace des couplages multiphysiques, où la dissipation est prise en compte de façon thermodynamiquement cohérente.
Des formulations pour des phénomènes de thermo-viscoélasitité divers sont présentées. Les mécanismes de couplage et la paramétrisation choisie pour les sources de dissipation sont discutés en détail.
Des approches variationnelles similaires peuvent être étendues à la dégradation des propriétés matériau, en tant que problème dissipatif. Avec les spécificités microstructurelles des polymères comme motivation, une formulation pour une classe de problèmes d'endommagement thermo-viscoélastique est proposée. Le model dépend d'hypothèses liant tous les phénomènes physiques à la même fonction d'endommagement, ce qu'amène à une structure naturellement séparable entre la solution d'un problème thermo-viscoélastique pour un état équivalent non-endommagé et un problème d'évolution d'endommagement.
Bien que capables de décrire plusieurs traits du comportement des polymères, les modèles variationnels proposés restent soumis aux limitations de la déscription locale d'endommagement, notamment la localisation factice. La Thick Level Set, approche récente à l'endommagement nonlocal basée sur l'utilisation de fonctions de niveau, offrant un passage entre la modélisation de l'endommagement et de la rupture, est explorée comme moyen de contourner ces limitations.

Mots-clés : Modélisation constitutive variationnelle. Comportement des polymères. Thermo-viscoélasticité. Endommagement viscoélastique. Endommagement nonlocal. Thick Level Set.

LIST OF FIGURES

Figure 2.1 Influencing factors towards polymer performance 48

Figure 2.2 Left, spherulitic structures observed in polyhydroxybutyrate (PHB) through transmitted cross-polarized light microscope [Source: University of Cambridge's DoITPoMS Micrograph Library]. Right, aspects of the microstructure of spherulites, semi-crystalline structures arising during the crystallization of polymers from the molten state. (CALLISTER, 2007) 55

Figure 2.3 Temperature dependent behavior of polymers as represented through relaxation tests: regions of material behavior. (CALLISTER, 2007) 58

Figure 2.4 Schematic view of the Heat Deflection Temperature test [Source: ASTM] 60

Figure 2.5 Effect of increasing temperature or decreasing strain-rate on the material behavior of semi-crystalline polymers: from brittle behavior (below the glass transition temperature), some yielding before fracture, large plastic deformations (plateau characteristic of necking during cold drawing) and rubber-like flow. Principle of time-temperature equivalence. 61

Figure 2.6 Dynamic Thermomechanical Analysis of polymers. Top left: scheme of the experimental set up showing the drive motor (1), the clamps (2) and the furnace (3). Top right: DTMA clamps for 3-point bending (1), shearing (2), compression (3) and tensile (4) testing. Bottom: sample results from a DTMA test – sharper identification of the glass transition temperature on the tan-delta curve [Source: TA Instruments] .. 64

Figure 2.7 Details evidencing stress crazing for fractured surfaces of polycarbonate. Left, crazes evident of the wake of a downward evolving crack tip. Right: remains of broken fibers in a fractured surface [Source: University of Cambridge's DoIT-PoMS Micrograph Library] 69

Figure 2.8 Shear bands forming in polymer tensile specimens explain necking and strain softening observed during standardized tensile tests [Source: MIT OpenCourseWare] 71

Figure 2.9 Example of non-uniform microstructure of block copolymers. Two-phase structure of SBS, a class of thermoplastic elastomer: rigid spheres of polystyrene surrounded by randomly distributed network of polybutadiene. 76

Figure 3.1 Reference and current configurations of a body [Source: adapted from (GURTIN; FRIED; ANAND, 2010)]. 83

Figure 3.2 Saddle-point structure of a thermomechanical problem around the incremental solution: representation of a thermomechanical functional for adiabatic shear banding problems. [Source: (SU; STAINIER; MERCIER, 2014)] 104

Figure 4.1 Generalized Kelvin-Voigt Maxwell rheological model for the simulation of non-linear viscoelasticity. 112

Figure 4.2 Physical representation of the multiplicative decomposition between elastic and inelastic strains for viscoelasticity. Viscous states (circled red) seen as an intermediate state. [Source: (FANCELLO; PONTHOT; STAINIER, 2006)] 115

Figure 4.3 Application of the variational thermo-viscoelasticity model to a uniaxial tensile test at different strain rates: joint determination of stress-strain and temperature-strain curves. ... 147

Figure 4.4 Uniaxial tensile test at different strain rates of a Kelvin-Voigt element with Ogden-type viscous behavior: joint determination of highly nonlinear stress-strain and temperature-strain curves. 148

Figure 4.5 Relaxation test of two Maxwell branches at different strain rates: apparent translation of curves sharing the same characteristic times. 150

Figure 4.6 Relaxation tests of a single Maxwell branch at different initial temperatures: lower viscous dissipation (as measured through entropy generation) for higher initial temperatures. Stress-time and entropy-time curves calculated by the thermo-viscoelasticity model. 151

Figure 4.7 Hysteresis loop in cyclic loading of Maxwell elements: stress-strain and temperature-strain curves. 152

Figure 4.8 Hysteresis loop in cyclic loading of a generalized Kelvin-Voigt/Maxwell rheological model: stress-strain and temperature-strain curves. 154

Figure 5.1 Graphic representation of the effective stress $\tilde{\boldsymbol{\sigma}}$. [Source: (MURAKAMI, 2012)] 160

Figure 5.2 Strain rate influence on the effective stress-strain behavior of a thermo-viscoelastic damage model - a single Maxwell branch. No observed softening, as expected for the undamaged

equivalent problem. 183
Figure 5.3 Strain rate influence on the damage variable-strain behavior of a thermo-viscoelastic damage model - a single Maxwell branch. Viscous strains evidenced as the guiding force behind damage evolution: higher values for the damage variables obtained for the lower stress cases. 184
Figure 5.4 Strain rate influence on the stress-strain behavior of a thermo-viscoelastic damage model - a single Maxwell branch. . 185
Figure 5.5 Strain rate influence on the temperature-strain behavior of a thermo-viscoelastic damage model - a single Maxwell branch. Initially, thermoelastic effects result in cooling. Later, viscous dissipation dominates and local heat generation ensues. . 186
Figure 5.6 Relaxation test of two Maxwell branches with damage at different strain rates: evolution of stress and temperature. 187
Figure 5.7 Relaxation test of two Maxwell branches with damage at different strain rates: evolution of damage variable and entropy. 189
Figure 5.8 Hysteresis loop in cyclic loading of Maxwell elements with damage: stress-strain and temperature-strain curves. 190
Figure 5.9 Hysteresis loop in cyclic loading of a generalized Kelvin-Voigt/Maxwell rheological model with damage: stress-strain and temperature-strain curves. 191
Figure 5.10 Evolution of the damage variable during the cyclic loading of two Maxwell branches (on top) and of the generalized Kelvin-Voigt/Maxwell rheological model (on the bottom). 192
Figure 6.1 Distribution of the damage variable as delimited by the Thick Level Set. [Source: (MOËS et al., 2011)] 199
Figure 6.2 Local coordinate system induced by the TLS: positions along the damage front s and normally along the level set thickness ϕ. [Source: (BERNARD; MOËS; CHEVAUGEON, 2012)] . . 200
Figure 6.3 View of the average energy restitution rate ($\bar{Y}^d$) along the thick level set. [Source: Kévin Moreau] 202
Figure 6.4 Diffused damage TLS models: areas of nonlocal (Ω^+) and local damage modeling (Ω^-) as determined by the gradient of the level-set function. [Source: Kévin Moreau] 203
Figure 6.5 Dynamic tensile loading of a one-dimensional bar divided into 500 elements. 211
Figure 6.6 Exponentially decaying applied forces at the extremities of the bar(measured in [N]) through time (in [s]) for all

the examples of TLS use. 212

Figure 6.7 Application of the TLS to an elastic local model of damage: development of a damage profile spread around the middle of the bar, instead of localized failure only at the central element of the bar. 212

Figure 6.8 Application of the TLS to a thermo-viscoelastic damage model: one single Kelvin-Voigt branch with low viscosity. Development of a slightly broader damage profile. 213

Figure 6.9 Predicted temperature profile for the TLS applied to a thermo-viscoelastic damage model: one single Kelvin-Voigt branch with low viscosity. Damage dissipation dominating heat generation. 214

Figure 6.10 Profile of temperature increase due to viscous effects only, in the application of the TLS to a thermo-viscoelastic damage model: one single Kelvin-Voigt branch with low viscosity. 215

Figure 6.11 Damage profile predicted by the application of the TLS to a thermo-viscoelastic damage model: one single Kelvin-Voigt branch with higher viscosity. 215

Figure 6.12 Predicted profile of temperature increase (in $[K]$) for the TLS applied to a thermo-viscoelastic damage model: one single Kelvin-Voigt branch with higher viscosity. Comparable viscous and damage dissipation. 216

Figure 6.13 Damage profile for the TLS applied to a thermo-viscoelastic damage model: one single Maxwell branch with higher viscosity. Broader damage profile. 217

Figure 6.14 Predicted temperature profile for the TLS applied to a thermo-viscoelastic damage model: one single Maxwell branch with low viscosity. Comparable viscous and damage dissipation. 217

Figure 7.1 Mesh used for the simulation of a plate with a central circular hole and mesh information. 225

Figure 7.2 Deformation of the plate with a central hole at three different time steps. Color scale shows the displacements along the x-axis, indicating localization of deformation next to the hole. 227

Figure 7.3 Temperature profile for three different time steps. Adiabatic conditions on the left, convection-conduction on the right. 229

Figure 7.4 Heat flux at three different time steps for the Kelvin-

Voigt thermo-viscoelasticity model. 230
Figure 7.5 Stresses at the final time step. Higher levels of stress closer to the right boundary for the convection/conduction case: thermal dilatation effect. 231
Figure 7.6 Temperature increase profile for the thermo-viscoelastic damage model at three different time steps. Lower convection coefficient on the left, higher on the right. 232
Figure 7.7 Heat flux at the intermediate time step. Higher convection coefficient working as a heat sink. 233
Figure 7.8 Damage profile for the thermo-viscoelastic damage model at three different time steps. Lower convection coefficient on the left, higher on the right. Different scales for each figure. 234
Figure 7.9 Temperature increase profile for the thermo-viscoelastic damage model at two different time steps. Lower conduction coefficient on the left, higher on the right. 235
Figure 7.10 Temperature increase profile for the thermo-viscoelastic damage model at the intermediate time step. Higher conduction counterbalances the heat sink effect of convection along the hole boundary. 236
Figure 7.11 Damage profile for the thermo-viscoelastic damage model at two different time steps. Lower conduction coefficient on the left, higher on the right. Same scale for each time step. . . 237
Figure 7.12 Damage and temperature increase profiles for the thermo-viscoelastic damage model at the final time step. Higher temperatures reached even for higher conduction: damage dissipation. 238
Figure 7.13 Stress evolution through time during a temperature scan of a thermo-viscoelasticity model: thermal softening is responsible for the decreasing amplitude of stress. 241
Figure 7.14 Entropy evolution through time during a temperature scan of a thermo-viscoelasticity model: thermoelastic effects and viscous dissipation. 242
Figure 7.15 Stress evolution through time during a temperature scan of a thermo-viscoelastic damage model: thermal softening and damage evolution are responsible for the decreasing amplitude of stress. 243
Figure 7.16 Entropy evolution through time during a temperature scan of a thermo-viscoelastic damage model: lower dissi-

pation levels than for the undamaged model. 243
Figure 7.17 Damage variable evolution during a temperature scan of a thermo-viscoelastic damage model: decreasing slope caused by stress softening. 244
Figure 7.18 Stress evolution through time during a frequency sweep of a thermo-viscoelasticity model: amplitude increase due to viscous effects. 244
Figure 7.19 Stress evolution through time during a frequency sweep of a thermo-viscoelastic damage model. 245
Figure 7.20 Damage variable evolution during a frequency sweep of a thermo-viscoelastic damage model: sharp spike in higher loading frequencies. 246
Figure 7.21 Stress evolution in a long duration tensile/compressive test of a thermo-viscoelasticity model: no temperature dependence of parameters results in constant amplitude. 246
Figure 7.22 Temperature evolution in a long duration tensile/-compressive test of a thermo-viscoelasticity model. 247
Figure 7.23 Stress evolution in a long duration tensile/compressive test of a thermo-viscoelastic damage model. 248
Figure 7.24 Temperature evolution in a long duration tensile/-compressive test of a thermo-viscoelastic damage model. 248
Figure 7.25 Damage variable evolution in a long duration tensile/compressive test of a thermo-viscoelastic damage model. . . . 249
Figure 7.26 Profile of imposed logarithmic strains in the dynamic stress-strain tests. 249
Figure 7.27 Profile of imposed logarithmic strains in the dynamic stress-strain tests. 250
Figure 7.28 Stress evolution in the dynamic stress-strain test of a thermo-viscoelasticity model: linear amplitude growth due to fixed temperature. 250
Figure 7.29 Stress evolution in the dynamic stress-strain test of a thermo-viscoelastic damage model: damage reaches 1 and the material can no longer bear loads. 251
Figure 7.30 Damage variable evolution in the dynamic stress-strain test of a thermo-viscoelastic damage model: sharp spike and failure. 251
Figure 7.31 Standard geometry for tensile plate test specimens according to ASTM D638. Types I, II and V indicated for plates with low thickness. Type III for plates of higher thick-

ness. Type IV for special comparisons between rigid and non-rigid materials. 253
Figure 7.32 Mesh used for the simulation of polymer tensile tests. 254
Figure 7.33 Distributed necking of a standard tensile test specimen. Geometries at three different imposed displacements $1mm$, $20mm$ and $50mm$. Uniform stress along the central process zone, no softening. 256
Figure 7.34 Distributed necking of a standard tensile test specimen. Uniform temperature levels in the process zone (left column). Heat fluxes (right column) concentrated along the thermal boundary on the right. 259
Figure 7.35 Temperature softening of a standard tensile test specimen. Decreasing stresses for increasing imposed displacements. Viscous dissipation causes temperature increase, which then reduces elastic and viscous properties. Uniform stress along the central process zone. 260
Figure 7.36 Temperature softening of a standard tensile test specimen. Uniform temperature levels in the process zone (left column). Heat fluxes (right column) constantly concentrated between the same coldest and hottest regions. 261
Figure 7.37 Damage-induced softening of a standard tensile test specimen. Stress levels (right column) decreasing as imposed strains increase. Transverse displacement (left column) concentrating in the narrower process zone as damage increases at first, then showing signs of localization in a single spot. 262
Figure 7.38 Damage-induced softening of a standard tensile test specimen. Temperature levels (left column) go from thermoelastic cooling to extremely localized heating due to damage dissipation. Damage (right column) spreads through the process zone before beginning to localize in a narrow band. 263

LIST OF TABLES

Table E.1 Material 1: standard material properties used for most examples of chapter 7 (1 Kelvin-Voigt element, 2 Maxwell elements) 313

Table E.2 Material 2: properties for thermo-viscoelasticity model used in figure 4.4 (1 Kelvin-Voigt element, Ogden viscous potential) 314

Table E.3 Material 3: material properties used for the final example of tensile testing in section 7.5 (1 Kelvin-Voigt element, 2 Maxwell elements) 315

LIST OF ABBREVIATIONS

Abbreviation	**Description**
CDM	Continuum Damage Mechanics
DTMA	Dynamic Themomechanical Analysis
FEM	Finite Element Method
GSM	Generalized Standard Materials
HDT	Heat Deflection Temperature
LATIN	Large Time Increment method
PGD	Proper Generalized Decomposition
TLS	Thick Level Set method
X-FEM	Extended Finite Element Method

LIST OF SYMBOLS

General mathematical notation

Symbol	Description
$(\bullet)$	Unless strictly necessary during the development of an equation, parentheses are only used to indicate function dependence and entities undergoing a given operation, as described below
$\zeta(\mathbf{A}_{n+1}, \mathbf{B}_{n+1}; \mathbf{C}_{n+\alpha})$	Generic function ζ of variables $\mathbf{A}$ and $\mathbf{B}$ evaluated at time $n+1$, with parametric dependence on variable $\mathbf{C}$ evaluated at a given time $n+\alpha$
$\frac{\partial}{\partial \mathbf{A}}(\zeta)$, $\frac{d}{d\mathbf{A}}(\zeta)$, $\mathrm{OP}(\zeta)$	Partial or total derivative of generic function ζ with respect to variable $\mathbf{A}$, generic operator OP applied to function ζ

Symbols defined in chapter 2

Symbol	Units	Description
T_m, T_c, T_g	$[K]$	Melting, crystallization and glass transition temperatures of polymers
E, E', E”	$[MPa]$	Young’s modulus, real (storage modulus) and imaginary (loss modulus) parts
$\tan\delta$	–	Relation between storage and loss moduli

Symbols defined in chapter 3

Symbol	Units	Description
Ω, dV	$[m^3]$, $[m^3]$	Reference configuration and its volume element
$\partial\Omega$, $d\Gamma$	$[m^2]$, $[m^2]$	Domain boundary in the reference configurations and its surface element
$\mathbf{X}$	$[m]$	Position vector at the reference configuration

Ω_t, dv, Γ_t	$[m^3]$, $[m^3]$, $[m^2]$	Current configuration, its volume element and boundary
$\mathbf{x}$	$[m]$	Position vector at the current configuration
χ	$-$	Displacement mapping between reference and current configurations
$\mathbf{v}$	$[m/s]$	Velocity vector of a material point
J	$-$	Jacobian
$\mathbf{F}$	$-$	Deformation gradient
$\mathbf{R}$	$-$	Rotation tensor
$\mathbf{V}$, $\mathbf{U}$	$-$	Left and right stretch tensors
$\mathbf{B}$, $\mathbf{C}$	$-$	Left and right Cauchy-Green strain tensors
$\mathbf{E}$	$-$	Green-St. Venant strain tensor
$\boldsymbol{\varepsilon}$	$-$	Logarithmic strain tensor
$\mathbf{L}$	$-$	Gradient velocity tensor
$\mathbf{D}$, $\mathbf{W}$	$-$	Rate of stretching and spin tensors
ρ_R, ρ	$[kg/m^3]$	Mass density in reference and current configurations
$\mathbf{t}$, $\mathbf{b}_0$	$[N/m^2]$, $[N/m^3]$	Surface tractions and body forces
a_R	$-$	Generic variable a measured in the reference configuration
$\boldsymbol{\sigma}$	$[MPa]$	Cauchy stress tensor
$\mathcal{W}^{ext}$, $\mathcal{W}^{int}$, $\mathcal{K}$	$[J/s]$	External power, internal stress power and kinetic energy
$\mathbf{P}$, $\mathbf{P}$	$[MPa]$	First and second Piola-Kirchhoff stress tensors
T	$[K]$	Absolute temperature (also, external temperature)
$\mathcal{E}$, e	$[J]$, $[J/kg]$	Internal energy and specific internal energy
$\mathcal{Q}$, $\mathbf{q}$, r	$[J/s]$, $[J/s.m^2]$, $[J/s.m^3]$	Heat flow, heat flux and volumetric heat generation
$\mathcal{S}$, $\mathcal{I}$, $\mathcal{J}$	$[J/s.K]$, $[J/K]$, $[J/s.K]$	Net entropy production, net internal entropy, entropy flow
η	$[J/K.kg]$	Entropy density

W, w	$[J/m^3]$, $[J/kg]$	Helmholtz free energy and specific Helmholtz free energy
$\mathcal{D}^{int}$	$[J/s]$	Internal dissipation
$\mathbf{Z}$, $\mathbf{Y}$	–	General notation for internal variables, and their conjugated thermodynamic forces
$\mathcal{C}$	$[J/m^3.K]$	Heat capacity
ψ, $\bar{\psi}$	$[J/m^3.s]$	Dissipation pseudo-potential, and an appropriate average of ψ along the time step
$\mathcal{H}$	$[J/s]$	Potential functional
$\partial_{\boldsymbol{\sigma}}\Omega$, $\partial_{\mathbf{q}}\Omega$	–	Neumann boundaries of imposed traction and heat fluxes
$\bar{\mathbf{t}}_R$, $\bar{\mathbf{q}}_R$	$[N/m^2]$, $[J/s.m^2]$	Imposed traction and heat fluxes on the boundaries of the material domain
$D_b[A](\delta b)$	–	Gâteaux-derivative of function A with respect to variations of variable b
$\mathcal{H}_n$	$[J]$	Incremental pseudo-potential at instant t_n
a_n, a_{n+1}, $a_{n+\alpha}$	–	Generic variable a evaluated at the start, at the end, and at some intermediate value of the time step
Δt	$[s]$	Size of the time step
φ	$[J/s]$	Irreversible heat conduction dissipation pseudo-potential
κ	$[J/s.K.M^2]$	Fourier conduction parameter
θ	$[K]$	Internal temperature
$\langle\psi\rangle$	$[J/s]$	Thermodynamic consistent average of the dissipation pseudo-potential along the time step
$\mathcal{H}_n^{eff}$	$[J]$	Effective incremental potential
$\mathbf{A}^c$, $\mathbf{A}^d$	–	Conservative and dissipative parts of the chosen stress measure $\mathbf{A}$

Symbols defined in chapter 4

Symbol	**Units**	**Description**
$\mathbf{F}^e$, $\mathbf{F}^v$	–	Elastic and viscous parts of the deformation gradient

$\mathbf{F}^{pr}$	–	Predictor deformation gradient
$\mathbf{F}^{vol}$, $\hat{\mathbf{F}}$	–	Volumetric and isochoric parts of the deformation gradient
$\hat{\mathbf{C}}^{e}$, c^{e}_{j}, $\mathbf{M}^{e}_{j}$	–	Right Cauchy-Green measure of isochoric elastic deformations, its eigenvalues and eigenvectors
$\mathbf{D}^{v}$, q_j, $\mathbf{M}^{v}_{j}$	–	Rate of viscous stretching tensor, its eigenvalues and eigenvectors
K_q, K_M	–	Sets of eigenvalues and eigenvectors
$\hat{\mathbf{C}}^{pr}$, $\boldsymbol{\varepsilon}^{pr}$, ϵ^{pr}_{j}	–	Right Cauchy-Green predictor, logarithmic predictor and its eigenvalues
W^{vol}, W^{th}, W^{e}	$[J/m^3]$	Volumetric, thermal accumulation and isochoric elastic parts of the Helholtz free energy
T_0	$[K]$	Reference temperature for the measurement of material properties
K, α	$[MPa]$, $[1/K]$	Bulk modulus and expansion coefficient
μ^{e}	$[MPa]$	Hencky shear modulus
μ^{e}_{i}, α^{e}_{i}	$[MPa]$, –	Ogden shear moduli, and exponents
ψ^{KV}	$[J/s.m^3]$	Kelvin-Voigt dissipation pseudo-potential
μ^{vKV}	$[MPa]$	Kelvin-Voigt Viscous Hencky shear modulus
Y^{KV}_{0}, $\bar{m}$, $\dot{\epsilon}^{KV}_{0}$	$[J]$, –, –	Kelvin-Voigt dissipation power law parameters
ψ^{MX}	$[J/s.m^3]$	Maxwell dissipation pseudo-potential
Y^{MX}_{0}, m, $\dot{\epsilon}^{MX}_{0}$	$[J]$, –, –	Maxwell dissipation power law parameters
$\mathbf{H}$	$[J/m^2.K]$	Thermodynamic force associated to the temperature gradient
$\mathcal{L}$	$[J]$	Lagrangian function
λ_i	–	Lagrange multipliers
$\mathcal{H}^{effInt}_{n}$, $\mathcal{H}^{effExt}_{n}$	$[J]$	Internal and external parts of the effective incremental potential

$\mathbb{C}$, $\mathbb{C}_{mech}$, $\mathbb{C}_{thm}$	–	Tensor modulus, its purely mechanical and thermomechanical parts
$\mathbb{C}^e$, $\mathbb{C}^v$, $\mathbb{C}^{vol}$	–	Isochoric elastic, viscous and volumetric contributions to the tensor modulus
$\mathbb{D}$, $\mathbb{D}_{th}$, $\mathbb{D}_{thm}$	–	Thermal tensor modulus, its purely thermal and thermomechanical parts

Symbols defined in chapter 5

Symbol	**Units**	**Description**
d	–	Damage variable (isotropic, scalar)
Y^d	$[J]$	Energy restitution rate, thermodynamic force associated to damage
ψ^d	$[J/s.m^3]$	Damage dissipation pseudo-potential
$\tilde{\sigma}$	$[MPa]$	Effective Cauchy stress
$\psi^\star$	$[J/s.m^3]$	Dual damage dissipation pseudo-potential
$\dot{\lambda}^p$	–	Plastic multiplier
H_Γ, H_b	–	Hardening and softening moduli of (KINTZEL; MOSLER, 2011)
α_Γ, α_b	–	Hardening and softening internal variables of (KINTZEL; MOSLER, 2011)
H_k, H_i	–	Kinematic and isotropic hardening moduli of (KINTZEL; MOSLER, 2011)
$\boldsymbol{\alpha}_k$, α_i	–	Kinematic and isotropic hardening variables of (KINTZEL; MOSLER, 2011)
$f(d)$	–	Damaging function
$\tilde{W}$, $\tilde{\psi}$	$[J/m^3]$, $[J/s.m^3]$	Helmholtz free energy and dissipation pseudo-potentials of the equivalent undamaged problem
Y_0^d, m', $\dot{d}_0$	$[J]$, –, –	Damage dissipation power law parameters

$\tilde{\mathbb{C}}$, $\tilde{\mathbb{C}}$	$-$	Mechanical and thermal tangent moduli of the equivalent undamaeg problem

Symbols defined in chapter 6

Symbol	**Units**	**Description**
$\bar{\epsilon}$, ω	$-$	Nonlocal weighted average of strains, weighting function
l_c	$[m]$	Characteristic length
ϕ	$-$	Level-set function
Γ_0, Γ_c	$-$	"Iso-zero" and "iso-l_c" contours of the level-set function
d'	$[1/m]$	Damage profile along the level-set thickness
s, ϕ	$-$	TLS coordinate system of: position along the damage front, and position normal to the front
v_n	$[m/s]$	Velocity of the damage front
$\rho(s)$	$[1/m]$	Radius of curvature of the damage front at point s
$g(s)$	$[N/m^2]$	Thermodynamic force conjugated to the front velocity
$\bar{\psi}^d$	$[J/s]$	Damage dissipation pseudo-potential expressed in terms of the pair g, v_n
$\bar{Y}^d$	$[J]$	Averaged energy restitution rate along the level-set thickness
Ω^+, Ω^-	$[m^3]$	Regions treated by nonlocal damage, and strictly by local damage models, in a diffused damage context
Y^c	$[J]$	Damage initiation threshold (critical value of Y^d)
G, G^c	$[J/s]$	Energy release rate of fracture mechanics, and its critical value for crack advancement

Symbols defined in chapter 7

Symbol	**Units**	**Description**
$\partial_{\mathbf{x}}\Omega$, $\partial_T\Omega$	$-$	Dirichlet boundaries of imposed displacements and temperatures
$N_a(\mathbf{X})$	$-$	Shape function associated to node a of the mesh
ζ_h	$-$	Approximation of generic field ζ related to Finite Element discretization h
nel	$-$	Number of elements
Θ_h, p_h, $\overline{\Theta_h^{el}}$, $\overline{p_h^{el}}$	$-$, $[MPa]$, $-$, $[MPa]$	Additional mixed formulations fields of volumetric strains and corresponding pressure, and their respective constant values over each element
$\hat{\mathcal{H}}_n^{eff}$	$[J]$	Incremental formulation recast under a mixed formulation

CONTENTS

1 INTRODUCTION 41

2 CHALLENGES RELATED TO THE CONSTITUTIVE MODELING OF POLYMERS 47

2.1 Introduction: determinants of polymer performance . 47

2.2 Classes of polymers: thermoplastics, thermosets and elastomers 49

2.3 Features of polymer behavior: viscoelasticity and thermomechanical coupling 52

2.4 Main features of polymer degradation: damage and rupture 65

2.5 Limitations of thermo-viscoelastic damage models in describing polymer-like material behavior 73

3 REVIEW OF VARIATIONAL FORMULATION TO DISSIPATIVE PROBLEMS 79

3.1 Introduction: constitutive modeling and variational approaches 79

3.2 Continuum mechanics and thermodynamics: kinematic relations, balance equations and thermodynamic principles 81

3.3 Constitutive modeling: Coleman-Noll procedure and internal variables 91

3.4 Variational approaches to mechanical dissipative problems: fundamentals of incremental constitutive updates applied to viscoplasticity, viscoelasticity and damage 94

3.5 Variational approach to thermomechanical dissipative problems: multiphysics coupling and symmetry of material tensors 100

4 VARIATIONAL FORMULATION OF THERMO-VISCOELASTICITY IN FINITE STRAINS 109

4.1 Introduction: thermomechanically coupled viscoelasticity and associated rheological models 109

4.2 Kinematic assumptions: multiplicative split of strains and exponential mapping of internal variables 114

4.3 Additive decomposition of the Helmholtz free energy and dissipation pseudo-potential: isotropic functions of eigenvalues of strains, nonlinear elastic and viscous behaviors and temperature dependence 119
4.4 Formulation of the thermomechanically coupled problem: variational constitutive updates 126
4.5 Derivation of the tangent moduli: mechanical part, thermomechanical coupling and heat capacity 135
4.6 An algorithmic view of the incremental variational constitutive updates 143
4.7 Finite thermo-viscoelasticity: limitations and modeling alternatives 144
4.8 Sample numerical tests: consistency tests at a single material point 146

5 THERMO-VISCOELASTIC DAMAGE IN A VARIATIONAL FRAMEWORK 157
5.1 Introduction: continuum damage mechanics and polymer damage 157
5.2 Review of an earlier variational formulation of damage 162
5.3 Thermo-viscoelastic damage: discussion on possible choices of internal variables and potentials 164
5.4 Variational formulation of damage coupled to thermo-viscoelasticity: internal variable updates and influence of damage on stress and entropy 168
5.5 Effect of damage on the derivation of the tangent moduli 173
5.6 An algorithmic view of the incremental variational constitutive updates 176
5.7 Thermo-viscoelastic damage: limitations and modeling alternatives 178
5.8 Sample numerical tests 183

6 NONLOCAL TREATMENT OF THERMOVISCOELASTIC-DAMAGE THROUGH THE THICK LEVEL SET METHOD 193
6.1 Introduction: spurious localization and nonlocal damage models 193
6.2 Brief overview of nonlocal damage models 194
6.3 The Thick Level Set approach to damage and fracture 197

6.4 Brief observations on the connection between the Thick Level Set and fracture mechanics 203
6.5 Thick Level Set regularization of the variational thermo-viscoelastic damage model 205
6.6 An algorithmic view of the variational incremental updates for the thermo-viscoelastic damage model regularized through the Thick Level Set 208
6.7 Sample numerical tests: TLS regularization of variational thermo-viscoelastic damage in one-dimensional dynamic simulation of a bar 210
7 APPLICATIONS OF THE PROPOSED MODELS 219
7.1 Implementation details: Zorglib/Matlib 219
7.2 Finite Element aspects: data structure, volumetric locking and thermomechanical coupling 220
7.3 Plate with a central hole 225
7.4 Reproduction of alternated loading conditions of the Dynamic Thermomechanical Analysis 241
7.5 Strain localization and damage-induced strain softening in tensile tests 253
8 CONCLUDING REMARKS AND FUTURE PERSPECTIVES 265
REFERENCES 271
APPENDIX A – Parametric dependence in general dissipation pseudo-potentials 285
APPENDIX B – Thermomechanical dissipation pseudo-potentials: contribution to entropy evolution 291
APPENDIX C – Thermo-viscoelasticity: derivatives with respect to eigenvalues of strain predictor 297
APPENDIX D – Thermo-viscoelastic damage: aspects of the derivation of tangent moduli 303
APPENDIX E – Material parameters used in the applications 313

1 INTRODUCTION

Polymers are a versatile and ever-growing class of materials. The development and design of new types of polymers has helped them move from simpler applications, for instance in packaging and non-critical components, towards fulfilling much more demanding tasks, often comprising the majority of components in highly complex structures, for instance in aerospace engineering. Engineers have mostly turned to them due to desirable general characteristics often associated with all polymers: light weight, strength, chemical resistance, thermal and electrical insulation.

Two main tendencies have accompanied the expansion of polymers to more advanced applications: increasing demands on load bearing and structural integrity, and rising cost of polymer-based components. Naturally, then, came the need for simulation tools suited to the accurate description of their behavior. In addition to numerical methods, such as the Finite Element Method widely employed in structural engineering, the simulation of polymer-like behavior poses particular challenges on the constitutive side. In fact, the development of efficient constitutive models capable of capturing the complex features of polymer-like material behavior is a challenge that has received extensive attention as the importance of polymers has grown over the last decades.

Although they share some general features, polymers constitute a vast family of materials, with wide ranging material properties suited to various different kinds of applications. In other words, some types of polymers, under certain conditions of application may be sufficiently well represented by simple constitutive models. However, in most cases, features such as large strains, rate dependence and multiphysics phenomena (particularly in the form of strong thermomechanical coupling) can be expected to dominate their material behavior.

The molecular and microstructural configurations that characterize polymers are responsible for this constitutive complexity. Understanding the way polymer chains are arranged and how they interact under different types of loads is a useful tool toward formulating accurate constitutive models.

In chapter 2, a brief description of polymer molecules and microstructures is presented. Based on the behavior of polymer chains under stress, an argument is made for constitutive models including rate dependence and large strain phenomena. The response to thermal loads is also briefly discussed, and classical concepts such as time-temperature equivalence are explored in justifying the need for the inclusion of thermomechanical coupling. Finally, as loads grow, the degradation of material properties and the appearance of cracks are then related to the compromising of polymer chains. A connection between damage and fracture mechanisms in polymers and thermo-viscoelastic phenomena is also established.

The microstructural arguments associated to polymer material behavior constitute at once the motivation and the challenges that must be addressed by the actual formulation. Extensive literature is available on all the individual constitutive features described in chapter 2. However, it can be challenging to develop a single model combining and coupling all different sources of dissipation, namely irreversibilities related to viscous strains, damage evolution and thermal phenomena. Solid bases are needed in order to formulate rich constitutive models accounting for various sorts of coupling, in a thermodynamically sound manner.

Starting from the seminal paper of Ortiz & Stainier (1999), a family of constitutive models for several types of dissipative problems has been formulated in a variational framework. Within the context of generalized standard materials, where internal variables are used to describe internal processes and convex dissipation pseudo-potentials are used to ensure positive dissipation (and thus, thermodynamic consistency), these models are based on incremental variational principles derived from rate forms of energy equations. Solutions are thus associated to stationarity points of incrementally built functionals.

In comparison to classical formulations, variational models can be shown to hold some interesting mathematical properties (such as the symmetry of material tensors, even in strongly coupled problems such as those arising in themomechanical applications (YANG; STAINIER; ORTIZ, 2006)) which in turn lead to advantageous implementation techniques (such as the use of well established optimization toolboxes in order to find the stationarity points of an energy-like functional).

Chapter 3 of this document brings further details on variational formulation of dissipative problems. A review of previous publications is made, with an emphasis on thermomechanical formulations. Thermodynamic consistency is achieved through convex dissipation pseudo-potentials. A full derivation of the general thermomechanical problem is presented, with all the balance and evolution equations arising from a single functional. A factorization used for all dissipative mechanisms is shown to be behind the symmetry of the formulation. The underlying saddle-point structure of the resulting optimization problem is presented.

As shown during the literature review of chapter 3, efforts to model some features of polymer behavior with variational formulations for dissipative problems have already been made. Large strain viscoelasticity of polymers has been explored in Fancello, Ponthot & Stainier (2006) for isothermal problems. Issues related to polymer viscoplasticity, with different forms of yield functions, were explored by Fancello, Vassoler & Stainier (2008). Furthermore, thermomechanically coupled models of viscoplasticity for adiabatic applications, such as those developed in Stainier & Ortiz (2010), have also been extended to describe polymer-like behavior in Selke (2009). So far, though, variational formulations of strongly coupled thermo-viscoelasticity in large strains, a necessity for many polymer applications as argued in chapter 2, have remained unexplored.

As a first central contribution, chapter 4 presents a full description of such a formulation. A generalized Kelvin-Voigt Maxwell rheological model serves as base for treating an arbitrary number of characteristic times, which translates into models of arbitrary complexity. Isotropic potentials depending on eigenvalues of strains are used. Different choices for the individual components of the free and dissipated energies are explored. Procedures for the update of stress and entropy are described. Tangent moduli are derived and thermomechanical coupling is extensively discussed.

As discussed in chapter 2, polymer behavior also shows to be complex in its degradation and failure mechanisms. Once more, microstructural complexities and the micromechanics of interactions between long polymer chains are responsible for the onset of particular phenomena such as stress crazing and shear banding, common cause of compromised material properties, as well as precursors to fracture in polymers. There are also strong indications that inelastic and rate dependent phenomena are strongly related to polymer damage behavior. These issues should be accounted for by constitutive models of polymer damage.

Abundant literature on polymer damage and fracture has also been developed throughout the years, both in the field of continuum damage mechanics and in the field of fracture mechanics. Damage and fracture, as essentially dissipative phenomena, can also be recast in the variational framework presented in chapter 3. The works of Kintzel & Mosler (2011) on damage of metals in fatigue applications are a first incursion into the matter.

One efficient way of coupling damage to the thermo-viscoelastic models (previously presented in chapter 4) is the subject of chapter 5, for the second main contribution of the present work. Based on a central hypothesis that damage is measured by a single isotropic variable and affects all volume depending phenomena equally, it is shown that a naturally staggered scheme arises: first, thermo-viscoelasticity is solved in the mold of chapter 4 for an equivalent state; then, the necessary ingredients necessary to determine damage evolution are available. The different guiding mechanisms for the evolution of damage are explored. The influence of damage dissipation upon tangent moduli and entropy evolution is also detailed. As in chapter 4, sample numerical examples are brought as an illustration of the capabilities of the proposed model.

After exploring the toolbox of variational methods to develop constitutive models capable of describing important features of polymer behavior, from fully sane to degraded material states, the focus shifts to the regularization of the proposed damage models and to the onset of fracture.

Spurious localization is a common occurrence for purely local damage models, such as those derived in chapter 5. When damage evolution at a material point only takes into account information related to itself, becoming essentially oblivious to the state of damage in adjacent regions, formulations may become artificially brittle. This happens since it is possible for a single point to surpass previously defined damage thresholds and evolve to fracture, all while its neighbors remain undamaged.

The field of nonlocal damage models (whose classical variants are reviewed in Peerlings et al. (2001)) has been developed to overcome the issue of spurious localization and its numerical counterpart of pathological mesh dependence. The main idea is to introduce some sort of regularization, so that each point has access to information of a given surrounding region.

A recent contribution to the field of nonlocal damage modeling, and to the transition between damage and fracture models, is the Thick Level Set approach (MOËS et al., 2011). Making use of the level set formalism, a new material parameter is inserted into the damage model, representing the minimum distance between sound and fully degraded material.

As argued in chapters 2 and 6, there is strong micromechanical reasons to include such a length into the modeling polymer damage, as evidenced, for instance, by the phenomenon of stress crazing.

The Thick Level Set approach is responsible for the regularization of damage behavior, and can be coupled to different local damage models. However, this possibility has yet to be explored in the literature.

Chapter 6 shows the application of the Thick Level Set to the local thermo-viscoelastic damage model of chapter 5, in the third contribution of this project. The central ingredients of the Thick Level Set method are initially presented. Different material models are then shown to be clearly compatible with the method. It suffices to adequately define the energy release rate, the thermodynamic force associated to the damage variable and driving force behind damage evolution. Sample 1-D examples, designed to induce localization in a single element, are tested to demonstrate how the method works. Viscosity is shown to have some regularizing effect upon damage evolution.

Finally, chapter 7 includes applications of the previously proposed models and techniques to more realistic problems. In order to do so, the models were implemented in ZorgLib/MatLib, an open source platform dedicated to multiphysics simulations developed at the Ecole Centrale de Nantes. Finite element aspects of the implementation of the developed models are briefly discussed, including strategies to circumvent volume locking issues and data structure for the coupled problems. Special attention is given to examples reproducing some of the most widely used tests in polymer characterization, bringing about a discussion on future efforts of validating the proposed models for polymer species of interest.

Concluding remarks on the developed models and perspectives for future works close the document. A recapitulation of the central contributions of the document with potential impacts is done. The focus is set on the various possible coupling aspects covered by the proposed models and on possible variations to account for behaviors outside the scope of the adopted constitutive hypotheses.

In the appendices, some lengthier algebraic operations that would otherwise render the text of the chapters less fluid can be found.

2 CHALLENGES RELATED TO THE CONSTITUTIVE MODELING OF POLYMERS

> *Chapter overview: Polymers are a class of materials of increasing engineering importance, constantly gaining ground on competing materials on various applications. Their properties, dominated by the microstructural arrangement of the long polymer chains, present both advantages and challenges. A knowledge of the micromechanics of motion between molecules is an essential tool for the constitutive modeling of polymers, the central goal of the present document. This chapter brings an overview of chemical and physical aspects governing polymer behavior giving rise to some of the most common features of their material behavior under thermal and mechanical loading. With regards to the following chapters, micromechanically-based arguments are made for the necessity of thermomechanically-coupled viscoelasticity models, for the inclusion of viscous effects into polymer damage models and for the inclusion of a characteristic length into fracture models.*

2.1 INTRODUCTION: DETERMINANTS OF POLYMER PERFORMANCE

Polymers have been constantly gaining ground on a variety of industrial contexts for several decades. Owing to intensive effort in the development of new materials and to technological advancements allowing for their large scale production and profitability, polymers are increasingly employed in substitution of metals both for large volume applications, such as all-purpose packaging, and for much more advanced applications, such as the automotive, air and space industries.

Characterized by their molecular composition, consisting of long chains of repetition units, polymers can exhibit a wide range of material properties. Long carbon chains often comprise the basic backbone of polymers and are responsible for much of their constitutive features, but the presence of other types of atoms or molecular groups, connected to the principal chains in different ways, can completely change the way polymers of similar composition behave. Even polymers of the very same chemical composition can exhibit varying properties, depending on factors such as the spatial arrangement of the chains (e.g. with respect to tacticity, the disposition of side groups along the principal chain) or the length of polymeric chains, among others. These factors strongly influence the microstructure (e.g. in the maximum degree of crystallinity for a given type of polymer) and macrostructure of a polymer component, which in turn define such features such as permeability and porosity, among many others.

This first group of determining factors to the material behavior of polymers is often referred to as *structure*.

The chemical structure of polymeric materials also strongly determine their intrinsic *properties*. A central property for the characterization of a polymer is its molar mass. It reflects the length of polymer chains and the degree of compactness in the volumetric arrangement of the chains. On the other hand, the presence of different chemical elements in the chains, and the corresponding chemical interactions between chains is of extreme importance in determining mechanical, thermal and electric properties of a type of polymer.

Alongside the chemical structure of the polymeric chains and their intrinsic properties, another determining factor to the constitutive response of polymeric materials is the *processing* employed in developing the final products. Different processing temperatures may have strong influence on the degree of crystallinity of a specimen, which in turn crucially determines factors such as strength and toughness. Marked differences in induced anisotropy can be observed in choosing between blow molding, extrusion or injection in the production phase of a component. Submitting a material of interest to vulcanization processes (common practice in the production of elastomers) or otherwise inducing the formation of cross-links between chains (giving birth to thermoset polymers) severely constrains the possibility of plastic straining, increasing thermal stability.

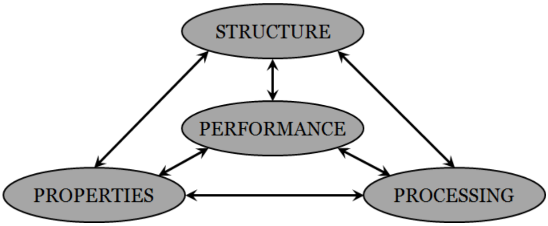

Figure 2.1 – Influencing factors towards polymer performance

There is very strong interplay between *structure*, *properties* and *processing* (as represented in figure 2.1, in a classical diagram in materials science literature), as alluded to in the previous paragraphs. The performance of polymers in industrial applications is determined by this tripod. Conversely, required performance parameters in the design phase lead to feedback on the need to modify every step of the production.

Polymers are often split into categories, corresponding to differences in regard to certain features of their structure, properties or processing. The goal of the present text is not to thoroughly explore all the aspects of polymers as a subject of interest of material scientists. Rather, it lies in identifying some general material behavior features shared by a large section of polymers, features that must taken into account in their constitutive modeling.

In order to contextualize the microstructurally-based discussion that makes up the core of the present chapter, a brief aside on the most general classification of polymer materials is made necessary.

2.2 CLASSES OF POLYMERS: THERMOPLASTICS, THERMOSETS AND ELASTOMERS

Bearing in mind the previously described factors that play a role in the performance of polymers in engineering applications, a first task is to properly define the three main classes of polymers: thermoplastics, thermosets and elastomers.

This is the most basic classification in the study of polymers, essentially related to the way polymer chains are distributed and linked within the microstructure. The chemical structure of polymer chains, often based on long sequences of covalently bonded carbon atoms, is explored in further detail in the following subsection.

For the time being, it shall be sufficient to distinguish between these covalent bonds[2.1] and the much weaker van der Waals bonds[2.2] that may develop between different chains or even different parts of the same chain. Van der Waals bonds are often referred to as secondary bonds (or physical bonds) in polymer science, in contrast to princi-

---

[2.1] Typically, covalent bonds display binding energies in the $60 - 700kJ/mol$ range (KAKANI, 2006). Single covalent bonds between carbons, a common occurrence in polymers, display binding energies of about $350kJ/mol$ (BILLMEYER, 2007).

[2.2] Depending on the type of interaction, which may include hydrogen bonds, dipole interactions or London forces between apolar molecules, van der Waals bonds have binding energies of $0,1 - 40kJ/mol$ (BILLMEYER, 2007).

pal covalent bonds (or chemical bonds) resulting from the process of polymerization.

Secondary bonds are more thermally unstable. Low variations in temperature may excite molecules to the point of breaking secondary bonds. Polymers where they play a central role exhibit what is called low dimensional stability, when subjected to changes in temperature. Principal bonds, on the other hand, are much more thermally stable, essentially immune to large temperature variations.

Through different processing parameters (depending also on the chemical structure and intrinsic properties of the elements that make up the smaller repetition units called monomers), three different scenarios can be found in the resulting microstructure: long polymer chains connected only through secondary bonds; polymer chains heavily connected by principal bonds (called crosslinks), forming a dense network of covalently bound chain sections; long entangled polymer chains connected at some points by crosslinks.

Thermoplastics are characterized by an absence of principal bonds between polymer chains. Different microstructural configurations are possible, from the heavily entangled amorphous state, to the much more organized crystalline state (see next subsection for more details), but the long principal chains only interact through secondary bonds. In turn, relative displacements between neighboring chains are not significantly restricted. Since secondary bonds between different parts of polymer molecules may disappear and reappear under thermal or mechanical loading, thermoplastics are said to have little "memory" of their initial dimensions. In other words, large inelastic strains are observed in thermoplastics, requiring models accounting for constitutive behaviors of plasticity and viscoelasticity. The underlying micromechanics will be discussed in the following subsection. It should be noted that thermoplastics can be promptly recycled, recovering initial properties when subjected to a melting cycle.

Thermosets are characterized by a large density of crosslinks between polymer chains. Though secondary bonds may develop, covalent bonds make up the backbone of the microstructure. Since these bonds are immune to temperature variations, thermosets have significant dimensional stability. As a consequence, thermomechanical coupling is of little to no importance in the constitutive modeling of thermosets. Under stress, their strongly crosslinked networks exhibit small deformations. Related mostly to rotations and stretching of covalent bonds, these deformations are mostly recovered when stress is released. The resulting material behavior is that of a more stiff material when compared to thermoplastics, with little to no inelastic deformations. Rupture is often very brittle. The most common example of thermosets are the various resins used in many engineering applications, for instance, in the production of composite materials such as carbon-epoxy fiber plies. Thermosets cannot be melted and recycled.

Finally, a state of heavily entangled molecules connected to each other at a few ”points of memory” through crosslinks is characteristic of elastomers[2.3]. The crosslinked network can be subjected to very large strains, since there are very long portions of entangled molecules between crosslinks. Large elastic returns are observed, since the amorphous (entangled) state is often the most thermodynamically stable. Different densities of crosslinks define different levels of deformable elastomers. For the most common elastomer, rubber, the content of sulphur used during the process of vulcanization defines the final density of crosslinks. As the density of crosslinks grows, the material behavior approaches that of thermosets. The complex elastic behavior of elastomers has been extensively studied and modelled, especially within the field of hyperelasticity, where the stress strain relations are derived from an energy-like potential (some topics of hyperelasticity are briefly discussed in chapter 3).

The models proposed in the present document are conceived with the challenges presented by the constitutive modeling of the large class of thermoplastics in mind, namely, the treatment of complex inelastic deformations and strong thermomechanical coupling. Most of the arguments presented in the following subsection are developed based on the most common features of microstructural behavior of thermoplastics. Their hierarchy of principal and secondary bonds under the influence of temperature and stresses determines in large part the macroscopically observed large inelastic strains, as will be discussed in the following sections.

For a deeper foray into a microstructurally-based presentation of the features of polymer behavior, including elastomers and thermosets, the interested reader is referred to Ward & Sweeney (2004), Canevarolo

---

[2.3] Due to the presence of crosslinks, some authors choose to classify elastomers as belonging to the family of thermosets. However, the completely distinct mechanical behavior of elastomers warrants its own family. In addition, it should be noted that the family of elastomers may also include some thermoplastic materials, such as poly(styrene-butadiene-styrene) (SBS), poly(styrene-ethylene/butylene-styrene) (SEBS) and thermoplastic polyurethane (TPU), and other block copolymers (made up of blocks of different repetition units or monomers). There, the role played by crosslinks, in restricting the movement of amorphous phases, is played by crystalline phases of one of the composing monomers.

(2006) and Callister (2007). The arguments presented in the following sections are indebted to these works of reference.

2.3 FEATURES OF POLYMER BEHAVIOR: VISCOELASTICITY AND THERMOMECHANICAL COUPLING

Even though polymers[2.4] constitute a wide class of materials, with very diverse material properties, some common features necessary to their accurate constitutive modeling can be identified. Characteristics such as light weight, low conduction and electrical isolation are often attributed to polymers in general. It is also widely known that many polymers (except for thermosets) keep their dimensional stability and mechanical properties in a fairly narrow range of temperature.

These characteristics can be attributed to the chain-like structure shared by all polymers and to the way this structure responds when subjected to loadings of various natures. This also hinges strongly on the degree of crystallinity obtained after processing, especially in relation to temperature dependence. This section is dedicated to exploring these general features and correlating them to the microstructure. Special attention is given to phenomena observed in thermoplastics.

In order to do so, a brief discussion on the long carbon-based chains that constitute the backbone of polymers is a good starting point. In the following, the focus rests on the main microstructural features that explain the macroscopic behavior of polymers. The interested reader is referred to material science literature for material properties and specifics of various polymer species.

Polymer molecules are formed by the repetition of smaller units called monomers, in large enough numbers so that the addition or subtraction of another monomer does not significantly affect the global properties (as defined by the International Union of Pure and Applied Chemistry - IUPAC). As a result, chains of polymers can contain several thousand monomers. Taking polyethylene, one of the most commonly used polymers, as an example, different varieties can have molecular weights ranging from $50.000 g/mol$ (low density polyethylene - LDPE) to around $3.000.000 g/mol$ (ultra high molecular weight polyethylene - UHMWPE) (BILLMEYER, 2007).

[2.4] As mentioned in the previous subsection, most arguments made from here on rely on features more strongly present in thermoplastics. Unless clearly stated otherwise, most general mentions to polymers are made with the thermoplastic structure in mind.

Even if ramifications are often present, the most usual resulting structure is dominated by a very long principal chain with large quantities of carbon atoms. When dominated by carbon atoms connected by single covalent bonds (as is the case of all polyolefins, a family characterized by homogeneous carbon linear chains), but also when oxygen atoms are interposed between carbon atoms in the principal chain (as for the commonly used heterogeneous chained polycarbonate), polymer chains are very flexible. The presence of double covalent bonds or of benzene rings in the principal chain (as for polyethylene terephtalate - PET), on the other hand, renders polymer chains more rigid, limiting movement and organization between chains.

The very long chains that characterize polymers on a molecular level are often found in very entangled states. As the distance between molecules or between different parts of the same molecule decreases, be it in points of entanglement or elsewhere, secondary bonds may form. Depending on the polarity of the molecules and the types of atoms they contain, different types of secondary bonds may develop. Classified either as hydrogen bonds or under the more general category of van der Waals bonds, and appearing between either polar or apolar molecules, secondary bonds are weaker than the primary covalent bonds that make up the principal chains, and are therefore more easily ruptured under loading. They remain, however, very important in providing resistance to straining in thermoplastics (where there is a negligible number of covalent bonds between chains, the so called crosslinks), as obstacles to the relative movement between molecules.

Length, ramification, flexibility and secondary bonding all play a fundamental role in determining the maximum crystallinity of a thermoplastic, together with the level of ramification, the presence, organization and size of side groups (functional groups connected laterally to the principal chains, often containing large numbers of atoms and deeply influencing the properties of the resulting polymer) as well as the ”width” of the actual principal chain. In some ways a measure of the maximum molecular compactness obtainable for a given type of thermoplastic, this reference value of crystallinity is hard to obtain in actual polymer components.

The reason for this lies in the understanding of the dynamics of the crystallization process and the temperatures that characterize it, and the transposition to practical contexts of polymer processing. Two qualitatively distinct microstructural states are often identified for polymers: the amorphous state, where molecules are heavily entangled and there is more empty space between them; and the crystalline state, where a higher level of molecular organization is observed, with aligned molecules developing well known patterns (such as the very common spherulites, shown in figure 2.2).

Often processed from the molten state, thermoplastics begin to develop secondary bonds between molecules or between different parts of the same molecule, as temperature decreases and molecular agitation subsides. Aforementioned factors such as size of side groups and their organization (crucially in their tacticity, a way of describing the identifiable pattern of the spatial distribution of side groups along the principal chain) determine the minimum distances that can be expected between molecules, and the density of secondary bonds that can be created. Highly organized states may develop. Constrained by an increasing number of secondary bonds, molecules may align forming large quantities of bonds in crystalline lamellae. Thermoplastic specimens may be in a completely crystalline phase, in what is sometimes called polymeric single crystals.

More often than not, though, single crystals are not observed alone in practice. Structures mixing crystalline and amorphous phases are much more usual. Different parts of long molecules often participate in separate crystalline plates, with entanglements and large empty spaces proper to amorphous phases dominating the interstices. This has been the object of extensive studies, ever since the pioneering works of Hermann Staudinger on macromolecules and the original ”fringed micelles” model of the 1920's, up to the microscopic observation and description of the most common semi-crystalline structures that develop during polymer processing. These frequently observed structures in polymers include the so called ”shish kebab” structure or spherulites (ball-like structures formed from crystal grains during cooling; see figure 2.2). The more slender, organized and flexible the polymer molecule is, the higher is its maximum level of crystallinity.

The process of crystallization as described above is heavily dependent on temperature. If temperatures are too high, molecules are too agitated for stable secondary bonds to develop. If temperature gradients are too steep, there is not enough time for them develop. The temperature at which the crystalline phases begin to develop is referred to as the crystallization temperature (T_c) of the polymer. On the other hand, when considering the heating process from a solid state, the crystalline phases become mobile and dissociate for temperatures higher than the melting temperature (T_m). Although essentially describing two sides of the same phenomenon (creation and dissociation of crystalline phases), the crystallization and melting temperatures are

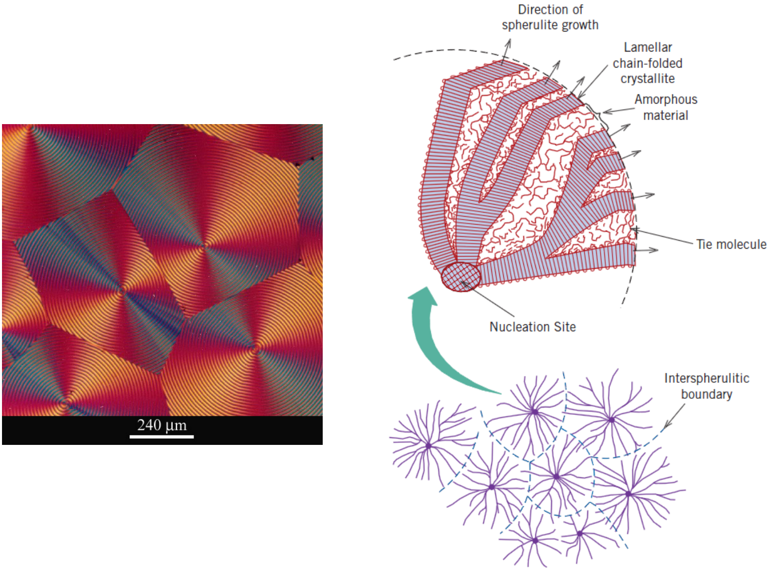
240 μm
Direction of spherulite growth
Lamellar chain-folded crystallite
Amorphous material
Tie molecule
Nucleation Site
Interspherulitic boundary

Figure 2.2 – Left, spherulitic structures observed in polyhydroxybutyrate (PHB) through transmitted cross-polarized light microscope [Source: University of Cambridge's DoITPoMS Micrograph Library]. Right, aspects of the microstructure of spherulites, semi-crystalline structures arising during the crystallization of polymers from the molten state. (CALLISTER, 2007)

different, due to the activation energy needed for the process to start. As for most properties of polymers, both the crystallization and melting temperatures are actually averages of a band along which the transitions occur, as the presence of different lengths of molecules and of different atoms in the polymer chains makes these transitions less sharp.

Maximum levels of crystallinity for a given polymer species would be obtained for quasi-isothermal processes, as the organization would freely develop along time. This is not realistically applicable to industrial contexts, where there are strong demands on productivity. Some presence of amorphous phases is always to be expected in finished polymer products. When high crystallinity is required of the final component due to demands on the thermomechanical performance in the envisioned application (differences between the behaviors of crystalline and amorphous phases will be discussed later on), the idea is to induce the formation of plenty of crystal grains (often through the use of additives) and to control the temperature of tools and molds to ensure a sufficient rate of grain growth. The longer the polymer chains, the longer it takes for crystals to grow, as the bending and arranging of the molecules takes longer.

While the crystallization and melting temperatures of polymers are important in understanding the process of crystallization, marking the temperature below which molecule excitation subsides enough for there to be secondary bonds and crystalline arrangement, perhaps the most important temperature related behavior of thermoplastics pertains to a different phenomenon: glass transition. As temperature decreases, from the molten state to below the melting temperature, molecules in the amorphous phase remain very mobile. Unconstrained by a sufficient number of secondary bonds, aside from a few points of entanglement, molecules in the amorphous phase are still sufficiently agitated in order to bend and reach different configurations. As temperatures continue to drop, glass transition is the phenomenon that represents the end of mobility for the amorphous molecules.

The glass transition temperature (T_g) is of central importance in the characterization of thermoplastic polymer species. Below the glass transition temperature, the amorphous phases no longer have the necessary energy to move and conform, which translates into a much more rigid and brittle macroscopic behavior. As mentioned above, restrictions upon polymer processing explain the presence of amorphous phases in a large majority of polymer components, even when the properties of the crystalline phase were desirable (higher density, stiffness, chemical and dimensional stability, among others). Other applications require properties more closely related to amorphous polymers (such as lower density, transparency and permeability, among many others). Therefore, the knowledge of the glass transition temperature is essential for polymer applications.

Even within the family of thermoplastics, different polymer species may have widely varying glass transition, crystallization and melting temperatures. For instance, low density polyethylene (used in the production of plastic films, kitchen utensils and toys) has $T_g = -30^oC$, while high density polyethylene (used for more resistant plastic bags, plastic boxes and storing units, buckets, wire coating), essentially a polymer of the same chemical composition, but with less ramified and longer principal chains, has $T_g = -100^oC$. Polycarbonate, used for the production of CD's, and extensively in the automotive industry (for instance in headlights and other impact resistant components), has a much higher T_g of 145^oC. Polylactic acid, a biodegradable polymer extensively used for in the manufacturing of medical implants, has a T_g of about 60^oC.

In other words, a combination of different possibilities can be encountered: highly crystalline or amorphous polymers used below the glass transition temperature or between the glass transition and melting temperatures. What is important in developing reliable constitutive models is to understand the main features of the macroscopic behavior of the materials of interest and how they may vary with changing temperatures. As touched upon above, some general guidelines can be drafted, characterizing the behavior of crystalline (or semi-crystalline) and amorphous polymers and how glass transition can be expected to affect it.

Roughly speaking, as crystallinity grows (or for a decreasing presence of the amorphous phase), for the same type of polymer subjected to the same temperature, the following properties tend to increase:

- density (molecules are more compactly organized)
- stiffness (bonds between organized molecules offer resistance to straining)
- hardness
- dimensional stability (less subject to heat dilatation)
- chemical stability (crystalline arrangement is stronger and leaves molecules less subject to external agents)

Meanwhile, the following properties are compromised:

- ultimate stretching (more crystalline materials tend to behave in a more brittle fashion, since within the crystal lamellae there is a great constrain on the relative movement between molecules, and breaking of principal chains happens before significant strains can take place)
- impact resistance (due to increased brittleness)
- tenacity (little to no dissipation in the form of inelastic deformation takes place)
- thermal expansion (dilatation is restricted in the compact lamellae)
- permeability (much less free space between molecules is present)

As mentioned earlier, going from application temperatures below the glass transition temperature to ones above it will usually lead to a reduction in stiffness and hardness, and to the passage from brittle to much more ductile behaviors. As the amorphous phases gain mobility, thermoplastic polymer chains are free to conform and accommodate the imposed loadings. In fact, operating between T_g and T_m can be expected to lead to large strains and induced anisotropy, as chains align in the direction of higher stresses. As a small side note, for polymers processed from the molten state down to below their glass transition temperature, heated molds or an annealing phase are often employed to remove this type of induced anisotropic behavior. Thermosets, on the other hand, have their behavior dominated by the large presence of crosslinks, which severely restricts movement between polymer chains.

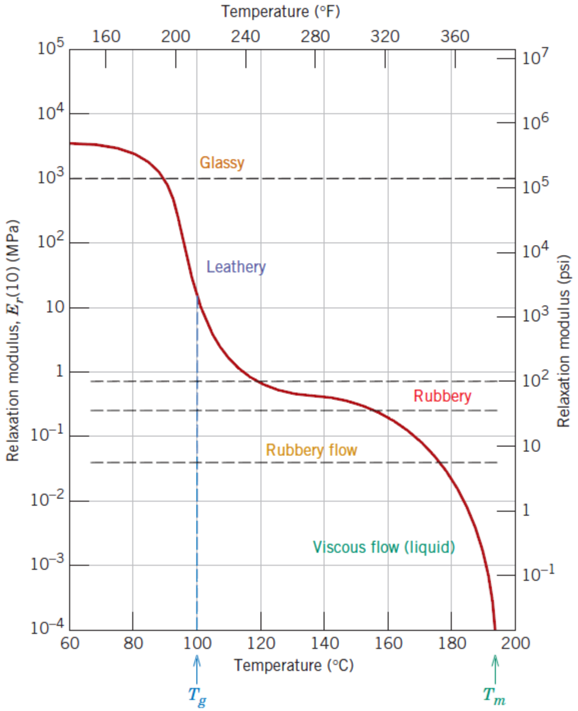

Figure 2.3 – Temperature dependent behavior of polymers as represented through relaxation tests: regions of material behavior. (CALLISTER, 2007)

The temperature dependent behavior of polymers is characterized in a variety of standardized tests, generating several curves of interest to the development of constitutive models. Among these tests, the stress relaxation tests can be used to evidence the transitions in material response as temperatures increase. By subjecting a specimen to a constant total strain and measuring stresses while temperature evolves, thermoplastics develop four identifiable bands of behavior (represented as the evolution of the stiffness modulus with temperature; see figure 2.3). For amorphous polymers, these bands are more evident than for semicrystalline ones, as increasing levels of crystallinity render the glass transition less important to the general mechanical behavior of the polymer.

The first band, with little variation with respect to temperature, marks the glassy region: below the glass transition temperature, the material is stiffer and brittler. As the glass transition takes place, a second band with strong temperature gradients can be identified, the leathery or viscoelastic region: increasing temperature excites molecules and leads to the breaking of secondary bonds, higher compliance and larger inelastic response. The third band (sometimes absent, depending on the polymer species), characterized by a second plateau, is the rubbery region: tight entanglements play the role of cross-links between chains, so that large strains are possible, but the elastic return is increased with respect to the viscoelastic phase. Finally, as temperatures climb towards melting, the fourth band appears, the flow region (separated into slower rubbery flow and viscous flow in figure 2.3): molecular agitation destroys all links between chains, and they become free to flow as a viscous fluid, so that elastic return tends to zero.

Quantifying the impact of growing temperature on material properties of polymers is the goal of another common characterization, the Heat Deflection Temperature (HDT) test. Using a constant central load applied to a beam specimen under controlled temperature conditions (as represented in figure 2.4), the HDT test is used as a means of identifying the limiting temperatures for engineering applications of thermoplastics. The result is the temperature for which the central distortion of the beam reaches a threshold (usually, $0,1in$), indicating compromised dimensional stability under loading. This means that the thermoplastic polymer in question is moving from a glassy phase into a viscoelastic phase, and creep-like behavior can begin to take place.

The influence of temperature on general material behavior can equivalently be plotted in stress-strain curves that can be expected for a thermoplastic polymer at different temperatures, as seen in figure 2.5. The opposite effect is also indicated when, instead of temperature, the

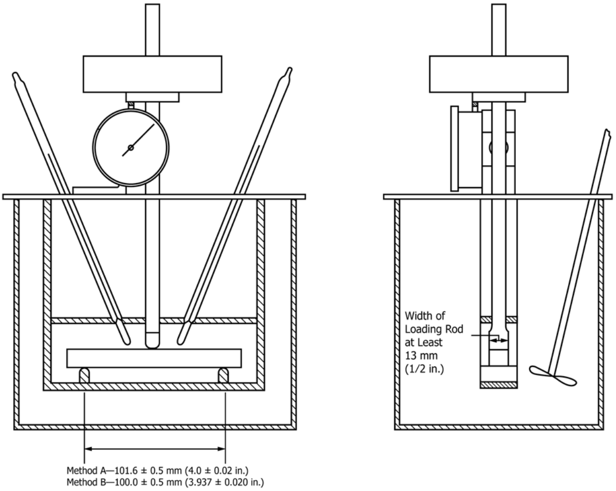
Width of
Loading Rod
at Least
13 mm
(1/2 in.)
Method A—101.6 ± 0.5 mm (4.0 ± 0.02 in.)
Method B—100.0 ± 0.5 mm (3.937 ± 0.020 in.)

Figure 2.4 – Schematic view of the Heat Deflection Temperature test [Source: ASTM]

strain rate of loading is increased. As the characteristic time of the applied loadings becomes shorter, as for impact loads or for high frequency cyclic tests, the characteristic time of the viscoelastic relaxation of polymers becomes comparatively too long for there to be high inelastic strains. In other words, as for any viscoelastic material, the response becomes increasingly rigid and brittle as strain rates grow. Conversely, the material behaves more like a viscous fluid as strain rates decrease.

These effects are the theme of extensive studies, in what is called the time-temperature equivalence observed for polymers. Based on hypotheses that thermodynamically similar activation phenomena occur for varying time scales and temperatures, a common practice in polymer characterization is the generation of master curves. In a master curve, results such as the viscoelastic creep behavior of a polymer species obtained at different temperatures are shifted and fitted to a single curve that represents the behavior of the polymer for a larger range of time scales and temperatures. Although often limited to low strain rates and within the linear viscoelastic regime, so as not to violate the underlying thermodynamics of activation, the practice of time-temperature superposition that leads to master curves finds extensive application for characterization purposes in engineering contexts.

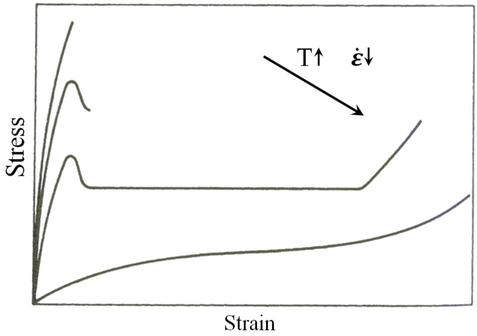

Figure 2.5 – Effect of increasing temperature or decreasing strain-rate on the material behavior of semi-crystalline polymers: from brittle behavior (below the glass transition temperature), some yielding before fracture, large plastic deformations (plateau characteristic of necking during cold drawing) and rubber-like flow. Principle of time-temperature equivalence.

The focus of the present work is in the development of constitutive models well suited to treat the complex material behavior exhibited in the viscoelastic phase of thermoplastics, where large strains and strong thermomechanical coupling are of great importance. For all the other phases, however, molecular and microstructural complexities generate phenomena including dissipation, hysteresis and some thermal coupling. This makes the use of simpler constitutive models of isothermal elasticity a daunting task. Some degree of viscoelasticity often needs to be included to account for accurate modeling, even for applications in the small strains regime, or below the glass transition temperature.

Combining elastic and inelastic deformations, the viscoelastic behavior of polymers is usually idealized as a combination of properties from an elastic solid and a viscous fluid in polymer science literature (BILLMEYER, 2007; CALLISTER, 2007; CANEVAROLO, 2006; KAKANI, 2006)[2.5], using the methodology of rheological models, where basic

---

[2.5] It should be noted that, in distinction with the nomenclature used in continuum mechanics texts, polymer scientists often use the term viscoelasticity to account for all inelastic phenomena, and not only for the deformations that can be fully recovered after a characteristic relaxation time. In that sense, what is under the umbrella of viscoelasticity in several polymer science texts includes both viscoelastic effects components such as springs, dashpots and dry friction elements have their easily describable behavior combined in various ways to reproduce complex experimental results. Several different models are used in describing various facets of polymer behavior, including the classical Kelvin-Voigt and Maxwell models. Further discussion upon available rheological models, their strengths and shortcomings, can be found in chapter 3 together with the formulation of thermo-viscoelasticity in a variational framework.

Once more focusing on the microstructure of polymers (especially that of thermoplastics), it is interesting to understand the origins of the two distinct features of their material response: elastic return and viscous flow. Elastic deformation, a conservative phenomenon, is closely associated to the rotation and stretching of covalent bonds present in the principal chains. Under stress, atoms are forced to move away from the more energetically stable state often called unloaded. When stress is removed, the previous configuration is recovered. Elastic response is idealized as time independent, occurring immediately (in phase, for cyclic loads) with the application of loads.

The inelastic part of deformations (associated to those of viscous fluids), on the other hand, is closely associated to dissipative phenomena, such as the breaking of secondary bonds or friction between chains. Under stress, especially in the viscoelastic region comprised between the glass transition and melting temperatures, large displacements between molecules can be expected. In that region, temperatures are high enough for the amorphous phases to move freely; temporary bonds between entangled molecules are much less stable, and may easily be broken, eliminating obstructions to movement.

One of the most widely used experimental procedures for the characterization of polymers, the Dynamic Thermomechanical Analysis (DTMA), is based on an assumed decomposition of the elastic modulus of the material of interest in real and imaginary parts ($E = E' + iE$"). In other words, the parameter takes into account a real portion, representing the instantaneous response in force with the imposed sinusoidal displacements, and an imaginary portion, representing the out

---

(in the aforementioned concept of continuum mechanics), plasticity (permanent deformations after yielding) and viscoplasticity (strain rate dependent plasticity).

The models developed within the present text are more closely related to the continuum mechanics tradition. In the interest of clear definitions of what is understood by the different types of inelastic behavior, the reader is referred to chapter 3. For the time being, it should be sufficient to recognize the difference in lexicon and to move along to more discussions on the influence of the microstructure upon the material response of polymers.

of phase response associated to fluid-like viscosity. The experimental set up consists of an isolated chamber inside which a standard specimen is cyclically tested with imposed displacements at moderate frequencies (usually around $1Hz$, keeping inertia effects negligible) for varying controlled temperature. Points of inflexion are apparent, both for the storage modulus (E', real part of the elastic modulus) and for the loss modulus (E", imaginary counterpart) around the glass transition temperature. The relation between loss and storage moduli is usually plotted in the so called "tan-delta" ($\tan \delta = E"/E'$), where a peak makes the identification of the glass transition temperature easier. In figure 2.6, a general overview on DTMA, including sample results from a thermoplastic polymer.

The matter of time scales is important when considering and modeling the inelastic behavior of polymers. The dissipative phenomena taking place in the microstructural level are strongly time dependent. Molecules move relative to their neighbors in finite time, in distinction to the idealized immediacy of elastic deformations. In other words, there is a characteristic time associated to the viscous part of material response. When unloaded for a long enough time, even polymer specimens that were previously highly stretched can be expected to exhibit considerable return, though some deformations may be in fact permanent.

This issue is crucial in the selection of material models for the simulation of polymer behavior. Although introductory literature on the materials science behind polymers frequently makes no distinction between all inelastic behaviors, the choice of a constitutive model is associated with modeling hypotheses on the nature, dependencies and relations between different physics. A wide range of material models has been used to accurately describe polymer-like inelastic behavior in applications of interest, depending on material, type of loading, loading rate and range, time scale of simulation, among other factors. A by no means exhaustive list of the main classes of models employed includes: plasticity (HAUDIN; MONASSE, 2001), viscoplasticity (BOYCE; PARKS; ARGON, 1988), isothermal viscoelasticity (DROZDOV, 1998) and thermomechanically coupled models (ARRUDA; BOYCE; JAYACHANDRAN, 1995).

Aside from applications within the small strains regime, with small strain rates and quasi-isothermal conditions, it is clear that the accurate description of thermoplastic polymer-like material behavior requires the inclusion of rate dependence (viscous phenomena) and temperature dependence. The microstructurally-based discussion up

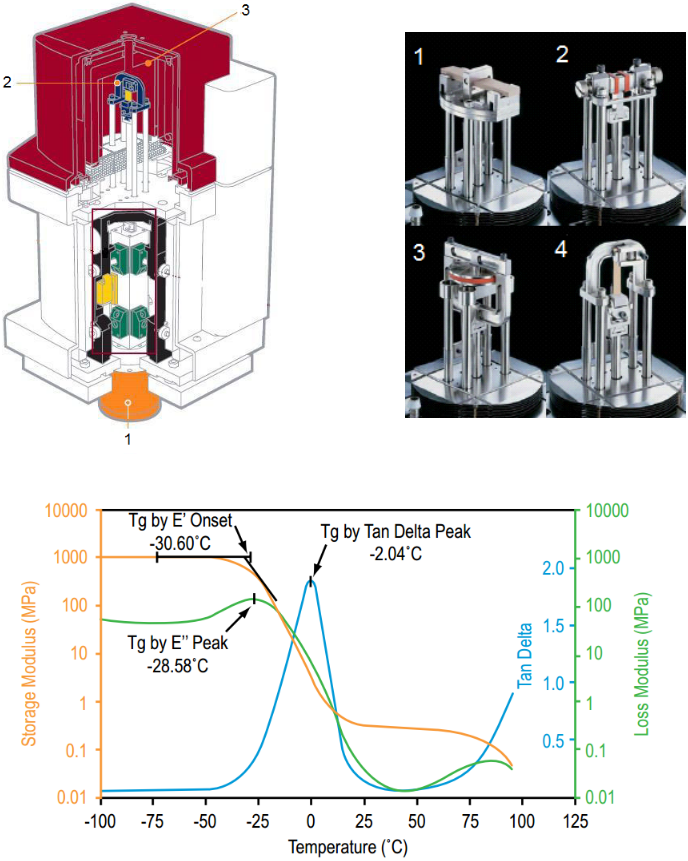

Figure 2.6 – Dynamic Thermomechanical Analysis of polymers. Top left: scheme of the experimental set up showing the drive motor (1), the clamps (2) and the furnace (3). Top right: DTMA clamps for 3-point bending (1), shearing (2), compression (3) and tensile (4) testing. Bottom: sample results from a DTMA test – sharper identification of the glass transition temperature on the tan-delta curve [Source: TA Instruments]

to this point, illustrated by examples taken from the literature and by brief presentations of a few extensively used characterization procedures, has hopefully been sufficient motivation for the necessity of consistent thermomechanically coupled viscoelasticity models for the constitutive modeling of thermoplastics.

However, throughout the above discussion no mention was given to degradation phenomena that may affect the material properties of polymers. So far, only the behavior of microstructurally sound material has been considered. Though viscoelasticity and other forms of inelastic behavior have been related to the breaking of secondary bonds and other forms of irreversibility, all the arguments were made considering that the material remained homogeneous, free of defects and with intact principal polymeric chains.

This scenario is sorely lacking in complexity as the point of interest moves from the behavior of a fully sound material to the mechanisms involving degradation and, eventually, rupture. While thermodynamically sound models, including thermomechanical coupling and complex forms of viscoelasticity (included in the framework developed in chapter 4), have great value in modeling polymer-like material behavior, additional information needs to be added to account for damaging mechanisms.

In the following subsection, once more, a phenomenological description of the degradation mechanisms taking place at the microstructural level is offered as motivation for the development of constitutive models based on the field of continuum damage mechanics, such as those presented in chapter 4.

2.4 MAIN FEATURES OF POLYMER DEGRADATION: DAMAGE AND RUPTURE

As explored earlier, microstructural explanations to macroscopically observable characteristics of polymer behavior can be developed. Experimental observations using techniques such as spectroscopy, electronic microscopes and specific characterization procedures have greatly increased the amount of available information, which in turn helps in developing models of increasing complexity. Through the knowledge of the chemical structure of the long principal polymeric chains and of the way they can form bonds and patterns of organization, one can explain such phenomena as strain rate dependence and temperature dependence. These features characterize the material response of polymers under loading, and justify the need for constitutive models incorporating ingredients of viscoelasticity and thermomechanical coupling. These models are crucial for an accurate description of the microstructurally sound polymer of interest.

As the end of life of polymer components comes into focus, a whole new set of phenomena starts taking place at the micro and macrostructural levels. Depending of the criteria utilized in order to determine the threshold for the application of a given component, a variety of effects may have to be modelled. In general, and in order to clarify the nomenclature used from here on, an argument can be made that one of two scenarios is possible. There may be noticeable degradation of material properties, jeopardizing the structural or functional integrity of a larger system within an engineering application - in this case, *damage* mechanisms come into play. Likewise, there may be catastrophic failure, with some part breaking up into multiple pieces through the nucleation and propagation of cracks - in which case, *fracture* mechanisms have to be accounted for.

Clearly, damage and rupture mechanisms are not independent from each other. Often considerable damage on material properties serves as an indicator for the imminent onset of fracture. In fact, the development of models that are able to describe the transition from damage to fracture is a topic of intense research, and one of the issues dealt with in the present document. Chapter 6 includes a description of the Thick Level Set model, a nonlocal approach to damage and fracture encompassing phenomena of both natures.

Classically, however, damage and fracture mechanisms have been approached in separate families of models by the continuum mechanics community, namely: continuum damage mechanics (following pioneering works by Kachanov) and fracture mechanics (originated in the works of Griffith). Since the basics of the classic continuum approaches will receive more extensive attention in chapters 5 and 6 and the subject of the present chapter is polymer behavior, the focus is once again shifted to the microstructure of polymers and its influence upon macroscopic behavior.

As discussed earlier, the long carbon-based chains that characterize the large class of polymers are also those responsible for the material properties exhibited by them. Consequently, the main factor causing degradation of material properties is the rupture of principal chains. In fact, some common measures of polymer degradation, either from mechanical or chemical sources (briefly discussed later on), are directly related to the reduction of the average molecular weight of polymer chains. Charged beyond the threshold of atomic bonding between their components, some chains may split into several shorter chains and reduce the elastic modulus, for example. This may happen for a few chains only, so as not to cause the total rupture of the component (other less stretched chains may accommodate the stress released by the ruptured fibres). Still, there may be a finite change in the values of material properties.

Unlike the breaking of secondary bonds, a dissipative phenomenon that explains different forms of inelastic deformations, when the much stronger principal bonds are broken, the general integrity of the material is more severely affected. While secondary bonds may form again elsewhere between other parts of polymer chains, the rupture of principal bonds is permanent. Formed from monomers generated during oil fracking processes using controlled temperature conditions and with the help of additives, principal chains are the result of the process of polimerization. The conditions for polimerization are seldom if ever present under application conditions, which precludes the possibility of "healing" broken chains.

Breaking principal bonds remains a dissipative process, though. While in composite materials the reinforcing fibers are often organized and aligned, in polymers, chains hardly follow a given controlled direction. Even in cases where large straining caused induced anisotropy, entanglements guarantee that neighbooring chains are not under the same loading condition. As secondary bonds begin to break, other chains bear more of the imposed loads, and the possibility that they break increases. In other words, as for inelastic deformations, there is clearly a time dependent component to damage in thermoplastic polymers, at least in the leathery or viscoelastic region of their behavior (see figure 2.3, in the previous subsection).

It should be noted, however, that crystallinity and temperature play an important role on the matter. For crystalline materials, such as metals, no such claim on the need for a time dependent component to damage modeling can be made unequivocally. Even for amorphous polymers operating under the glass transition temperature, brittle fracture usually occurs, indicating a clean and instantaneous break of a large number of polymer chains, once their resistance to loading has been reached. As a general rule of thumb, it can only be argued that when viscoelastic effects dominate material behavior (that is, when there is an amorphous phase and the material is used in applications above the glass transition temperature), the damage modeling of polymer chains should take into account some sort of time or strain rate dependence. Due to time-temperature equivalence effects, a similar claim can support the need for the inclusion of temperature dependence as well.

Specific loading conditions and modeling assumptions can lead to different choices for polymer damage constitutive modeling. For instance, quasi-static load imposition and isothermal conditions are often assumed for several applications. Still, damage remains associated with the breaking of secondary bonds and the onset of inelastic behavior, as principal fibers are ever more responsible for bearing the applied loads. In these cases, a common assumption, often made for metallic materials, is the coupling of damage to plastic deformations in Lemaître-type damage models (a very brief discussion on Lemaître models of damage is made in chapter 5; for more details on the models, the interested reader is referred to Lemaître (1996) and Lemaître & Desmorat (2005); for applications of damage coupled to plasticity for polymers, one of many examples can be found in Fancello et al. (2014)).

Other factors besides loading conditions can act as the driving force behind material degradation in polymers. Their chemical structure can be affected by various factors, such as ultraviolet radiation and exposure to aggressive chemicals. This type of phenomenon is usually called ageing. Ageing plastics are known to become fragile and brittle, a reflection of a chemical damage process taking place through time. The physics underlying such phenomena is markedly different from that of loading-based damage, and therefore require different tools and couplings when it comes to modeling. The models proposed in chapter 5 of the present work do not deal with chemically driven damage, and are restricted to thermomechanical loading driven damage.

While the breaking of principal bonds that make up polymer chains can be described as the main mechanism behind damage of polymers, other phenomena that evidence reduced material integrity can also take place. Sometimes, modern observation techniques can help visualize effects of a slightly larger length scale. For instance, microcracks and microvoids are a common appearance in damaged specimens, in polymers as in metals. As it will be discussed in further detail in chapter 5, a classic approach to the constitutive modeling of continuum damage mechanics uses, as a measure of damage, the volume occupied by microvoids in a representative volume element. In other words, this approach associates damage to the appearance of voids, volumes not filled by a bulk material that can bear the applied mechanical loads.

In figure 2.7, there is clear evidence of the development of microvoids in the fracture surface of a polycarbonate specimen. Instead of a flat fracture surface, expected when brittle failure occurs, a much more rough texture can be observed, with the remnants of broken polymer fibers clearly evident. The presence of these features in a fractured surface indicates a region of compromised material integrity that triggered fracture failure.

From the experimental observation of damaged specimens arises the bridge between damage and fracture mechanics. While in damage modeling microvoids and microcracks are considered infinitesimal, having only volumetric influence upon material properties, fracture modeling starts from a finite crack. It is clear, then, that coalescence of microvoids and microcracks into larger cracks serves as a *de facto* boundary of application between the two classical families of constitutive modeling.

Focusing now on failure and fracture of polymers, two characteristic features are often observed: stress crazing and shear banding. A brief overview of the physics underlying these phenomena serves a useful primer on some of the micro and mesostructural aspects of polymer fracturing.

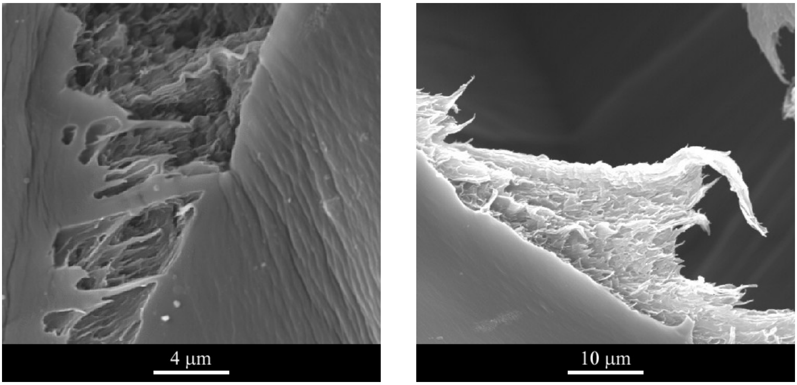

Figure 2.7 – Details evidencing stress crazing for fractured surfaces of polycarbonate. Left, crazes evident of the wake of a downward evolving crack tip. Right: remains of broken fibers in a fractured surface [Source: University of Cambridge's DoITPoMS Micrograph Library]

Stress crazing, seen in figure 2.7, is in fact the main representation of the generation of microvoids and microcracks within loaded polymer specimens. As secondary bonds break and principal chains align with the loading direction, some of the forces that kept the bulk material homogeneous are lost. In addition, some principal bonds may start to break in certain locations, giving rise to fibril-like structures around a growing network of microvoids.

Experimental measures show a slight local increase in volume (or reduced material density) in regions where stress crazing develops. The remnants of broken crazes are mostly observed for specimens fractured under tensile loading conditions, only rarely for compressive loadings. Stress crazing is also the main reason for the rough fracture surfaces observed in ductile polymers. Associated to large inelastic deformations, crazing usually accompanies considerable plastic and viscous deformations, and is absent when brittle behavior dominates.

After the onset of stress crazing, as loading continues, microvoids coalesce and give birth to cracks. As evidenced in figure 2.7, these so called crazes are often present in the wake of an evolving crack. They can be considered a means of increasing tenacity and fracture toughness, by serving as obstacles to crack advancement (BILLMEYER, 2007; CALLISTER, 2007).

The presence of crazes as precursors to cracks suggests some interesting choices in terms of modeling fracture in thermoplastics. Under one point of view, the fibrils on the wake of the crack exert forces that tend to close the crack tips, a phenomenon that constitutes the core of cohesive zone damage models. This has been the model of choice in the modeling of polymer fracture in Bjerke & Lambros (2003), Zreid, Fleischhauer & Kaliske (2013).

Under a second point of view, regarding microvoids as evidence of partial damage (since the bulk material remains capable of bearing loads) and cracks as complete damage, there is a clear development of a minimum length between sound and totally degraded portions of material. Microscopic observations of fractured thermoplastic specimens in the viscoelastic region seem to support the existence of such a characteristic length (as observed in figure 2.7). For models that endeavor to bridge the modeling gap between continuum damage mechanics and fracture mechanics, the inclusion of such a characteristic length is crucial in managing the change in modeling tools. The Thick Level Set model, the nonlocal damage model of choice in the present document (described in detail in chapter 6), was developed to deal with this type of phenomenon.

Another common occurrence before fracture in polymers is shear banding. Extensively studied for metals, shear bands are preferred directions of plastic flow formed under loading as the microstructure is led to move and conform. In thermoplastic polymers, the alignment of principal chains tends to create bands where secondary bonds can more easily be broken and greater inelastic flow is possible. As principal chains become more loaded, they may start to break, precluding even further the possibility of elastic returns.

Appearing both in tensile and compressive loading conditions, shear bands are responsible for strain localization in polymers. The common necking observed in standard tensile specimens reflects the appearance of shear bands in 45^o angles with respect to the applied loading direction, as represented in figure 2.8. As some principal bonds break, polymer fibers rearrange and further align. Strains localize in the most loaded region and form a neck, where two situations are experimentally observed: either the neck ”spreads” to the full length of the specimen, or concentration continues and the neck becomes narrower as it approaches failure.

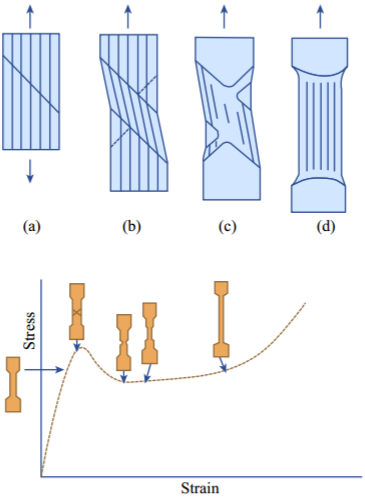

Figure 2.8 – Shear bands forming in polymer tensile specimens explain necking and strain softening observed during standardized tensile tests [Source: MIT OpenCourseWare]

Both the loading pattern and the characteristics of the inelastic behavior of the polymer of interest will determine which of the paths is followed. Different constitutive models are then needed to properly capture these features of material behavior. Typically, when strain localization in the form of necking takes place, models of viscoplasticity (therefore incorporating permanent strains and strain-rate sensitivity) are needed. Although plasticity models are not the focus of the present work, it should be noted that different models for the shape and evolution of the yield surface can be used to fit the observed phenomena.

As it will discussed in chapter 3, a common assumption, supported by strong experimental evidences (in pure shear tests, for example), is that inelastic deformations are volume preserving. Shear bands, consisting essentially of concentrated plastic deformations in small bands, is also often observed to be isochoric. Plastic deformations are facilitated within the bands, happening at much higher rates than elsewhere. In fact, most efforts to model the physics behind shear bands take advantage of mathematical tools that introduce discontinuities in displacement velocity fields. In other words, shear bands can be regarded as regions of plastic instability, where large inelastic flows take place.

Shear bands are a theme of interest in the field of thermomechanically coupled constitutive models. As for other phenomena related to the breaking of secondary bonds, shear bands are of a dissipative nature. Strong local heat generation accompanies the onset of shear bands. Given that the velocity of displacements becomes so high within a shear band, a common modeling assumption is that there is not enough time for the heat to dissipate and flow to other parts of the body, i.e., adiabatic conditions are present. This led to the development of the classical family of models dedicated to Adiabatic Shear Bands, as in the later discussed variational approach of Su, Stainier & Mercier (2014) for metals (where the occurrence of shear bands is also common) and the many works related in chapter 9 of Dodd & Bai (2012), among many others. As heat is locally generated in rates higher than conduction can dissipate, material parameters can become affected and trigger even further strain localization, through softening.

Within the present text, shear bands and strain localization are of general interest as thermomechanically coupled phenomena, and of specific interest as frequent precursors to failure in polymers. Locations of strain localization are often locations of crack generation. Since high plastic deformations occur, ductile fracture (and the associated stress crazing previously discussed) is the usual failure mechanism. It should be noted, though, that the models of viscoelasticity developed in chapters 4−6, which do not include plastic deformations, are not well suited to the description of adiabatic shear bands.

Therefore, the interest here is merely in contextualizing the micromechanics preceding different modes of failure in polymers. In addition, in relating failure in polymers to dissipative and time-dependent phenomena, the central goal is to justify the necessity of including viscous phenomena into accurate models of degradation and failure of polymers.

2.5 LIMITATIONS OF THERMO-VISCOELASTIC DAMAGE MODELS IN DESCRIBING POLYMER-LIKE MATERIAL BEHAVIOR

Before moving on to the core of this work, where constitutive models encompassing time and temperature dependence in both the fully sound and degraded behavior of polymers are devised and later extended to include nonlocal information ruling the passage from damage to fracture, it is necessary to go into some of the possible limitations of the chosen models.

Using similar microstructurally-based arguments, some phenomena commonly observed in polymers can be shown to fall outside the scope of the models developed in chapters 4, 5 and 6 of the present document, namely models of thermomechanically coupled viscoelastic damage. Mentions to some of these shortcomings have already been sprinkled through the previous subsections, but a more centralized view merits its own space.

While the need to include time and temperature-dependent phenomena to account for several facets of polymer behavior has hopefully been well established at this point, the specific choice of the classes of these phenomena is crucial in accounting for different features.

As discussed earlier, materials science literature on polymers often makes no distinction between different inelastic phenomena. Moving on to constitutive modeling efforts, choices on the matter have to be made. In those choices lies the source of the limitations of said constitutive models in reproducing experimentally-observed phenomena.

It is clear that the behavior of secondary bonds introduces a time-dependence absent from pure plasticity models. However, as discussed earlier, secondary bonds may break and form between different parts of the polymer network during loading, so that full recovery of original dimensions is often impossible. The time scale of interest is an issue, though.

Some experimental tests indicate that the recovery of original dimensions may continue in very long time scales: some polymer species seem to keep the ability of going back to a more relaxed internal state.

In that sense, the choice of viscoelasticity models, as done in the following, can be justified, as long as appropriate characteristic times are included. These can often be much longer than those of the loading periods. Some of the presented examples will account for that possibility.

However, it must be admitted that within the time scales of most applications, viscoplasticity models (or some combination between viscoelasticity and plasticity) do seem to be more in tune with the observed phenomena. Shear bands and other strain localization phenomena may still appear in thermomechanically coupled viscoelasticity models, as will become evident in some applications present later on, but the correspondence between classical shear banding models may become more difficult, especially in identifying the same geometrical features of the shear bands, something that is not explored in the present text.

Another discussion absent in the following chapters and often observed in experiments with polymers approaching failure is the issue of induced anisotropy, something that was mentioned earlier when discussing stress crazing phenomena.

The models developed in the present text are all isotropic. Based on the hypothesis of a random statistical orientation of long polymer chains throughout the material, schematically represented in the structure of spherulites shown in figure 2.2, isotropy of material properties can be easily lost as loading approaches the limiting resistance of the polymer sample.

The micromechanics of induced anisotropy has been previously discussed: it involves the breaking of secondary bonds and the orientation of principal chains along the direction of higher tension. As this happens, mechanical properties in transverse directions can differ greatly from the direction aligned with loading. Models that do not account for local fiber directions are intrinsically unable to account for these phenomena.

This is one of the main motivations behind the development of constitutive models featuring a mathematical description of polymer chains and links, such as the one in Arruda, Boyce & Jayachandran (1995). This type of modeling is clearly challenging. The appropriate number of chains, their length and the angles between them are dependent both on the polymer species and on processing conditions. Additionally, the description of fiber orientation in a real specimen requires the description of surface features introduced during fabrication. The complexity of such a model is greatly increased, and its application constrained to very specific conditions.

In contrast, the models developed in the present work are conceived as of more general application. They encompass the guiding micromechanical phenomena of polymer behavior, but do not go into the actual description of the microstructural features of polymers. This can compromise the ability to describe all the complex phenomena observed experimentally. In other words, the goal of the proposed models is to offer qualitatively accurate models without the complexities of describing the internal fiber configuration parameters. Through the use of several characteristic times in viscoelasticity and of a characteristic length in the nonlocal damage modeling, however, the proposed models can remain general in structure (and thus more easily related to other widely used constitutive models and computational tools) while approximating the observed phenomena. As will be shown in chapter 6, the introduction of a characteristic length for the transition between damage and fracture allows for the identification of preferred damaging directions and introduce localization and crack initiation, ultimately giving rise to fibril-like structures (cohesive tones) closely resembling in stress crazing of polymers, even for a locally isotropic model.

In such a locally-simpler model, though, the rational description of all micromechanical mechanisms, closely linked to the description of fiber directions, gives way to a more phenomenological approach, where sensitivity analysis and curve fitting become more important in quantitatively matching what is experimentally observed.

Assuming isotropy can also become an issue when dealing with block copolymers, where polymer chains are constituted by more than one type of repeating unit or monomer grouped in separate blocks along the polymer chains. In these cases, it is common to find non-uniform microstructures. Instead of a network of randomly distributed polymer chains, different parts of polymer chains may develop inclusion-like structures. The different properties of these separate phases combine in giving such copolymers their macroscopic properties.

Examples of such polymers include SBS, composed of styrene and butadiene monomers organized in alternated polystyrene and polybutadiene chains, a large class of thermoplastic elastomers (materials with the inner structure of thermoplastics but the macroscopic behavior associated to elastomers). Polystyrene sections of various chains organize in inclusion-like spheres, exhibiting much larger stiffness than that of the randomly distributed and flexible sections of polybutadiene, and working like crosslinks in classic elastomers. Figure 2.9 shows a schematic representation of the structure of SBS.

Using an isotropic model for these cases is equivalent to a strong

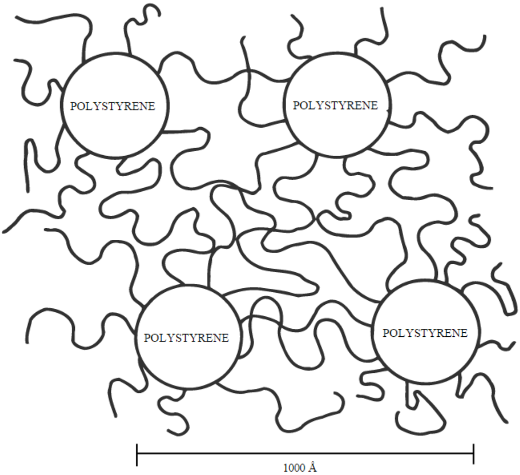

Figure 2.9 – Example of non-uniform microstructure of block copolymers. Two-phase structure of SBS, a class of thermoplastic elastomer: rigid spheres of polystyrene surrounded by randomly distributed network of polybutadiene.

simplification, and may lead to poor models, seen as the microstructural interfaces can serve as initiating locations for localization phenomena. This class of problems is clearly more suited to a multiscale approach, which falls outside the scope of the present text. As an alternative, the models present in the following chapters do offer the possibility of reproducing complex macrostructural properties through the use of an arbitrary number of rheological elements and of nonlinear functions for each portion of accumulated energy in the material. This remains a simplification of cases where the microstructure is non-uniform, though.

Another possible issue for the models devised in the following is the mechanism linking damage and heat capacity. As argued earlier, thermal properties, as mechanical ones, are related to the microstructure of polymers. Long polymer chains dominate the response to both mechanical and thermal loading, through a resistance to stretching and temperature-induced molecule excitation. With the onset of damage, these properties are altered. Breaks in principal chains severely reduced the material's ability of bearing loads - thus, compromising macro properties such as the elastic and viscous moduli. On the other hand, the effect on thermal properties can be different.

The concept of time-temperature equivalence discussed earlier correlates thermal excitation to the easier breaking of secondary bonds, in turn leading to higher viscous strains. This accounts for thermomechanical coupling, though, leaving aside purely thermal effects such as conduction and heat accumulation. As the material is damaged, the principle of time-temperature equivalence offers no evident explanation for the evolution of thermal properties.

Although in the classical theory damage is linked to the appearance of microvoids where no bulk material is present to bear imposed stresses, evidence obtained for various materials shows that in a thermomechanically coupled context, these voids should not completely lose their thermal capacity. A possible microstructural argument is that in fact the voids are not completely empty spaces, but rather regions of severely degraded material disconnected from neighboring regions. The mechanical effect is that of a void, but the remnants of material are still able to accumulate energy when their their temperature is altered.

The issue of damage in thermomechanically coupled problems has been explored, for example, in Canadija & Mosler (2013), where it is argued that a damaging function should not be applied to the heat accumulation terms of a variational formulation of metal fatigue.

This was not done in the models presented in this work. In keeping with a desired modular approach to damage, whereby the construction of the variational structure aims at a post-processing of damage from an undamaged problem in the space of equivalent strains, all the energy terms present in this undamaged equivalent state are equally affected by the same damaging function. Thus, damage acts the same way upon both thermal, mechanical and coupled terms. Such a choice is thus limited.

It should be noted, however, that not applying any damage effects to heat capacity seems to pose its own, though smaller, problems. The integrity of polymer chains remains the determining factor towards the soundness of the material response. Even if the ability of accumulating energy is not fully lost in a fully degraded polymer, it would seem to be altered. Shorter portions of broken polymer chains will respond differently to increasing temperature. Unbound by strong principal bonds, shorter chains would seem to be at more of a liberty to vibrate under increasing temperature, which would translate into lower heat capacities.

The actual situation seems to lie between the limiting cases of a fully undamaged and a fully damaged heat capacity term. This discussion falls outside the scope of the present work, but it should be kept in mind when applying the proposed models. Some short observations on different modeling choices are spread through the text, providing ideas for future works, should the issue become a limitation for given applications.

Still pertaining to the effects of damage over the material response to various kinds of loading, a final important limitation of the proposed models is due to the choice of a single damage mechanism. Based on the microstructural argument that the damage variable is a unified measure of the degradation of the bulk material, the use of a single damaging function to all portions of accumulated energy can prove to be too simplistic.

While the elastic response of polymers is linked to the resistance of polymer chains to stretching (and thus to the increase of the distance between atoms covalently bonded atoms), it was argued that inelastic (viscous) strains are more closely related to breaks in secondary bonds. As discussed above, thermal properties present their own evolution mechanisms when damage begins. With this in mind, the adoption of a single measure of damage seems ill advised.

Throughout the text, some modeling alternatives are presented, with different damage variables acting upon each part of the model. The evolution of each damage variable would then have its own driving mechanism.

Once more, the goal of devising a thermodynamically sound blueprint for incorporating damage to previously existing constitutive models was kept in mind. In choosing a single damage driving mechanism encompassing a variety of phenomena, it was possible to construct models keeping extensive modularity. Although some simplification is implied in combining degradation of diverse sources, the proposed framework this is done in constitutes an asset in extending the proposed course of action to other realms of application in the future.

Keeping in mind both the advantages and the possible drawbacks of thermo-viscoelastic damage models for the description of polymer behavior, it is now possible to move on to the central part of this text, where such models are developed within the framework of variational formulations.

3 REVIEW OF VARIATIONAL FORMULATION TO DISSIPATIVE PROBLEMS

Chapter overview: Variationally based constitutive models are available for a wide class of material models. Traditionally developed for conservative systems, where they were associated to well established variational principles such as that of minimum action (in Hamiltonian formulations) or of minimum potential energy, variational approaches have been extended to include dissipative problems. These models, based on incremental variational principles derived from rate formulations, are able to describe phenomena ranging from traditional plasticity and rate dependent problems all the way to various complex forms of coupled multiphysics problems. Following an introduction to some basic continuum mechanics concepts and notations, this chapter presents the foundations of variational constitutive modeling, particularly of the family of models originated by Ortiz & Stainier (1999). An overview of currently available models is offered, with larger emphasis on issues related to large strains, viscoelasticity (FANCELLO; PONTHOT; STAINIER, 2006), thermomechanical coupling (YANG; STAINIER; ORTIZ, 2006; STAINIER; ORTIZ, 2010) and damage (KINTZEL; MOSLER, 2011).

3.1 INTRODUCTION: CONSTITUTIVE MODELING AND VARIATIONAL APPROACHES

Variational models have long been a staple of physical modeling. They include, as the first notable examples, principles of least action, postulated since Maupertuis (early in the $XVIII^{th}$ century) and central to Lagrangian mechanics (late $XVIII^{th}$ century), evoking the tendency of natural processes to follow a path of least resistance. With the advent of calculus of variations, they received proper mathematical formulations in describing a variety of physical phenomena, ranging from classical mechanics, to optics and electromagnetism.

Within this context, the construction of Lagrangian functions, obtained from the subtraction of kinetic and potential energies involved for a given process, provides the necessary tools for the derivation of equilibrium equations. The underlying variational principle being the stationarity of the action during a natural process. The derivation of Euler-Lagrange equations remains, to this day, current practice in the field of calculus of variations and a powerful tool in the development of physical models of various sorts.

Later on, in the XIX^{th} century, associated to the principle of energy conservation, the development of Hamiltonian physics brought about tools for reformulations of classical problems within a new framework. Hamiltonian functions, the sum of kinetic and potential energies, are considered stationary for conservative processes. Hamiltonian formalism would become essential towards the development of quantum mechanics.

What these two classical branches of physical modeling have in common is an energy-based approach to the description of balance and equilibrium equations ruling a problem of interest. At their core lies postulation of an underlying variational principle of stationarity, which then leads to the recasting of the problem in an optimization light. Furthermore, both Lagrangian and Hamiltonian physics were initially restricted to conservative problems, precluding the treatment of dissipative phenomena, such as friction and viscosity, in the field of mechanics.

Continuum mechanics texts have made extensive use of such classical variational formulations in constitutive modeling, that is, in describing the material specific relations between variables of interest. Among others, two notable examples should be mentioned: principle of minimum potential energy and hyperelasticity. The principle of minimum potential energy of elastostatics states that the solution of a problem is the displacement field that minimizes the potential energy, given imposed conditions. Hyperelasticity models, and their application to rubber-like nonlinear elasticity, are founded upon the existence of a potential energy function, optimized with respect to independent variables to obtain stresses.

Both of these examples are strictly variational, in the sense that the energy-based functional is valid for all time. In other words, a single canonical function describes the response of the material for any point in time. This is only possible for time-independent processes and conservative processes, as the various forms of dissipation take place through time.

For that reason, the field of constitutive modeling developed separately of classical variational methods. Many materials of interest exhibit essentially dissipative behaviors, such as when permanent deformations appear, when stress response is shown to be dependent on the imposed strain rate or when heat flow is present.

Only if the definition of variational formulations is loosened is it possible to extend them to non-conservative problems. In that sense, the principle of maximum dissipation, central to the development of plasticity and other inelastic models, as an energy-based technique for the derivation of internal variable evolution equations, can be regarded as the main variational tool for dissipative applications.

A broader concept of variational formulations is behind the development of a family of constitutive models, starting from Ortiz & Stainier (1999), where the concept of incrementally variational models was first discussed. Starting from rate formulations, postulating the interconvertibility between all forms of energies, be them conserved or dissipated, it is possible to obtain time-discrete formulations that are variational within sufficiently small time steps. The present chapter explores the central concepts behind these variational formulations for dissipative problems (sometimes referred to as the family of variational constitutive updates) and the currently available models within this framework.

Before going into the subject, though, a brief review of central concepts of continuum mechanics is sketched. Requirements for the proposed constitutive models, kinematic relations, balance equations and thermodynamic principles are presented in classical form. The goal of all presented variational models shall be to obtain similar relations from energy-based functionals.

3.2 CONTINUUM MECHANICS AND THERMODYNAMICS: KINEMATIC RELATIONS, BALANCE EQUATIONS AND THERMODYNAMIC PRINCIPLES

The present subsection, far from being a self-contained text on the mechanics and thermodynamics of continua, aims merely at setting the notation for the remainder of the text while presenting the necessary relations to properly describe thermomechanically coupled material models, which constitute the core of the present works. High quality texts on continuum mechanics abound, including (MALVERN, 1969; HOLZAPFEL, 2000; BONET; WOOD, 2008; GURTIN; FRIED; ANAND, 2010; SOUZA NETO; PERIC; OWEN, 2011), works to which are referred those interested in deeper details and discussions. Meanwhile, the focus is set on enumerating the main ingredients to constitutive modeling of materials, namely: kinematics, balance equations and thermodynamics. Notations and nomenclature adopted approach those of Gurtin, Fried & Anand (2010), chosen as base text for the special attention devoted to thermodynamic issues.

As per custom, a body occupying a region of space is associated to two distinct configurations: the reference configuration and the current configuration. The reference configuration (denoted Ω from here on), arbitrarily chosen (though often related to an unloaded state), is assumed fixed in time. Every point of the material in the reference configuration is defined by a position vector $\mathbf{X}$, with respect to the chosen frame of reference. The current configuration (denoted Ω_t from here on), on the other hand, is the position occupied by the body of interest at a given time t. Every material point in the current configuration has a position vector $\mathbf{x}$, related to the equivalent point $\mathbf{X}$ in the reference configuration by the time dependent one-to-one mapping $\mathbf{x} = \chi(\mathbf{X}, t)$ (see figure 3.1). The velocity of a material point is then given by the material time derivative[3.1] of the displacement map ($\mathbf{v} = \dot{\chi}(\mathbf{X}, t) = \frac{\partial \chi(\mathbf{X},t)}{\partial t}$).

The volume of the material is commonly associated to the Jacobian, defined as $J(\mathbf{X}, t) = \det \nabla\chi(\mathbf{X}, t)$, and must be always greater than zero so that volumes do not vanish.

Equations can be described in terms of variables proper to the reference configuration (Lagrangian or material expressions) or in terms of variables proper to the current configuration (be it following a portion of material through time, in what can be called updated Lagrangian formulations; or rather focusing on a fixed position in space through which material can flow, in Eulerian or spatial expressions). In the present text, as for others where large strains are of interest, there is a general preference for Lagrangian expressions. The reasons behind this choice are discussed opportunely.

When dealing with the motion of a body, more than only the position of its points, it is necessary to map infinitesimal neighborhoods around them or vectors originating from them, in order to properly describe deformations. The deformation gradient is the second order tensor[3.2] that maps spatial vectors to corresponding material vectors, and is defined as:

$$\mathbf{F} = \nabla\chi(\mathbf{X}, t) = \frac{\partial \mathbf{x}}{\partial \mathbf{X}} \tag{3.1}$$

The deformation gradient can be decomposed into rotation ($\mathbf{R}$) and stretch tensors, respectively responsible for the change in direction

---

[3.1] For fixed material coordinates $\mathbf{X}$.

[3.2] Second order tensors are denoted by bold uppercase letters.

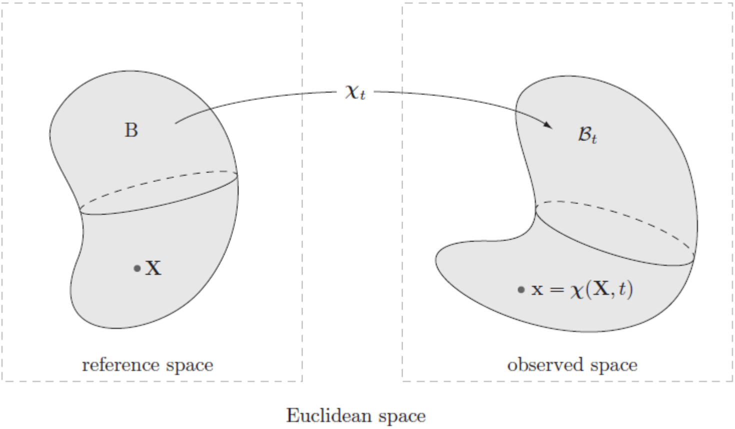

Figure 3.1 – Reference and current configurations of a body [Source: adapted from (GURTIN; FRIED; ANAND, 2010)].

and length of the mapped vector. Depending on the assumed order of the operations, left ($\mathbf{V} = \sqrt{\mathbf{F}\mathbf{F}^T}$, mapping spatial vectors to spatial vectors) and right ($\mathbf{U} = \sqrt{\mathbf{F}^T\mathbf{F}}$, mapping material vectors to spatial vectors) stretch tensors can appear in the classic polar decomposition of the deformation gradient:

$$\mathbf{F} = \mathbf{V}\mathbf{R} = \mathbf{R}\mathbf{U} \tag{3.2}$$

Some additional measures of deformation can be derived, namely the left ($\mathbf{B}$) and right ($\mathbf{C}$) Cauchy-Green tensors, and the Green-Lagrange tensor ($\mathbf{E}$) defined as:

$$\mathbf{C} = \mathbf{F}^T\mathbf{F} = \mathbf{U}^2 \qquad \mathbf{B} = \mathbf{F}\mathbf{F}^T = \mathbf{V}^2 \qquad \mathbf{E} = \frac{1}{2}\left[\mathbf{F}^T\mathbf{F} - \mathbf{1}\right] \tag{3.3}$$

All the above mentioned tensors can be decomposed spectrally in terms of principal directions and stretches of the right and left stretch tensors[3.3], something that will be useful later on in the treatment of large strains:

[3.3] Vectors are denoted by bold lowercase letters (with the exception of the previously defined material position vector $\mathbf{X}$), scalars by regular lowercase letters.

$$\begin{aligned} \mathbf{U} &= \sum_{i=1}^{3} \gamma_i \mathbf{m}_i \otimes \mathbf{m}_i & \mathbf{V} &= \sum_{i=1}^{3} \gamma_i \mathbf{l}_i \otimes \mathbf{l}_i \\ \mathbf{C} &= \sum_{i=1}^{3} \gamma_i^2 \mathbf{m}_i \otimes \mathbf{m}_i & \mathbf{B} &= \sum_{i=1}^{3} \gamma_i^2 \mathbf{l}_i \otimes \mathbf{l}_i \\ \mathbf{E} &= \sum_{i=1}^{3} \frac{1}{2} \left[\gamma_i^2 - 1\right] \mathbf{m}_i \otimes \mathbf{m}_i \end{aligned} \tag{3.4}$$

By defining logarithms of tensors as operations on the principal stretches, conserving the principal directions, it is possible to define the logarithmic strain tensor as:

$$\boldsymbol{\varepsilon} = \ln \mathbf{U} = \sum_{i=1}^{3} \ln \gamma_i \mathbf{m}_i \otimes \mathbf{m}_i \tag{3.5}$$

Another second order tensor of interest, carrying information on the evolution of the deformation gradient in time, is the gradient velocity **L**. As any other tensor, it can be additively decomposed in symmetric and skew-symmetric tensors, which bear information on the rates of stretching (**D**) and spin (**W**), respectively:

$$\begin{gathered} \mathbf{L} = \operatorname{grad} \mathbf{v} = \frac{\partial \mathbf{v}}{\partial \mathbf{x}} \qquad \mathbf{L} = \dot{\mathbf{F}}\mathbf{F}^{-1} \\ \mathbf{L} = \mathbf{D} + \mathbf{W} \qquad \mathbf{D} = \frac{1}{2}\left[\mathbf{L} + \mathbf{L}^T\right] \qquad \mathbf{W} = \frac{1}{2}\left[\mathbf{L} - \mathbf{L}^T\right] \end{gathered} \tag{3.6}$$

In addition to the kinematic relations listed up to this point, balance equations of different natures must be respected for the body of interest. Either expressed in integral form over the domain or in local form, valid for arbitrarily small volumes, balance equations represent the conservation of different physical quantities. Depending on the chosen volume, be it in material, spatial or control volumes (i.e., volumes fixed in space, through which matter can flow, not used for any of the formulations proposed in the present text), balance equations take on different forms.

As a first example, since mass cannot be created or vanish in a non-relativistic context, a balance of mass on a given volume must be respected. Following the volume occupied by the material through time, the amount of mass (commonly represented as the volume integral of the mass density $\rho(\mathbf{x}, t)$; in material notation, $\rho_0(\mathbf{X})$) must remain constant, as in equation 3.7a:

$$\int_{\Omega} \rho_0(\mathbf{X}) dv_0(\mathbf{X}) = \int_{\Omega_t} \rho(\mathbf{x},t) dv(\mathbf{x},t) \quad \dot{\overline{\int_{\Omega_t} \rho(\mathbf{x},t) dv(\mathbf{x},t)}} = 0 \tag{3.7a}$$

$$\int_{\Omega_t} \left[\dot{\rho} + \rho \mathrm{div}\mathbf{v}\right] dv = 0 \qquad \dot{\rho} + \rho \mathrm{div}\mathbf{v} = 0 \tag{3.7b}$$

Equation 3.7b (where the dependence on the spatial coordinates $\mathbf{x}$ and time is dropped for brevity) shows two time-dependent terms: the proper material time derivative of mass density ($\dot{\rho}$) and the mass flow due to the velocity ($\rho\mathrm{div}\mathbf{v}$). This comes naturally from the application of the Reynolds transport theorem to the mass density field. The second expression of equation 3.7b shows the local form of mass balance, valid for any arbitrary spatial volume, that convects with the body.

Another quantity that is conserved is linear momentum. When subjected to surface tractions (denoted $\mathbf{t}(\mathbf{n},\mathbf{x},t)$, where $\mathbf{n}(\mathbf{x},t)$ denotes the unit normal to the infinitesimal area $d\Gamma$ about point $\mathbf{x}$; representing forces applied to the surface of the body $\partial\Omega_t$) and body forces (denoted $\mathbf{b}_0(\mathbf{x},t)$; representing volume dependent forces, such as gravitational pull), the body's linear momentum (calculated by the integral $\int_{\Omega_t} \rho\mathbf{v}dv$) varies in order to maintain mechanical equilibrium, as in equation 3.8a.

An alternative form of the balance of linear momentum is usual, based on the first measure of stress. Cauchy stress ($\boldsymbol{\sigma}$), a spatial second order tensor, is related to surface tractions through $\mathbf{t}(\mathbf{n},\mathbf{x},t) = \boldsymbol{\sigma}(\mathbf{x},t)\mathbf{n}$, following Cauchy's theorem. This definition leads to equation 3.8b.

$$\int_{\partial\Omega_t} \mathbf{t}(\mathbf{n},\mathbf{x},t) d\Gamma + \int_{\Omega_t} \mathbf{b}_0(\mathbf{x},t) dv = \dot{\overline{\int_{\Omega_t} \rho\mathbf{v} dv}} \tag{3.8a}$$

$$\int_{\partial\Omega_t} \boldsymbol{\sigma}(\mathbf{x},t)\mathbf{n} d\Gamma + \int_{\Omega_t} \mathbf{b}_0(\mathbf{x},t) dv = \dot{\overline{\int_{\Omega_t} \rho\mathbf{v} dv}} \tag{3.8b}$$

It is possible to adopt a different definition of body forces, including inertial terms ($\mathbf{b} = \mathbf{b}_0 - \rho\dot{\mathbf{v}}$), which allows for a more economical notation of linear and angular momentum balances.

Angular momentum also has to be conserved. Obtained through the vector product of the linear momentum balance by a position vector ($\mathbf{r}$), angular momentum equations are provided below.

$$\int_{\partial\Omega_t} \mathbf{r} \times \mathbf{t}(\mathbf{n},\mathbf{x},t) d\Gamma + \int_{\Omega_t} \mathbf{r} \times \mathbf{b}(\mathbf{x},t) dv = 0 \tag{3.9a}$$

$$\int_{\partial\Omega_t} \mathbf{r} \times \boldsymbol{\sigma}(\mathbf{x},t)\mathbf{n}d\Gamma + \int_{\Omega_t} \mathbf{r} \times \mathbf{b}(\mathbf{x},t)dv = 0 \tag{3.9b}$$

A straightforward application of the divergence theorem to the balance of linear momentum allows for the substitution of the surface integral by a volume integral, yielding alternative expressions, in integral (equation 3.10a) and local (equation 3.10b, where the dependence on $\mathbf{x}$ and time were dropped for brevity) forms. It is possible to prove that, given the balances of linear and angular momentum, the Cauchy stress tensor is symmetric.

$$\int_{\Omega_t} \left[\mathrm{div}\boldsymbol{\sigma}(\mathbf{x},t) + \mathbf{b}(\mathbf{x},t)\right] dv = 0 \tag{3.10a}$$

$$\mathrm{div}\boldsymbol{\sigma} + \mathbf{b} = 0 \qquad \mathrm{div}\boldsymbol{\sigma} + \mathbf{b}_0 = \rho\dot{\mathbf{v}} \tag{3.10b}$$

In order to obtain an energy balance equation, since forces are power conjugate to velocities, it suffices to operate the dot product of the applied forces with the velocity field $\mathbf{v}$. Given the symmetry of the Cauchy stress tensor and applying the divergence theorem to the product $\boldsymbol{\sigma}(\mathbf{x},t)\mathbf{n}.\mathbf{v}$, the balance of mechanical power follows in equation 3.11[3.4].

$$\int_{\partial\Omega_t} \boldsymbol{\sigma}\mathbf{n}.\mathbf{v}d\Gamma + \int_{\Omega_t} \mathbf{b}_0.\mathbf{v}dv = \int_{\Omega_t} \boldsymbol{\sigma} : \mathbf{D}dv + \dot{\overline{\int_{\Omega_t} \frac{1}{2}\rho\mathbf{v}.\mathbf{v}}} \tag{3.11}$$

The terms on the left-hand side of the equality are commonly called the external power ($\mathcal{W}_{ext}(\Omega_t)$). The first term on the right-hand side ($\mathcal{W}_{int}(\Omega_t) = \int_{\Omega_t} \boldsymbol{\sigma} : \mathbf{D}dv$) is the internal stress power, while the last term is the rate of kinetic energy ($\dot{\mathcal{K}}(\Omega_t) = \dot{\overline{\int_{\Omega_t} \frac{1}{2}\rho\mathbf{v}.\mathbf{v}}}$). For quasi-static applications, inertial terms can be disregarded, and the power balance is calculated only between internal and external power sources.

Aside from Cauchy stresses, other measures of stress are frequently used. Notable among them are the First and Second Piola-Kirchhoff stress tensors, used for the expression of balance equations in reference form.

The First Piola-Kirchhoff stress tensor ($\mathbf{P}$) relates forces measured in the material configuration to tractions acting upon areas in the reference configuration. It can be obtained from the Cauchy stress as: $\mathbf{P} = J\boldsymbol{\sigma}\mathbf{F}^{-T}$, and is therefore not necessarily symmetric. It is possible

---

[3.4] Alternatively, by considering velocities as test functions in the lead up to equation 3.11, the classical principle of virtual power can be formulated.

to show the local form of the mechanical equilibrium equation 3.10b reads, in referential version (where $\mathbf{v}_R$ and $\mathbf{b}_{0R}$ are the velocity and body force fields in Lagrangian coordinates):

$$\mathrm{Div}\mathbf{P} + \mathbf{b}_{0R} = \rho_R \dot{\mathbf{v}}_R \tag{3.12}$$

The Second Piola-Kirchhoff stress tensor ($\mathbf{S}$), in turn, relates forces measured in the reference configuration to areas measured in the reference configuration. It transforms from the Cauchy stress as: $\mathbf{S} = \mathbf{F}^{-1}\mathbf{P} = \mathbf{F}^{-1}J\boldsymbol{\sigma}\mathbf{F}^{-T}$, keeping the symmetry property.

Each stress measure must paired with appropriate measures of strains in order to yield energy units in the balance of mechanical power (equation 3.11). The deduction is omitted here, but it can be shown that the following pairs are stress conjugate:

$$\int_{\Omega_t} \boldsymbol{\sigma} : \mathbf{D}dv = \int_{\Omega} \mathbf{P} : \dot{\mathbf{F}}dV = \int_{\Omega} \frac{1}{2}\mathbf{S} : \dot{\mathbf{C}}dV \tag{3.13}$$

Keeping within an energetic framework, the following balance principle that must be respected in all thermodynamic processes is the energy balance, expressed in the First Law of Thermodynamics. It expresses the interconvertibility between different forms of energy.

So far, only mechanical sources of energy have been explored: external power input, internal stress power and kinetic energy. In order to move on to the first law of thermodynamics in a thermomechanical setting, it is necessary to introduce other quantities of interest to fully define the thermodynamic state. While for the purely mechanical side of things, position (and derived quantities such as velocity, stretch and strain) and force were able to characterize the problem, when thermal effects are included two additional quantities arise: absolute temperature (T) and entropy (η).

In order to encompass all different forms of energy that can be stored in a volume of material (in a thermomechanical context, either through internal stresses or through heat capacity, as will be explored further along), the internal energy ($\mathcal{E}_R(\Omega) = \int_\Omega \rho_R \mathrm{e}_R(\mathbf{X}, \eta_R, t)dV$ in referential form, $\mathcal{E}(\Omega_t) = \int_{\Omega_t} \rho \mathrm{e}(\mathbf{x}, \eta, t)dv$ in current coordinates) is defined. The internal energy can be shown to serve as a potential for temperature, in the sense that: $T = \frac{\partial \mathrm{e}}{\partial \eta}$.

The thermal counterpart to the external power input is the heat flow, including all forms of thermal energy input, i.e. heat conduction through the surface and volumetric heat generation ($\mathcal{Q}_R(\Omega) = \int_{\partial\Omega} -\mathbf{q}_R.\mathbf{n}_R d\Gamma_R + \int_\Omega \mathrm{r}_R dV$ in referential form, $\mathcal{Q}(\Omega_t) = \int_{\partial\Omega_t} -\mathbf{q}.\mathbf{n}d\Gamma +$

$\int_{\Omega_t} \mathrm{r} dv$ in spatial form)

The conservation of energy, therefore, imposes that the rate of change in accumulated forms of energy (internal or kinetic) be equal to the input power rate (external forces or heat flow), as expressed in equation 3.14:

$$\overline{\mathcal{K}(\Omega_t) + \mathcal{E}(\Omega_t)}^{\cdot} = \mathcal{W}_{ext}(\Omega_t) + \mathcal{Q}(\Omega_t) \tag{3.14a}$$

$$\overline{\int_{\Omega_t} \frac{1}{2}\rho\mathbf{v}.\mathbf{v} + \int_{\Omega_t} \rho e dv}^{\cdot} = \int_{\partial\Omega_t} [\boldsymbol{\sigma}\mathbf{n}.\mathbf{v} - \mathbf{q}.\mathbf{n}]\, d\Gamma + \int_{\Omega_t} [\mathbf{b}_0.\mathbf{v} + \mathrm{r}]\, dv \tag{3.14b}$$

Using the definition of internal stress power and the divergence theorem on heat flux terms, it is possible to arrive at the following forms for the first law of thermodynamics in current (equation 3.15, in global and local forms) and referential coordinates (equation 3.16, in global and local forms).

$$\overline{\int_{\Omega_t} \rho e dv}^{\cdot} = \int_{\Omega_t} [\boldsymbol{\sigma} : \mathbf{D} - \mathrm{div}\mathbf{q} + \mathrm{r}]\, dv, \quad \forall dv \tag{3.15a}$$

$$\rho\dot{\mathrm{e}} = \boldsymbol{\sigma} : \mathbf{D} - \mathrm{div}\mathbf{q} + \mathrm{r} \tag{3.15b}$$

$$\overline{\int_{\Omega} \rho_R \mathrm{e}_R dV}^{\cdot} = \int_{\Omega} \left[\mathbf{P} : \dot{\mathbf{F}} - \mathrm{Div}\mathbf{q}_R + \mathrm{r}_R\right] dV, \quad \forall dV \tag{3.16a}$$

$$\rho_R\dot{\mathrm{e}}_R = \mathbf{P} : \dot{\mathbf{F}} - \mathrm{Div}\mathbf{q}_R + \mathrm{r}_R \tag{3.16b}$$

While the first law of thermodynamics states the possibility of interconversion between different forms of energies, it poses no restriction on the direction of such conversions. All that is guaranteed is that no energy is lost. However, natural processes do have a preferential direction. The introduction of entropy aims at measuring the so called "arrow of time" of thermodynamic processes.

Usually associated to the degree of disorder due to the local agitation of molecules (GURTIN; FRIED; ANAND, 2010), entropy can be either transported ($\mathcal{J}(\Omega_t)$) or locally generated. The underlying principle guiding all thermodynamic processes is that, for every material region, the net entropy production $\mathcal{S}(\Omega_t)$ must be equal or greater than zero. Denoting $\mathcal{I}(\Omega_t) = \int_{\Omega_t} \rho\eta dv$ as the net internal entropy (where η is the entropy density), the general expression of the Second Law of

Thermodynamics reads:

$$\mathcal{S}(\Omega_t) = \dot{\mathcal{I}}(\Omega_t) - \mathcal{J}(\Omega_t) \geq 0 \tag{3.17}$$

Other than a measure of disorder, entropy is equivalently a measure of irreversibility of thermodynamic processes. For instance, heat flows naturally from hotter to colder parts of the body. The process is irreversible, in the sense that, in order to pump heat from colder to hotter regions, it is necessary to provide power. Thus, it is possible to equate the direction of heat flux with the direction of entropy flux for natural processes, weighted by temperature (T). Local heat generation can also be associated to local entropy generation, yielding the classical Clausius-Duhem form of the second law of thermodynamics of equation 3.18:

$$\overline{\int_{\Omega_t} \rho \eta dv}^{\,\cdot} \geq -\int_{\partial\Omega_t} \frac{\mathbf{q}}{T} . \mathbf{n} d\Gamma + \int_{\Omega_t} \frac{\mathrm{r}}{T} dv \tag{3.18}$$

As it was done for the first law of thermodynamics, an application of the divergence theorem produces a local version of equation 3.18, as follows:

$$\rho\dot{\eta} + \operatorname{div}\left[\frac{\mathbf{q}}{T}\right] - \frac{\mathrm{r}}{T} \geq 0 \tag{3.19}$$

Simple manipulations for allow a mixture of the first (equations 3.15 and 3.16) and second laws of thermodynamics in local version, respectively for reference and current coordinates as follows in equations 3.20 and 3.21.

$$\rho\left[\dot{\mathrm{e}} - T\dot{\eta}\right] - \boldsymbol{\sigma} : \mathbf{D} + \frac{1}{T}\mathbf{q} . \operatorname{grad} T \leq 0 \tag{3.20}$$

$$\rho_R\left[\dot{\mathrm{e}}_R - T\dot{\eta}_R\right] - \mathbf{P} : \dot{\mathbf{F}} + \frac{1}{T}\mathbf{q}_R . \nabla T \leq 0 \tag{3.21}$$

Dealing with the internal energy may not be of practical interest, seeing as it counts entropy as one of its natural independent variables, a quantity that can be challenging to measure. A new measure of energy can be introduced through a Legendre-Fenchel transform of the internal energy, in order to handle temperature as an independent variable. The specific Helmholtz free energy (w in material coordinates, w_R in reference coordinates)[3.5] is therefore defined as:

[3.5] Different measures of free energy are often related to physical interpretations

$$w(\mathbf{x}, T, t) = \inf_{\eta} \left[\mathrm{e}(\mathbf{x}, \eta, t) - T\eta \right] \tag{3.22}$$

And equation 3.20, sometimes referred to as the free energy imbalance, becomes:

$$\rho \left[\dot{w} + \eta \dot{T} \right] - \boldsymbol{\sigma} : \mathbf{D} + \frac{1}{T}\mathbf{q} . \operatorname{grad} T \leq 0 \tag{3.23}$$

Since heat flux and temperature gradient always have opposing directions, the term $\mathbf{q} . \operatorname{grad} T$ will always be less than or equal to zero. Therefore, a reduced (though stronger) version of the second law of thermodynamics, often referred to as the Clausius-Planck inequality, reads as follows, where the concept of internal dissipation ($\mathcal{D}_{int}$) was introduced:

$$\mathcal{D}_{int} = \boldsymbol{\sigma} : \mathbf{D} - \rho \left[\dot{w} + \eta \dot{T} \right] \geq 0 \tag{3.24a}$$

$$\mathcal{D}_{intR} = \mathbf{P} : \dot{\mathbf{F}} - \rho_R \left[\dot{w}_R + \eta_R \dot{T} \right] \geq 0 \tag{3.24b}$$

It is possible to introduce the definition of internal dissipation into the local forms of the first law (3.15 and 3.16, in current and reference coordinates respectively), in what is commonly referred to as the entropy form of the first law of thermodynamics and constitutes an expression for the evolution of entropy:

$$T\dot{\eta} = -\mathrm{div}\mathbf{q} + \mathcal{D}_{int} + \mathrm{r} \tag{3.25a}$$

$$T\dot{\eta_R} = -\mathrm{Div}\mathbf{q}_R + \mathcal{D}_{intR} + \mathrm{r}_R \tag{3.25b}$$

So far, only balance equations and thermodynamic principles have been presented. For every thermodynamic process, these relations must be respected. However, they bring no information on the relations between variables (for instance, how the Cauchy stress tensor relates to the displacement field, or how entropy evolves with changes in temperature). That is the role of constitutive equations.

---

of the type of available energy they represent. Obtained through Legendre-Fenchel transforms of the internal energy (which represents the sum of all types of microscopic energies that can be volumetrically stored), every new measure of energy has its own set of natural independent variables. In this context, enthalpy, for instance, corresponds to available energy for processes at constant pressures; its natural independent variables are pressure, entropy and time. The Helmholtz free energy, on the other hand, constitutes the available energy in isothermal processes, and is therefore often used in purely mechanical applications.

3.3 CONSTITUTIVE MODELING: COLEMAN-NOLL PROCEDURE AND INTERNAL VARIABLES

While the previously presented equations remain valid for all materials, constitutive equations characterize specific material behaviors. The goal is to build consistent equations relating different physical quantities as follows (for brevity, only reference configuration versions are presented and time dependence is omitted; the Helmholtz free energy is defined from its specific counterpart as $W_R = \rho_R w_R$):

$$W_R = W_R(\mathbf{X}, T) \tag{3.26a}$$

$$\eta_R = \eta_R(\mathbf{X}, T) \tag{3.26b}$$

$$\mathbf{P} = \mathbf{P}(\mathbf{X}, T) \tag{3.26c}$$

In order for such equations to bear significant meaning, two central requirements have to be met: thermodynamic consistency and frame-indifference (in other words, an independence with respect to changes to the observation frame[3.6]). Therefore, instead of using the position $\mathbf{X}$, a frame dependent measure, the right Cauchy-Green strain tensor ($\mathbf{C}$, defined in equation 3.3) is often preferred. Its power conjugate measure of stress, the second Piola-Kirchhoff tensor, is then adopted for consistency.

In addition, the description of internal processes of dissipation, representing various features such as viscosity, plasticity, damage, or others, needs the inclusion of more internal variables. The variables that carry this sort of information can be of different natures, be it scalar, vectorial or tensorial (they are generally denoted $\mathbf{Z}$ in the following), according to the corresponding physical phenomenon.

The set of constitutive equations then has the following form:

$$W_R = W_R(\mathbf{C}, \mathbf{Z}, T) \tag{3.27a}$$

$$\eta_R = \eta_R(\mathbf{C}, \mathbf{Z}, T) \tag{3.27b}$$

$$\mathbf{S} = \mathbf{S}(\mathbf{C}, \mathbf{Z}, T) \tag{3.27c}$$

Starting from equation 3.23, and the set of independent variables

---

[3.6] The internal energy (and entropy, as scalar fields) should be the same when measured by different inertial observers. Since the first Piola-Kirchhoff stress tensor is shown not to be frame invariant, it is sometimes preferable to deal with the second Piola-Kirchhoff stress tensor ($\mathbf{S}$), the power conjugate to the rate of the right Cauchy-Green stress tensor.

$\mathbf{C}, \mathbf{Z}, T$, it is possible to arrive at a common form for a dissipation inequality:

$$\left[\frac{\partial W}{\partial \mathbf{C}} : \dot{\mathbf{C}} + \frac{\partial W}{\partial T} : \dot{T} + \frac{\partial W}{\partial \mathbf{Z}} : \dot{\mathbf{Z}} + \rho_R \eta_R \dot{T}\right] - \frac{1}{2}\mathbf{S} : \dot{\mathbf{C}} + \frac{1}{T}\mathbf{q}_R . \nabla T \leq 0 \tag{3.28}$$

The above equation 3.28 must be valid for all admissible thermodynamic processes. A key step in proposing new constitutive models, the so called Coleman-Noll procedure consists in testing the dissipation inequality for any such virtual processes. Equations relating different physical quantities, the objective behind constitutive modeling, come as a result.

By admitting a process where $\dot{\mathbf{C}} \neq 0$, while $\dot{T}, \dot{\mathbf{Z}} = 0$, the following constitutive relation for (conservative) stresses is evidenced:

$$\mathbf{S}(\mathbf{C}, \mathbf{Z}, T) = 2\frac{\partial W}{\partial \mathbf{C}} \tag{3.29}$$

Equivalently, for a process where $\dot{T} \neq 0$, while $\dot{\mathbf{C}}, \dot{\mathbf{Z}} = 0$, it is clear that the Helmholtz free energy serves as a potential for entropy, with respect to temperatures:

$$\rho_R \eta_R(\mathbf{C}, \mathbf{Z}, T) = -\frac{\partial W}{\partial T} \tag{3.30}$$

Substituting these results back into equation 3.28, all that remains is a reduced dissipation inequality:

$$\left[\frac{\partial W}{\partial \mathbf{Z}} : \dot{\mathbf{Z}}\right] + \frac{1}{T}\mathbf{q}_R . \nabla T \leq 0 \tag{3.31}$$

As stress and strain, or temperature and entropy, internal variables are energy-conjugate to thermodynamic forces conveniently defined as: $\mathbf{Y} = -\frac{\partial W}{\partial \mathbf{Z}}$. Then, by comparing to equation 3.23 it is clear that internal dissipation corresponds to:

$$\mathcal{D}_{intR} = \rho_R \mathbf{Y} : \dot{\mathbf{Z}} \geq 0 \tag{3.32}$$

In other words, guaranteeing non-negative internal dissipation, defined with respect to internal variables and conjugate thermodynamic forces as in the above equation 3.32, is equivalent to respecting the second law of thermodynamics. In other words, the development of thermodynamically consistent material models hinges on the definition of the evolution equations of internal variables and the constitutive equation for their conjugated thermodynamic forces.

The variational approach to constitutive modeling of dissipative processes is essentially a tool towards this goal, as will be discussed in the following subsection. It should be made clear, though, that the Coleman-Noll procedure is general, and helps to determine restrictions upon the proposed constitutive equations whatever the chosen method of formulating constitutive equations may be.

Before moving along to the next subsection, though, a brief look upon issues related to purely thermal and thermomechanically coupled problems is necessary.

Heat capacity is a useful process in describing thermomechanical processes. Reflecting a material's ability of accumulating energy through increase of temperature, heat capacity is defined as: $\mathcal{C} = \frac{\partial \mathrm{e}}{\partial T}|_{fixed\mathbf{C}}$. Alternatively, heat capacity can be expressed in terms of Helmholtz free energy (using equation 3.22).

$$\mathcal{C}(\mathbf{C},\mathbf{Z},T) = T\frac{\partial \eta_R}{\partial T} = -T\frac{\partial^2 W}{\partial T^2} \tag{3.33}$$

Strictly positive heat capacities are imposed, for all temperatures. By the above equation 3.33, this is equivalent to stating that entropy must be monotonically increasing with temperature and that the Helmholtz free energy must be strictly concave with respect to temperature.

For coupled thermomechanical processes, the coupling term is determined by the derivative of stresses with respect to temperature (or the cross derivative of the Helmholtz free energy with respect to strains and temperatures, for a more energy-based point of view). From equation 3.29 and using equation 3.33, it becomes clear that constitutive equations for stress and heat capacity cannot be defined independently.

$$\begin{aligned}
\frac{\partial \mathbf{S}}{\partial T} &= 2\frac{\partial}{\partial T}\left(\frac{\partial W}{\partial \mathbf{C}}\right) = 2\frac{\partial}{\partial \mathbf{C}}\left(\frac{\partial W}{\partial T}\right) = -2\frac{\partial \eta_R}{\partial \mathbf{C}} \\
\frac{\partial^2 \mathbf{S}}{\partial T^2} &= -2\frac{\partial}{\partial T}\left(\frac{\partial \eta_R}{\partial \mathbf{C}}\right) = -2\frac{\partial}{\partial \mathbf{C}}\left(\frac{\partial \eta_R}{\partial T}\right) = -\frac{2}{T}\frac{\partial \mathcal{C}}{\partial \mathbf{C}}
\end{aligned} \tag{3.34}$$

3.4 VARIATIONAL APPROACHES TO MECHANICAL DISSIPATIVE PROBLEMS: FUNDAMENTALS OF INCREMENTAL CONSTITUTIVE UPDATES APPLIED TO VISCOPLASTICITY, VISCOELASTICITY AND DAMAGE

The use of internal variables to describe internal processes, as described in the previous section, has been standard practice in the field of constitutive modeling for decades. The need of variables to store information related to dissipative processes clearly became a necessity as soon as the move from elastic materials to inleastic materials was made.

Devising a set of internal variables is not a task to be done freely, though. In the interest of developing thermodynamically consistent material models, internal variables and their associated thermodynamic forces are required to obey equation 3.32.

Early work by Halphen & Nguyen (1975) helped define a class of materials for which this central constraint would always be respected. Generalized standard materials (GSM) were defined as those whose thermodynamic forces ($\mathbf{Y}$) associated to internal variables ($\mathbf{Z}$) could be derived from a dissipative pseudo-potential (denoted $\psi(\dot{\mathbf{Z}})$), holding the property of convexity with respect to the rate of internal variables. In doing so, the product $\mathbf{Y} : \dot{\mathbf{Z}}$ is guaranteed to be positive, ensuring positive dissipation and thermodynamic consistency. The concept has since been applied to model a variety of material behaviors, in various modeling frameworks.

Taking tools from the early works on standard dissipative solids (a subclass of generalized standard materials where maximum dissipation is guaranteed, and the flow rule for internal variables is associative), in order to ensure the respect of the second law of thermodynamics, Ortiz & Stainier (1999) proposed taking a variational approach to the modeling of dissipative behavior. Viscoplasticity was the focus of their first modeling efforts.

While classical variational approaches to constitutive modeling were restricted to conservative problems (such as in elasticity and hyperelasticity, as previously discussed), since potentials, in a strict sense, uniquely describe a conservative problem, for all time and loading, the novel approach[3.7] was able to deal with dissipative problems through

---

[3.7] It should be noted that energy-based approaches to dissipative problems have long been available. The principle of maximum dissipation clearly has a variational character, and has been used from the early models of plasticity and other inelastic behaviors in determining the evolution of internal variables. In this context, accordincremental variational principles. In other words, by assuming that dissipative problems could be accurately described by a more loosely defined potential (incrementally built and taking into account the dissipation behavior of interest), the toolbox of variational modeling could be extended to a much broader family of problems.

Dissipative problems, even in more standard approaches that do not make use of variational structures, are frequently solved incrementally. Dissipation occurs through time, and material behavior can be history dependent. Thus, the determination of intermediate states between sufficiently small time steps is necessary.

The same is true in the variational approach to dissipative problems. Solutions are calculated incrementally, in sufficiently small time steps, so that all eventual time-discrete approximations of evolution equations keep within an error tolerance. What is different is assuming the problem to be variational within a time step, that is, assuming the problem to be ruled by an *incremental variational principle*, including both conservative and dissipative variations of energy. Determining incremental solutions can then be done using optimization tools. Furthermore, by imposing some mathematical properties on the potentials, mathematical features such as the existence of solutions or symmetry of material tensors (absent from non-variational approaches to thermomechanics, for example) can be guaranteed.

Variational formulations for dissipative problems typically start from energy-based equations in rate form (equation 3.35, for purely mechanical problems), stating the interconversion between different types of accumulated and dissipated energies. Classical potentials (Helmholtz free energy W, for one possibility) are used to describe conservative parts of energy, stored elastically, through heat capacity, or otherwise. Dissipation pseudo-potentials (ψ, with units of power, depending on the rates of independent variables and possibly of their history), convex with respect to the rates of internal variables as in the framework of standard dissipative solids, are used to describe internal processes. Both conservative and dissipative contributions are gathered in a single functional, dependent on the rates of independent variables, together with the external power input representing the corresponding boundary value problem($\mathcal{W}_{ext}(\Omega) = \int_{\partial_\sigma \Omega} \bar{\mathbf{t}}_R . \mathbf{v}_R d\Gamma + \int_\Omega \mathbf{b}_R . \mathbf{v}_R dV$, as previously

---

ing to Mosler & Bruhns (2009), the central contribution in Ortiz & Stainier (1999) is in the discretization of the variational principle, whose stationarity conditions yield all the necessary equations (both internal variable evolution, as in maximum dissipation, and equilibrium relations). This feature is the reason behind the sometimes used name of variational constitutive updates, to the family of models derived from Ortiz & Stainier (1999).

defined in equation 3.11). This functional is assumed to be stationary, in the spirit of energy conservation. Internal dependence on the referentially measured velocities are implicit in $\dot{\mathbf{C}}$.

$$\mathcal{H}(\mathbf{v}_R, \dot{\mathbf{Z}}) = \int_{\Omega} \left[\dot{W}(\mathbf{C}, \mathbf{Z}) + \psi(\dot{\mathbf{C}}, \dot{Z}; \mathbf{C}, \mathbf{Z}) \right] dV - \mathcal{W}_{ext}(\Omega) \qquad (3.35)$$

The assumed stationarity of the global functional translates to its Gâteaux derivatives with respect to independent variables. In variational fashion, then, through the stationarity with respect to strains and internal variables, the equations for mechanical equilibrium and evolution of internal variables are respectively recovered in equations 3.36[3.8]. The definitions of the right Cauchy-Green strain tensor and the property of the Helmholtz free energy of serving as a potential for the second Piola-Kirchhoff stress tensor are assumed known *a priori*.

$$\begin{aligned} D_{\mathbf{v}}[\mathcal{H}](\delta \mathbf{v}) = & \int_{\Omega} \left[\frac{\partial W}{\partial \mathbf{C}} + \frac{\partial \psi}{\partial \dot{C}} \right] : \nabla \delta \mathbf{v} dV \\ & - \int_{\partial_{\sigma}\Omega} \bar{\mathbf{t}}_R . \delta \mathbf{v} d\Gamma - \int_{\Omega} \mathbf{b}_R . \delta \mathbf{v} dV = 0, \quad \forall adm \delta \mathbf{v} \qquad (3.36a) \end{aligned}$$

$$D_{\dot{\mathbf{Z}}}[\mathcal{H}](\delta \dot{\mathbf{Z}}) = \int_{\Omega} \left[\frac{\partial W}{\partial \mathbf{Z}} + \frac{\partial \psi}{\partial \dot{\mathbf{Z}}} \right] : \delta \dot{\mathbf{v}} dV = 0, \quad \forall adm \delta \dot{\mathbf{Z}} \qquad (3.36b)$$

It is interesting to observe the possible appearance of a stress-like term depending on the dissipation pseudo-potential ($\frac{\partial \psi}{\partial \dot{C}}$). While the Helmholtz free energy carries information on the conservative part of stress, stored elastically in the bulk of the material, the dissipation pseudo-potential is responsible for carrying information on non-conservative stresses. These sort of stresses, appearing due to the imposed strain rate, have a viscous character. They are often called dissipative stresses, and are important in modeling the stress-strain behavior of polymers and other strain rate dependent materials.

In contrast to other standard approaches to constitutive modeling of dissipative materials, in Ortiz & Stainier (1999) and papers deriving from it, the choice is not to apply time discretization to internal variable evolution equations, but rather, to the full variational

---

[3.8] The choice of velocity as an independent field was done in order for the final equations to match the definition of external power input. It is possible to choose $\dot{\mathbf{C}}$ as the independent variable, but it requires rewriting the external power output. The resulting equations remain equivalent to mechanical equilibrium.

principle, expressed in rates in the general form of equation 3.35. This yields incremental variational equations of the following form, representing the full boundary value problem (where boundary and body forces are taken at the end of the time step - their indexes $n+1$ are dropped, for simplicity of notation):

$$\begin{aligned}
&\mathcal{H}_n(\mathbf{x}_{n+1}, \mathbf{Z}_{n+1}; \mathbf{x}_n, \mathbf{Z}_n) = \\
&\int_\Omega \left[W(\mathbf{C}_{n+1}, \mathbf{Z}_{n+1}) - W(\mathbf{C}_n, \mathbf{Z}_n) + \Delta t \psi \left(\frac{\Delta \mathbf{C}}{\Delta t}, \frac{\Delta \mathbf{Z}}{\Delta t}; \mathbf{C}_{n+\alpha}, \mathbf{Z}_{n+\alpha} \right) \right] dV \\
&\qquad - \int_{\partial_\sigma \Omega} \bar{\mathbf{t}}_R . [\mathbf{x}_{n+1} - \mathbf{x}_n] d\Gamma - \int_\Omega \mathbf{b}_R . [\mathbf{x}_{n+1} - \mathbf{x}_n] dV \qquad (3.37)
\end{aligned}$$

At every time step, from a known initial state (at time t_n) and by imposing some form of load (through force or strain increments, for instance), the goal is to find the values of the remaining physical quantities at the end of the time step (at time t_{n+1}). Velocities are approximated by a simple difference scheme ($\mathbf{v}_{n+1} = (\mathbf{x}_{n+1} - \mathbf{x}_n)/\Delta t$), allowing the displacement field to be used as independent variable.

The Helmholtz free energy is a state function, meaning that its rate is exactly the difference between its values at t_n (assumed known) and t_{n+1} divided by the time step Δt. Meanwhile, dissipation is an instantaneous rate of energy. Its time discretization hinges on the choice of an appropriate intermediate value[3.9], evaluated at some point $t_{n+\alpha}$ (for a fully implicit scheme, clearly, $\alpha = 1$; for a fully explicit scheme, $\alpha = 0$). The size of the time step determines the amount of error being introduced through this assumption. As time steps become smaller, consistency is guaranteed, as the underlying rate form is recovered.

Once again, stationarity with respect to independent variables $(\mathbf{x}_{n+1}, \mathbf{Z}_{n+1})$ yields the necessary equations to determine the desired values of stresses and internal variables at the end of the increment, in so called variational constitutive updates. It is important to remember that, although the second law of thermodynamics does not come out explicitly from the incremental potential $\mathcal{H}_n$, the use of convex pseudo-potentials with respect to the rate of internal variables guarantees positive internal dissipation.

[3.9] In order to distinguish from the dissipation pseudo-potential in rates, it is usual to adopt the notation $\overline{\psi}$ in the incremental context. This has not been done throughout this text so as not to further burden the notations. Both the description of the independent variables and the context will make clear when rate or incremental forms are implied.

While mechanical equilibrium takes into account forces acting upon the boundary of the body, and is therefore of a global character, the optimization with respect to internal variables are essentially local. As will be explored in the following chapters, this can lead to a separation of problems, the global optimization being done upon an effective potential, for which the internal variables have already been determined.

These concepts, initially presented for viscoplastic problems in Ortiz & Stainier (1999), were general enough to encompass a variety of dissipative material behaviors, some of which are briefly reviewed below, with an emphasis on their new contributions. For every problem of interest, adequate choices of internal variables and corresponding dissipation pseudo-potentials are needed to properly account for different physics. Additionally, different forms of stored energy can appear in different contexts. In this context, it is common to assume the hypothesis of additive decomposition of the Helmholtz free energy.

In Fancello, Vassoler & Stainier (2008), a variety of plasticity models was included in the variational framework. Spectral quantities of plastic strains were chosen as internal variables. Isotropic potentials, depending only on the principal values of plastic strains, were used to model linear, exponential and logarithmic modes of hardening, in various combinations. The Helmholtz free energy potential included plastically stored energy by means of hardening. The optimization with respect to internal variables was shown to resemble classic predictor-corrector schemes of plasticity: an initial elastic predictor was used to determine the sign of the derivative with respect to the plastic increment, and to decide if plastic minimization was necessary.

Later on, making use of a different parameterization of plastic dissipation, non-associative plasticity (MOSLER; BRUHNS, 2009) and kinematic hardening (MOSLER, 2010) were variationally modeled by Mosler and co-workers. It is important to note that, according to Mosler (2010), non-associative plasticity does not fit the traditional framework of standard dissipative solids which derive from the principle of maximum dissipation for associative materials (where the direction of flow is normal to the yield surface). It is shown that a reparameterization of dissipation with respect to stresses, instead of only the rate of internal variables, gives more flexibility in determining flow directions independently from yield surfaces, and allows for modeling of Armstrong-Frederick plasticity, for example. The same type of reparameterization of dissipation, together with a split of plastic strains in volumetric and isochoric parts, has been used in Mosler & Bruhns

(2009) to account for other non-associative plasticity models with pressure dependence, such as Mohr-Coulomb and Drucker-Prager.

In Fancello, Ponthot & Stainier (2006) and Fancello, Ponthot & Stainier (2008), the framework of variational modeling of dissipative materials was extended to large strain viscoelasticity, a class of models essential for the description of polymer-like behavior. As in Fancello, Vassoler & Stainier (2008) for plasticity, isotropic potentials depending on eigenvalues of inelastic strains (more specifically, viscous strains) were chosen, something that constitutes an efficient tool in dealing with large strain phenomena. The optimization with respect to principal directions of viscous strains was shown to be analytically solvable, and equivalent to having colinearity between elastic and viscous strain tensors. More details on the full development of the large strains viscoelastic treatment can be found in the following chapter, as a way of coupling a very similar model to thermal effects is explored in detail.

Damage phenomena, essentially dissipative, were also modeled with variational constitutive updates in Kintzel & Mosler (2011). Used as a tool to represent low cycle phenomena in metals, two different types of damage models were framed variationally. The brittle damage model, more closely related to classical models of elastic damage, was based on an evolution of damage variables dependent exclusively on elastic strains. The ductile damage model, on the other hand, bearing similarities to Lemaître-type plastic damage models (LEMAÎTRE, 1996), had the evolution of damage variables coupled to that of the plastic increment at every time step. In addition, the proposed formulation lent itself to an uncoupled update of plastic and damage variables, in other words, plasticity could be solved in an equivalent stress state. That constitutes the inspiration behind the proposed approach in chapter 4, for the thermomechanically coupled viscoelastic damage model. More details on the full formulation are discussed there.

Other classes of problems, such as single crystal plasticity (ORTIZ; REPETTO, 1999; STAINIER; CUITIÑO; ORTIZ, 2002), composite materials (BRASSART et al., 2012) and plasticity of metallic foams (WEINBERG; MOTA; ORTIZ, 2006; VASSOLER, 2009), among others, have been modeled with variational methods. These classes of models are less applicable to the constitutive modeling of polymer-like behavior, and are therefore merely mentioned here, without futher details.

More than just another tool in developing constitutive models, though, variational constitutive updates are used for their mathematical properties. The structure of variational formulations can be explored to prove consistency of proposed material models, convergence with respect to known analytic solutions and proofs of existence of solutions, that help validate the framework (see, for example, Brassart & Stainier (2012)). It can also serve as a tool toward the easy evaluation of derivatives in sensitivity analysis, used for the identification of material parameters (FANCELLO et al., 2008), among others. Error estimation efforts are also aided by the mathematical properties of variational formulations, as in Radovitzky & Ortiz (1999), for example. Multiscale approaches, where scale transitions are ruled by energy minimization rules, can also make use of the variational framework, as in Miehe (2002) and Bleier & Mosler (2013). Other works make use of the variational structure in mesh refinement strategies, where energy concentration in a single element in comparison to its neighbors serves as a criterion for mesh refinement, as in Mosler & Ortiz (2007) and Mosler & Ortiz (2009), where the element bisection technique of Rivara (1997) is applied.

3.5 VARIATIONAL APPROACH TO THERMOMECHANICAL DISSIPATIVE PROBLEMS: MULTIPHYSICS COUPLING AND SYMMETRY OF MATERIAL TENSORS

Thermomechanical problems bring about a new series of challenges. Although the basic framework of variational formulations remains the same, a straightforward extension of previous concepts may lead to the loss of symmetry of material operators and other convenient mathematical properties that constitute the main advantages of variational methods. Dealing with thermomechanical problems in a variationally consistent manner is the central objective of Yang, Stainier & Ortiz (2006).

An extensive review of the variational approach to various thermomechanically coupled problems was recently done by Stainier (2013). The interested reader is referred to this review chapter in order to find more extensive details, as the focus of the present subsection is restricted to exploring the parameterization of dissipation introduced in Yang, Stainier & Ortiz (2006) that constitutes the core of the of the models proposed in chapters 3 and 4 of the present document, and is responsible for the symmetric structure of the resulting formulation. As in the former subsection, a few brief paragraphs with the main contributions of different articles closes this subsection.

The first step in developing the variational formulation to thermomechanical problems is defining an appropriate set of independent variables. As previously discussed, referential notations are preferred, in order to circumvent issues of material frame indifference, while encompassing the most general case of finite strains. Additionally, absolute temperatures T (rather than entropy η_R, which is more difficult to measure directly) are chosen as basic thermal quantities. This leads to the use of the Helmholtz free energy W instead of the internal energy e_R. In order to keep the formulation as general as possible, a general set of internal variables ($\mathbf{Z}$) is used.

Recalling previous definitions, in a general thermomechanical problem, external power input encompasses mechanical and thermal portions. The mechanical external power input reads: $\mathcal{W}_{ext}(\Omega) = \int_{\partial_{\sigma}\Omega} \bar{\mathbf{t}}_R.\mathbf{v}d\Gamma + \int_{\Omega} \mathbf{b}_R.\mathbf{v}dV$. Thermal power input then reads, in referential form: $\mathcal{Q}(\Omega) = -\int_{\partial_{\mathbf{q}}\Omega} \bar{\mathbf{q}}_R.\mathbf{n}_R d\Gamma + \int_{\Omega} \mathrm{r}_R dV$[3.10].

Since heat conduction only happens naturally from hot to cold regions, heat flow within a material domain inserts an additional source of dissipation, represented in pseudo-potential $\varphi\left(\frac{\nabla T}{T}; \mathbf{C}, \mathbf{Z}, \theta\right)$. The most common form for this source of dissipation is the classical Fourier law of conduction, presented in the equation below.

$$\mathbf{q}_R = -\kappa \nabla T \tag{3.38}$$

It involves, in fact, assuming a constitutive relation between the heat flux vector and the temperature gradient. This can be represented through a conduction potential depending on related variable $\mathbf{G} = -\frac{\nabla T}{T}$, as follows:

$$\varphi\left(\mathbf{G}; \mathbf{C}, \mathbf{Z}, \theta\right) = \frac{1}{2}\kappa \mathbf{G}.\mathbf{G} \tag{3.39a}$$

$$\frac{\partial \varphi}{\partial \mathbf{G}} = \frac{\mathbf{q}_R}{T} = -\kappa \frac{\nabla T}{T} \tag{3.39b}$$

A general notation is kept through the end of this chapter. Clearly, in order to ensure positive dissipation due to conduction, dissipation pseudo-potential φ must be convex and non-negative, following the pioneering work of Biot (1958).

The underlying variational principle is once again derived from

---

[3.10] As will be explored in a few paragraphs, a temperature factor will be employed to all dissipative behaviors. This will include the irreversibility of heat flux and bulk heat generation. The external thermal power input will then be noted $\mathcal{Q}\left(\Omega, \frac{T}{\theta}\right)$

a rate form potential, stating the interconvertibility between different forms of energy. The counterpart to equation 3.35, representing the thermomechanical boundary value problem reads as follows:

$$\begin{aligned}\mathcal{H}(\mathbf{v}_R, \dot{\mathbf{Z}}, \dot{T}) = \int_\Omega \Big\{ & \dot{W}(\mathbf{C}, \mathbf{Z}, T) + \rho_R \eta_R \dot{T} \\ & + \psi\left(\frac{T}{\theta}\dot{\mathbf{C}}, \frac{T}{\theta}\dot{Z}; \mathbf{C}, \mathbf{Z}, \theta\right) + \varphi\left(\frac{\nabla T}{T}; \mathbf{C}, \mathbf{Z}, \theta\right)\Big\} dV \\ & - \mathcal{W}_{ext}(\Omega) - \mathcal{Q}\left(\Omega, \frac{T}{\theta}\right) \end{aligned} \quad (3.40)$$

Some comments should be made about the above equation 3.40. First of all, as for all variational formulations of dissipative problems, the functional is built, and should not be associated to specific meaning on its own. There is clearly an energy-like character behind it, but the minutiae behind the chosen variables becomes justified when it comes to the optimization with respect to independent variables.

Two different measures of temperature appear in equation 3.40: the external temperature T, an observable quantity; and the internal temperature θ, sometimes called the equilibrium temperature, which is a thermodynamic property associated to local thermal equilibrium[3.11]. If local thermal equilibrium is assumed *a priori*, in other words, if the point is assumed to be in thermal equilibrium internally (so that there is no lag between external temperature and entropy), the external and internal temperatures coincide and the factor $\frac{T}{\theta}$ tends to 1. This need not be the case, though, and both variables are kept. The ratio between external and internal temperatures is then used to parameterize all dissipative behaviors, as evidenced by the dependencies of the dissipation pseudo potential: $\psi\left(\frac{T}{\theta}\dot{\mathbf{C}}, \frac{T}{\theta}\dot{Z}; \mathbf{C}, \mathbf{Z}, \theta\right)$.

The use of this factorization is the crucial step in obtaining a symmetric material tensor for the thermomechanical problem. The choice of the term $\frac{T}{\theta}$ is explored in detail in Yang, Stainier & Ortiz (2006). It constitutes, in fact, a sort of integrating factor that both keeps consistency (when local thermal equilibrium is respected) and makes the dissipation pseudo-potential keep its potential-like charac-

---

[3.11] The internal temperature is in fact the thermodynamic property conjugated to entropy by means of the internal energy. That is, the internal energy serves as a potential for the internal temperature as: $\theta(\mathbf{C}, \mathbf{Z}, \eta_R) = \dfrac{\partial e_R}{\partial \eta_R}$

ter. The importance of this factor will become evident when the optimization with respect to independent variables is carried out.

Before doing so, though, a possible time discretization of the rate form is proposed. By identifying the external temperature to the unknown temperature T_{n+1} at the end of the time step, and the internal temperature θ to the temperature T_n at the beginning of the time step (thus introducing a sort of time lag between the quantities, equivalent to a slight error when it comes to local thermal equilibrium), the incremental potential for the thermomechanical boundary value problem then becomes:

$$\begin{aligned}
&\mathcal{H}_n(\mathbf{x}_{n+1}, \mathbf{Z}_{n+1}, T_{n+1}; \mathbf{x}_n, \mathbf{Z}_n, T_n) = \\
&\int_\Omega \{[W(\mathbf{C}_{n+1}, \mathbf{Z}_{n+1}, T_{n+1}) - W(\mathbf{C}_n, \mathbf{Z}_n, T_n) + \rho_R \eta_n [T_{n+1} - T_n]] \\
&\qquad + \Delta t \left\langle \psi \left(\frac{T_{n+1}}{T_n} \frac{\Delta \mathbf{C}}{\Delta t}, \frac{T_{n+1}}{T_n} \frac{\Delta \mathbf{Z}}{\Delta t}; \mathbf{C}_{n+\alpha}, \mathbf{Z}_{n+\alpha}, T_{n+\alpha} \right) \right\rangle \\
&\qquad + \Delta t \left\langle \varphi \left(\frac{\nabla T_{n+1}}{T_{n+1}}; \mathbf{C}_{n+\alpha}, \mathbf{Z}_{n+\alpha}, T_{n+\alpha} \right) \right\rangle \Bigg\} dV \\
&\qquad - \int_{\partial_{\boldsymbol{\sigma}}\Omega} \bar{\mathbf{t}}_R . \mathbf{v} d\Gamma - \int_\Omega \mathbf{b}_R . \mathbf{v} dV \\
&\qquad + \Delta t \int_{\partial_{\mathbf{q}}\Omega} \frac{T_{n+1}}{T_n} \bar{\mathbf{q}}_R . \mathbf{n}_R d\Gamma - \Delta t \int_\Omega \frac{T_{n+1}}{T_n} \mathrm{r}_R dV
\end{aligned} \tag{3.41}$$

In the time discrete version of the potentials, entropy and density (measured at the reference configuration; the subindex R was dropped for brevity) are taken as the values in the beginning of the time step, at instant t_n. Furthermore, from here on, the known value of the Helmholtz free energy at instant t_n is shortly noted as: $W_n = W(\mathbf{C}_n, \mathbf{Z}_n, T_n)$.

While the principle of minimum potential energy is associated to minimization operations with respect to displacements and internal variables, the principle of maximum thermal dissipation is associated to a maximum operation with respect to temperatures. In other words, the underlying variational principle reflects the classical inf-sup character of thermomechanical problems, when temperatures are considered independent variables. At every time step, the solution lies at a saddle-point, as determined by the equation below, and represented in figure 3.2 for a sample problem.

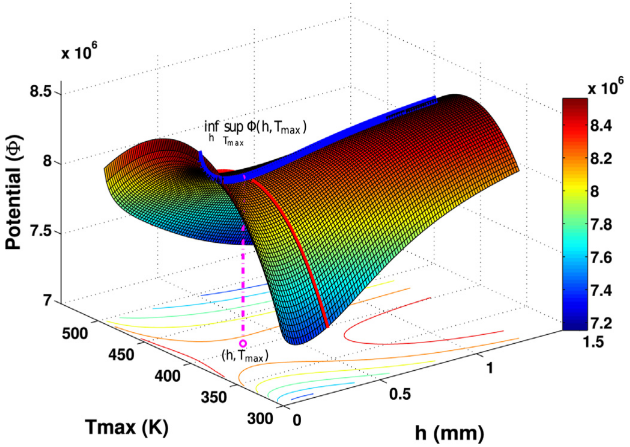

Figure 3.2 – Saddle-point structure of a thermomechanical problem around the incremental solution: representation of a thermomechanical functional for adiabatic shear banding problems. [Source: (SU; STAINIER; MERCIER, 2014)]

$$\inf_{\mathbf{x}_{n+1},\mathbf{Z}_{n+1}} \sup_{T_{n+1}} \mathcal{H}_n(\mathbf{x}_{n+1}, \mathbf{Z}_{n+1}, T_{n+1}; \mathbf{x}_n, \mathbf{Z}_n, T_n) \tag{3.42}$$

Stationarity conditions with respect to the set of independent variables yields all the necessary equations to fully describe the thermomechanical problem, a feature of the family of models based on variational constitutive updates. The minimization with respect to displacements yields a temperature factorized version of mechanical equilibrium. Equations for the evolution of internal variables result from the minimization with respect to $\mathbf{Z}_{n+1}$. Finally, an entropy form of the first law of thermodynamics (equivalent to equation 3.25) is obtained from the maximization with respect to temperature:

$$\begin{aligned} D_{\mathbf{x}_{n+1}}[\mathcal{H}_n](\delta\mathbf{x}_{n+1}) &= \int_{\Omega} \left[\frac{\partial W}{\partial \mathbf{C}_{n+1}} + \frac{T_{n+1}}{T_n} \left\langle \frac{\partial \psi}{\partial \dot{C}} \right\rangle \right] : \nabla \delta\mathbf{x}_{n+1} dV \\ &- \int_{\partial_{\boldsymbol{\sigma}}\Omega} \bar{\mathbf{t}}_R . \delta\mathbf{x}_{n+1} d\Gamma - \int_{\Omega} \mathbf{b}_R . \delta\mathbf{x}_{n+1} dV = 0, \quad \forall adm \delta\mathbf{x}_{n+1} \end{aligned} \tag{3.43a}$$

$$D_{\mathbf{Z}_{n+1}}[\mathcal{H}_n](\delta\mathbf{Z}_{n+1}) = \int_\Omega \left[\frac{\partial W}{\partial \mathbf{Z}_{n+1}} + \frac{T_{n+1}}{T_n}\left\langle\frac{\partial \psi}{\partial \dot{\mathbf{Z}}}\right\rangle\right]\delta\mathbf{Z}_{n+1} dV = 0, \quad \forall adm \delta\mathbf{Z}_{n+1} \tag{3.43b}$$

$$\begin{aligned} D_{T_{n+1}}[\mathcal{H}_n](\delta T_{n+1}) = \int_\Omega \Bigg\{ & \left[\frac{\partial W}{\partial T_{n+1}} + \rho_R \eta_n\right] \\ & + \frac{\Delta t}{T_n}\left\langle \frac{\partial \psi}{\partial \dot{C}} : \dot{C} + \frac{\partial \psi}{\partial \dot{Z}} : \dot{Z}\right\rangle + \Delta t \left\langle \frac{\partial \varphi}{\partial \mathbf{G}} : \mathbf{G}\right\rangle \Bigg\} \delta T_{n+1} dV \\ + \int_{\partial_{\mathbf{q}}\Omega} \frac{\Delta t}{T_n} \bar{\mathbf{q}}_R . \mathbf{n}_R \delta T_{n+1} d\Gamma & - \int_\Omega \frac{\Delta t}{T_n} \mathrm{r}_R \delta T_{n+1} dV = 0, \quad \forall adm \delta T_{n+1} \end{aligned} \tag{3.43c}$$

Unlike equations 3.43a and 3.43c, where there is information from a neighborhood respectively through strain and heat flux measures, the evolution of internal variables of equation 3.43b is strictly local. This is the nature of many internal variables. It allows a separation of local and global effects in the optimization of the incremental potential $\mathcal{H}_n$. An effective version of the incremental potential, after the minimization with respect to internal variables is often used:

$$\mathcal{H}_n^{eff}(\mathbf{x}_{n+1}, T_{n+1}) = \inf_{\mathbf{Z}_{n+1}} \mathcal{H}_n \tag{3.44}$$

In equation 3.43a, the necessary information to update stresses in a pseudo-hyperelastic fashion is available. Conservative ($\mathbf{S}^c_{n+1}$) and dissipative parts ($\mathbf{S}^d_{n+1}$) of stress appear naturally from the incremental potential:

$$\mathbf{S}^c_{n+1} = 2\frac{\partial W}{\partial \mathbf{C}_{n+1}} \qquad \mathbf{S}^d_{n+1} = 2\frac{T_{n+1}}{T_n}\frac{\partial \psi}{\partial \dot{C}} \tag{3.45}$$

By applying the divergence theorem to the heat flux term, it is possible to arrive at a local form for the entropic form of the first law of thermodynamics of equation 3.43c. Since the Helmholtz free energy serves as a potential for entropy ($\eta_{n+1} = -\frac{\partial W}{\partial T_{n+1}}$), the following equation constitutes an entropy update. An incremental version of internal dissipation clearly appears, factored by temperature: $\frac{\Delta t}{T_n}\left\langle \frac{\partial \psi}{\partial \dot{C}} : \dot{C} + \frac{\partial \psi}{\partial \dot{Z}} : \dot{Z}\right\rangle$. Two dissipation sources appear: one due to the imposed strain rate (as will be seen in the following chapter, this is equivalent to Kelvin-Voigt viscoelasticity) and another due to the evolution of internal variables (a flexible term, which can encompass, among others, plastic, damage and Maxwell viscoelasticity):

$$\left[\frac{\partial W}{\partial T_{n+1}} + \rho_R \eta_n\right] + \frac{\Delta t}{T_n}\left\langle \frac{\partial \psi}{\partial \dot{C}} : \dot{C} + \frac{\partial \psi}{\partial \dot{Z}} : \dot{Z} \right\rangle + \frac{\Delta t}{T_n}\mathrm{Div}\mathbf{q}_R - \frac{\Delta t}{T_n}\mathrm{r}_R = 0 \tag{3.46}$$

Going back to equation 3.41, an aside on the employed notation for the dissipation pseudo-potential is necessary. Once more, as for the purely mechanical case, since dissipation takes place along the time step, an adequate average measure along the time step has to be chosen. In Stainier (2011), the problem with a simple use of an intermediate point $n+\alpha$ for thermomechanical problems was discussed. Inconsistencies with respect to energy conservation arise if adaptations are not made to the time discretization of dissipation. Although the development is omitted here, it can be shown that energy consistency is achieved through the use of an average measure of the following type:

$$\begin{aligned}
&\left\langle \psi\left(\frac{T_{n+1}}{T_n}\frac{\Delta \mathbf{C}}{\Delta t}, \frac{T_{n+1}}{T_n}\frac{\Delta \mathbf{Z}}{\Delta t}; \mathbf{C}_{n+\alpha}, \mathbf{Z}_{n+\alpha}, T_{n+\alpha}\right)\right\rangle = \\
&\qquad \frac{T_n}{T_{n+1}}\psi\left(\frac{T_{n+1}}{T_n}\frac{\Delta \mathbf{C}}{\Delta t}, \frac{T_{n+1}}{T_n}\frac{\Delta \mathbf{Z}}{\Delta t}; \mathbf{C}_{n+\alpha}, \mathbf{Z}_{n+\alpha}, T_n\right) \\
&\quad + \frac{T_{n+1} - T_n}{T_{n+1}}\psi\left(\frac{T_{n+1}}{T_n}\frac{\Delta \mathbf{C}}{\Delta t}, \frac{T_{n+1}}{T_n}\frac{\Delta \mathbf{Z}}{\Delta t}; \mathbf{C}_{n+\alpha}, \mathbf{Z}_{n+\alpha}, T_{n+\alpha}\right)
\end{aligned} \tag{3.47}$$

The proposed framework for thermomechanical problems clearly holds the property of symmetric material tensors. Since all dissipative behaviors are factored by the temperature term $\frac{T_{n+1}}{T_n}$, cross derivatives with respect to strains and temperature commute. For naïve formulations of thermomechanically-coupled problems, this would not be the case. Having symmetric material operators brings about advantages in implementation, and allows for proofs of existence and convergence of solutions.

The novel parameterization used originally in Yang, Stainier & Ortiz (2006), where many typical thermomechanical problems were shown to fit the modeling structure presented above, has since been extended to other problems.

A hybrid semi-analytic approach to adiabatic shear banding in metals (for a phenomenological point of view of adiabatic shear bands as a feature of polymer behavior, see chapter 2) was variationally developed in Su, Stainier & Mercier (2014). A self catalyzed phenomenon, involving the formation of preferential plastic flow bands where thermal softening occurs, further accelerating plastic flow locally, adiabatic shear bands are a challenging subject to model with traditional thermomechanical approaches (see figure 3.2 for a representation of the saddle-point structure of the thermomechanical problem). The variational framework provided a solid base for the development of efficient models.

The mathematical properties of variational formulations can be explored in order to improve convergence properties of the optimization algorithms. While Newton-Raphson schemes are commonly used for their versatility, other strategies are possible. In Bouery (2012), viscoelasticity problems with strong temperature dependence of material parameters (simulating phenomena such as glass transition) were used to test the advantages of using Uzawa-type schemes instead of classical Newton-Raphson.

A common approach to thermomechanical problems is to utilize staggered schemes, solving cheaper purely thermal and purely mechanical problems sequentially, instead of the more computationally expensive fully coupled problem. The convergence and stability properties of staggered schemes have been the subject of several publication, such as Armero & Simo (1992) and Armero & Simo (1993), among others. Variational methods can also be used in conjunction with staggered schemes (one such scheme is fully developed in chapter 6, although for the separation of damage and viscoelasticity instead of the separation of mechanical and thermal effects). This is the subject explored in Ramabathiran & Stainier (2013), for strongly coupled thermoviscoelastic material models.

A special case of the general thermomechanical problem is when adiabatic conditions are present. In the absence of heat flux, be it thanks to insulation or due to very short simulations times (not long enough for there to be significant energy flow through conduction or convection), the non-local character of equation 3.43c disappears. The determination of energy balance and entropy evolution becomes an essentially local matter, as for other internal variables (equation 3.43b). Temperature can then be treated as an additional internal variable, and equation 3.44 becomes:

$$\mathcal{H}_n^{eff}(\mathbf{x}_{n+1}) = \inf_{\mathbf{Z}_{n+1}} \sup_{T_{n+1}} \mathcal{H}_n \tag{3.48}$$

In Stainier & Ortiz (2010) and Selke (2009), adiabatic problems were analyzed under this point of view. The partition of plastic work, classically simulated through the lens of previously imposed Taylor-Quinney factors, is then a natural result of the energy balance at every time step.

Other works following the same modeling techniques include Canadija & Mosler (2011), where the strategy developed in Mosler & Bruhns (2009) for the inclusion of kinematic hardening into the variational context is coupled to thermal effects in the large strain regime.

Having explored the fundamentals of variational formulations for dissipative problems in the previous section, and for the inclusion of general thermomechanically coupled problems in the present section, the necessary background is set for the development of consistent material models capable of accurately encompassing the main features of polymer-like material behavior, micromechanically outlined in chapter 2, namely: strongly coupled thermo-viscoelasticity (subject of chapter 4) and viscoelastic damage (subject of chapter 5). The proposed models are fully developed, and extensive discussion on the underlying hypothesis, both energetic and kinematic, is presented.

4 VARIATIONAL FORMULATION OF THERMO-VISCOELASTICITY IN FINITE STRAINS

> *Chapter overview: A fundamental class of models for the accurate simulation of polymer-like material models, large strains thermo-viscoelasticity can be formulated in a variational framework. The present chapter brings a full description of the model. After a brief overview of previous works on thermomechanically coupled viscoelasticity and the most commonly used rheological models, the basic underlying hypotheses behind the proposed variational model are presented, emphasizing the adopted multiplicative decomposition and the exponential mapping of viscous strains. Full expressions for the additively decomposed portions of the Helmholtz free energy and dissipation pseudo-potential are developed. The incremental problem, related to the time-discretization of the variational principle, is framed as an optimization problem, yielding all the necessary equations towards the update of stresses, entropy and internal variables. A crucial step for the implementation of the model in the code of choice, the material tensor is then derived. Summing up the contributions, still with the implementation in mind, an algorithm for the incremental problem is developed. Finally, some sample results demonstrating the capabilities of the model close the chapter.*

4.1 INTRODUCTION: THERMOMECHANICALLY COUPLED VISCOELASTICITY AND ASSOCIATED RHEOLOGICAL MODELS

In chapter 2, during a fairly comprehensive (although by no means exhaustive) discussion on the micromechanics of polymer-like material behavior, some arguments were developed on the need for thermomechanically-coupled viscoelasticity models for the accurate modeling of polymer behavior.

Dominated by the microstructural arrangement of long covalently bonded chains, often entangled and developing weaker secondary bonds (of van der Waals type) in points of proximity between different portions of chains, polymers often exhibit dissipative behavior when subjected to loading. Thermoplastics especially can be subjected to large inelastic strains, as evidenced by phenomena such as hysteresis under cyclic loads, permanent deformations even after no loads are present, or time-dependent straining under creep conditions, among many others. These features of material behavior can be associated to the breaking of secondary bonds and the rearrangement of polymer chains under the influence of loading (sometimes leading to induced anisotropy).

Temperature and time play an important role in determining the constitutive response of polymers. Molecular excitation induced by increasing temperatures, for instance, may lead to more unstable secondary bonds, and is behind the glass transition that characterizes polymer-like behavior, as the amorphous phase of heavily entangled chains becomes mobile. Conversely, increasing strain rates leave no time for polymer chains to accommodate the imposed loads, burdening principal chains before secondary bonds have been broken, and leading primary covalent bonds to be prematurely destroyed, as material behavior becomes ever more rigid and brittle. These effects were shown in figure 2.5.

As polymers have grown in importance for engineering applications, much work has been devoted to the development of dedicated material models, encompassing all the experimentally observed features of constitutive behavior. Some examples of previous models of thermo-viscoelasticity, outside the scope of variational models for dissipative problems, will soon be discussed. Before, though, still in keeping with the micromechanics of polymers, it is important to explore one of the main tools used in the development of constitutive models as they relate to polymer-like behavior: rheological models.

Materials science literature constantly calls upon a combination of elastic solids and viscous fluids to describe the material behavior of polymers. As discussed in chapter 2, this is what lies beneath some of the most common parameter identification procedures, such as the Dynamic Thermomechanical Analysis (DTMA). When the storage and loss moduli are identified, there is an implicit material model including one elastic spring and one viscous element (commonly referred to as a dashpot). What is apparent, though, is that being restricted to a single linear elastic element and a single linear viscous element can lead to models suited for a very short range of applications. Hence, the parameters identified during a DTMA test are often limited to the small strains regime.

In order to develop richer models, capable of capturing the nonlinearity of polymer behavior, two (often equivalent) choices are available: either increasing the complexity of those two single representative elements, or including an arbitrary number of other similarly simple elements. As both choices require the identification of a larger number of material parameters, the mathematical flexibility of the latter makes it the most commonly used.

By combining simple rheological elements representing elastic, viscous or plastic behavior, in different numbers and arrangements (in series or in parallel), it is possible to develop a wide range of material models to fit various types of material behavior.

In viscoelasticity, two classic simple combinations exist: Kelvin-Voigt and Maxwell models. Kelvin-Voigt viscoelasticity is modeled by an elastic element and a dashpot in parallel. Maxwell viscoelasticity exhibits a series of an elastic element and a dashpot. Each model has its advantages and drawbacks. For instance, Maxwell models are not indicated for creep applications, while Kelvin-Voigt models may have difficulties modeling some relaxation features.

By combining different numbers of Kelvin-Voigt and Maxwell elements, a variety of material models can be reproduced with rheological models. In the present document, a choice for an arbitrary model was made, combining one Kelvin-Voigt element (accounting for creep phenomena) in parallel to an arbitrary number of Maxwell elements (accounting for an arbitrary number of characteristic relaxations times, as well as for complex elastic behavior). This is represented in figure 4.1.

Thermal effects are not evident on figure 4.1. However, viscous dissipation phenomena taking place in the dashpots of the proposed generalized rheological model are the driving force of local heat generation. Further thermomechanical coupling is considered through the temperature dependence of material properties of elasticity (originating classical thermoelastic effects that shall be explored opportunely) and viscosity. This will be made clear in the following subsections, during the full derivation of the variational model.

Meanwhile, it is important to acknowledge previous contributions to the field of thermoviscoelasticity. The thermodynamic basis for thermomechanically-coupled viscoelasticity was initially set by Coleman & Noll (1963), where requirements for the constitutive equations of internal energy, temperature, heat conduction and stress (including elastic and viscous parts) were established.

Since then, myriad of approaches can be found in the literature. Some of the publications on the subject, starting from the early mathematical analysis works such as that of Taylor, Pister & Goudreau (1970)

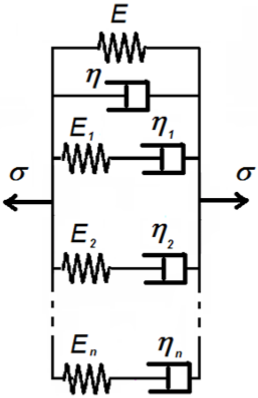

Figure 4.1 – Generalized Kelvin-Voigt Maxwell rheological model for the simulation of non-linear viscoelasticity.

on linear thermoviscoelasticity (restricted to the small strains regime), constitute an extension of previous works on thermoelasticity.

Another family of material models came about following Oden & Armstrong (1971), who modeled a class of materials with memory, called thermorheologically simple materials (whose material behavior depends exclusively on the history of variables of strain and temperature at the same point) and able to deal with nonlinearity of viscous behavior. Several papers have since been dedicated to mathematical aspects of nonlinear thermoviscoelasticity, following the proof of existence of smooth solutions by Dafermos (1982).

In contrast to other works, in Drozdov (1996), an approach separated from the time-temperature superposition principle was proposed for linear thermoviscoelasticity, allowing for temperature dependence of material properties and different evolution parameters for different characteristic times. Temperature dependent material parameters are also included in the approach of Holzapfel & Simo (1996), where the additional challenge of dealing with large strains behavior is faced - a volumetric-deviatoric split of strains is proposed, motivated by evidences of starkly different bulk and isochoric behavior in viscoelastic solids: such a split is used later on in this document. A general approach based on the molecular chain theory and also capable of dealing with finite strain behavior (in a way that generalizes the model developed by Holzapfel & Simo (1996)) is proposed by Huang (1999).

In Huang, Dui & Yang (2013), the common practice of using internal variables is correlated to the multiplicative split of inelastic strains in thermoviscoelasticity.

With respect to polymer material behavior, thermoviscoelasticity models have been applied to model shape memory polymers (SUN et al., 2002; NGUYEN et al., 2008; CHEN; NGUYEN, 2011), creep (LUO et al., 2012), rubber viscoelasticity (HASLACH; ZENG, 1999; DROZDOV; DORFMANN, 2002), and the validation of the constitutive behavior of several species of polymers (such as the work of Drozdov & Christiansen (2008) and Cheng, Wang & Huang (2010) for polyethylene), among other effects. Molecular chain models of thermoviscoelasticity, founded upon the formation and destruction of statistically-measured links and activation energies, are available such as in Cheng, Wang & Huang (2010) and Drozdov & Dorfmann (2002). In Bird & Curtiss (1998), an equivalence between predicted temperature evolution equations obtained through thermoviscoelasticity and polymer molecular theory models is demonstrated. Evolution equations based on the maximum dissipation principle are derived in Haslach & Zeng (1999) for thermoviscoelasticity.

However, despite the wide availability of constitutive models (of which the above list constitutes but a very a small sample), it should be noted that in engineering contexts, the intricacies of thermomechanical coupling often lead to the choice of models limited to some conditions of application, namely, disconsidering temperature dependence of material properties or restricting the range of application to relatively short relaxation times. Simpler models of linear thermo-viscoelasticity remain commonly used. Although applications require models accounting for the complexity of observed phenomena, the difficulty in devising tests and identifying the proper number of material parameters serves as a deterrent to the use of more complete models.

In the following subsections, the goal is to propose such a complete and flexible model, capable of dealing with strong thermomechanical coupling and other sources of nonlinearity, including various characteristic times and nonlinear elastic behavior. The variational framework described in the previous chapter serves as a basis from where all the necessary equations ruling the problem can be derived, no matter the chosen level of complexity included in individual terms of free energy and dissipation. In this sense, the proposed model generalizes simpler models (such as those of linear thermoviscoelasticity) while keeping enough information to model more complex phenomena, such as large strain behavior, the motivation behind the kinematic assumptions described in the following subsection.

Before moving on to the following section, though, it should be mentioned that the recently published book chapter by Stainier (2013), which brings an overview of the variational formulation of thermo-mechanically coupled problems, already includes a section on thermo-viscoelasticity. The present document brings a full description of such a variational formulation, with larger focus on the internal variable, stress and entropy updates, as well as tangent operators. In addition, the capabilities of the proposed model are demonstrated through as yet unpublished implemented applications.

4.2 KINEMATIC ASSUMPTIONS: MULTIPLICATIVE SPLIT OF STRAINS AND EXPONENTIAL MAPPING OF INTERNAL VARIABLES

As discussed in chapter 2, polymer behavior is often characterized by large strains (with the exception of thermosets, whose crosslinked molecular chain inhibits large displacements between polymer chains). Accurate models for the description of polymers in a wide range of applications are therefore required to deal with large strains, so as not to have very limited ranges of application. However, large strains are a source of nonlinearity and represent a challenge in the formulation of constitutive models. Oftentimes this translates into more computationally costly models than linearized versions specializing in certain ranges of problems.

Since the goal of this section is to develop a general framework capable of dealing with the most important features of polymer behavior, though, the issue of large strains needs to be properly tackled. The current subsection brings the main kinematic assumptions behind a consistent treatment of large strains for the assumed rheological model. The development here follows that of Fancello, Ponthot & Stainier (2006) for isothermal viscoelastic models.

The first kinematic ingredient of the proposed formulation is the multiplicative decomposition of elastic and inelastic strains due to Kröner (1959), Lee (1969), and thoroughly discussed by Gurtin & Anand (2005).

$$\mathbf{F} = \mathbf{F}^e \mathbf{F}^v \tag{4.1}$$

This type of decomposition can be physically interpreted as equivalent to the existence of an intermediate inelastic strain state where the material would immediately go back to, if the elastic strains were to be instantly removed (see figure 4.2). This interpretation may be clearer in plasticity, where plastic strains are permanent. The intermediate state then becomes the new stress-free state. In viscoelasticity, on the other hand, the intermediate state does not constitute a stress-free state nor an equilibrium one. With the passage of time, relaxation takes place and the body returns to the original stress-free state at time $t = 0$ (which may conveniently be chosen as the reference configuration).

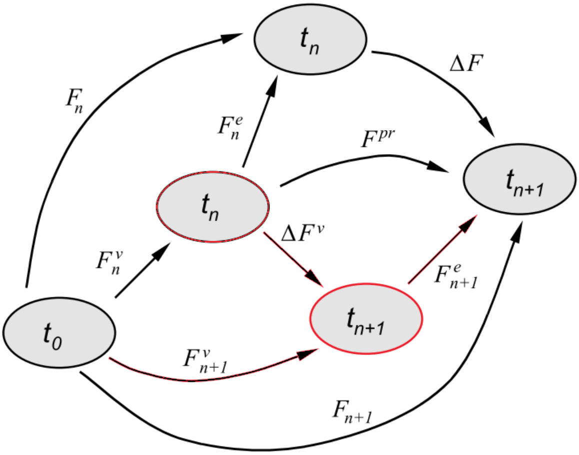

Figure 4.2 – Physical representation of the multiplicative decomposition between elastic and inelastic strains for viscoelasticity. Viscous states (circled red) seen as an intermediate state. [Source: (FANCELLO; PONTHOT; STAINIER, 2006)]

In a time-discrete context, the multiplicative decomposition leads to incremental measures of deformation. In that sense, the incremental deformation gradient ($\Delta\mathbf{F}$) is responsible for taking the body from the deformed state at t_n to its deformed state at t_{n+1}. Equivalently, the intermediate viscous states $\mathbf{F}_n^v$ and $\mathbf{F}_{n+1}^v$ are related by a viscous strain increment ($\Delta\mathbf{F}^v$), as represented in figure 4.2.

Another practice originally devised for plasticity problems is the use of predictor-corrector schemes. From a known total imposed deformation gradient $\mathbf{F}_{n+1}$, in order to find the corresponding intermediate state $\mathbf{F}_{n+1}^v$, it is often convenient to start local internal variable updates with a predictor state $\mathbf{F}^{pr}$, considered a fully elastic increment from the previous intermediate state. In other words, a first assumption of fully elastic strain increment is made, before checking for convergence in the mechanical equilibrium equations. Clearly, unlike plasticity, there is no threshold to overcome for the onset of viscous deformations.

In addition to the multiplicative decomposition into elastic and inelastic parts of the deformation gradient, a second ingredient of the proposed formulation pertains to the differences between isochoric and volumetric behavior. As discussed by Holzapfel & Simo (1996), the development of material models must take into account the observed differences between bulk and deviatoric behavior of inelastic materials. Any tensor may be decomposed in volumetric and isochoric parts. Therefore, it may be of interest to separate the deformation gradient in volumetric ($\mathbf{F}^{vol}$) and isochoric ($\hat{\mathbf{F}}$) parts:

$$\mathbf{F} = \mathbf{F}^{vol}\hat{\mathbf{F}} \qquad \mathbf{F}^{vol} = J^{\frac{1}{3}}\mathbf{I} \qquad \hat{\mathbf{F}} = J^{-\frac{1}{3}}\mathbf{F} \tag{4.2}$$

A common assumption, initially based on the mechanisms of metal plasticity (namely the movement of dislocations along the crystalline network), is that inelastic deformations are volume-preserving[4.1]. The same assumption is made here. Therefore, all viscous strains are considered isochoric ($\det \mathbf{F}^{v} = 1$), while the elastic strains may include isochoric and volumetric parts. Mixing together both multiplicative decompositions:

$$\mathbf{F} = \mathbf{F}^{vol}\hat{\mathbf{F}}^{e}\mathbf{F}^{v} \tag{4.3}$$

It should be noted that the hypothesis of isochoric viscous strains for thermoplastic polymers is a limiting one. Experimental evidences on the existence of inelastic volumetric strains have been extensively reported for various polymer species. An extension of Vassoler (2009) to viscoelasticity can be envisioned as a future enhancement of the proposed models, as discussed in subsection 4.7.

In relating equation 4.3 to the proposed rheological model of figure 4.1, deformations on Maxwell branches are considered isochoric ($\hat{\mathbf{F}} = \hat{\mathbf{F}}^{e}\mathbf{F}^{v}$, so that the Maxwel springs are only subjected to isochoric elastic strains) while the elastic deformations on the single Kelvin-Voigt branch are considered fully volumetric.

It is possible to derive alternative measures of deformation based on the decomposition of strains. Specifically, it will be useful to de-

---

[4.1] Exceptions to this assumption abound, such as in the treatment of plasticity in metal foams of (VASSOLER, 2009) and many others where volumetric plasticity needs to be considered.

fine the right Cauchy-Green measure of elastic strains on the Maxwell branches as follows, and its spectral decomposition, as the proposed formulation makes use of isotropic potentials depending on eigenvalues of strains:

$$\hat{\mathbf{C}}^e = \hat{\mathbf{F}}^{eT}\hat{\mathbf{F}}^e = \sum_{j=1}^{3} c_j^e \mathbf{M}_j^e \otimes \mathbf{M}_j^e \tag{4.4}$$

Viscoelasticity is a class of time-dependent material behavior. It is therefore important to define viscous gradient velocity tensors, and to determine flow rules for viscous strains. Assuming irrotational viscous strains ($\mathbf{W}^v = 0$), the viscous gradient velocity tensor ($\mathbf{L}^v$), which is equal to the rate of viscous stretching ($\mathbf{D}^v$), reads (with its spectral decomposition):

$$\begin{aligned} \mathbf{D}^v = \mathrm{sym}(\mathbf{L}^v) = \mathbf{L}^v = \dot{\mathbf{F}}^v\mathbf{F}^{v-1} &= \sum_{j=1}^{3} q_j \mathbf{M}_j^v \otimes \mathbf{M}_j^v \\ \dot{\mathbf{F}}^v &= \mathbf{D}^v\mathbf{F}^v \end{aligned} \tag{4.5}$$

In the equation above, eigenvalues of viscous strains were separated into an amplitude vector q_j and directions of viscous strains $\mathbf{M}_j^v$. Later on, they shall be taken as internal variables, and are subjected to the following constraints, related to the properties of eigenvalues and eigenvectors of isochoric tensors (whence the set K_q, enforcing a null sum of eigenvalues; Sym is the set of symmetric tensors):

$$\begin{aligned} q_j \in \mathrm{K}_q &= \left\{ q_j \in \mathbb{R} : \sum_{i=1}^{3} q_i = 0 \right\} \\ \mathbf{M}_j^v \in \mathrm{K}_M &= \{\mathbf{N}_i \in \mathrm{Sym} : \mathbf{N}_i.\mathbf{N}_i = 1; \mathbf{N}_i.\mathbf{N}_j = 0, i \neq j\} \end{aligned} \tag{4.6}$$

In order to fully define the viscous flow rule in the incremental context, some form of mapping between the rate of viscous stretching and the incremental viscous strains is needed. The exponential mapping of inelastic strains, used, among many others, in (WEBER; ANAND, 1990; FANCELLO; PONTHOT; STAINIER, 2006; FANCELLO; VASSOLER; STAINIER, 2008; SELKE, 2009), allows for strain increments respecting the previously mentioned hypotheses of isochoric viscous strains.

$$\mathbf{F}^v_{n+1} = \Delta\mathbf{F}^v\mathbf{F}^v_n = \Delta\mathbf{R}\exp\left[\Delta t\sum_{j=1}^{3} q_j\mathbf{M}^v_j\otimes\mathbf{M}^v_j\right]\mathbf{F}^v_n \tag{4.7}$$

$$\Delta\mathbf{F}^v = \Delta\mathbf{R}\exp\left[\Delta t\mathbf{D}^v\right] = \Delta\mathbf{R}\exp\left[\Delta t\sum_{j=1}^{3} q_j\mathbf{M}^v_j\otimes\mathbf{M}^v_j\right] \tag{4.8}$$

$$\Delta\mathbf{C}^v = \Delta\mathbf{F}^{vT}\Delta\mathbf{F}^v = \mathbf{F}^{v-T}_n\mathbf{C}^v_{n+1}\mathbf{F}^{-1}_n = \exp\left[\Delta t\mathbf{D}^v\right]^2 \tag{4.9}$$

$$\mathbf{D}^v = \frac{1}{2\Delta t}\ln\Delta\mathbf{C}^v \tag{4.10}$$

The tensor $\Delta\mathbf{R}$ is the incremental counterpart of the rotation tensor $\mathbf{R}$ in the above equations. Since $\Delta\mathbf{R}^T\Delta\mathbf{R} = \mathbf{I}$, it vanishes from the incremental mapping of the right Cauchy-Green viscous strain tensor.

The same type of development in terms of the exponential mapping can be done for the predictor state (later used as an initial step in the update of internal variables) and for the isochoric elastic state (which characterizes the elastic behavior of each Maxwell branch of the generalized rheological model).

$$\hat{\mathbf{F}}^{pr} = \hat{\mathbf{F}}_{n+1}\mathbf{F}^{v-1}_n \qquad \hat{\mathbf{C}}^{pr} = \mathbf{F}^{v-T}_n\hat{\mathbf{C}}_{n+1}\mathbf{F}^{v-1}_n \tag{4.11}$$

$$\hat{\mathbf{F}}^e_{n+1} = \hat{\mathbf{F}}_{n+1}\mathbf{F}^{v-1}_{n+1} = \hat{\mathbf{F}}^{pr}\left[\Delta\mathbf{F}^v\right]^{-1} = \hat{\mathbf{F}}^{pr}\left[\exp[\Delta t\mathbf{D}^v]\right]^{-1} \tag{4.12}$$

Provided that the tensors of rate of viscous stretching ($\mathbf{D}^v$) and right Cauchy-Green predictor ($\hat{\mathbf{C}}^{pr}$) are colinear (that is, if they share principal directions $\mathbf{M}_j$) the following relation can also be used:

$$\hat{\mathbf{C}}^e_{n+1} = \hat{\mathbf{F}}^{eT}_{n+1}\hat{\mathbf{F}}^e_{n+1} = \hat{\mathbf{C}}^{pr}\left[\exp[\Delta t\mathbf{D}^v]\right]^{-2} \tag{4.13}$$

Additionally, corresponding logarithmic measures of strains may defined and used as independent variables later on. The elastic logarithmic strain tensor and the logarithmic predictor are defined and relate to the rate of viscous stretching as follows:

$$\boldsymbol{\varepsilon}^{e}_{n+1} = \frac{1}{2}\ln \hat{\mathbf{C}}^{e}_{n+1} \qquad \boldsymbol{\varepsilon}^{pr} = \frac{1}{2}\ln \hat{\mathbf{C}}^{pr} \tag{4.14}$$

$$\boldsymbol{\varepsilon}^{e}_{n+1} = \boldsymbol{\varepsilon}^{pr} - \Delta t \mathbf{D}^{v} \tag{4.15}$$

Once more, provided the colinearity of tensors $\mathbf{D}^{v}$, $\hat{\mathbf{C}}^{pr}$ and the elastic right Cauchy-Green ($\hat{\mathbf{C}}^{e}_{n+1}$), the above relations can be written in terms of eigenvalues of strains as follows (in a form reminiscent of predictor-corrector schemes in small strains):

$$\begin{gathered} \hat{\mathbf{C}}^{e}_{n+1} = \sum_{j=1}^{3} c^{e}_{j}\mathbf{M}_j \otimes \mathbf{M}_j \qquad \boldsymbol{\varepsilon}^{e}_{n+1} = \sum_{j=1}^{3} \epsilon^{e}_{j}\mathbf{M}_j \otimes \mathbf{M}_j \\ \boldsymbol{\varepsilon}^{pr} = \sum_{j=1}^{3} \epsilon^{pr}_{j}\mathbf{M}_j \otimes \mathbf{M}_j \end{gathered} \tag{4.16}$$

$$\epsilon^{e}_{j} = \frac{1}{2}\ln c^{e}_{j} = \epsilon^{pr}_{j} - \Delta q_j \qquad \text{with} \quad \Delta q_j = \Delta t q_j \tag{4.17}$$

Although the reasoning behind such a notation using only the principal values of strains may seem obscure for the moment, it will soon be clarified. In the following subsections, it will be demonstrated that, as a consequence of choosing isotropic potentials depending only on eigenvalues of viscous strains, the colinearity of these tensors comes as a consequence of the optimization of the problem with respect to the eigenvectors of strains $\mathbf{M}_j$, which can be done analytically.

Before moving on to the optimization aspects of the proposed formulation, though, the next subsection is dedicated to the discussion of the additive decomposition of the Helmholtz free energy potential and the dissipation pseudo-potential. Specific forms for the proposed potentials are explored.

4.3 ADDITIVE DECOMPOSITION OF THE HELMHOLTZ FREE ENERGY AND DISSIPATION PSEUDO-POTENTIAL: ISOTROPIC FUNCTIONS OF EIGENVALUES OF STRAINS, NONLINEAR ELASTIC AND VISCOUS BEHAVIORS AND TEMPERATURE DEPENDENCE

Two crucial steps precede the actual variational formulation of dissipative problems, in the vein of Ortiz & Stainier (1999): the choice of the set of internal variables that shall describe the internal dissipative processes (in the context of generalized standard materials), and the choice of the potentials representing the various forms of energies involved, both stored and dissipated.

The previous subsection brought definitions of strain measures that will be used as internal variables. Together with temperature, eigenvalues of viscous strains will be responsible for storing the information describing thermal and mechanical dissipative processes that characterize polymer behavior. The main goal was to provide the necessary tools towards a solid treatment of large strains, an important source of nonlinearity in constitutive modeling.

The general set of independent variables for the Helmholtz free energy potential, previously described, in chapter 3, as $W(\mathbf{C}, \mathbf{Z}, T)$, becomes then, with the adopted choices of internal variables to describe viscous strains:

$$W(\mathbf{C}, \mathbf{Z}, T) = W(\mathbf{C}, q_j, \mathbf{M}_j^v, T) \tag{4.18}$$

In the present subsection, the second step is discussed, starting from stored energy and moving along to dissipated energy.

The common assumption of an additively-decomposed Helmholtz free energy is made here. Separate portions of energy are used to describe all the possible forms of storing energy. This sort of decomposition is closely related to the choice of rheological model. Individual rheological elements represent different forms of energy. Springs represent elastically-stored energy. Dashpots, viscosity-related dissipation.

As mentioned earlier, and following the choices made in Fancello, Ponthot & Stainier (2006), Fancello, Vassoler & Stainier (2008), Selke (2009), isotropic potentials depending on eigenvalues of strains are used. Although this restricts the possible forms of potentials, there is still enough freedom for the inclusion of various different types of material behaviors, as will be explored in the following paragraphs.

The spring of the single Kelvin-Voigt branch is chosen as a starting point. Since both rheological elements of a Kelvin-Voigt branch are subjected to the same imposed displacement (i.e., the total displacement field), no internal variable is needed in order to describe either the viscous dissipation or the elastically-stored energy. Hence, no dependence on the set of internal viscous variables q_j and $\mathbf{M}_j$ appears.

Stemming from the observed differences in bulk and deviatoric behaviors in many inelastic materials, a term dedicated to the volumetric contribution of the elastically-stored energy is defined, depending only on the volume changes to which the material is subjected through the Jacobian $\det \mathbf{F} = J$. A first term responsible for thermomechanical coupling accounts for the influence of temperature induced volumetric dilatation, with the common expansion coefficient α. Also, the bulk modulus $K(T)$ is assumed to be temperature dependent, inducing further coupling between mechanical and thermal responses. For simplicity, all deviatoric elastic contributions to stored energy are assumed to be borne by Maxwell branches.

The adopted final expression for the volumetric elastic energy stored in the spring of the Kelvin-Voigt branch then reads as follows (the temperature dependence of the bulk modulus is assumed linear, but no restriction to more complex dependencies is imposed):

$$W^{vol}(J,T) = \frac{1}{2} K(T) \left[\ln J\right]^2 - 3K_0\alpha[T - T_0] \ln J \tag{4.19}$$

$$K(T) = K_0 - K_1[T - T_0] \tag{4.20}$$

The term T_0 is a reference temperature for the measurement of the bulk modulus (which equals K_0 at that temperature).

Every Maxwell branch[4.2] also has a spring representing elastically-stored energy. Complying with previous assumptions, all strains undergone by the elements of the Maxwell branches are isochoric. Isotropic potentials depending on eigenvalues of strains are used. Hence, the general dependence on isochoric elastic strains (through the previously defined right Cauchy-Green measure $\hat{\mathbf{C}}^e$) is substituted by specific dependence on their eigenvalues (c_j^e). However, eigenvalues of logarithmic strains (ϵ_j^e) will be preferred as independent variables.

$$W^e(\hat{\mathbf{C}}^e, T) = W^e(c_1^e, c_2^e, c_3^e, T) = W^e(\epsilon_1^e, \epsilon_2^e, \epsilon_3^e, T) \tag{4.21}$$

It is possible to show that classic elasticity models can be represented with this type of isotropic potential. For instance, Hencky elasticity, generalizing linear elasticity, can be formulated as follows:

$$W^e(\epsilon_1^e, \epsilon_2^e, \epsilon_3^e, T) = \mu^e(T) \sum_{j=1}^{3} [\epsilon_j^e]^2 \tag{4.22}$$

[4.2] No index is used to identify different Maxwell branches here, in order to keep notations simple. During the description of the minimization procedure behind internal variable updates, the proper distinctions will be made.

Thermomechanical coupling is included in the model through temperature dependent shear moduli. Once again, a simple linear dependence on temperature of the shear modulus μ^e is assumed, but there is no restriction to more complex relations:

$$\mu^e(T) = \mu_0^e - \mu_1^e[T - T_0] \tag{4.23}$$

Nonlinear elasticity models may also be described by isotropic potentials. Ogden elasticity, which can be shown to encompass Neo-Hookean elasticity for specific choices of material parameters, is thus modeled as follows:

$$W^e(\epsilon_1^e, \epsilon_2^e, \epsilon_3^e, T) = \sum_{i=1}^{3} \sum_{j=1}^{3} \frac{\mu_i^e(T)}{\alpha_i^e} \left[[\exp \epsilon_j^e]^{\alpha_i^e} - 1 \right] \tag{4.24}$$

The exponents α_i^e are considered independent of temperature.

One final form of storing energy in the proposed material model is thermally, through heat capacity. Clearly, there are no rheological elements representing this sort of energy accumulation in the generalized Kelvin-Voigt/Maxwell model of figure 4.1. Rheological models are often devised to model purely mechanical problems. When thermomechanical instances are present, additional care must be taken so as not to leave behind all possible thermal effects.

The final portion of the Helmholtz free energy, representing thermal heat storage, reads as follows, where the heat capacity $\mathcal{C}(T)$ may exhibit temperature dependence, provided that it is coherent with equation 3.33. No dependence on strains is assumed, which means that this portion of the Helmholtz free energy does not contribute to thermomechanical coupling.

$$W^{th}(T) = \rho_R \mathcal{C}(T) \left[[T - T_0] - T \log \frac{T}{T_0} \right] \tag{4.25}$$

Finally, putting all the ingredients together, the additive decomposition of the Helmholtz free energy then reads (where K Maxwell branches are considered in the rheological model, and index j refers to the three eigenvalues of strains):

$$W(\mathbf{C}, q_j, \mathbf{M}_j^v, T) = W^{vol}(J, T) + W^{th}(T) + \sum_{k=1}^{K} \sum_{j=1}^{3} W^{ek}(\epsilon_j^e, T) \tag{4.26}$$

Having explored all the sources of stored energy that go into the Helmholtz free energy potential, the focus can be shifted to the sources of energy dissipation.

In an incremental context, the general dependence of the dissipation pseudo-potential was previously described in equation 3.41, for thermomechanically-coupled problems in the variational framework. All dissipative processes were factored by a temperature ratio, giving equations for the internal dissipation of the desired form and guaranteeing symmetry of the material tensor. Now, using spectral quantities of viscous strains as independent variables, this can be rewritten as:

$$\psi\left(\frac{T_{n+1}}{T_n}\frac{\Delta\mathbf{C}}{\Delta t}, \frac{T_{n+1}}{T_n}\frac{\Delta\mathbf{Z}}{\Delta t}; \mathbf{C}_{n+\alpha}, \mathbf{Z}_{n+\alpha}, T_{n+\alpha}\right) = \\ \psi\left(\frac{T_{n+1}}{T_n}\frac{\Delta\mathbf{C}}{\Delta t}, \frac{T_{n+1}}{T_n}\frac{\Delta q_j}{\Delta t}; \mathbf{C}_{n+\alpha}, q_{jn+\alpha}, T_{n+\alpha}\right) \quad (4.27)$$

The first source of energy dissipation is the Kelvin-Voigt dashpot. As for the Kelvin-Voigt spring, it is subjected to the full imposed deformations (and, more importantly in this case, to the total imposed strain rate), and does not require the use of internal variables in order to describe viscous dissipation.

Isotropic potentials depending only on eigenvalues of strains are once more used, due to their ability of encompassing a broad variety of viscosity behaviors. For instance, Hencky-style viscous dissipation can be of the form:

$$\psi^{KV}\left(\frac{T_{n+1}}{T_n}\frac{\Delta\mathbf{C}}{\Delta t}; \mathbf{C}_{n+\alpha}, T_{n+\alpha}\right) = \mu^{vKV}(T)\sum_{j=1}^{3}\left[\frac{T_{n+1}}{T_n}\Delta c_j\right]^2 \quad (4.28)$$

Equivalently, nonlinear models of viscous dissipation may be formulated with isotropic pseudo-potentials, provided they respect the basic property of convexity with respect to internal variables. In doing so, positive internal dissipation is ensured, as is the respect of the second law of thermodynamics.

One such possible model is the following power law for viscous dissipation, which shall be used in some applications presented later on:

$$\psi^{KV}\left(\frac{T_{n+1}}{T_n}\frac{\Delta \mathbf{C}}{\Delta t};\mathbf{C}_{n+\alpha},T_{n+\alpha}\right)=\\ \sum_{j=1}^{3}\left\{\frac{\overline{m}}{\overline{m}+1}Y_0^{KV}\dot{\epsilon}_0^{KV}\left[\frac{T_{n+1}}{T_n}\frac{\Delta c_j/\Delta t}{\dot{\epsilon}_0^{KV}}\right]^{\frac{1}{\overline{m}}+1}\right\} \tag{4.29}$$

It should be noted that, since the dissipation pseudo-potential takes into account only the imposed strain rate, there is only a single characteristic time (and thus, one single relaxation mechanism) represented in the Kelvin-Voigt branch.

The dashpots at each Maxwell branch are the remaining source of dissipation in the proposed rheological model. The freedom to add an arbitrary number of Maxwell branches allows for the inclusion of dissipative phenomena of various characteristic times. Internal variables are needed in order to represent the split between viscous and elastic strains in each Maxwell branch. In accordance to the other parts of the proposed model, the variables of choice are eigenvalues of viscous strains (q_j). In order to keep notations simple, no indexes are used to represent different Maxwell branches here, though they will be present in the following subsection, when describing the internal variable update procedure. Both Hencky (equation 4.30) and power law (equation 4.31) dissipation pseudo-potentials are presented:

$$\psi^{MX}\left(\frac{T_{n+1}}{T_n}\frac{\Delta q_j}{\Delta t};q_{jn+\alpha},T_{n+\alpha}\right)=\mu^v(T)\sum_{j=1}^{3}\left[\frac{T_{n+1}}{T_n}\frac{\Delta q_j}{\Delta t}\right]^2 \tag{4.30}$$

$$\psi^{MX}\left(\frac{T_{n+1}}{T_n}\frac{\Delta q_j}{\Delta t};q_{jn+\alpha},T_{n+\alpha}\right)=\\ \sum_{j=1}^{3}\left\{\frac{m}{m+1}Y_0^{MX}\dot{\epsilon}_0^{MX}\left[\frac{T_{n+1}}{T_n}\frac{\Delta q_j/\Delta t}{\dot{\epsilon}_0^{MX}}\right]^{\frac{1}{m}+1}\right\} \tag{4.31}$$

The additive decomposition of the dissipation pseudo-potential then reads (where K Maxwell branches are considered in the rheological model):

$$\psi\left(\frac{T_{n+1}}{T_n}\frac{\Delta\mathbf{C}}{\Delta t},\frac{T_{n+1}}{T_n}\frac{\Delta q_j^k}{\Delta t};\mathbf{C}_{n+\alpha},q_{jn+\alpha}^k,T_{n+\alpha}\right)=$$
$$\psi^{KV}\left(\frac{T_{n+1}}{T_n}\frac{\Delta\mathbf{C}}{\Delta t};\mathbf{C}_{n+\alpha},T_{n+\alpha}\right)$$
$$+\sum_{k=1}^{K}\sum_{j=1}^{3}\psi^{MXk}\left(\frac{T_{n+1}}{T_n}\frac{\Delta q_j^k}{\Delta t};q_{jn+\alpha}^k,T_{n+\alpha}\right)\quad(4.32)$$

Before moving along to the actual variational formulation of thermo-visco-elasticity, it should be noted that some authors may choose to include the dissipation due to heat flux inside the general dissipation pseudo-potential, which can help somewhat shorten the equations. In essence, this translates into combining pseudo-potentials ψ and φ into a unified dissipation potential Ψ:

$$\Psi\left(\frac{T_{n+1}}{T_n}\frac{\Delta\mathbf{C}}{\Delta t},\frac{T_{n+1}}{T_n}\frac{\Delta q_j^k}{\Delta t},\frac{\nabla T_{n+1}}{T_n};\mathbf{C}_{n+\alpha},q_{jn+\alpha}^k,T_{n+\alpha}\right)=$$
$$\psi\left(\frac{T_{n+1}}{T_n}\frac{\Delta\mathbf{C}}{\Delta t},\frac{T_{n+1}}{T_n}\frac{\Delta q_j^k}{\Delta t};\mathbf{C}_{n+\alpha},q_{jn+\alpha}^k,T_{n+\alpha}\right)+\varphi\left(\frac{\nabla T_{n+1}}{T_n};T_{n+\alpha}\right)\quad(4.33)$$

Despite the convenience of including all dissipative behaviors in a single functional, this notation choice has a central drawback. In keeping the distinction, local effects relating to the evolution of internal variables and coupling terms (related to ψ) are more clearly separated from the nonlocal nature of irreversible heat dissipation (related to φ).

In addition, as discussed in chapter 3, instead of assuming *a priori* the respect of a Fourier-type conduction law, a general notation using a conduction dissipation pseudo-potential (depending on the temperature gradient, and possibly parametrically of temperature $\varphi(\frac{\nabla T_{n+1}}{T_n};T_{n+\alpha})$) remains more flexible to include other types of relations between temperature gradients and heat dissipation. The associated thermodynamic force (which in the case of Fourier's law is nothing more than $\mathbf{H}=\frac{\partial\varphi}{\partial\nabla T}=-\frac{1}{T}\mathbf{q}$), then pairs with the temperature gradient to yield the dissipated energy through irreversible heat conduction in the second law of thermodynamics as follows:

$$\left[\frac{\partial W}{\partial \mathbf{Z}} : \dot{\mathbf{Z}}\right] - \mathbf{H}.\nabla T \leq 0 \tag{4.34}$$

This is an alternative version of equation 3.31. In the present text, however, Fourier conduction law is assumed known *a priori*, and the general notation using φ gives way to the dissipation term $\frac{1}{T}\mathbf{q}\nabla T$.

Having defined the set of independent variables needed to model the problem and built specific forms of all the involved energy potentials and pseudo-potentials, it is now time to move to the actual variational formulation of thermo-viscoelasticity, the subject of the following subsection.

4.4 FORMULATION OF THE THERMOMECHANICALLY COUPLED PROBLEM: VARIATIONAL CONSTITUTIVE UPDATES

In order to put problems of thermo-viscoelasticity in a variational framework, the first step is going back to the underlying variational principle discussed in chapter 3. Formulated in rate form (equation 3.40) and representing the interconvertibility between different types of energies, for general thermomechanical problems in an incremental setting, the variational principle states that the solution lies at stationarity points of the following functional of equation 3.41.

$$\begin{aligned}
&\mathcal{H}_n(\mathbf{x}_{n+1}, \mathbf{Z}_{n+1}, T_{n+1}; \mathbf{x}_n, \mathbf{Z}_n, T_n) = \\
&\int_\Omega \{[W(\mathbf{C}_{n+1}, \mathbf{Z}_{n+1}, T_{n+1}) - W(\mathbf{C}_n, \mathbf{Z}_n, T_n) - \rho_R \eta_n [T_{n+1} - T_n]] \\
&\qquad + \Delta t \left\langle \psi\left(\frac{T_{n+1}}{T_n}\frac{\Delta \mathbf{C}}{\Delta t}, \frac{T_{n+1}}{T_n}\frac{\Delta \mathbf{Z}}{\Delta t}; \mathbf{C}_{n+\alpha}, \mathbf{Z}_{n+\alpha}, T_{n+\alpha}\right)\right\rangle \\
&\qquad\quad + \Delta t \left\langle \varphi\left(\frac{\nabla T_{n+1}}{T_{n+1}}; \mathbf{C}_{n+\alpha}, \mathbf{Z}_{n+\alpha}, T_{n+\alpha}\right)\right\rangle\} \, dV \\
&\qquad\qquad - \int_{\partial_\sigma \Omega} \bar{\mathbf{t}}_R.\mathbf{v} d\Gamma - \int_\Omega \mathbf{b}_R.\mathbf{v} dV \\
&\qquad\qquad + \Delta t \int_{\partial_\mathbf{q}\Omega} \frac{T_{n+1}}{T_n} \bar{\mathbf{q}}_R.\mathbf{n}_R d\Gamma - \Delta t \int_\Omega \frac{T_{n+1}}{T_n} \mathrm{r}_R dV
\end{aligned} \tag{4.35}$$

As indicated by the terms of imposed tractions and heat fluxes (respectively, $\bar{\mathbf{t}}_R$ and $\bar{\mathbf{q}}_R$) along regions of the boundary $\partial\Omega$, the expression above constitutes an incremental variational formulation of the full boundary value problem. Dissipation due to irreversible heat conduction is assumed to follow a Fourier law with no parametric dependence on temperature, so that its thermodynamically-appropriate average along the time step (denoted $\langle\bullet\rangle$) reduces to Δt times the dissipation rate.

All variables are assumed known at time t_n, and the functional $\mathcal{H}_n$ is rebuilt at every time step to account for the history dependent behavior. In relation to the postulated variational principle and to the proposed set of internal variables, the solution procedure for thermo-viscoelastic problems can be expressed as the search for:

$$\inf_{\mathbf{C}_{n+1}, q_{jn+1}, \mathbf{M}^v_{jn+1}} \sup_{T_{n+1}} \mathcal{H}_n \tag{4.36}$$

The internal variable update is strictly local. Therefore, it is possible to derive an effective global expression for the problem, by previously performing the point-wise minimization with respect to variables of viscous strains q_{jn+1} and $\mathbf{M}^v_{jn+1}$:

$$\begin{aligned}&\mathcal{H}^{eff}_n(\mathbf{C}_{n+1}, T_{n+1}; \mathbf{C}_n, q_{jn}, \mathbf{M}^v_{jn}, T_n) = \\ &\inf_{q_{jn+1}, \mathbf{M}^v_{jn+1}} \mathcal{H}_n(\mathbf{C}_{n+1}, q_{jn+1}, \mathbf{M}^v_{jn+1}, T_{n+1}; \mathbf{C}_n, q_{jn}, \mathbf{M}^v_{jn}, T_n)\end{aligned} \tag{4.37}$$

It is important to note that the chosen internal variables of viscous strains must respect the properties of eigenvalues and eigenvectors. As previously discussed, these variables must be of the following form (equation 4.6):

$$\begin{aligned} q_j \in \mathrm{K}_q &= \left\{ q_j \in \mathbb{R} : \sum_{i=1}^{3} q_i = 0 \right\} \\ \mathbf{M}^v_j \in \mathrm{K}_M &= \{\mathbf{N}_i \in \mathrm{Sym} : \mathbf{N}_i . \mathbf{N}_i = 1; \mathbf{N}_i . \mathbf{N}_j = 0, i \neq j\} \end{aligned} \tag{4.38}$$

Hence, the internal variable update procedure consists of a constrained optimization problem. The above restrictions may be implemented by means of Lagrange multipliers, a standard procedure in optimization literature (ARORA, 2004). A Lagrangian function $\mathcal{L}$ is built as follows:

$$\begin{aligned}\mathcal{L}(q_j,\mathbf{M}_j^v) = \mathcal{H}_n^{eff}(\mathbf{C}_{n+1},T_{n+1};\mathbf{C}_n,q_{jn},\mathbf{M}_{jn}^v,T_n) + \lambda_0[q_1+q_2+q_3]\\ + \lambda_1[\mathbf{M}_1^v.\mathbf{M}_1^v - 1] + \lambda_2[\mathbf{M}_2^v.\mathbf{M}_2^v - 1] + \lambda_3[\mathbf{M}_3^v.\mathbf{M}_3^v - 1]\\ + \lambda_4[\mathbf{M}_1^v.\mathbf{M}_2^v] + \lambda_5[\mathbf{M}_1^v.\mathbf{M}_3^v] + \lambda_6[\mathbf{M}_2^v.\mathbf{M}_3^v] \end{aligned} \quad (4.39)$$

The optimization with respect to eigenvectors can be performed analytically, and has important repercussions. In Fancello, Ponthot & Stainier (2006), it is used to demonstrate that, as a consequence of using isotropic potentials depending only on eigenvalues of viscous strains, tensors of the rate of viscous stretching ($\mathbf{D}^v$), elastic isochoric strains ($\hat{\mathbf{C}}^e$) and predictor strain increment ($\hat{\mathbf{C}}^{pr}$) must be colinear. This analytic minimization is performed here as briefly as possible, so as not to burden the text.

Starting from the Lagrangian function defined in equation 4.39 above, where the restrictions on independent variables of viscous strains are imposed through the Lagrange multipliers λ, stationarity with respect to eigenvectors of viscous strains reads:

$$\frac{\partial \mathcal{L}}{\partial \mathbf{M}_i^v}[\delta \mathbf{M}_i^v] = 0, \mathbf{M}_i^v \in \mathbf{K}_M \quad (4.40)$$

It shall be useful to go back to the definitions of the logarithmic elastic strain tensor and its relation to the predictor state and the rate of viscous stretching.

$$\boldsymbol{\varepsilon}^e = \sum_{j=1}^{3} \epsilon_j^e \mathbf{M}_j^e \otimes \mathbf{M}_j^e = \boldsymbol{\varepsilon}^{pr} - \Delta t \mathbf{D}^v = \boldsymbol{\varepsilon}^{pr} - \sum_{j=1}^{3} \Delta q_j \mathbf{M}_j^v \otimes \mathbf{M}_j^v \quad (4.41)$$

$$\frac{\partial \epsilon_i^e}{\partial \boldsymbol{\varepsilon}^e} = \mathbf{M}_i^e \qquad \frac{\partial \boldsymbol{\varepsilon}^e}{\partial \mathbf{M}_i^v} = -\Delta q_i \quad (4.42)$$

Optimizing with respect to the first eigenvector $\mathbf{M}_1^v$, the stationarity condition reads as follows (indexes for individual Maxwell branches are dropped for economy of notation):

$$\begin{aligned}\frac{\partial \mathcal{L}}{\partial \mathbf{M}_1^v}[\delta \mathbf{M}_1^v] = \frac{\partial W^e}{\partial \mathbf{M}_1^v}.\delta \mathbf{M}_1^v + 2\lambda_1[\mathbf{M}_1^v.\delta \mathbf{M}_1^v]\\ + \lambda_4[\mathbf{M}_2^v.\delta \mathbf{M}_1^v] + \lambda_5[\mathbf{M}_3^v.\delta \mathbf{M}_1^v] = 0, \forall \delta \mathbf{M}_1^v \in \mathrm{Sym}\end{aligned} \quad (4.43)$$

Since the variations of the first eigenvector ($\delta\mathbf{M}_1^v$) of viscous strains are arbitrary, they can be taken equal to $\mathbf{M}_1^v$, $\mathbf{M}_2^v$ and $\mathbf{M}_3^v$, yielding expressions for the Lagrange multipliers:

$$2\lambda_1 = -\frac{\partial W^e}{\partial \mathbf{M}_1^v}.\mathbf{M}_1^v \tag{4.44}$$

$$\lambda_4 = -\frac{\partial W^e}{\partial \mathbf{M}_1^v}.\mathbf{M}_2^v \tag{4.45}$$

$$\lambda_5 = -\frac{\partial W^e}{\partial \mathbf{M}_1^v}.\mathbf{M}_3^v \tag{4.46}$$

Taking these results and going back to the optimality condition now yields:

$$\begin{aligned}\frac{\partial \mathcal{L}}{\partial \mathbf{M}_1^v}[\delta\mathbf{M}_1^v] = \Bigg\{ \frac{\partial W^e}{\partial \mathbf{M}_1^v} - \left[\frac{\partial W^e}{\partial \mathbf{M}_1^v}.\mathbf{M}_1^v\right]\mathbf{M}_1^v - \left[\frac{\partial W^e}{\partial \mathbf{M}_1^v}.\mathbf{M}_2^v\right]\mathbf{M}_2^v \\ - \left[\frac{\partial W^e}{\partial \mathbf{M}_1^v}.\mathbf{M}_3^v\right]\mathbf{M}_3^v \Bigg\}.\delta\mathbf{M}_1^v = 0, \forall \delta\mathbf{M}_1^v \in \mathrm{Sym}\end{aligned} \tag{4.47}$$

Using the definitions of logarithmic elastic tensors presented above, it is possible to expand the term $\frac{\partial W^e}{\partial \mathbf{M}_1^v}$ as follows:

$$\frac{\partial W^e}{\partial \mathbf{M}_1^v} = \sum_{i=1}^{3} \frac{\partial W^e}{\partial \epsilon_i^e}\frac{\partial \epsilon_i^e}{\partial \boldsymbol{\varepsilon}^e}\frac{\partial \boldsymbol{\varepsilon}^e}{\partial \mathbf{M}_i^v} = -\left[\sum_{i=1}^{3}\frac{\partial W^e}{\partial \epsilon_i^e}\mathbf{M}_i^e\right]\Delta q_i \tag{4.48}$$

Finally, putting all these results together results in the following expression for the optimality condition:

$$\begin{aligned}\frac{\partial \mathcal{L}}{\partial \mathbf{M}_1^v}[\delta\mathbf{M}_1^v] = \Bigg\{ \sum_{i=1}^{3}\frac{\partial W^e}{\partial \epsilon_i^e}\mathbf{M}_j^e - \sum_{i=1}^{3}\frac{\partial W^e}{\partial \epsilon_i^e}[\mathbf{M}_i^e.\mathbf{M}_1^v]\mathbf{M}_1^v \\ - \sum_{i=1}^{3}\frac{\partial W^e}{\partial \epsilon_i^e}[\mathbf{M}_i^e.\mathbf{M}_2^v]\mathbf{M}_2^v \\ - \sum_{i=1}^{3}\frac{\partial W^e}{\partial \epsilon_i^e}[\mathbf{M}_i^e.\mathbf{M}_3^v]\mathbf{M}_3^v \Bigg\}.\delta\mathbf{M}_1^v = 0, \forall \delta\mathbf{M}_1^v \in \mathrm{Sym}\end{aligned} \tag{4.49}$$

The same procedure is done for the remaining eigenvectors, $\mathbf{M}_2^v$ and $\mathbf{M}_3^v$, rendering similar equations to the one above. Given the orthogonality conditions between eigenvectors, these equations can only be satisfied if $\mathbf{M}_i^v = \mathbf{M}_i^e$. The optimality conditions with respect to eigenvectors of viscous strains thus yields the colinearity between tensors $\mathbf{D}^v$, $\hat{\mathbf{C}}^e$ and $\hat{\mathbf{C}}^{pr}$.

From here on, the optimization with respect to eigenvectors $\mathbf{M}_j^v$ is assumed *a priori*, as the colinearity of the tensors and consequent relations between their eigenvalues (equation 4.17) are used throughout.

Completing the internal variable update, it is necessary to optimize with respect to the eigenvalues of viscous strains. They represent the amplitude of viscous stretching during the time step. A reduced form of the Lagrangian may now be written:

$$\mathcal{L}(q_j) = \mathcal{H}_n^{eff}(\mathbf{C}_{n+1}, T_{n+1}; \mathbf{C}_n, q_{jn}, \mathbf{M}_{jn}^v, T_n) + \lambda_0[q_1 + q_2 + q_3] \quad (4.50)$$

Stationarity with respect to the directions q_j yields a system of nonlinear equations, which may be solved iteratively with standard Newton-Raphson schemes. In light of the choices of Helmholtz free energy and dissipated energy, specific expressions for the system of equations may easily be derived:

$$r_j = \frac{\partial \mathcal{L}}{\partial q_j} = 0, \quad j = 1, 2, 3 \quad (4.51)$$

$$\begin{aligned} r_j = \frac{\partial W}{\partial q_j} + \lambda + \frac{T_{n+1}}{T_n}\frac{1}{\Delta t}\Delta t \frac{\partial \langle \psi \rangle}{\partial q_j} \\ = \frac{\partial W^e}{\partial \epsilon_j^e}\frac{\partial \epsilon_j^e}{\partial q_j} + \lambda_0 + \frac{T_{n+1}}{T_n}\left\langle \frac{\partial \psi}{\partial \dot{q}_j} \right\rangle = 0 \quad (4.52) \end{aligned}$$

$$r_j = -\frac{\partial W^e}{\partial \epsilon_j^e} q_j + \lambda_0 + \frac{T_{n+1}}{T_n}\left\langle \frac{\partial \psi}{\partial \dot{q}_j} \right\rangle = 0 \quad (4.53)$$

The equations above are what would be obtained for dissipative terms exhibiting no history dependence on the value of q_j. In this case, the term $\frac{T_{n+1}}{T_n}\left\langle \frac{\partial \psi}{\partial \dot{q}_j} \right\rangle$ is what remains of the actually performed derivative $\Delta t \frac{\partial \langle \psi \rangle}{\partial q_j}$. In the presence of parametric dependence on q_j, additional terms appear. For a full presentation of the handling of parametric dependence and the thermodynamically accurate average of dissipation $\langle\psi\rangle$, the reader is referred to appendices A and B of this document.

There are four unknowns in the system of equations above: the three directions of viscous flow q_j and the Lagrange multiplier λ. The final equation to complete the system comes from the stationarity of the Lagrangian with respect to the Lagrange multipliers, i.e. the imposed restrictions:

$$r_4 = \frac{\partial \mathcal{L}}{\partial \lambda_0} = 0 \tag{4.54}$$

$$r_4 = \sum_{j=1}^{3} q_j = 0 \tag{4.55}$$

Newton-Raphson schemes are used for the internal variable updates of all examples presented in this document.

Once the values of viscous strains have been calculated for all material points, the effective incremental functional $\mathcal{H}_n^{eff}$ is used to determine the stress field in hyperelastic fashion. As discussed earlier, the optimality condition[4.3] with respect to the imposed strains results in the mechanical equilibrium equation, including internal and external power:

$$\frac{\partial \mathcal{H}_n^{eff}}{\partial \mathbf{C}_{n+1}} = 0 \tag{4.56}$$

It is possible to separate internal ($\mathcal{H}_n^{effInt}$) and external ($\mathcal{H}_n^{effExt}$) sources of power and dissipation additively as follows, where it is evident that the optimization with respect to internal variables of viscous strains does not influence the external power input and dissipation[4.4].

$$\mathcal{H}_n^{eff} = \mathcal{H}_n^{effInt} + \mathcal{H}_n^{effExt} \tag{4.57}$$

[4.3] A certain abuse of notation must be recognized here. Rigorously, Gâteaux derivatives with respect to independent variables should be performed, with respect to admissible variations, following the notation employed in chapter 3. Here, notations for common derivatives are used, as they translate more directly to derivatives of the different portions of the free and dissipated energies.

[4.4] For brevity of notation, the value of the Helmholtz free energy at time t_n is simply denoted: $W_n = W(\mathbf{C}_n, \mathbf{Z}_n, T_n)$.

$$
\begin{aligned}
\mathcal{H}_n^{effInt} &= \inf_{\mathbf{Z}_{n+1}} \int_\Omega \mathcal{H}_n^{loc} dV = \\
&\inf_{\mathbf{Z}_{n+1}} \int_\Omega \{[W(\mathbf{C}_{n+1}, \mathbf{Z}_{n+1}, T_{n+1}) - W_n + \rho_R \eta_n [T_{n+1} - T_n]] \\
&+\Delta t \left\langle \psi \left(\frac{T_{n+1}}{T_n} \frac{\Delta \mathbf{C}}{\Delta t}, \frac{T_{n+1}}{T_n} \frac{\Delta \mathbf{Z}}{\Delta t}; \mathbf{C}_{n+\alpha}, \mathbf{Z}_{n+\alpha}, T_{n+\alpha} \right) \right\rangle \right\} dV
\end{aligned}
\tag{4.58}
$$

$$
\begin{aligned}
\mathcal{H}_n^{effExt} &= \Delta t \{\mathcal{W}_{ext} + \mathcal{Q} + \varphi\} = \\
&\Delta t \left\{ - \int_{\partial_{\boldsymbol{\sigma}}\Omega} \bar{\mathbf{t}}_R . \dot{\mathbf{x}}_{n+1} d\Gamma - \int_\Omega \mathbf{b}_R . \dot{\mathbf{x}}_{n+1} dV \right. \\
&\left. + \int_{\partial_{\mathbf{q}}\Omega} \frac{T_{n+1}}{T_n} \bar{\mathbf{q}}_R . \mathbf{n}_R d\Gamma - \int_\Omega \left[\frac{1}{T_n} \mathbf{q}_R . \nabla T_{n+1} + \frac{T_{n+1}}{T_n} \mathrm{r}_R \right] dV \right\}
\end{aligned}
\tag{4.59}
$$

Clearly, the optimization with respect to the internal variables can be done locally in equation 4.58, as there are no gradient terms involved. The strictly local portion of the effective incremental potential (denoted $\mathcal{H}_n^{loc}$ above) may be used in order to determine the stress update at time t_{n+1}. The procedure is done in hyperelastic-like[4.5] fashion as follows:

$$
\mathbf{P}_{n+1} = 2\mathbf{F}_{n+1} \frac{\partial \mathcal{H}_n^{loc}}{\partial \mathbf{C}_{n+1}} \tag{4.60}
$$

Once again, the specifics of this derivative are directly related to the proposed generalized rheological model. The Kelvin-Voigt spring is only responsible for the volumetric part of deformations, storing energy at a rate determined by the bulk modulus. The Maxwell springs, in turn, store the isochoric elastic energy according to the shear modulus (or the equivalent combination of material parameters of the chosen model). Since every Maxwell branch is in mechanical equilibrium, no explicit contribution coming from the Maxwell dashpots appears (although they are very much present, influencing the split of elastic

---

[4.5] It is not possible to talk about proper hyperelasticity, since the proposed variational formulation includes dissipative terms, and assumed actually variationally only within a sufficiently small time step and viscous strains at every branch). Additionally, the Kelvin-Voigt dashpot is subjected to the imposed total strain rate, and contributes additively to the stress field.

$$\mathbf{P}_{n+1} = 2\mathbf{F}_{n+1}\left[\frac{\partial W^{vol}}{\partial J_{n+1}}\frac{\partial J_{n+1}}{\partial \mathbf{C}_{n+1}} + \frac{\partial W^{e}}{\partial \hat{\mathbf{C}}_{n+1}}\frac{\partial \hat{\mathbf{C}}_{n+1}}{\partial \mathbf{C}_{n+1}} \right. \\ \left. +\Delta t\left\langle\frac{\partial \psi^{KV}}{\partial \dot{\mathbf{C}}_{n+1}}\right\rangle\frac{\partial \dot{\mathbf{C}}_{n+1}}{\partial \mathbf{C}_{n+1}}\right] \tag{4.61}$$

Before putting together all this information and performing the hyperlastic-like stress update, some useful identities must be derived. The derivative of the Jacobian of $\mathbf{C}$ with respect to itself is given by:

$$\frac{\partial J}{\partial \mathbf{C}} = \frac{J}{2}\mathbf{C}^{-1} \tag{4.62}$$

Next, the derivative of the isochoric part of $\mathbf{C}$ with respect to itself is then given by:

$$\frac{\partial \hat{\mathbf{C}}}{\partial \mathbf{C}} = J^{-\frac{2}{3}}\left[\mathcal{I} - \frac{1}{3}\mathbf{C}\otimes\mathbf{C}^{-1}\right] \tag{4.63}$$

Going back to the hyperelastic-like stress update of equation 4.60, taking into account the additive decomposition of stored and dissipated energies, it now reads as follows:

$$\mathbf{P}_{n+1} = 2\mathbf{F}_{n+1}\left\{J^{-\frac{2}{3}}\left[\frac{\partial W^{e}}{\partial \hat{\mathbf{C}}_{n+1}} - \frac{1}{3}\left(\frac{\partial W^{e}}{\partial \hat{\mathbf{C}}_{n+1}} : \mathbf{C}_{n+1}\right)\mathbf{C}_{n+1}^{-1}\right] \right. \\ \left. +\frac{\partial W^{vol}}{\partial J_{n+1}}\frac{J_{n+1}}{2}\mathbf{C}_{n+1}^{-1} + \frac{T_{n+1}}{T_n}\left\langle\frac{\partial \psi^{KV}}{\partial \dot{\mathbf{C}}_{n+1}}\right\rangle\right\} \tag{4.64}$$

The following notation is used for the deviatoric part of a second order tensor:

$$\mathrm{DEV}(\mathbf{A}) = \left[\mathbf{A} - \frac{1}{3}(\mathbf{A} : \mathbf{C})\mathbf{C}^{-1}\right] \tag{4.65}$$

This slims the notation on the previous equation somewhat, and renders the influence of individual rheological elements to the stress tensor clearer:

$$\mathbf{P}_{n+1} =$$

$$\mathbf{F}_{n+1}\left\{\overbrace{\underbrace{J^{-\frac{2}{3}}\mathrm{DEV}\left(2\frac{\partial W^{e}}{\partial \hat{\mathbf{C}}_{n+1}}\right)}_{\text{MX springs}}+\underbrace{\frac{\partial W^{vol}}{\partial J_{n+1}}J_{n+1}\mathbf{C}_{n+1}^{-1}}_{\text{K-V spring}}}^{\text{Conservative stress}}+\overbrace{\underbrace{\frac{T_{n+1}}{T_{n}}\left\langle\frac{\partial \psi^{KV}}{\partial \dot{\mathbf{C}}_{n+1}}\right\rangle}_{\text{K-V dashpot}}}^{\text{Dissipative stress}}\right\} \tag{4.66}$$

Only the specific expressions for the derivatives of the potentials with respect to their independent variables remain to be calculated. This is determined by the final form of the potentials chosen for each portion of stored and dissipated energy, and is therefore omitted from the text here. However, it is important to remember that, granted the optimization with respect to viscous directions, the colinearity of predictor, viscous and isochoric elastic tensors can be used in order to derive simple relations on eigenvalues of strains only.

Analogously to what has just been derived for stresses, the entropy update is also obtained variationally. As discussed in the previous chapter, the Helmholtz free energy serves as a potential for entropy[4.6] (see equation 3.30):

$$\rho_R \eta_{n+1} = -\frac{\partial W}{\partial T_{n+1}} \tag{4.67}$$

In the variational framework for thermomechanical problems, stationarity with respect to temperature yields the final necessary equation to fully describe the problem, namely, the first law of thermodynamics in entropy form[4.7].

$$\frac{\partial \mathcal{H}_{n}^{eff}}{\partial T_{n+1}} = 0 \tag{4.68}$$

Recalling all the temperature dependent behavior allowed in the proposed forms of the potentials proposed in the previous subsection, and other sources of thermomechanical coupling, the entropy update equation reads as follows (the divergence theorem is used to remove

---

[4.6] As the effective incremental potential is formulated in reference configuration, the entropy measure derived from it is also related to the reference configuration η_R. In the incremental expressions presented here, though, the index R was dropped for simplicity, so as not to meddle with the index for time increment $n+1$

[4.7] See footnote 4.3 for a disclaimer on the used notation.

boundary integrals, and a local form of the equation is presented):

$$\rho_R \eta_{n+1} = -\left[\frac{\partial W^e}{\partial T_{n+1}} + \frac{\partial W^{vol}}{\partial T_{n+1}} + \frac{\partial W^h}{\partial T_{n+1}}\right] = \overbrace{\left[\Delta t \frac{\dot{c}_j}{T_n}\left\langle \frac{\partial \psi^{KV}}{\partial \dot{c}_j}\right\rangle + \Delta t \frac{\dot{q}_j}{T_n}\left\langle \frac{\partial \psi^{MX}}{\partial \dot{q}_j}\right\rangle\right]}^{\text{Internal dissipation}=\mathcal{D}_{int}} + \rho_R \eta_n + \Delta t \mathrm{Div}\left(\frac{\mathbf{q}_R}{T_n}\right) + \Delta t \frac{\mathrm{r}_R}{T_n} \qquad (4.69)$$

Clearly, viscous dissipation on the dashpots in Maxwell and Kelvin-Voigt branches is the source of internal dissipation (as defined earlier, for general dissipative solids: $\mathcal{D}_{int} = \mathbf{Y} : \dot{\mathbf{Z}} \geq 0$).

Furthermore, as previously discussed in the presentation of the thermodynamic basis of constitutive modeling, constitutive equations for heat capacity (defined in equation 3.33 as the derivative of entropy with respect to temperature) cannot be defined independently from constitutive equations for stress[4.8]. This is clear in the proposed variational formulation, based on the properties of the Helmholtz free energy as a potential for stress and entropy.

Due to the factorization of dissipative processes with the temperature term $\frac{T_{n+1}}{T_n}$ proposed in Yang, Stainier & Ortiz (2006), it is possible to see that cross derivatives of the effective incremental potential (with respect to independent variables of temperature and strains) commute, in a clear demonstration of the symmetry of the formulation. Further details on symmetry will become evident in the following subsection, where the material tensor is derived.

4.5 DERIVATION OF THE TANGENT MODULI: MECHANICAL PART, THERMOMECHANICAL COUPLING AND HEAT CAPACITY

Efficient implementation of constitutive models often demands the derivation of tangent moduli. Coming into play mainly during stress update routines, the tangent moduli (sometimes referred to as material tensors) are commonly defined as the total derivative of stress with respect to strains (for purely mechanical problems), and are therefore

---

[4.8] See equation 3.34 for details on the coupling terms.

fourth-order tensors:

$$\mathbb{C}_{mech} = \frac{d}{d\mathbf{C}_{n+1}} \left(\frac{\partial \mathcal{H}_n^{loc}}{\partial \mathbf{C}_{n+1}} \right) \tag{4.70}$$

In the thermomechanically-coupled context, since temperature is an independent variable, additional tangent moduli come into play, accounting for both purely thermal effects and thermomechanical coupling.

The thermomechanical coupling term $\mathbb{C}_{thm}$, can be defined as the total derivative of the entropy with respect to strains (or equivalently, from the derivative of strains with respect to temperature, as the formulation is symmetric), and is therefore a second order tensor.

$$\mathbb{C}_{thm} = \frac{d}{d\mathbf{C}_{n+1}} \left(\frac{\partial \mathcal{H}_n^{loc}}{\partial T_{n+1}} \right) \tag{4.71}$$

The purely thermal tangent term $\mathbb{D}$, as discussed later on in this section, can be seen as a modified heat capacity, and is generally defined as:

$$\mathbb{D} = \frac{d}{dT_{n+1}} \left(\frac{\partial \mathcal{H}_n^{loc}}{\partial T_{n+1}} \right) \tag{4.72}$$

In the special case of adiabatic problems, as pointed out in the discussion leading up to equation 3.48, the absence of temperature gradient terms linked to heat conduction renders the temperature update strictly local. In other words, temperature can be treated as an additional internal variable. Thermomechanical coupling terms $\mathbb{C}_{thm}$ similar to those defined above still appear, though. Instead of a simple partial derivative, the tangent modulus accounts for the total variation, which can be shown to include two distinct terms: one purely mechanical and one due to thermomechanical coupling.

$$\begin{aligned} \mathbb{C} = \frac{d}{d\mathbf{C}_{n+1}} \left(\frac{\partial \mathcal{H}_n^{loc}}{\partial \mathbf{C}_{n+1}} \right) \\ = \underbrace{\frac{\partial}{\partial \mathbf{C}_{n+1}} \frac{\partial \mathcal{H}_n^{loc}}{\partial \mathbf{C}_{n+1}}}_{\mathbb{C}_{mech}} + \underbrace{\frac{\partial}{\partial T_{n+1}} \frac{\partial \mathcal{H}_n^{loc}}{\partial \mathbf{C}_{n+1}} \frac{\partial T_{n+1}}{\partial \mathbf{C}_{n+1}}}_{\mathbb{C}_{thm}} \end{aligned} \tag{4.73}$$

The first term ($\mathbb{C}_{mech}$), the second derivative with respect to imposed strains, can be easily be calculated from the proposed expressions of the potentials. The second term ($\mathbb{C}_{thm}$), now including the derivative $\frac{\partial T_{n+1}}{\partial \mathbf{C}_{n+1}}$, accounts for all the thermomechanical coupling terms.

Stresses are additively decomposed as follows, as in equation 4.66, in first Piola-Kirchhoff form:

$$\mathbf{P}^{e}_{n+1} = \mathbf{F}_{n+1} J^{-\frac{2}{3}} \mathrm{DEV} \left(2 \frac{\partial W^{e}}{\partial \hat{\mathbf{C}}_{n+1}} \right) \tag{4.74}$$

$$\mathbf{P}^{vol}_{n+1} = \mathbf{F}_{n+1} \frac{\partial W^{vol}}{\partial J_{n+1}} J_{n+1} \mathbf{C}^{-1}_{n+1} \tag{4.75}$$

$$\mathbf{P}^{v}_{n+1} = \mathbf{F}_{n+1} \frac{T_{n+1}}{T_{n}} \left\langle \frac{\partial \psi^{KV}}{\partial \dot{\mathbf{C}}_{n+1}} \right\rangle \tag{4.76}$$

So too is the tensor modulus, which can be expressed as follows:

$$\mathbb{C}_{mech} = \mathbb{C}^{e}_{mech} + \mathbb{C}^{vol}_{mech} + \mathbb{C}^{v}_{mech} \tag{4.77}$$

The individual parts are derived from the following expressions. A slight abuse of notation in the viscous term has to be recognized, where the average along the time step is used rather freely:

$$\mathbb{C}^{e}_{mech} = \frac{d}{d\mathbf{C}_{n+1}} \frac{\partial W^{e}}{\partial \mathbf{C}_{n+1}} \tag{4.78}$$

$$\mathbb{C}^{vol}_{mech} = \frac{d}{d\mathbf{C}_{n+1}} \frac{\partial W^{e}}{\partial \mathbf{C}_{n+1}} \tag{4.79}$$

$$\mathbb{C}^{v}_{mech} = \frac{d}{d\mathbf{C}_{n+1}} \left(\frac{T_{n+1}}{T_{n}} \left\langle \frac{\partial \psi^{KV}}{\partial \mathbf{C}_{n+1}} \right\rangle \right) \tag{4.80}$$

In addition to the purely mechanical terms outlined above, thermomechanically-coupled parts are present for each of the terms: the tangent modulus of the Kelvin-Voigt spring ($\mathbb{C}^{vol}_{thm}$), that of the Maxwell springs ($\mathbb{C}^{e}_{thm}$) and the one related to the Kelvin-Voigt dashpot ($\mathbb{C}^{v}_{thm}$).

So as not to encumber the text with lengthy derivations, only the deduction of the Maxwell springs tangent moduli (mostly $\mathbb{C}^{e}_{mech}$, but also some aspects of $\mathbb{C}^{e}_{thm}$) is presented here. In many ways, it constitutes the most interesting example, since the internal variables of viscous strains play a central role, whereas the other terms of the tensor modulus involve only the global variables of temperature and total strains.

As alluded to earlier, the proposed variational formulation is consistent with predictor-corrector schemes. In figure 4.2, the predictor tensor is graphically represented. The predictor state is a natural choice for the initialization of Newton-Raphson schemes to determine the internal variable update. It is therefore common to use eigenvalues of the predictor state as independent variables (which is equivalent to using eigenvalues of viscous strains, as they are related through equation 4.17). The numerical tests presented at the end of the present chapter received such a treatment. The rest of the derivation of the tangent modulus was performed using this format.

The definition of the right Cauchy-Green predictor (equation 4.11) is recalled:

$$\hat{\mathbf{C}}^{pr} = \mathbf{F}_n^{v-T} \hat{\mathbf{C}}_{n+1} \mathbf{F}_n^{v-1} \tag{4.81}$$

Now, going back to the definition of the tensor modulus of the Maxwell springs, it is possible to use the chain rule as follows:

$$\mathbb{C}^e = \frac{d}{d\mathbf{C}_{n+1}} \frac{\partial W^e}{\partial \mathbf{C}_{n+1}} = \frac{d}{d\hat{\mathbf{C}}_{n+1}} \left(\frac{\partial W^e}{\partial \mathbf{C}_{n+1}} \right) \frac{\partial \hat{\mathbf{C}}_{n+1}}{\partial \mathbf{C}_{n+1}} \tag{4.82}$$

In addition, recalling the expression for the derivative of the isochoric part of the right Cauchy-Green tensor with respect to itself, given in equation 4.63, it is possible to isolate the strictly kinematic from the actual constitutive aspects. In order to keep notations fairly simple, it is desirable to restrict focus to the isochoric part of tensor $\mathbf{C}_{n+1}$, by redefining this part of the tangent modulus as follows:

$$\mathbb{C}^e = \frac{d}{d\hat{\mathbf{C}}_{n+1}} \left(\frac{\partial W^e}{\partial \hat{\mathbf{C}}_{n+1}} \right) \tag{4.83}$$

As before, the chain rule is applied, yielding expressions based on the predictor state. Indicial notation is used. The index $n+1$ pertaining to the time step is dropped for simplicity. The terms in brackets, derivatives of the predictor state with respect to the isochoric part of the right Cauchy-Green strain tensor, give rise to fourth order identity tensors, denoted $\mathcal{I}_{ijkl}$.

$$\begin{aligned}
\mathbb{C}^{e}_{ijkl} &= \frac{d}{d\hat{\mathbf{C}}_{kl}}\left(\frac{\partial W^{e}}{\partial \hat{\mathbf{C}}_{ij}}\right) \\
&= \frac{d}{d\hat{\mathbf{C}}_{kl}}\left(\frac{\partial W^{e}}{\partial \hat{\mathbf{C}}^{pr}_{mt}}\frac{\partial \hat{\mathbf{C}}^{pr}_{mt}}{\partial \hat{\mathbf{C}}_{ij}}\right) = \frac{d}{d\hat{\mathbf{C}}^{pr}_{pq}}\left(\frac{\partial W^{e}}{\partial \hat{\mathbf{C}}^{pr}_{mt}}\frac{\partial \hat{\mathbf{C}}^{pr}_{mt}}{\partial \hat{\mathbf{C}}_{ij}}\right)\frac{\partial \hat{\mathbf{C}}^{pr}_{pq}}{\partial \hat{\mathbf{C}}_{kl}} \\
&= \frac{d}{d\hat{\mathbf{C}}^{pr}_{pq}}\frac{\partial W^{e}}{\partial \hat{\mathbf{C}}^{pr}_{mt}}\left[\frac{\partial\left(\hat{\mathbf{F}}^{v-T}_{mr}\hat{\mathbf{C}}_{rs}\hat{\mathbf{F}}^{v-1}_{st}\right)}{\partial \hat{\mathbf{C}}_{ij}}\right]\left[\frac{\partial\left(\hat{\mathbf{F}}^{v-T}_{pu}\hat{\mathbf{C}}_{uv}\hat{\mathbf{F}}^{v-1}_{vq}\right)}{\partial \hat{\mathbf{C}}_{kl}}\right] \\
&= \hat{\mathbf{F}}^{v-1}_{rm}\hat{\mathbf{F}}^{v-1}_{up}\left(\frac{d}{d\hat{\mathbf{C}}^{pr}_{pq}}\frac{\partial W^{e}}{\partial \hat{\mathbf{C}}^{pr}_{mt}}\right)\hat{\mathbf{F}}^{v-1}_{st}\hat{\mathbf{F}}^{v-1}_{vq}\mathcal{I}_{rsij}\mathcal{I}_{uvkl} \\
&= \hat{\mathbf{F}}^{v-1}_{im}\hat{\mathbf{F}}^{v-1}_{kp}\left(\frac{d}{d\hat{\mathbf{C}}^{pr}_{pq}}\frac{\partial W^{e}}{\partial \hat{\mathbf{C}}^{pr}_{mt}}\right)\hat{\mathbf{F}}^{v-1}_{jt}\hat{\mathbf{F}}^{v-1}_{lq}
\end{aligned} \tag{4.84}$$

In the above equation, pre and post multiplication by the viscous strain gradient is a purely kinematic operation. The actual constitutive information lies in the term in parentheses of the last expression.

As mentioned earlier for the total tensor modulus for the special case of adiabatic problems, taking the total variation with respect to imposed strains generates two distinct parts: one purely mechanical and a thermomechanical coupling term:

$$\frac{d}{d\hat{\mathbf{C}}^{pr}}\frac{\partial W^{e}}{\partial \hat{\mathbf{C}}^{pr}} = \frac{\partial}{\partial \hat{\mathbf{C}}^{pr}}\frac{\partial W^{e}}{\partial \hat{\mathbf{C}}^{pr}} + \frac{\partial}{\partial T}\frac{\partial W^{e}}{\partial \hat{\mathbf{C}}^{pr}}\frac{\partial T}{\partial \hat{\mathbf{C}}^{pr}} \tag{4.85}$$

It is useful to recall the following definitions (where the colinearity of the viscous and predictor tensors may be used):

$$\hat{\mathbf{C}}^{pr} = \sum_{j=1}^{3} c^{pr}_{j}\mathbf{M}^{pr}_{j}\otimes\mathbf{M}^{pr}_{j} \tag{4.86a}$$

$$\boldsymbol{\varepsilon}^{pr} = \frac{1}{2}\ln\hat{\mathbf{C}}^{pr} = \sum_{j=1}^{3}\epsilon^{pr}_{j}\mathbf{M}^{pr}_{j}\otimes\mathbf{M}^{pr}_{j}, \quad \text{with} \quad \epsilon^{pr}_{i} = \frac{1}{2}\ln c^{pr}_{i} \tag{4.86b}$$

$$\epsilon^{pr}_{i} = \epsilon^{e}_{i} - \Delta q_{i}, \quad \text{with} \quad \Delta q_{i} = \Delta t q_{i} \tag{4.86c}$$

Taking the mechanical term ($\mathbb{C}^{e}_{mech}$) as a first step, it now reads:

$$\begin{aligned}\frac{\partial W^e}{\partial \hat{\mathbf{C}}^{pr}} &= \sum_{j=1}^{3} \frac{\partial W^e}{\partial c_j^{pr}} \frac{\partial c_j^{pr}}{\partial \hat{\mathbf{C}}^{pr}} = \sum_{j=1}^{3} \frac{\partial W^e}{\partial c_j^{pr}} \mathbf{M}_j^{pr} \\ &= \sum_{j=1}^{3} \frac{\partial W^e}{\partial \epsilon_j^e} \frac{\partial \epsilon_j^e}{\partial \epsilon_j^{pr}} \frac{\partial \epsilon_j^{pr}}{\partial c_j^{pr}} \mathbf{M}_j^{pr} = \sum_{j=1}^{3} \frac{\partial W^e}{\partial \epsilon_j^e} \frac{1}{2c_j^{pr}} \mathbf{M}_j^{pr} \qquad (4.87)\end{aligned}$$

Taking into account the proposed structure of the Helmholtz free energy and dissipation terms, namely their proposed isotropy (translated in their explicit dependence on principal values of viscous strains), two terms are involved in calculating the total second derivative: a first term related to the variation of viscous eigenvectors with respect to strains, and a second term related to the variation of viscous eigenvalues.

$$\begin{aligned}&\frac{d}{d\hat{\mathbf{C}}^{pr}} \left(\frac{\partial W^e}{\partial \hat{\mathbf{C}}^{pr}} \right) = \\ &\qquad \frac{\partial}{\partial c_j^{pr}} \left(\frac{\partial W^e}{\partial \hat{\mathbf{C}}^{pr}} \right) \frac{\partial c_j^{pr}}{\partial \hat{\mathbf{C}}^{pr}} + \frac{\partial}{\partial \mathbf{M}_j^{pr}} \left(\frac{\partial W^e}{\partial \hat{\mathbf{C}}^{pr}} \right) \frac{\partial \mathbf{M}_j^{pr}}{\partial \hat{\mathbf{C}}^{pr}} \qquad (4.88)\end{aligned}$$

By using properties of spectral decomposition, it is possible to write:

$$\begin{aligned}&\frac{\partial}{\partial \mathbf{M}_j^{pr}} \left(\frac{\partial W^e}{\partial \hat{\mathbf{C}}^{pr}} \right) \frac{\partial \mathbf{M}_j^{pr}}{\partial \hat{\mathbf{C}}^{pr}} = \\ &\left[\frac{\partial W^e}{\partial \epsilon_j^e} \frac{1}{2c_j^{pr}} \right] \frac{\partial \mathbf{M}_j^{pr}}{\partial \hat{\mathbf{C}}^{pr}} = \left[\frac{\partial W^e}{\partial \epsilon_j^e} \frac{1}{2c_j^{pr}} \right] \mathbf{M}_j^{pr} \otimes \left(c_j^{pr} \mathcal{I} - \hat{\mathbf{C}}^{pr} \right)^{-1} \qquad (4.89)\end{aligned}$$

In turn, the constitutive essence of the mechanical part of the Maxwell tangent modulus, obtained by the partial derivative with respect to the eigenvalues of strains, reads as follows:

$$\frac{\partial}{\partial c_j^{pr}}\left(\frac{\partial W^e}{\partial \epsilon_i^e}\frac{1}{2c_i^{pr}}\right) = \frac{\partial^2 W^e}{\partial \epsilon_i^e \partial c_j^{pr}}\frac{1}{2c_i^{pr}} - \frac{\partial W^e}{\partial \epsilon_i^e}\frac{1}{2[c_j^{pr}]^2}\delta_{ij}$$

$$= \frac{\partial^2 W^e}{\partial \epsilon_i^e \partial \epsilon_i^e}\underbrace{\left[\frac{\partial \epsilon_i^e}{\partial \epsilon_j^{pr}}\right]}_{\text{I}}\frac{1}{4c_i^{pr}c_j^{pr}} - \frac{\partial W^e}{\partial \epsilon_i^e}\frac{1}{2[c_j^{pr}]^2}\delta_{ij} \qquad (4.90)$$

What is left to determine is the derivative marked I in the last equation. It is possible to show that it can be calculated using the same tangent matrix used for the update of internal variables. It suffices to take derivatives of stationarity equations of the Lagrangian function (conditions r_i and r_4 in 4.52 and 4.55, respectively) with respect to the eigenvalues of the predictor state and solve the resulting nonlinear system. For details, the interested reader is referred to appendix C of the present document. The procedure is analogous to that of the appendix in (SELKE, 2009), for themomechanically-coupled viscoplasticity problems.

Next, going back to the expression for the adiabatic problem, the thermomechanical part ($\mathbb{C}^e_{thm}$) can be derived as follows, using the same set of relations:

$$\frac{\partial}{\partial T}\left(\frac{\partial W^e}{\partial \hat{\mathbf{C}}^{pr}}\right)\frac{\partial T}{\partial \hat{\mathbf{C}}^{pr}} =$$

$$\left\{\left[\sum_{i=1}^{3}\frac{\partial^2 W^e}{\partial T \partial \epsilon_i^e}\frac{1}{2c_i^{pr}}\right]\underbrace{\left[\frac{\partial T}{\partial \epsilon_j^{pr}}\right]}_{\text{II}}\left[\frac{1}{2c_j^{pr}}\right]\right\}\mathbf{M}_j^{pr} \qquad (4.91)$$

The determination of the derivative marked II in the equation above can be done taking the derivative of the first law of thermodynamics (obtained variationally by the stationarity of the incremental potential with respect to temperature) with respect to the eigenvalues of the elastic predictor. Details can likewise be found in appendix C.

Having dealt with the purely mechanical and the thermomechanical coupling parts of the tangent modulus, it is important to discuss the tangent operator responsible for the purely thermal response of the material. In chapter 3, during the discussion on the continuum mechanics and thermodynamics behind constitutive modeling, the heat capacity was defined in equation 3.33 as follows:

$$\mathcal{C}(\mathbf{C}, \mathbf{Z}, T) = T\frac{\partial \eta_R}{\partial T} = -T\frac{\partial^2 W}{\partial T^2} \tag{4.92}$$

Given the role of the Helmholtz free energy as a potential for entropy, it is clear that the heat capacity, the second temperature derivative in the purely thermal context, can be regarded as a counterpart to the tensor modulus. In fact, if the tensor modulus is derived from the total variation of the stresses (in turn derived from internal part of the effective potential $\mathcal{H}_n^{effInt}$) with respect to the imposed strains, one way of analogously defining a heat capacity-like quantity (denoted $\mathbb{D}$, to differentiate from the previous definition of the heat capacity) is through the total variation of entropy (also derived from the effective potential as in equation 4.69) with respect to temperature:

$$\mathbb{D} = \frac{d}{dT_{n+1}}\frac{\partial \mathcal{H}_n^{loc}}{\partial T_{n+1}} \tag{4.93}$$

It can be shown to be a modified version of the classical definition of the heat capacity. It includes the second temperature derivative of the Helmholtz free energy, as well as internal dissipation terms and the value of entropy at the previous time step.

Finally, the total tangent operator ($\mathbb{T}$), including purely mechanical, thermo-mechanically-coupled and purely thermal terms can be shown to be symmetric and has the following structure:

$$\mathbb{T} = \begin{bmatrix} \mathbb{C}_{mech} & \mathbb{C}_{thm} \\ \mathbb{C}_{thm} & \mathbb{D} \end{bmatrix} \tag{4.94}$$

Symmetric tangent operators are an advantage of the thermomechanical formulation proposed in Yang, Stainier & Ortiz (2006) and derived articles over other formulations. In fact, the authors show that even trying to naïvely generate a variational formulation of thermomechanics is not guaranteed to render tangent operators fully symmetric. It is only through the use of the temperature factor for all dissipation mechanisms that this property is guaranteed. This in turn accelerates the solution procedure, since it allows for the use of techniques that take advantage of the symmetries.

4.6 AN ALGORITHMIC VIEW OF THE INCREMENTAL VARIATIONAL CONSTITUTIVE UPDATES

Throughout the present chapter, all the necessary components of the variational formulation of thermo-viscoelasticity were laid out. First, a set of internal variables was chosen and specific forms of the potentials were explored. The actual variational formulation was then described, based on the time discretization of the rate-based variational principle. Special attention was given to the strictly local internal variable update. Next, expressions for stress and entropy update were derived. Finally, the steps toward consistent tangent moduli were presented.

However, the full presentation of the model involves many intermediary steps, often not directly involved in the implementation of the model. A clear picture of the necessary effort to implement the proposed variational model comes from an algorithmic overview of the necessary operations, the subject of this very short subsection.

The full thermodynamic state is assumed known at time t_n, namely, all the independent variables ($\mathbf{C}_n$, T_n, q_{jn}, $\mathbf{M}_{jn}$), their power conjugates or thermodynamic forces (especially stresses $\mathbf{P}_n$ and entropy η_n) and the value of the stored free energy (W_n). At time t_{n+1}, the load is considered applied through imposed values of the global variables: $\mathbf{C}_{n+1}$ and T_{n+1}. The variational constitutive update procedure then follows:

1. From the imposed value of $\mathbf{C}_{n+1}$ and from the known value of $\mathbf{C}_n$, the predictor state $\mathbf{C}^{pr}_{n+1}$ is determined through equation 4.11. A spectral decomposition is performed, determining the eigenvectors shared by the Maxwell viscous strains tensor, as a consequence of the stationarity condition with respect to internal variables $\mathbf{M}^v_j$ (equation 4.49).

2. The internal variable update, essentially local, is performed by solving the nonlinear system of equations 4.52 and 4.55. A Newton-Raphson scheme is used, based on the construction of a tangent matrix to this system of equations. At this point, in addition to the imposed global variables, all the internal variables are known.

3. The value of the Helmholtz free energy at the end of the time step (W_{n+1}) is stored. Additionally, an effective incremental potential is built through equations 4.57, 4.58 and 4.59.

4. Stresses at the end of the time step ($\mathbf{P}_{n+1}$) are updated in hyperelastic-like fashion through equation 4.66.

5. Entropy is also updated from the stationarity of the effective incremental potential, through equation 4.69.

6. Tangent moduli can also be calculated through expressions like equations 4.73 and 4.93. For the case of imposed forces or heat fluxes (instead of displacements and temperatures), the tangent moduli are used to assess convergence with respect to the mechanical equilibrium equation (equation 4.56), and the entropy form of the first law of thermodynamics (equation 4.68, which gives rise to equation 4.69), until total strains and temperature fields are correctly calculated.

7. All the values of the independent variables, stress conjugates and stored energy are then stored, and the algorithm may continue to the next time step.

This type of algorithm was used in the implementation of the proposed model of thermo-viscoelasticity. Some simple numerical results are shown in the final subsection of this chapter, in order to illustrate the main features that can be reproduced by the model.

With the discussion in section 2.5 on the limitations of the proposed models in mind, some modeling alternatives are discussed in the next subsection.

4.7 FINITE THERMO-VISCOELASTICITY: LIMITATIONS AND MODELING ALTERNATIVES

In chapter 2, a microstructural description of the behavior of polymer chains under various kinds of loading established the need for the inclusion of large strains phenomena, viscosity effects and temperature dependence in modeling efforts.

The finite thermo-viscoelasticity model presented in the previous subsections aims at providing the necessary tools to tackle these requirements, while remaining a fairly simply structured and versatile. In other words, instead of leaning on a richer set of internal variables to account for microstructural complexity, such as polymer fiber orientation, or including constitutive elements able to deal with different kinds of deformations, such as plasticity, the proposed model offers the possibility of including a variety of phenomena by the addition of an arbitrary number of viscoelastic rheological elements to the generalized structure of figure 4.1.

While this has the advantage of encompassing both simpler and more elaborate material models in a unified framework, it can also lead to some limitations. For instance, as exposed in section 2.5, while polymers exhibit recovery of original dimensions along very large time periods, which is in tune with the use of viscoelasticity elements with characteristic times of diverse magnitudes, observed phenomena are often more in tune with (visco)plasticity models, for the time frame of reference. This is issue is not addressed in the present text.

However, as mentioned in the review of variational formulations of chapter 3, thermomechanically-coupled viscoplasticity has been studied in the same variational approach employed here in the works of Stainier & Ortiz (2010), Stainier (2011), Stainier (2013) and Selke (2009), among others. The inclusion of viscoplasticity rheological elements into the model of figure 4.1, which would require a complete overhaul of the proposed model, starting from the choice of internal variables, on to the description of yield functions and down to the update of internal variables, strains and tensor moduli, is left for future works.

An issue that can be addressed in briefer terms within the present subsection is the hypothesis of isochoric viscous strains. A staple of the inelastic modeling of metals, this assumption is commonly adopted in the constitutive modeling of different classes of materials. It was the chosen strategy here, although, as mentioned earlier, there is evidence pointing to the existence of volumetric inelastic deformations in polymers. In the following, the impact of considering volumetric viscous strains is considered.

If viscous strains were free of the isochoric constraint, their set of eigenvalues would no longer be restricted to the set K_q of equation 4.6. In turn, this would eliminate the constrained optimization with respect to eigenvalues q_j in the Lagrangian of equations 4.39 and 4.50, thus eliminating Lagrange multiplier λ_0.

Additionally, the exponential mapping of viscous increments, adopted in large part because of its property of providing isochoric viscous strains, could be substituted by a different class of functions.

Clearly, though, the main change to the proposed model would come from the addition of dissipative terms to the dissipation pseudo-potentials. Terms of the following kind would be expected, with a renewed set of parameters to identify:

$$\psi^{vol}\left(\frac{T_{n+1}}{T_n}\frac{\Delta J^v}{\Delta t}; J^v_{n+\alpha}, T_{n+\alpha}\right), \qquad \text{where } J^v = \det \mathbf{F}^v \tag{4.95}$$

As for the addition of any new dissipation source, this adds new terms to the internal dissipation during entropy update, changes the stress update expressions and alters all tangent moduli due to thermomechanical coupling. Details on these procedures are left for future works, but the developments for volumetric plastic strains developed in Vassoler (2009) can serve a starting point for the inclusion of volumetric viscoelasticity into the proposed model presented earlier.

4.8 SAMPLE NUMERICAL TESTS: CONSISTENCY TESTS AT A SINGLE MATERIAL POINT

In order to evaluate the types of material behaviors that can be described with the proposed variational model of thermo-viscoelasticity, consistency tests in a single material point are usually performed.

Through simply imposed boundary conditions on a fictitious element, a considerable range of phenomena can be simulated, including: uniaxial tests in compression or tension, pure shearing tests, cyclic loading, relaxation and creep test, among many others. These tests constitute the first step before moving on to larger scale applications, where geometry effects start to have an influence.

All the following examples were run using displacement-driven loading cycles.

Since a single material point is considered, heat flux loses most of its original sense, as there are no neighboring elements and therefore no temperature gradients. Clearly, simple ways to circumvent this limitation could have been used, for example, by imposing temperatures through time so as to simulate the effect of conduction, or by adding a scalar heat exchange term depending on the difference between local and reference temperatures. This was not done here, though. Furthermore, no heat generation was considered. In other words, adiabatic conditions were considered for all the examples.

In doing so, it is possible to clearly identify the local generation of heat through dissipation, due to the assumed full thermomechanical coupling. For every application, such a term is present. When temperatures are imposed, the excess heat generated locally has to be dissipated through heat conduction in order to keep isothermal con-

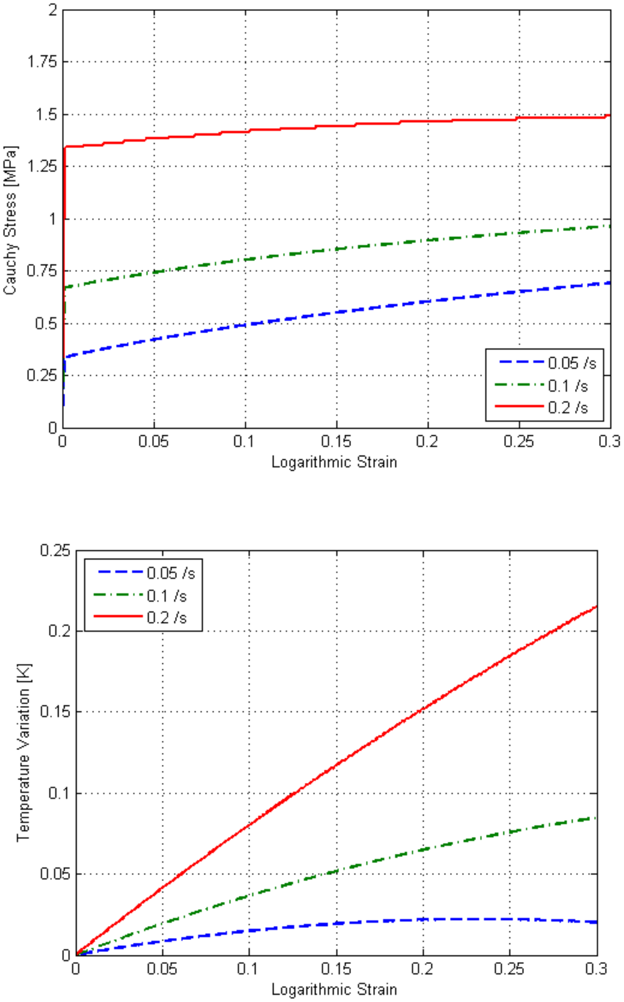

Figure 4.3 – Application of the variational thermo-viscoelasticity model to a uniaxial tensile test at different strain rates: joint determination of stress-strain and temperature-strain curves.

ditions. On the other hand, when heat flux is imposed, temperature increases both due to this imposed heat power and to local heat generation. In this context, studying adiabatic cases is an elegant way of isolating the contribution of internal dissipation towards the local variation of temperature.

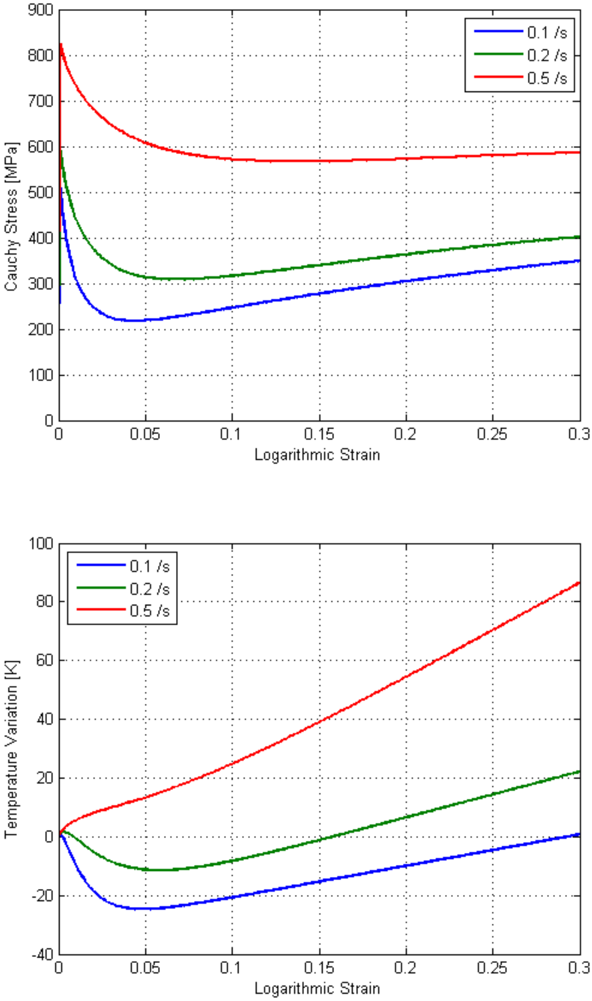

Figure 4.4 – Uniaxial tensile test at different strain rates of a Kelvin-Voigt element with Ogden-type viscous behavior: joint determination of highly nonlinear stress-strain and temperature-strain curves.

Assuming adiabatic conditions has deep effects upon the mathematical structure of the problem, since temperature becomes an additional internal variable and can be updated locally (STAINIER; ORTIZ, 2010; SELKE, 2009). The optimality condition with respect to temperature (equation 4.68, no longer including gradient terms) can then be included into the nonlinear system of equations of equations 4.52 and 4.55. This changes the tangent operators used in the Newton-Raphson scheme (for details, in an adiabatic thermo-viscoplastic setting, the interested reader is referred to Selke (2009)).

The first example is a tensile test performed at three different strain rates, in figure 4.3. In the underlying rheological model of figure 4.1, one Kelvin-Voigt branch is used in conjunction to two Maxwell branches. In doing so, many characteristic relaxation times are present: one associated to the Kelvin-Voigt dashpot, and two associated to the Maxwell dashpots. Hencky-type potentials are used for the elastic part of the stored energy W^e and for the dissipation potentials. Material parameters are not chosen to represent any specific kind of material. Rather, the results of this first test are to be taken merely qualitatively, evidencing the unified determination of stress-strain and temperature-strain curves and the possibility of describing strong strain rate dependence, a typical phenomenon in polymers. Simple adjustments of material parameters would be sufficient to change the observed behavior, so as to fit with experiments.

The markedly different behavior of Ogden-type potentials is evidenced in figure 4.4. A single Kelvin-Voigt element is employed (a spring in parallel to a dashpot). The elastic potential is of Hencky-type, quadratic in eigenvalues of elastic strains. The viscous potential, on the other hand, is modeled with an Ogden-type potential. This brings a dose of non-linearity to the model clearly reflected in the predicted stress and temperature behaviors. Three different characteristic times are captured in the proposed Ogden potential, and their interplay is responsible for the initial spike in stresses, followed by some softening before stiffening once more.

Strain rate influence can also be simulated through the common relaxation tests. While displaying limitations when used under creep conditions (when a constant force is applied), Maxwell rheological elements perform well in relaxation. By running relaxations tests at three different imposed strain rates, in figure 4.5, the underlying character explored in the time-temperature equivalence principle is evidenced qualitatively. It should be noted, however, that thermomechanical coupling affects material parameters through the relaxation process, and large

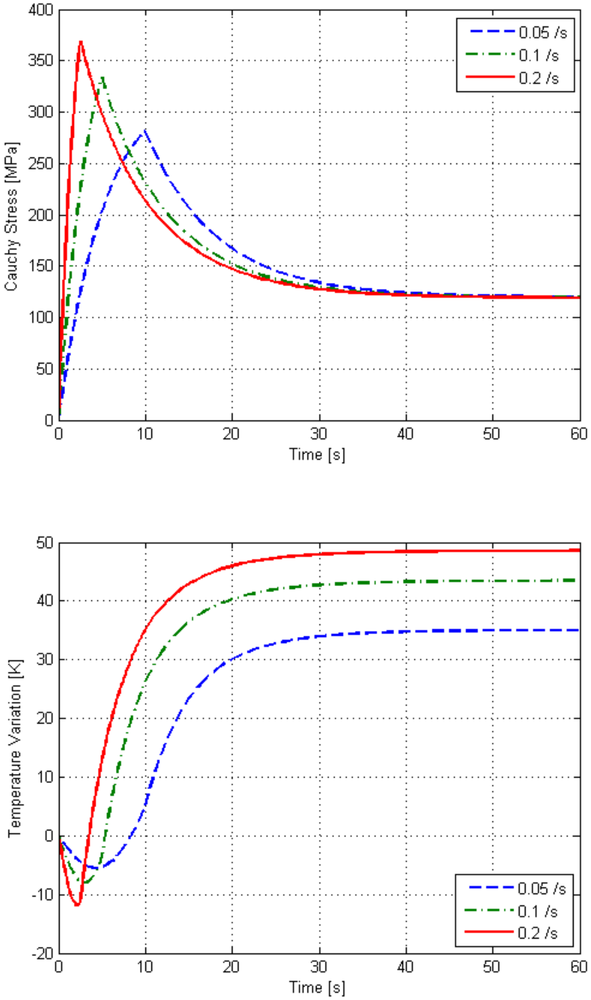

Figure 4.5 – Relaxation test of two Maxwell branches at different strain rates: apparent translation of curves sharing the same characteristic times.

strain behavior (a source of nonlinearity) is being simulated, and the hypotheses behind time-temperature equivalence are thus not present.

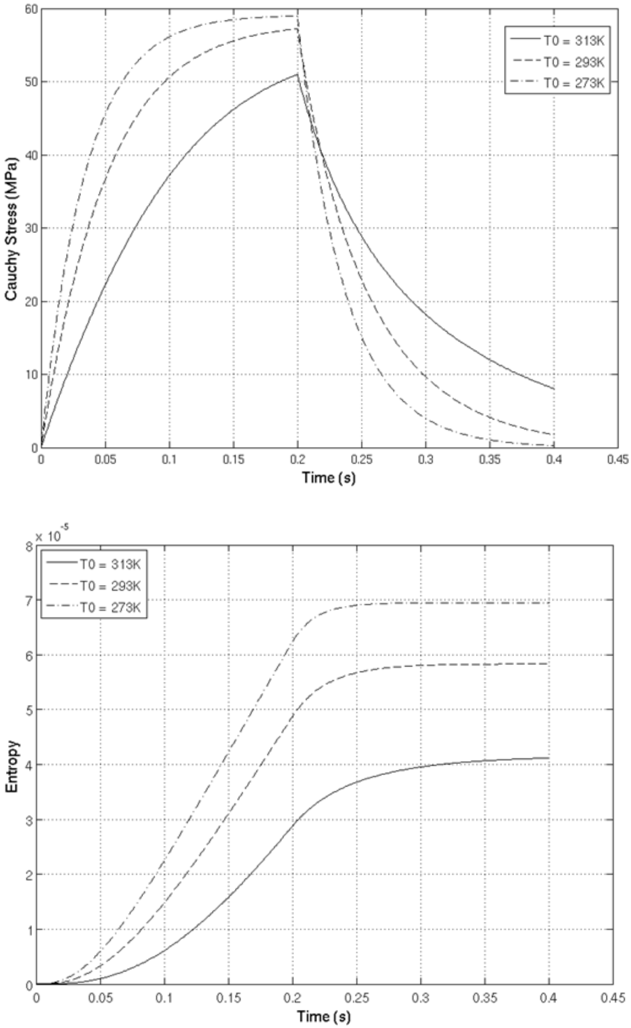

Figure 4.6 – Relaxation tests of a single Maxwell branch at different initial temperatures: lower viscous dissipation (as measured through entropy generation) for higher initial temperatures. Stress-time and entropy-time curves calculated by the thermo-viscoelasticity model.

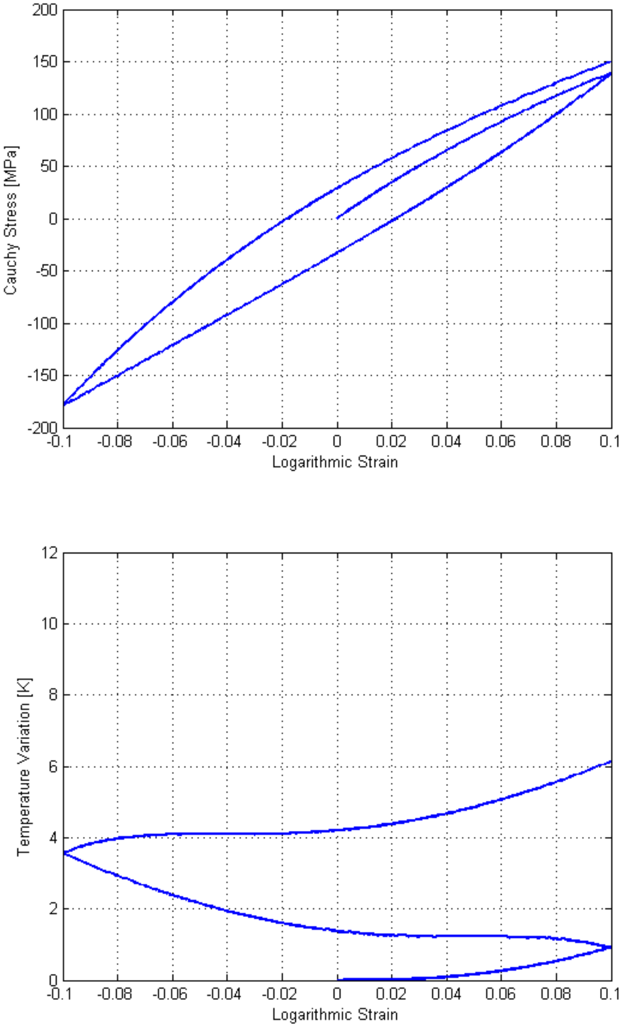

Figure 4.7 – Hysteresis loop in cyclic loading of Maxwell elements: stress-strain and temperature-strain curves.

Two Maxwell elements in parallel with a spring (no Kelvin-Voigt dashpot is present) are used. In all three cases, the material is stretched to a logarithmic strain of 0.3 at the respective strain rates, and is later kept at the same strain level. The higher the initial strain rate, the lower are the viscous strains experienced by the Maxwell dashpots, and therefore relaxation toward the equilibrium strain (due to the spring in parallel) is faster. However, due to the increased stress levels, viscous dissipation is higher, and local temperature generation increases[4.9]. Initially, due to the thermoelastic effect, temperatures decrease. As viscous strains grow, local dissipation begins to dominate and local heating is observed.

All the stress-strain curves look like translations along the plane, and a common master curve could be derived. Since two relaxation times are present, though, the task is no longer trivial.

Another example shows the influence of temperature on material parameters, as shown in figure 4.6. A single Maxwell branch is used in relaxation conditions. Through viscosity effects in the Maxwell branch, elastic strains in the spring are relaxed as viscous flow continues in the dashpot. Different initial temperatures are simulated. For higher temperatures, viscosity parameters are lower, and thus lower levels of stress are attained. In turn, the viscous dissipation estimated by the model, the product of the non-conservative stress by the rate of viscous straining integrated through the process (as measured by the entropy increase, as in equation 4.69), is lower for the higher initial temperature.

Cyclic loading tests are often used in order to demonstrate the dissipative character of viscous strains. Whereas for hyperelastic materials loading and unloading follows the same path by definition, since the constitutive response is fully determined by by the Helmholtz free energy potential, for viscoelastic materials hysteresis is to be expected. In a stress-strain curve, the area between loading and unloading conditions is proportional to the energy dissipated in irreversible straining.

Figure 4.7 shows the result of a tensile loading cycle of two Maxwell branches in parallel to a spring. Figure 4.8 shows the results of the same test on a model adding a Kelvin-Voigt dashpot to the same two Maxwell branches and spring of figure 4.7. The difference in behavior between the two types of rheological models becomes clearer.

The Kelvin-Voigt dashpot introduces more dissipation into the model and is responsible for the immediate spike in stress due to the imposition of a strain rate. Since it is connected in parallel to the other elements, it is instantly subjected to the full imposed strain rate.

[4.9] No temperature dependence of material parameters was considered in this example, and therefore the equilibrium level of strains is the same for all three loading conditions, despite temperature diferences.

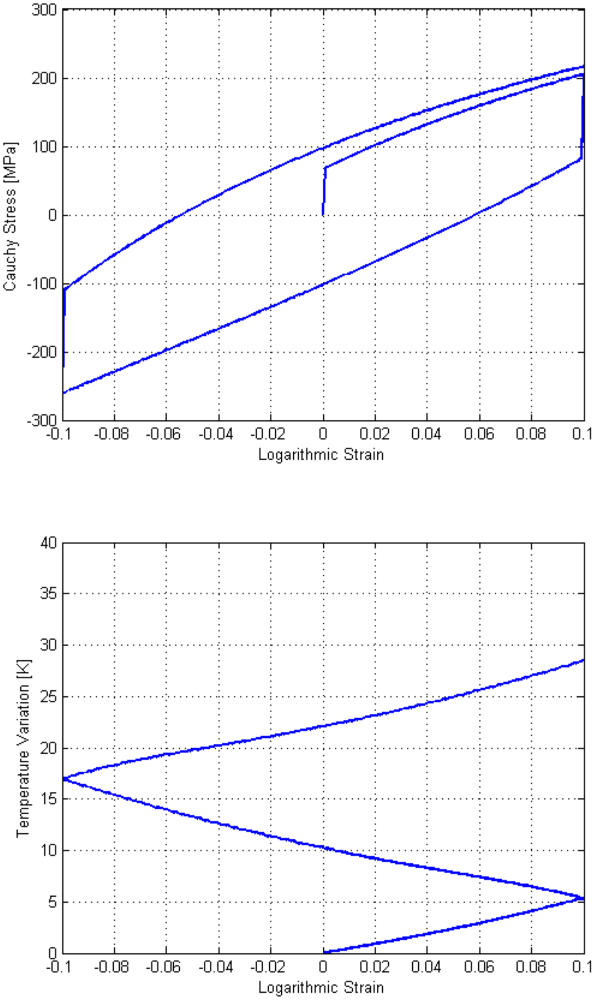

Figure 4.8 – Hysteresis loop in cyclic loading of a generalized Kelvin-Voigt/Maxwell rheological model: stress-strain and temperature-strain curves.

Maxwell dashpots, on the other hand, are eased into the imposed loads since their springs act as a buffer.

Since the examples are run in adiabatic conditions, the temperature can only increase monotonically. Once again, the different observed shapes of the temperature evolution curves bring evidence of the difference between Maxwell and generalized Kelvin-Voigt/Maxwell rheological models.

For Maxwell model, viscous strains, the central dissipation mechanism, develop slower. The slope of the temperature evolution then increases along the loading step. When Kelvin-Voigt dissipation is present, on the other hand, the dashpot in parallel is constantly submitted to the full imposed strain rate. Temperature increase behaves more linearly.

5 THERMO-VISCOELASTIC DAMAGE IN A VARIATIONAL FRAMEWORK

Chapter overview: Having developed a local model that accounts for the thermomechanical coupling and strain rate dependence crucial to the description of polymer-like material behavior, focus is now shifted to the issue of degradation of their properties. In order to do so, following the spirit employed in previous chapters, a brief overview of micromechanical aspects influencing damage behavior in polymers is given, with an emphasis on the physics driving degradation processes. Next, a very brief presentation on the origins and hallmarks of continuum damage mechanics is given, before moving along to earlier works in recasting damage in the same variational framework detailed in chapters 3 and 4. Finally, a specific variational structure for a coupled thermoviscoelastic-damage is developed. Inspired by the work done in Kintzel & Mosler (2011), special forms of the Helmholtz free energy potential and of the dissipation pseudo-potential are proposed. These lead to a natural uncoupling between the update of viscous variables and that of the damage variable, in a scheme based on an equivalent strain space. A full derivation of the internal variable updates is presented, as well as the modified expressions for stress and entropy updates, together with their corresponding tangent operators. Some sample numerical applications are used to illustrate the capabilities of the proposed model.

5.1 INTRODUCTION: CONTINUUM DAMAGE MECHANICS AND POLYMER DAMAGE

The physical mechanisms behind the constitutive response of a class of materials differ greatly depending on the degree of degradation. The way material degradation manifest itself can completely change the micromechanical aspects of deformation and entropy, in keeping within thermomechanical contexts.

This subject was explored in chapter 2 for polymers. Phenomena such as stress crazing and shear banding, common precursors to failure in polymers, reflect stark changes at the microstructural level, in comparison to the fully undamaged state. While models for sound material are based on the arrangement of polymer chains and the type of bonding they can develop at the application conditions, degradation can introduce other features that bear just as much responsibility to the overall material response.

Post failure microscopy, as in figure 2.7, often evidence the formation of microvoids and microcracks, which can coalesce to form macroscale counterparts. Before they coalesce and form free surfaces, however, degradation clearly has a volumetric character. This is true not only for polymers, the focus of the present document, but also in metals and other kinds of materials. Either through repeated loading (fatigue) or large imposed loads (over a certain threshold, in elasticity or plasticity), the bulk of the material can be degraded and starts to behave differently from the fully sound state.

Accordingly, the constitutive modeling of these phenomena is also done volumetrically, and represents degradation through compromised material properties. These kinds of models are the central occupation of the field of continuum damage mechanics (CDM).

Originated from the pioneering works of Kachanov (originally published in 1958, and reissued with comments in Kachanov (1999)) and Rabotnov (whose ideas on creep rupture were initially published in 1968, and later extended in Rabotnov (1969)), and receiving fundamental contributions by Lemaître and coworkers (summarized in two books: Lemaître (1996) and Lemaître & Desmorat (2005)), continuum damage mechanics is based on some key concepts that allow for a complete description of degradation in various contexts. A very brief overview of some of these concepts is brought in the following paragraphs.

In CDM, internal variables are used to store the information of degradation. When damage acts isotropically on the material, an assumption made for the model proposed in this chapter, a single scalar variable can be used. Damage mechanisms can also introduce anisotropy, and thus require a tensorial description (VOYIADJIS; YOUSEF; KATTAN, 2012).

The evolution of the internal variables is connected to assumed driving mechanism of damage. The first damage models, still useful for materials exhibiting brittle failure, correlated damage (represented by the variable d) to elastic strains. Thus, the damage variable was responsible for reducing the values of the Young's modulus (E) in a one dimensional small strains problem as below:

$$W(\epsilon, d) = [1 - d]\frac{1}{2}E\epsilon^2 \qquad \boldsymbol{\sigma} = \frac{\partial W}{\partial \epsilon} = [1 - d]E\epsilon \tag{5.1}$$

As will become clear in the formulation of the variational damage model, the elastic stored energy would then act as the sole thermodynamic force corresponding to the evolution of the damage variable (in the spirit of the notation used up to this point, Y^d (also a scalar quantity), commonly called the energy restitution rate; it can be derived from the Helmholtz free energy W, as well as from the damage dissipation potential $\psi^d(\dot{d})$):

$$Y^d = -\frac{\partial W}{\partial d} = \frac{\partial \psi^d}{\partial \dot{d}} = \frac{1}{2}E\epsilon^2 \tag{5.2}$$

It becomes clear that the energy release rate consists of the energy that would be absorbed by the material, had its properties not been compromised by damage. This is in close relation to the second main idea of damage formulations, that of effective stress ($\tilde{\boldsymbol{\sigma}}$, defined in equation 5.3 below).

Physical interpretations of damage are often sought. The relation to microvoids and microcracks is usually evoked. The scalar damage variable is taken to be zero for fully sound material, when no volume is occupied by voids. A fully damaged material is associated to a damage variable equal to one, another way of representing the volume ratio occupied by voids. When no bulk material is left, there is nothing to bear the imposed loads and the material fails. In this sense, the effective stress acting upon any given point is nothing more than the stress felt by volume of bulk material left at that point, after discounting the volume occupied by voids.

$$\tilde{\boldsymbol{\sigma}} = \frac{\boldsymbol{\sigma}}{1 - d} = E\epsilon \tag{5.3}$$

Figure 5.1 brings a schematic representation of the concept of effective stress.

Other points of view are possible for such interpretations. As the material becomes degraded, the term $1 - d$ reduces the elastically stored energy for the same strain ϵ. In fact, it is possible to regard the effective stress ($\tilde{\boldsymbol{\sigma}}$) as the stress acting upon an undamaged material for it to exhibit the same imposed strain. Thus, the constitutive equations for strain can keep the same format as for the undamaged material, provided that effective stresses are used in place of the actual

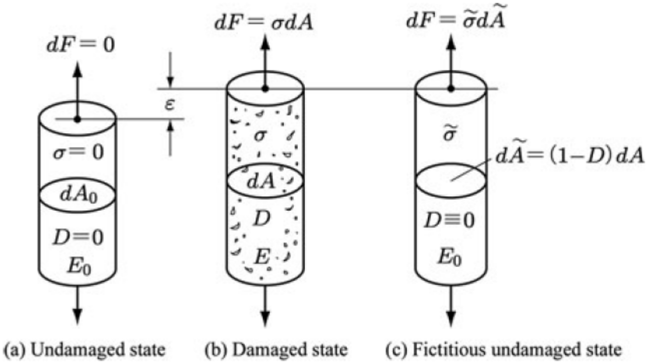
$dF=0$
$dF=\sigma dA$
$dF=\tilde{\sigma}d\tilde{A}$
ε
$\sigma=0$
dA_0
$D=0$
E_0
σ
dA
D
E
$\tilde{\sigma}$
$d\tilde{A}=(1-D)dA$
$D\equiv 0$
E_0
(a) Undamaged state
(b) Damaged state
(c) Fictitious undamaged state

Figure 5.1 – Graphic representation of the effective stress $\tilde{\boldsymbol{\sigma}}$. [Source: (MURAKAMI, 2012)]

stresses. This is commonly known as the principle of strain equivalence (LEMAÎTRE; DESMORAT, 2005).

Instead of assuming constitutive relations for strains to be equivalent in damaged and undamaged material, it is also possible to consider the strain energy to have equivalent forms in damaged and undamaged states. This is commonly called the strain energy equivalence principle (due originally to the work in Cordebois & Sidoroff (1982) for anisotropic damage, and later applied in different contexts, such as in Grammenoudis, Reckwerth & Tsakmakis (2009a, 2009b)), and has implications on the derivation of the constitutive equations. Basically, the influence of damage is stored in the tangent operators in such a model (so that, for undamaged material, the regular stiffness tensor $\mathbb{C}$ is used, while for the damaged material, a modified tensor has to be used, depending on the value of the chosen strain variables: $\tilde{\mathbb{C}}(d)$). The subject of strain energy equivalence falls outside the scope of the presently proposed models of damage.

Sensitivity to the direction of imposed stress is a common feature required of damage models. Damaged material is often shown to behave differently under tension or compression. This is due to the closure of the voids and cracks represented by the chosen damage variable. The variational model proposed in the present text does not take into account the void closure effect.

The main contributions of Lemaître and co-workers to the field of continuum damage mechanics pertained to the development of plasticity-driven damage. The details of said models fall outside the scope of the present document. In addition to the reference books (LEMAÎTRE, 1996; LEMAÎTRE; DESMORAT, 2005), the interested reader can find an application of said Lemaître-models in an article by Fancello et al. (2014). In the present subsection, it should be sufficient to view Lemaître type models as allowing for a damage function to act upon the plastic parts of energy, reducing the yield stress and the plastically-stored energy in the material as damage progresses.

Starting from dual dissipation pseudo-potentials (nothing more than Legendre-Fenchel transforms of the dissipation pseudo-potentials used up to this point, as defined in equation 5.4 below; including plastic dissipation, denoted $\psi^{p\star}(\boldsymbol{\sigma}, \mathbf{Y})$, and damage dissipation, denoted $\psi^{d\star}(\boldsymbol{\sigma}, \mathbf{Y})$), it is possible to show that damage evolution equations can then be derived from the stationarity condition with respect to the energy release rate, as in equation 5.5 below, with the plastic multiplier $\dot{\lambda}^p$ appearing naturally:

$$\psi^\star(\boldsymbol{\sigma}, Y^d) = \sup_{\dot{\epsilon}, \dot{d}} \left[\boldsymbol{\sigma}\dot{\epsilon} + Y^d \dot{d} - \psi(\dot{\epsilon}, \dot{d}) \right] \tag{5.4}$$

$$\dot{d} = \dot{\lambda}^p \frac{\partial \psi^\star}{\partial Y^d} \qquad \dot{\epsilon} = \dot{\lambda}^p \frac{\partial \psi^\star}{\partial \boldsymbol{\sigma}} \tag{5.5}$$

There are abundant options to couple damage to various types of plasticity models in this very general mold. Equivalently, when viscoelasticity dominates material behavior, it is possible to couple the action of the damage variable and its evolution to the viscous dissipation phenomena. These thermoviscoelastic damage models are of great interest for the modeling of polymer damage. A notable example of such a formulation, which has served as a base for many polymer damage applications (GOVINDJEE; SIMO, 1992; KALISKE; NASDALA; ROTHERT, 2001; KUMAR; TALREJA, 2003; YANG; KIM; LEE, 2012), can be found in Simo (1987), where the challenges of finite strain modeling are discussed.

The thermo-viscoelastic damage model presented in the present chapter fits this tradition of models. Viscous dissipation is the main driving force for damage evolution, although coupling with elasticity is also assumed. The variational framework described in previous chapters is used, with a specific structure leading to a natural split between viscous and damage update. Before moving on to the details of the proposed formulation, though, it is important to explore an available variational model of damage, the subject of the following subsection.

5.2 REVIEW OF AN EARLIER VARIATIONAL FORMULATION OF DAMAGE

The variational approach to dissipative phenomena originated in Ortiz & Stainier (1999) (often referred to as variational constitutive updates) and presented in detail on chapter 3 can also be applied to damage problems. Provided that the dissipation pseudo-potential due to damage is a convex function of its arguments, there is a guarantee of respecting the second law of thermodynamics, and all the necessary equations that rule the problem come from the same energy-like potential function.

Kintzel and Mosler, in the article Kintzel & Mosler (2011), were the first to recast damage in this variational framework. Presenting low cycle fatigue in metals as research topic, they proposed the use of two different types of damage mechanisms to account for the different observed phenomena: brittle and ductile damage.

When high cycle fatigue causes rupture, classical models of elastic damage are efficiently used, resulting in brittle failure. In that case, the yield stress is never surpassed, no plasticity is present. Observations of the fracture surface show sharp and smooth surfaces, indicating the formation of large surfaces at once, with little energy absorption.

In low cycle fatigue, on the other hand, stress levels are usually higher, and an onset of permanent deformations is commonly present. In fact, a combination of effects is usually to be expected. Fracture surfaces are thus much rougher, a result of ruptured fibrils and ductile fracture, although some sharper fascia can appear. The energy for the generation of the fractured surface is much higher.

The proposed brittle damage model lets an isotropic damage variable act upon the elastic part of stored energy only. It is therefore reminiscent of the early models of the form of equation 5.1. However, plasticity is considered present, and two internal variables are assigned to account for softening (α_b) and hardening (α_Γ) induced by damage evolution. Different hardening (H_Γ) and softening (H_b) moduli are considered. The Helmholtz free energy of the brittle damage model reads:

$$W(\boldsymbol{\varepsilon}^e, \alpha_\Gamma, \alpha_b, d) = [1-d]Y^d(\boldsymbol{\varepsilon}^e) + H_\Gamma \frac{\alpha_\Gamma^2}{2} + H_b \frac{\alpha_b^2}{2} \tag{5.6}$$

In the spirit of generalized standard materials, convex dissipation pseudo-potentials are used to ensure positive internal dissipation and respect of the second law of thermodynamics. The plastic dissipation mechanisms are considered independent of the damage variable, as the dissipation inequality reads:

$$\mathcal{D} = \underbrace{-\frac{\partial W}{\partial \alpha_\Gamma}\dot{\alpha_\Gamma} - \frac{\partial W}{\partial \alpha_b}\dot{\alpha}_b}_{\text{plastic dissipation}} + Y^d \dot{d} \leq 0 \tag{5.7}$$

The ductile damage model, in contrast, is characterized by the damaging term $(1-d)$ being allowed to affect the plastically-stored portions of energy as well. Both kinematic hardening (described by a general tensorial variable $\boldsymbol{\alpha}_k$ and modulus H_k) and isotropic hardening (described by a general scalar variable α_i and modulus H_i) are considered.

$$W(\boldsymbol{\varepsilon}^e, \boldsymbol{\alpha}_k, \alpha_i, d) = [1-d]\left[\frac{1}{2}\boldsymbol{\varepsilon}^e : \mathbb{C} : \boldsymbol{\varepsilon}^e + H_k \frac{\boldsymbol{\alpha}_k : \boldsymbol{\alpha}_k}{2} + H_i \frac{\alpha_i^2}{2}\right] \tag{5.8}$$

Now all the plastic dissipation terms depend explicitly on the damaging term $(1-d)$, as follows:

$$\begin{aligned} \mathcal{D} = \overbrace{-\frac{\partial W}{\partial \boldsymbol{\varepsilon}^p}\dot{\boldsymbol{\varepsilon}}^p - \frac{\partial W}{\partial \boldsymbol{\alpha}_k}\dot{\boldsymbol{\alpha}}_k - \frac{\partial W}{\partial \alpha_i}\dot{\alpha}_i}^{\text{plastic dissipation}} + Y^d \dot{d} = \\ [1-d]\left[\boldsymbol{\sigma} : \dot{\boldsymbol{\varepsilon}}^p + H_k \boldsymbol{\alpha}_k : \dot{\boldsymbol{\alpha}}_k + H_i \alpha_i \dot{\alpha}_i\right] + Y^d \dot{d} \leq 0 \end{aligned} \tag{5.9}$$

It is clear that the terms in brackets in the above expression 5.9 are precisely the plastic dissipation terms that would take place for an undamaged material. In other words, the strain equivalence principle can be applied to the proposed ductile damage model, which makes the update of plastic variables uncoupled from the update of damage variables. Since the same type of damage dependence (represented by the classic damaging term $(1-d)$) acts upon all terms, elastic and plastic, the elastoplasticity problem can be solved in an equivalent strain space.

This type of idea, based on the strain equivalence principle of continuum damage mechanics, underlies the thermo-viscoelastic damage model fully developed in the following subsections.

5.3 THERMO-VISCOELASTIC DAMAGE: DISCUSSION ON POSSIBLE CHOICES OF INTERNAL VARIABLES AND POTENTIALS

As discussed in the last chapters, variational approaches to dissipative problems depend on two preliminary definitions: that of the set of independent variables, with carefully chosen internal variables to represent the dissipation phenomena; and that of the form of the individual components of the Helmholtz free energy and of the dissipation pseudo-potential.

These definitions are proposed using the same kinematic hypotheses of the previous chapter. Both the Helmholtz free energy and the dissipation pseudo-potential are considered additively decomposed. Large strain kinematics are considered, with spectral quantities of viscous strains used as independent internal variables.

This is achieved with appropriate choices of potentials. In keeping with the general spirit of the undamaged model, modified versions of the potentials for the thermo-viscoelasticity problem are proposed.

The inclusion of damage is done assuming the existence of a damaging function $f(d)$ that acts multiplicatively upon the undamaged version of the corresponding potentials. The most classical form of the damaging function, as shown in the previous subsection, is simply $f(d) = (1-d)$, where the damage variable always has values between 0 (fully sound material) and 1 (total degradation). Different forms of the damaging function are possible, though, and thus a general notation is kept.

Also, in the general case, different parts of the potential can have different damaging functions. Therefore, the new definitions for the different portions of the Helmholtz free energy read as follows (where the potentials in the undamaged state of thermo-viscoelasticity are denoted with an overhead tilde, $\tilde{W}$):

$$W(\mathbf{C}, q_i, \mathbf{M}_j^v, T, d) =$$

$$f^{vol}(d)\tilde{W}^{vol}(J,T) + f^{th}(d)\tilde{W}^{th}(T) + \sum_{k=1}^{K}\sum_{j=1}^{3} f^{ek}(d)\tilde{W}^{ek}(\epsilon_j^e, T) \quad (5.10)$$

A central assumption of the present model is that a single damaging function acts equally upon all the parts of the Helmholtz free energy, so that the above equation can be simplified as:

$$W(\mathbf{C}, q_i, \mathbf{M}_j^v, T, d) = f(d)\tilde{W}(\mathbf{C}, q_i, \mathbf{M}_j^v, T) \tag{5.11}$$

It is clear that all the freedom to define a variety of material models remains present. The same isotropic potentials depending on eigenvalues of strains can be employed in the thermo-viscoelastic damage model.

Additionally, since the goal is to couple damage evolution to viscous processes, damaging functions are also introduced into the dissipation pseudo-potential. Following the ductile damage model proposed in Kintzel & Mosler (2011), the same unified damage function is used, so as to obtain the following structure in an incremental context(where different sources of dissipation in the undamaged state of thermo-viscoelasticity are marked with an overhead tilde, $\tilde{\psi}^{KV}$ and $\tilde{\psi}^{MX}$):

$$\begin{aligned}
\psi\left(\frac{T_{n+1}}{T_n}\frac{\Delta\mathbf{C}}{\Delta t}, \frac{T_{n+1}}{T_n}\frac{\Delta q_j^k}{\Delta t}, \frac{T_{n+1}}{T_n}\frac{\Delta d}{\Delta t}; \mathbf{C}_{n+\alpha}, q_{jn+\alpha}^k, d_{n+\alpha}, T_{n+\alpha}\right) = \\
f(d)\tilde{\psi}^{KV}\left(\frac{T_{n+1}}{T_n}\frac{\Delta\mathbf{C}}{\Delta t}; \mathbf{C}_{n+\alpha}, T_{n+\alpha}\right) \\
+\sum_{k=1}^{K}\sum_{j=1}^{3} f(d)\tilde{\psi}^{MXk}\left(\frac{T_{n+1}}{T_n}\frac{\Delta q_j^k}{\Delta t}; q_{jn+\alpha}^k, T_{n+\alpha}\right) \\
+\psi^d\left(\frac{T_{n+1}}{T_n}\frac{\Delta d}{\Delta t}; d_{n+\alpha}, T_{n+\alpha}\right)
\end{aligned} \tag{5.12}$$

Clearly, the new dissipation pseudo-potential includes both the damaged version of the thermo-viscoelastic one ($\tilde{\psi}$), as well as a potential describing the dissipation due to the evolution of the damage variable (ψ^d).

$$\begin{aligned}
\psi\left(\frac{T_{n+1}}{T_n}\frac{\Delta\mathbf{C}}{\Delta t}, \frac{T_{n+1}}{T_n}\frac{\Delta q_j^k}{\Delta t}, \frac{T_{n+1}}{T_n}\frac{\Delta d}{\Delta t}; \mathbf{C}_{n+\alpha}, q_{jn+\alpha}^k, d_{n+\alpha}, T_{n+\alpha}\right) = \\
f(d)\tilde{\psi}\left(\frac{T_{n+1}}{T_n}\frac{\Delta\mathbf{C}}{\Delta t}, \frac{T_{n+1}}{T_n}\frac{\Delta q_j^k}{\Delta t}; \mathbf{C}_{n+\alpha}, q_{jn+\alpha}^k, T_{n+\alpha}\right) \\
+\psi^d\left(\frac{T_{n+1}}{T_n}\frac{\Delta d}{\Delta t}; d_{n+\alpha}, T_{n+\alpha}\right)
\end{aligned} \tag{5.13}$$

The damage dissipation pseudo-potential is also taken as a convex function of its arguments, ensuring that the second law of thermodynamics is not violated. As for the other dissipation terms, it can be shown during the Coleman-Noll procedure that, since the thermodynamic force associated to damage does not generate external stress (as for all internal variables), it can be derived both from the Helmholtz free energy and from the dissipation pseudo-potential. Therefore, the energy restitution rate reads as follows:

$$Y^d = -\frac{\partial W}{\partial d} = -\frac{\partial f(d)}{\partial d}\tilde{W} = \frac{\partial \psi^d}{\partial \dot{d}} \tag{5.14}$$

The above equation, responsible for the evolution of the damage variable (usually nonlinearly), will be shown to come as a consequence of a stationarity condition in the underlying variational principle.

Different forms of the damage dissipation pseudo-potential lead to different models of damage. In the present document, a type of power law of the following form is employed in the examples:

$$\psi^d \left(\frac{T_{n+1}}{T_n} \frac{\Delta d}{\Delta t}; d_{n+\alpha}, T_{n+\alpha} \right) = \left\{ \frac{m'}{m'+1} Y_0^d \dot{d}_0 \left[\frac{T_{n+1}}{T_n} \frac{\Delta d/\Delta t}{\dot{d}_0} \right]^{\frac{1}{m'}+1} \right\} \tag{5.15}$$

Before moving on to the actual variational formulation of the thermo-viscoelastic damage problem, some discussions on the physical meaning behind the proposed structure of potentials should be outlined.

The choice of a single damaging function for all the potentials and dissipation pseudo-potentials can seem simplistic. For some applications it may actually show to be insufficient. However, it bears a strong connection to the physical interpretation of damage as a measure of volume degradation. As microvoids and microcracks form, and the damage variable approaches $d = 1$, all the phenomena taking place at the volume level are affected. All the portions of the Helmholtz free energy and the dissipation pseudo-potential are related to phenomena taking place throughout the bulk of the material, and would then feel the consequences of the creation and growth of voids.

However, it should be clear that questions on the soundness of this argument arise when it comes to the purely thermal accumulation W^{th}. As exposed in the model presented in the conference paper

Canadija & Mosler (2013), experimental results obtained for metals indicate that the ability to store energy by means of heat capacity is not significantly affected by damage. This would point to the use of the exact same form of the potential, in both the damaged and undamaged versions of the problem: $W^{th} = \tilde{W}^{th}$, in the proposed notation.

These issues on the choice of a single damage variable and of which parts of the energy are affected by damage, initially raised in section 2.5, are further explored in section 5.7. Possible damage modeling alternatives are explored, their physical interpretation is discussed and the contrast to the models presented here are brought to evidence.

From the way the potentials are constructed, it is clear that the damaging function diminishes the capabilities of energy storage and viscous dissipation. In other words, since dissipation is assumed to take place throughout the volume, as it becomes damaged, there is less viscous dissipation for the same viscous strain increment (of amplitude $\Delta t q_j = \Delta q_j$). Damage evolution then accounts for additional dissipation. The internal dissipation is given as follows[5.1], in the thermomechanically-coupled context proposed by Yang, Stainier & Ortiz (2006):

$$\begin{aligned}\mathcal{D}_{int} &= \frac{\partial \psi}{\partial \dot{\mathbf{Z}}} : \dot{\mathbf{Z}} \\ &= f(d) \quad \underbrace{\left[\frac{\dot{c}_j}{T_n} \left\langle \frac{\partial \tilde{\psi}^{KV}}{\partial \dot{c}_j} \right\rangle + \frac{\dot{q}_j}{T_n} \left\langle \frac{\partial \tilde{\psi}^{MX}}{\partial \dot{q}_j} \right\rangle \right]}_{\text{Thermo-viscoelastic internal dissipation } = \tilde{\mathcal{D}}_{int}} \quad + Y^d . \dot{d} \geq 0 \qquad (5.16)\end{aligned}$$

Having defined the set of independent variables and the forms of the potentials and dissipation pseudo-potentials, it is now time to move on to the variational formulation of thermo-viscoelastic damage, with an emphasis on the uncoupled nature of the internal variable updates.

[5.1] As for previous mentions to the contributions of different sources of dissipation to entropy evolution, the reader is referred to appendix B. Full expressions appropriately accounting for the derivatives of temperature averages along the time step, denoted by $\langle \psi \rangle$, are provided. Suffice it to say that the notation used in equation 5.16 is only accurate for dissipation pseudo-potentials exhibiting no parametric dependence on temperature.

5.4 VARIATIONAL FORMULATION OF DAMAGE COUPLED TO THERMO-VISCOELASTICITY: INTERNAL VARIABLE UPDATES AND INFLUENCE OF DAMAGE ON STRESS AND ENTROPY

As in chapter 4, the variational formulation of the thermomechanically coupled problem of thermo-viscoelastic damage is derived from a rate form variational principle. Presented initially in equation 3.41 (reproduced below for reading convenience), in incremental form, it represents the interconversion between different types of energies. Energy input through external forces or heat fluxes along regions of the boundary $\partial\Omega$ evidence that the following functional is an incremental representation of the full boundary value problem:

$$\begin{aligned}
&\mathcal{H}_n(\mathbf{x}_{n+1}, \mathbf{Z}_{n+1}, T_{n+1}; \mathbf{x}_n, \mathbf{Z}_n, T_n) = \\
&\int_\Omega \{[W(\mathbf{C}_{n+1}, \mathbf{Z}_{n+1}, T_{n+1}) - W(\mathbf{C}_n, \mathbf{Z}_n, T_n) + \rho_R \eta_n [T_{n+1} - T_n]] \\
&\qquad + \Delta t \left\langle \psi \left(\frac{T_{n+1}}{T_n} \frac{\Delta \mathbf{C}}{\Delta t}, \frac{T_{n+1}}{T_n} \frac{\Delta \mathbf{Z}}{\Delta t}; \mathbf{C}_{n+\alpha}, \mathbf{Z}_{n+\alpha}, T_{n+\alpha} \right) \right\rangle \\
&\quad - \Delta t \frac{1}{T_n} \mathbf{q}_R . \nabla T_{n+1} \bigg\} dV - \Delta t \int_{\partial_\sigma \Omega} \bar{\mathbf{t}}_R . \dot{\mathbf{x}}_{n+1} d\Gamma - \Delta t \int_\Omega \mathbf{b}_R . \dot{\mathbf{x}}_{n+1} dV \\
&\qquad\qquad + \Delta t \int_{\partial_\mathbf{q} \Omega} \frac{T_{n+1}}{T_n} \bar{\mathbf{q}}_R . \mathbf{n}_R d\Gamma - \Delta t \int_\Omega \frac{T_{n+1}}{T_n} \mathrm{r}_R dV \qquad (5.17)
\end{aligned}$$

Now, the general set of internal variables denoted $\mathbf{Z}$ includes eigenvalues and eigenvectors of viscous strains at the Maxwell rheological elements (q_j and $\mathbf{M}_j^v$, respectively) as well as damage. Following the forms for the potentials given in the previous subsection, the incremental potential now reads:

$$
\begin{aligned}
&\mathcal{H}_n(\mathbf{C}_{n+1}, q_{jn+1}, \mathbf{M}^v_{jn+1}, d_{n+1}, T_{n+1}; \mathbf{C}_n, q_{jn}, \mathbf{M}^v_{jn}, d_n, T_n) = \\
&\quad \int_\Omega \Big\{ \Big[f(d_{n+1}) \tilde{W}(\mathbf{C}_{n+1}, q_{jn+1}, \mathbf{M}^v_{jn+1}, T_{n+1}) \\
&\qquad - f(d_n)\tilde{W}_n + \rho_R \eta_n [T_{n+1} - T_n] \Big] \\
&\quad + \Delta t f(d_{n+1}) \left\langle \tilde{\psi} \left(\frac{T_{n+1}}{T_n} \frac{\Delta \mathbf{C}}{\Delta t}, \frac{T_{n+1}}{T_n} \frac{\Delta q_j}{\Delta t}; \mathbf{C}_{n+\alpha}, q_{jn+\alpha}, T_{n+\alpha} \right) \right\rangle \\
&\quad + \Delta t \left\langle \psi^d \left(\frac{T_{n+1}}{T_n} \frac{\Delta d}{\Delta t}; d_{n+\alpha}, T_{n+\alpha} \right) \right\rangle - \Delta t \frac{1}{T_n} \mathbf{q}_R . \nabla T_{n+1} \Big\} dV \\
&\quad - \Delta t \int_{\partial_{\boldsymbol{\sigma}} \Omega} \bar{\mathbf{t}}_R . \dot{\mathbf{x}}_{n+1} d\Gamma - \Delta t \int_\Omega \mathbf{b}_R . \dot{\mathbf{x}}_{n+1} dV \\
&\quad + \Delta t \int_{\partial_{\mathbf{q}} \Omega} \frac{T_{n+1}}{T_n} \bar{\mathbf{q}}_R . \mathbf{n}_R d\Gamma - \Delta t \int_\Omega \frac{T_{n+1}}{T_n} \mathrm{r}_R dV
\end{aligned}
\tag{5.18}
$$

In the spirit of all the articles derived from Ortiz & Stainier (1999), so called variational constitutive updates are derived from the stationarity conditions of the incremental functional $\mathcal{H}_n$.

$$
\inf_{\mathbf{C}_{n+1}, q_{jn+1}, \mathbf{M}^v_{jn+1}, d_{n+1}} \sup_{T_{n+1}} \mathcal{H}_n \tag{5.19}
$$

The update with respect to internal variables remains strictly local, since no terms with gradients of internal variables appear in the incremental potential. Once more, the idea is then to build an effective incremental potential ($\mathcal{H}^{eff}_n$), for which the internal variables have already been determined:

$$
\begin{aligned}
&\mathcal{H}^{eff}_n(\mathbf{C}_{n+1}, T_{n+1}; \mathbf{C}_n, q_{jn}, \mathbf{M}^v_{jn}, d_n, T_n) = \\
&\inf_{q_j, \mathbf{M}^v_j, d|_{n+1}} \mathcal{H}_n(\mathbf{C}_{n+1}, q_{jn+1}, \mathbf{M}^v_{jn+1}, d_{n+1}, T_{n+1}; \mathbf{C}_n, q_{jn}, \mathbf{M}^v_{jn}, d_n, T_n)
\end{aligned}
\tag{5.20}
$$

The same constraints on the eigenvalues and eigenvectors of viscous strains (equation 4.6) apply. Therefore, the same type of Langrangian function of equation 4.39 is built:

$$
\begin{aligned}
&\mathcal{L}(q_j, \mathbf{M}_j^v, d) = \\
&\quad \mathcal{H}_n(\mathbf{C}_{n+1}, T_{n+1}; \mathbf{C}_n, q_{jn}, \mathbf{M}_{jn}^v, d_n, T_n) + \lambda_0[q_1 + q_2 + q_3] \\
&\quad\quad + \lambda_1[\mathbf{M}_1^v.\mathbf{M}_1^v - 1] + \lambda_2[\mathbf{M}_2^v.\mathbf{M}_2^v - 1] + \lambda_3[\mathbf{M}_3^v.\mathbf{M}_3^v - 1] \\
&\quad\quad\quad + \lambda_4[\mathbf{M}_1^v.\mathbf{M}_2^v] + \lambda_5[\mathbf{M}_1^v.\mathbf{M}_3^v] + \lambda_6[\mathbf{M}_2^v.\mathbf{M}_3^v] \qquad (5.21)
\end{aligned}
$$

Since the adopted damage variable is scalar, the damaging function $f(d)$ has no influence on the determination of the direction of viscous flow, $\mathbf{M}_j^v$. Once again, it is possible to show that the optimality condition of the incremental potential with respect to the directions of viscous flow ($\frac{\partial \mathcal{L}}{\partial \mathbf{M}_j^v}[\delta \mathbf{M}_j^v] = 0$) yields as a result the colinearity of viscous straining ($\mathbf{D}^v$), isochoric elastic ($\hat{\mathbf{C}}^e$) and predictor tensors ($\mathbf{C}^{pr}$). It appears that, had the proposed model accounted for anisotropic damage, a change in the directions of viscous flow would be expected.

Next, the optimization with respect to the eigenvalues of viscous strains (q_j) is performed. From the Lagrangian function 5.21, the analogous form to equation 4.52 now reads as follows[5.2]:

$$
\begin{aligned}
r_j = \frac{\partial \mathcal{L}}{\partial q_j} &= f(d)\left[-\frac{\partial \tilde{W}^e}{\partial \epsilon_j^e} q_j + \frac{T_{n+1}}{T_n}\left\langle \frac{\partial \tilde{\psi}}{\partial \dot{q}_j} \right\rangle\right] + \lambda_0 \\
&= f(d)\left[-\frac{\partial \tilde{W}^e}{\partial \epsilon_j^e} q_j + \tilde{\lambda}_0 + \frac{T_{n+1}}{T_n}\left\langle \frac{\partial \tilde{\psi}}{\partial \dot{q}_j} \right\rangle\right] = 0 \qquad (5.22)
\end{aligned}
$$

Since the damaging function $f(d)$ is simply a scalar number, an equivalent Lagrange multiplier can be defined as: $\tilde{\lambda}_0 := f(d)\lambda_0$. It clearly equals the Lagrange multiplier obtained in the undamaged problem.

If the damage function is not equal to zero (which happens unless full degradation is reached, and the material has completely lost the ability to bear loads), it can be crossed out, leaving the same nonlinear equations for the update of viscous variables as for the undamaged problem. In other words, due to the construction of the potentials, the update of viscous variables is uncoupled from that of damage, in accordance with the principle of equivalent strains.

[5.2] As for equation 4.52, the notation used above corresponds to viscous dissipation pseudo-potentials independent on the history of internal variables q_j. The general case is dealt with in appendix A.

The equation obtained from the optimum condition with respect to the Lagrange multiplier λ_0 (precisely the same as in equation 4.55) closes the nonlinear system of equations needed to conclude the update of viscous variables.

With the updated viscous strains in hand, the internal update with respect to the damage variable can be performed. It is obtained from the stationarity condition of the incremental potential with respect to the damage variable:

$$\frac{\partial \mathcal{H}_n}{\partial d} = 0 \tag{5.23}$$

From the forms of proposed potentials, this results in a nonlinear equation as follows (where the simple form $f(d) = 1-d$ is used to obtain the second equation, a thermomechanical incremental approximation to the definition of the energy restitution rate of equation 5.14):

$$r_d = \frac{\partial f(d)}{\partial d}\left[\tilde{W}^{vol} + \tilde{W}^{e} + \tilde{W}^{th} + \Delta t \left\langle \tilde{\psi} \right\rangle\right] + \frac{T_{n+1}}{T_n}\left\langle \frac{\partial \psi^d}{\partial \dot{d}} \right\rangle = 0 \tag{5.24a}$$

$$\frac{T_{n+1}}{T_n}\left\langle \frac{\partial \psi^d}{\partial \dot{d}} \right\rangle = \left[\tilde{W}^{vol} + \tilde{W}^{e} + \tilde{W}^{th} + \Delta t \left\langle \tilde{\psi} \right\rangle\right] = Y^d \tag{5.24b}$$

It should be noted that the notation used above is rigorously correct only for damage dissipation pseudo-potentials strictly dependent on the rate of damage. In fact, the term $\frac{T_{n+1}}{T_n}\left\langle \frac{\partial \psi^d}{\partial \dot{d}} \right\rangle$ is what remains of the full term $\Delta t \frac{\partial \langle \psi^d \rangle}{\partial d_{n+1}}$ in such a case, with the common approximation of the rate of damage by a difference scheme such as: $\dot{d} = \frac{d_{n+1} - d_n}{\Delta t}$. If there is a parametric dependence on the history of the damage variable, additional terms appear. For a more detailed description on the treatment of parametric dependence and of the thermodynamically consistent dissipation average along the time step denoted by $\langle \psi \rangle$, the reader is referred to appendices A and B to the present document.

A usual assumption for non-healing materials is that damaging is an ever-increasing variable. Negative damage and damage over $d = 1$ are also prohibited. This means that the optimization problem above is constrained. Instead of using Lagrange multipliers, though, another option is to impose these restrictions during the solution of the nonlinear equation (due to the form of the damage dissipation pseudo-potential equation 5.24 above).

Furthermore, it may also be convenient to work with damage increment ($\Delta d = d_{n+1} - d_n$) in a time-discretized context, in which case the monotonic increase of damage would translate into imposing non-negative damage increments at every time step. Although the details of the implementation of these constraints are omitted, this was done in the provided examples that close the present chapter.

The internal variable optimization phase is thus concluded, and the effective incremental potential $\mathcal{H}_n^{eff}$ can be built. The structure of the chosen potentials translated into a naturally separated update of viscous and damage variables, as demonstrated above. Stationarity conditions of the effective incremental potential now yield the remaining equations necessary to fully describe the thermomechanically-coupled problem, namely mechanical equilibrium and the entropy form of the first law of thermodynamics.

As discussed in the previous chapter for the undamaged problem, stresses can be updated in hyperelastic-like fashion as follows, where a similar split between internal and external parts of the effective incremental potential of equation 4.57 can be performed:

$$\mathbf{P}_{n+1} = 2\mathbf{F}_{n+1} \frac{\partial \mathcal{H}_n^{effInt}}{\partial \mathbf{C}_{n+1}} \tag{5.25}$$

It is easy to derive relations for the effective stress acting upon a given point of the material ($\tilde{\mathbf{P}}_{n+1}$) as:

$$\begin{aligned}\mathbf{P}_{n+1} &= f(d_{n+1})\tilde{\mathbf{P}}_{n+1} \\ &= f(d_{n+1}) \left\{ 2\mathbf{F}_{n+1} \left[\frac{\partial \tilde{W}^e}{\partial \hat{\mathbf{C}}_{n+1}} \frac{\partial \hat{\mathbf{C}}_{n+1}}{\partial \mathbf{C}_{n+1}} + \frac{\partial \tilde{W}^{vol}}{\partial J_{n+1}} \frac{\partial J_{n+1}}{\partial \mathbf{C}_{n+1}} \right.\right. \\ &\qquad \left.\left. + \Delta t \left\langle \frac{\partial \tilde{\psi}^{KV}}{\partial \dot{\mathbf{C}}_{n+1}} \right\rangle \frac{\partial \dot{\mathbf{C}}_{n+1}}{\partial \mathbf{C}_{n+1}} \right] \right\}\end{aligned} \tag{5.26}$$

The kinematic derivatives presented in the previous subsection, together with specific forms for the free energy potentials give the final form of the updated stress.

Finally, the stationarity condition of the effective incremental potential with respect to the global variable of temperature (in fact, a maximum condition, as discussed in chapter 3, giving the thermomechanical problem a saddle-point character) has to be evaluated:

$$\frac{\partial \mathcal{H}_n^{eff}}{\partial T_{n+1}} = 0 \tag{5.27}$$

Given that the Helmholtz free energy serves as a potential for entropy, and using the divergence theorem to move heat flux terms from the boundaries to the volume, a local form of the first law of thermodynamics including entropy is obtained:

$$\begin{aligned} \rho_R \eta_{n+1} &= -f(d_{n+1}) \left[\frac{\partial \tilde{W}^e}{\partial T_{n+1}} + \frac{\partial \tilde{W}^{vol}}{\partial T_{n+1}} + \frac{\partial \tilde{W}^h}{\partial T_{n+1}} \right] \\ &\overbrace{= f(d_{n+1}) \left[\Delta t \frac{\dot{c}_j}{T_n} \left\langle \frac{\partial \tilde{\psi}^{KV}}{\partial \dot{c}_j} \right\rangle + \Delta t \frac{\dot{q}_j}{T_n} \left\langle \frac{\partial \tilde{\psi}^{MX}}{\partial \dot{q}_j} \right\rangle \right] + \Delta t \frac{\dot{d}_j}{T_n} \left\langle \frac{\partial \psi^d}{\partial \dot{d}} \right\rangle}^{\text{Internal dissipation}=\mathcal{D}_{int}} \\ &\quad + \rho_R \eta_n + \Delta t \mathrm{Div} \left(\frac{\mathbf{q}_R}{T_n} \right) + \Delta t \frac{\mathrm{r}_R}{T_n} \end{aligned} \tag{5.28}$$

As discussed for the optimality conditions with respect to viscous and damage variables, the notation used above is rigorous only for dissipation pseudo-potentials exhibiting no parametric dependence on temperature. In this case, terms like $f(d_{n+1}) \Delta t \frac{\dot{q}_j}{T_n} \left\langle \frac{\partial \tilde{\psi}^{MX}}{\partial \dot{q}_j} \right\rangle$ are what remains of the actual full term $\Delta t \frac{\partial \langle \psi^{MX} \rangle}{\partial T_{n+1}}$. Full expressions for the contributions to the increase of entropy of each dissipation source in a general case can be found in appendix B.

5.5 EFFECT OF DAMAGE ON THE DERIVATION OF THE TANGENT MODULI

The inclusion of damage also has an influence on the tangent operators of the thermo-viscoelasticity model. The definition of the tangent modulus as the total derivative of stress with respect to strains is recalled below.

$$\mathbb{C} = \frac{d}{d\mathbf{C}_{n+1}} \left(\frac{\partial \mathcal{H}_n^{effInt}}{\partial \mathbf{C}_{n+1}} \right) \tag{5.29}$$

All the discussion of the previous chapter applies to the damaged model as well: the split between purely mechanical and thermomechanical parts, and the additive decomposition corresponding to the split of the Helmholtz free energy and dissipation pseudo-potential.

The influence of damage can be explored in a simpler setting, starting from the definition of effective stress in equation 5.26.

$$\mathbb{C} = \frac{d}{d\mathbf{C}_{n+1}} \left(\frac{\partial \mathcal{H}_n^{effInt}}{\partial \mathbf{C}_{n+1}} \right) = \frac{d}{d\mathbf{C}_{n+1}} \left(f(d_{n+1}) \frac{1}{2} \mathbf{F}_{n+1}^{-1} \tilde{\mathbf{P}}_{n+1} \right) \tag{5.30}$$

Once more, it is possible to distinguish between two terms coming from the equation above, one corresponding to the developments presented in the previous chapter (under notation $\tilde{\mathbb{C}}$) and another due to damage coupling. The internal effective incremental potential of the undamaged thermo-viscoelastic problem is used. Following the notation used heretofore, it is denoted $\tilde{\mathcal{H}}_n^{effInt}$.

$$\mathbb{C} = f(d_{n+1}) \tilde{\mathbb{C}} + \frac{\partial f(d_{n+1})}{\partial d_{n+1}} \underbrace{\frac{\partial d_{n+1}}{\partial \mathbf{C}_{n+1}}}_{\mathrm{I}} \frac{\partial \tilde{\mathcal{H}}_n^{effInt}}{\partial \mathbf{C}_{n+1}} \tag{5.31}$$

It can be seen that the effective stress can be defined in the adopted notation as the last term in the equation above: $\frac{1}{2}\mathbf{F}_{n+1}\tilde{\mathbf{P}}_{n+1} = \frac{\partial \tilde{\mathcal{H}}_n^{effInt}}{\partial \mathbf{C}_{n+1}}$.

Since the formulation is symmetric, the cross-derivative term (marked I in the equation above) can be calculated either from the total damage derivative of the mechanical equilibrium equation, or from the total derivative with respect to strains $\mathbf{C}_{n+1}$ of the damage update equation 5.24, as sketched below[5.3]:

$$\frac{dr_d}{d\mathbf{C}_{n+1}} = \frac{d}{d\mathbf{C}_{n+1}} \left(-Y^d + \frac{T_{n+1}}{T_n} \left\langle \frac{\partial \psi^d}{\partial \dot{d}} \right\rangle \right) = 0 \tag{5.32a}$$

$$-\frac{\partial r_d}{\partial \mathbf{C}_{n+1}} + \frac{1}{\Delta t} \frac{T_{n+1}}{T_n}^{2} \left\langle \frac{\partial^2 \psi^d}{\partial \dot{d}^2} \right\rangle \frac{\partial d_{n+1}}{\partial \mathbf{C}_{n+1}} = 0 \tag{5.32b}$$

$$\frac{\partial d_{n+1}}{\partial \mathbf{C}_{n+1}} = \frac{\frac{\partial Y^d}{\partial \mathbf{C}_{n+1}}}{\frac{1}{\Delta t} \frac{T_{n+1}}{T_n}^{2} \left\langle \frac{\partial^2 \psi^d}{\partial \dot{d}^2} \right\rangle} = \frac{\frac{\partial \tilde{\mathcal{H}}^{effInt}}{\partial \mathbf{C}_{n+1}}}{\frac{1}{\Delta t} \frac{T_{n+1}}{T_n}^{2} \left\langle \frac{\partial^2 \psi^d}{\partial \dot{d}^2} \right\rangle} \tag{5.32c}$$

[5.3] Where notations match the case of a dissipation pseudo-potential exhibiting no parametric dependence on the history of the damage variable.

Clearly, the general case of history dependent dissipation pseudo-potentials includes additional terms. Further details of the derivation and expressions for the tangent moduli can be found in appendix D to the present document.

Next, the thermal counterpart to the tensor modulus $\mathbb{C}$ has to be evaluated. It carries both the information of the heat capacity ($\mathbb{D}_{th}$) and the thermomechanical coupling ($\mathbb{D}_{thm}$) as defined in equation 4.93 for the thermo-viscoelastic problem without damage.

The same reasoning used for the tensor modulus $\mathbb{C}$ can be used for its thermal counterpart $\mathbb{D}$. Thus, two terms can be identified, one derived in the undamaged problem (in the notation currently in use, $\tilde{\mathbb{D}}$), and another due to damage coupling effects. Since all dissipation mechanisms are coupled to the temperature term $\frac{T_{n+1}}{T_n}$, in addition to the cross-derivative term, the second derivative of the damage dissipation pseudo-potential appears:

$$\begin{aligned}\mathbb{D} &= \frac{d}{dT_{n+1}}\left(\frac{\partial \mathcal{H}_n^{effInt}}{\partial T_{n+1}}\right)\\ &= f(d_{n+1})\tilde{\mathbb{D}} + \Delta t\left\langle \frac{\partial^2 \psi^d}{\partial \dot{d}^2}\right\rangle + \frac{\partial}{\partial T_{n+1}}\underbrace{\frac{\partial d_{n+1}}{\partial T_{n+1}}}_{\text{II}}\frac{\partial \mathcal{H}^{effInt}}{\partial T_{n+1}}\end{aligned} \tag{5.33}$$

The cross-derivative term, marked II in the equation above, can be calculated from either the temperature derivative of the damage evolution equation 5.24 as sketched below for the case of damage pseudo-potentials with no history dependence, or from the derivative with respect to damage of equation 5.28, as the proposed model is fully symmetric.

$$\frac{dr_d}{dT_{n+1}} = \frac{d}{dT_{n+1}}\left(-Y^d + \frac{T_{n+1}}{T_n}\left\langle\frac{\partial \psi^d}{\partial \dot{d}}\right\rangle\right) = 0 \tag{5.34a}$$

$$-\frac{\partial r_d}{\partial T_{n+1}} + \frac{1}{\Delta t}{\frac{T_{n+1}}{T_n}}^2\left\langle\frac{\partial^2 \psi^d}{\partial \dot{d}^2}\right\rangle\frac{\partial d_{n+1}}{\partial T_{n+1}} = 0 \tag{5.34b}$$

$$\frac{\partial d_{n+1}}{\partial T_{n+1}} = \frac{\frac{\partial Y^d}{\partial T_{n+1}} + \left[\frac{1}{T_n}\left\langle\frac{\partial \psi^d}{\partial \dot{d}}\right\rangle + \frac{1}{\Delta t}{\frac{T_{n+1}}{T_n}}^2\left\langle\frac{\partial^2 \psi^d}{\partial \dot{d}^2}\right\rangle\right]}{\frac{1}{\Delta t}{\frac{T_{n+1}}{T_n}}^2\left\langle\frac{\partial^2 \psi^d}{\partial \dot{d}^2}\right\rangle} \tag{5.34c}$$

Expressions for the general case, including parametric dependence and exploring the terms included in the average dissipation along the time step $\langle\psi\rangle$, as well as the final form of tangent moduli $\mathbb{C}^{th}$, $\mathbb{D}^{th}$ and $\mathbb{D}$ are derived in detail in appendix D.

5.6 AN ALGORITHMIC VIEW OF THE INCREMENTAL VARIATIONAL CONSTITUTIVE UPDATES

As done in the previous chapter for the variational model of thermo-visco-elasticity, an algorithmic view of the necessary operations of the proposed thermo-viscoelastic damage model is proposed. Given the naturally separated update of viscous and damage variables, a comparison with the algorithm for thermo-viscoelasticity is interesting, and brings up the principle of strain equivalence discussed at the beginning of this chapter.

Once more, a displacement and temperature driven process is considered (though short comments on stress and heat flux driven processes are made in step 7). At the start of the time step, at instant t_n, all independent variables are considered known ($\mathbf{C}_n$, T_n, q_{jn}, $\mathbf{M}_{jn}$ and d_n), as well as their power conjugates and thermodynamic forces (especially stresses $\mathbf{P}_n$ and entropy η_n) and the stored energy in the Helmholtz free energy (W_n). At time t_{n+1}, the load is considered applied through imposed values of the global variables: $\mathbf{C}_{n+1}$ and T_{n+1}

1. From the imposed value of $\mathbf{C}_{n+1}$ and from the known value of $\mathbf{C}_n$, the predictor state $\mathbf{C}^{pr}_{n+1}$ is determined through equation 4.11. A spectral decomposition is performed, determining the eigenvectors shared by the Maxwell viscous strains tensor, as a consequence of the stationarity condition with respect to internal variables $\mathbf{M}^v_j$ (equation 4.49).

2. The internal variable update, essentially local, can be split into two parts because of the chosen form for the potentials (as demonstrated in equation 5.22). The update of viscous variables is performed exactly as before, by solving the nonlinear system of equations 4.52 and 4.55. A Newton-Raphson scheme is used, based on the construction of a tangent matrix to this system of equations. At this point, in addition to the imposed global variables, only the viscous internal variables are known. Damage remains to be determined.

3. Damage update is then performed through the usually nonlinear equation 5.24, with the known values of viscous strains in hand.

4. With the values of all internal variables, the value of the Helmholtz free energy at the end of the time step (W_{n+1}) can now be stored. Additionally, an effective incremental potential is built through equation 5.20, where a split between internal and external parts similar to the one in equation 4.57 can be done.

5. Stresses at the end of the time step ($\mathbf{P}_{n+1}$) are updated in hyperelastic-like fashion through equation 5.26, where the concept of effective stress ($\tilde{\mathbf{P}}_{n+1}$) is present.

6. Entropy is also updated from the stationarity of the effective incremental potential, through equation 5.28.

7. As for the thermo-viscoelastic model without damage, tangent moduli can be calculated through expressions like equations 4.73 (mechanical part $\mathbb{C}$) and 4.93 (thermal part $\mathbb{D}$), modified by the inclusion of damage through equations 5.31 and 5.33, respectively. For the case of imposed forces or heat fluxes (instead of displacements and temperatures), the tangent moduli are used to assess convergence with respect to the mechanical equilibrium equation (defined, in the damaged case, exactly as in equation 4.56), and the entropy form of the first law of thermodynamics (defined as in equation 5.27, which gives rise to equation 5.28), until total strains and temperature fields are correctly calculated.

8. All the values of the independent variables, stress conjugates and stored energy are then stored, and the algorithm may continue to the next time step.

One such algorithm was the basis for the implementation of a simple example, presented in the final subsection of this chapter, illustrating the characteristics of a model of fully-coupled thermo-viscoelastic damage with naturally separable update of viscous and damage variables.

Before doing this, though, going back to the discussion in section 2.5 on possible drawbacks of the proposed models, a primer on modeling alternatives capable of circumventing certain limitations related to the implementation of damage is offered in the following subsection.

5.7 THERMO-VISCOELASTIC DAMAGE: LIMITATIONS AND MODELING ALTERNATIVES

The proposed model of thermo-viscoelastic damage detailed in this chapter, though accounting for a variety of phenomena and for couplings between them, can have limitations in dealing with some features observed in polymer-like material behavior. As discussed in section 2.5, they mostly relate to the choice of the damage model and to the way it is assumed to affect different portions of accumulated and dissipated energy.

Below, it will be made clear that these issues are not related to variational formulations as a whole, but rather to the specific modeling choice advocated in this chapter. Although previously exposed, the reasons behind the choices made here will be explored once again, focusing on the advantages of the used framework.

The first possible limitation of the proposed model resides in the way damage acts upon the thermal accumulation term W^{th}. It is assumed here that the damaging function reduces the material's ability of storing thermal energy in the same way it does the ability of storing elastic energy or dissipating viscous energy. In a classical CDM setting, this would mean that the microvoids and microcracks present in the damaged state of figure 5.1 no longer conserve the possibility of storing thermal energy. In Canadija & Mosler (2013), for instance, it is argued that, for metals, that is not the case, and even damaged material conserves heat capacity. If similar evidence can also be found for a given class of polymers, then the chosen path presented in this chapter would be lacking.

It can be easily seen, though, that no extensive change to the structure of the variational model needs to be made to accomodate for such an occurrence. It would suffice to redefine the Helmholtz free energy potential of equation 5.10 as follows:

$$W(\mathbf{C}, q_i, \mathbf{M}_j^v, T, d) = f(d)\tilde{W}^{vol}(J, T) + W^{th}(T) + \sum_{k=1}^{K}\sum_{j=1}^{3} f(d)\tilde{W}^{ek}(\epsilon_j^e, T) \tag{5.35}$$

The structure of the variational formulation would remain naturally staggered, since W^{th} does not come into play in the determination of viscous strains directions or magnitudes. Changes appear in the definition of entropy and in the damage update, as a heat accumulation term no longer appears in the definition of the energy restitution rate:

$$\rho_R \eta_{n+1} = -\frac{\partial W}{\partial T_{n+1}} = -f(d_{n+1}) \left[\frac{\partial \tilde{W}^e}{\partial T_{n+1}} + \frac{\partial \tilde{W}^{vol}}{\partial T_{n+1}} \right] - \frac{\partial W^{th}}{\partial T_{n+1}} \quad (5.36)$$

$$\frac{T_{n+1}}{T_n} \left\langle \frac{\partial \psi^d}{\partial \dot{d}} \right\rangle = \left[\tilde{W}^{vol} + \tilde{W}^e + \Delta t \left\langle \tilde{\psi} \right\rangle \right] = Y^d \quad (5.37)$$

Expressions for the modified tangent terms of thermomechanical coupling ($\mathbb{C}_{thm}$ or $\mathbb{D}_{thm}$) and purely thermal effects ($\mathbb{D}_{th}$) are omitted here, but can be obtained in straightforward fashion.

By choosing not to apply the damaging function to W^{th}, the material conserves its original heat capacity even though damage evolves. The microvoids and microcracks classically related to damage would then be portions of material disconnected from their environs, thus unable to bear stresses, however still filled with the same amount of mass, thus able to store energy thermally.

Conversely, in the presented model, the driving mechanism behind the evolution of damage also includes the heat capacity term. Going back to the same sort of microstructural argument presented in chapter 2, this means that, as the temperature increases and the molecules become more excited, secondary bonds become less stable and the probability of rupture of principal bonds increases, compromising the integrity of the material. This effect is lost in the version of the equations presented above. Furthermore, even if damage reaches 1 and the material can no longer bear any mechanical load, the compromising of polymer chains due to damage would seem to have some effect on their ability to store thermal energy.

In other words, it is possible to argue that the real effect of damage on heat capacity lies somewhere between the limiting cases presented in previous sections of this chapter and that sketched in the equations above. This is left as a subject for future works.

Still reflecting upon the driving mechanism behind damage evolution and on the choice of a single damage variable to account for all degradation sources, a second possible issue arises. Such a model might appear to be simplistic, as elastic strains, viscous and thermal effects all contribute equally to the evolution of the single damage variable.

A natural solution would be to have individual damage variables and damaging functions for each portion of energy. In other words, the free energy potential would be defined as:

$$W(\mathbf{C}, q_i, \mathbf{M}_j^v, T, d^e, d^{th}, d^{ek}) = \\ f^e(d^e)\tilde{W}^{vol}(J,T) + f^{th}(d^{th})W^{th}(T) \\ + \sum_{k=1}^{K}\sum_{j=1}^{3} f^{ek}(d^{ek})\tilde{W}^{ek}(\epsilon_j^e, T) \quad (5.38)$$

Each viscous dissipation term would be defined as:

$$\psi^{vk}\left(\frac{T_{n+1}}{T_n}\frac{\Delta q_j^{vk}}{\Delta t}, d_j^{vk}; q_{jn+\alpha}^{vk}, d_{n+\alpha}^{vk}, T_{n+\alpha}\right) \\ = f^{vk}(d^{vk})\tilde{\psi}^{vk}\left(\frac{T_{n+1}}{T_n}\frac{\Delta q_j^{k}}{\Delta t}; q_{jn+\alpha}^{vk}, T_{n+\alpha}\right) \quad (5.39)$$

And the damage dissipation would include contributions from all different damage sources:

$$\psi^{d}\left(\frac{T_{n+1}}{T_n}\dot{d}^{e}, \frac{T_{n+1}}{T_n}\dot{d}^{th}, \frac{T_{n+1}}{T_n}\dot{d}^{ek}, \frac{T_{n+1}}{T_n}\dot{d}^{vk}; \\ d_{n+\alpha}^{e}, d_{n+\alpha}^{th}, d_{n+\alpha}^{ek}, d_{n+\alpha}^{ek}, T_{n+\alpha}\right) \quad (5.40)$$

The interaction between damage variables in such a model would need to be determined. Fully uncoupled variables would be allowed to vary individually from 0 to 1, and failure would then be related to the attainment of 1 of one of these variables. On the other hand, a combined failure criterion could be devised, whereby some mix of all damage variables would be evaluated in determining failure. A simple sum of the different damage mechanisms would be simplest example of such a strategy.

Though richer in describing damage mechanisms, such a model would entail a drastic increase in the number of parameters. With no standards on the definitions of what constitutes each part of damage (or on how to isolate various sources of damage) or on the tests necessary to identify a set of parameters, this seems like a daunting task.

Additionally, this would mean the end of the staggered structure of the proposed formulation, as the optimality condition with respect to viscous internal variables would now involve two different damaging functions. It would become impossible to uncouple the update of viscous and damage variables - each Maxwell branch would be a system of equations including viscous and damage optimality conditions. Thus, for Maxwell branch k, it would be necessary to solve the following system:

$$\begin{aligned} r_j &= \frac{\partial \mathcal{L}}{\partial q_j} \\ &= -f^{ek}(d^{ek}) \frac{\partial \tilde{W}^e}{\partial \epsilon^e_j} q_j + f^{vk}(d^{vk}) \frac{T_{n+1}}{T_n} \left\langle \frac{\partial \tilde{\psi}^{vk}}{\partial \dot{q}_j} \right\rangle + \lambda_0 = 0 \end{aligned} \tag{5.41a}$$

$$r_{d^{ek}} = \frac{\partial \mathcal{L}}{\partial d^{ek}} = \frac{\partial f^{ek}(d^{ek})}{\partial d^{ek}} \tilde{W}^{ek} + \frac{T_{n+1}}{T_n} \left\langle \frac{\partial \psi^{dek}}{\partial \dot{d}^{ek}} \right\rangle = 0 \tag{5.41b}$$

$$r_{d^{vk}} = \frac{\partial \mathcal{L}}{\partial d^{vk}} = \frac{\partial f^{vk}(d^{vk})}{\partial d^{vk}} \Delta t \tilde{\psi}^{vk} + \frac{T_{n+1}}{T_n} \left\langle \frac{\partial \psi^{dvk}}{\partial \dot{d}^{vk}} \right\rangle = 0 \tag{5.41c}$$

It is easy to see that a possible solution to the loss of the staggered structure would then be using the same damaging function to both the elastic and viscous parts of every Maxwell branch. The matter of identifying parameters for several damaging functions would remain, however.

Another way the staggered structure of the internal variable updates could be lost is through the inclusion of any kind of dependence on the value of other internal variables in the damage dissipation, be it parametric of explicit. This translates into assuming a pseudo-potential of the following respective forms:

$$\psi^d \left(\frac{T_{n+1}}{T_n} \frac{\Delta d}{\Delta t}; q_{jn+\alpha}, d_{n+\alpha}, T_{n+\alpha} \right) \tag{5.42a}$$

$$\psi^d \left(\frac{T_{n+1}}{T_n} \frac{\Delta d}{\Delta t}, \frac{T_{n+1}}{T_n} \frac{\Delta q_j}{\Delta t}; q_{jn+\alpha}, d_{n+\alpha}, T_{n+\alpha} \right) \tag{5.42b}$$

The optimality condition with respect to internal viscous variables would then read:

$$\begin{aligned} r_j &= \frac{\partial \mathcal{L}}{\partial q_j} \\ &= -f(d)\left[\frac{\partial \tilde{W}^e}{\partial \epsilon_j^e} q_j + \lambda_0 + \frac{T_{n+1}}{T_n}\left\langle \frac{\partial \tilde{\psi}}{\partial q_j}\right\rangle\right] + \frac{T_{n+1}}{T_n}\left\langle \frac{\partial \psi^d}{\partial q_j}\right\rangle = 0 \end{aligned} \tag{5.43}$$

Clearly, crossing out the damaging function $f(d)$ is no longer possible, and the update of the damage variable has to be done simultaneously to that of the viscous variables.

This would be the case, for instance, if a damage initiation threshold determined by the magnitude of viscous strains q_j were to be introduced. In fact, this type of dependence is a common staple of many damage models.

The thermo-viscoelastic damage model presented in previous subsections does not deal with damage thresholds: damage initiates as soon as there is loading. It should be clear that the loss of the staggered structure of internal variable updates would only happen if the introduced threshold is a function of other internal variables. Damage initiation thresholds depending on the amount of accumulated damage, or considered as a (possibly temperature dependent) material property would not cause these kinds of changes. Their inclusion in the proposed variational context is straightforward, and is analogous to the treatment of yield functions in plasticity.

Similar issues with regards to the loss of a naturally-staggered sequence in the internal variable updates arise in models where a single damage variable is differently affected by effects of diverse natures or occurring at various time scales. Equation 5.10 shows a possible way of having a richer model, with different damaging functions acting upon different parts of the additively decomposed Helmholtz free energy potential. Even with a single scalar damage variable d, this would represent a richer model.

However, as soon as different damaging functions act upon different portions of energy, the staggered structure that allows for the post-processing of damage after the update of viscous variables in an equivalent strains disappears. In turn, more extensive changes need to be made to previously implemented constitutive models, and the potential for modularity is lost.

Devising a framework for the inclusion of damage driven by various sources of energy in a readily applicable way was one of the main concerns during the development of the present work, and thus models such as those presented in the previous equations were not explored.

5.8 SAMPLE NUMERICAL TESTS

In order to demonstrate the capabilities of the proposed variational model of thermo-viscoelastic damage, different aspects of some examples are evaluated. Displacement-driven uniaxial tensile tests at three different strain rates are run, in order to show the influence of the imposed strain rate upon the evolution of all internal variables, stresses and entropy.

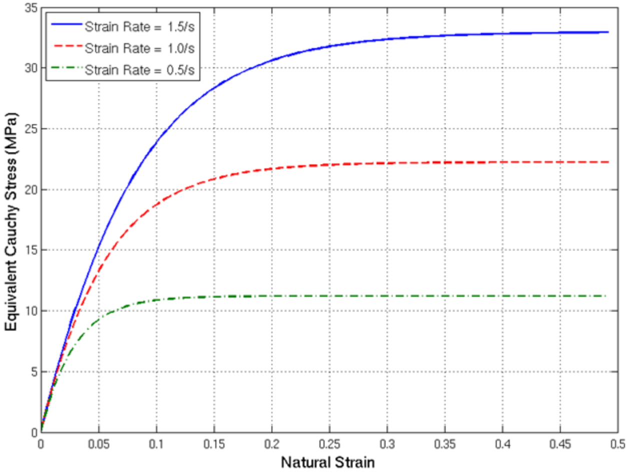

Figure 5.2 – Strain rate influence on the effective stress-strain behavior of a thermo-viscoelastic damage model - a single Maxwell branch. No observed softening, as expected for the undamaged equivalent problem.

As in the last chapter, consistency tests at a single Gauss point are run, so as to isolate the constitutive effects from the domain geometry. Adiabatic conditions are considered, so that temperature becomes an internal variable reflecting the amount of locally generated heat through thermomechanical coupling and dissipation. Material parameters are not chosen to represent any specific kind of material, and results should be interpreted qualitatively. If future works demand the fitting of the proposed model to experimental results, the variational structure and the easiness to calculate derivative and symmetric tan-

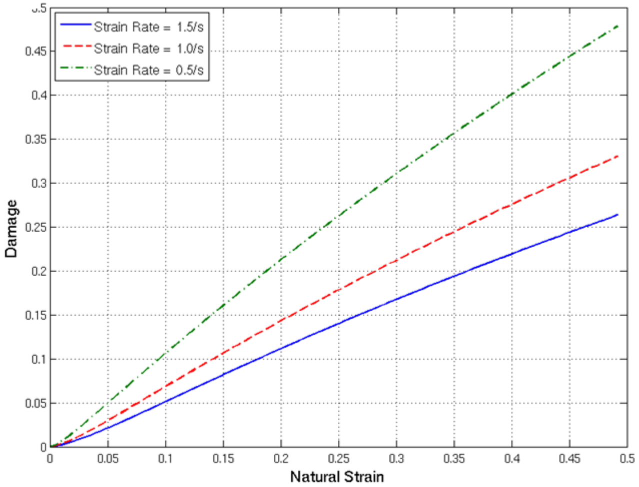

Figure 5.3 – Strain rate influence on the damage variable-strain behavior of a thermo-viscoelastic damage model - a single Maxwell branch. Viscous strains evidenced as the guiding force behind damage evolution: higher values for the damage variables obtained for the lower stress cases.

gent operators make it well-lent to the task.

A single Maxwell rheological element is simulated in the first example, with no spring in parallel.

As shown in detail in previous sections, the proposed model of thermo-viscoelastic damage is built upon specifically chosen forms of free energy and dissipation, leading to a naturally separable structure. The update of the damage variable can be uncoupled from that of the viscous strains. This was shown to be consistent with the assumed hypothesis of strain equivalence. In essence, the update of viscous variables takes place in the undamaged space of equivalent strains. This first step of the internal variable update corresponds to performing the same uniaxial tensile tests in the undamaged model presented in chapter 4. This gives rise to effective stresses following the same type of thermo-viscoelastic behavior. In figure 5.2, the predicted curves of effective stress-strains are presented. As the imposed strain rate increases, so does the value of effective stress.

With the updated values of viscous strains in hand, it is then

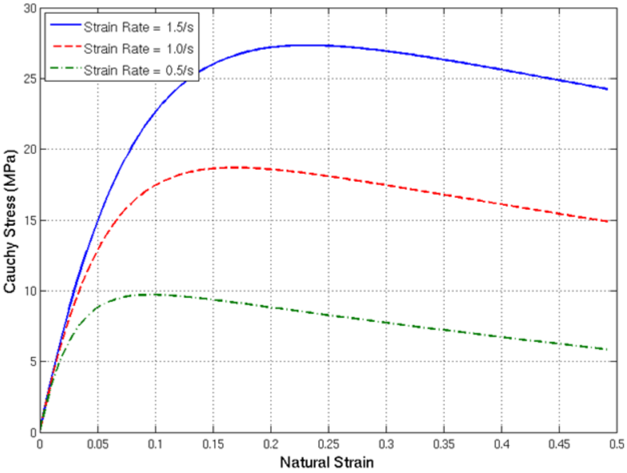

Figure 5.4 – Strain rate influence on the stress-strain behavior of a thermo-viscoelastic damage model - a single Maxwell branch.

possible to evaluate the evolution of the damage variable (as in equation 5.24). Viscous strains are the main guiding force of damage evolution. Therefore, where viscous strains are lower, so is the damage measure. In a Maxwell model, higher strain rates translate into lower viscous strains, as the spring is forced to bear the imposed loads while the dashpot has not had enough time for relaxation. These effects are shown in figure 5.3.

The update of damage variables concludes the local optimization procedure. Stresses can then be updated in hyperelastic-fashion, from the internal part of the effective incremental potential ($\mathcal{H}_n^{effInt}$) as described in equation 5.25. Due to damage evolution, real stresses acting upon the simulated material point exhibit softening, as shown in figure 5.4. The so called Mullins effect commonly observed in polymers is often simulated with models allowing for such a softening due to viscoelastic damage. Further investigation on the application of the model proposed here to the description of the Mullins effect is necessary, though.

Since the proposed thermomechanical constitutive model is fully coupled, the evolution of temperature and entropy come naturally as a result of the optimization of the effective incremental potential. Figure 5.5 shows an interesting competition of effects. In Maxwell models,

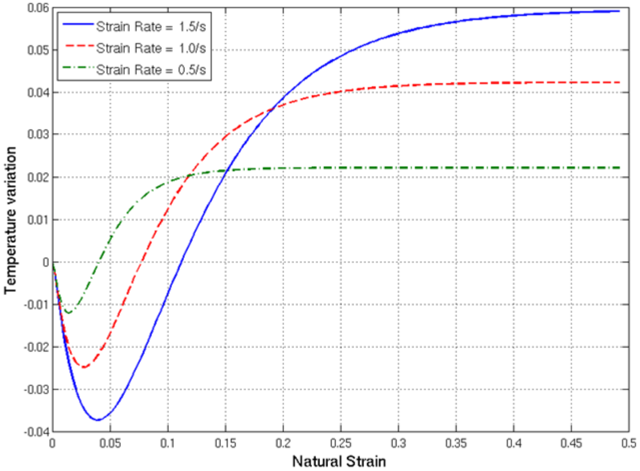

Figure 5.5 – Strain rate influence on the temperature-strain behavior of a thermo-viscoelastic damage model - a single Maxwell branch. Initially, thermoelastic effects result in cooling. Later, viscous dissipation dominates and local heat generation ensues.

as loads are applied, the spring is led to bear all the initial instantaneous deformations. Some time has to pass before viscous flow can take place at the dashpot, due to the characteristic relaxation time introduced via the material's viscous parameters. Hence, at the beginning, the elastically stored energy potential dominates the incremental potential. Thermoelastic cooling, typical of isentropic elastic processes, dominates the evolution of temperature at first. Next, however, as viscous strains start to take place, internal dissipation grows in magnitude and local heat generation (recalling that adiabatic conditions are considered) takes over. Temperatures then start to increase, in a clear demonstration of the nature of thermomechanical coupling.

Next, following the sample tests presented in the previous chapter, a comparison of the damaged model with its undamaged counterpart is done for relaxation tests. The same rheological model (two Maxwell branches and a spring in parallel) and material parameters used previously in the relaxation tests of chapter 4 are kept, but potentials are modified by the damaging factor $(1 - d)$ as well as a damage dissipation pseudo-potential are added to the model. Test conditions remain the same: the material is loaded to a logarithmic strain of 0.3

at the indicated strain rate and later kept there.

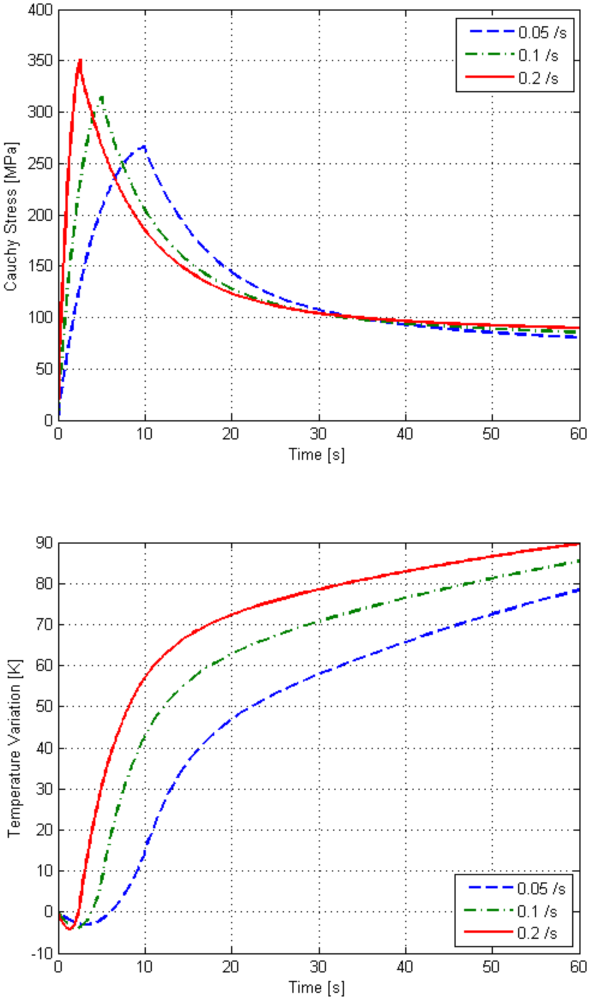

Figure 5.6 – Relaxation test of two Maxwell branches with damage at different strain rates: evolution of stress and temperature.

Figure 5.6 shows the evolution of the actual stress through time for three different initial strain rates, as well as the corresponding temperature evolution. Unlike the thermo-viscoelasticity model, now stresses do not converge to the same equilibrium level. As viscous strains evolve during the second phase of the test, the damage variable evolves differently for each case and different stress levels are obtained.

The profile of temperature evolution follows the same pattern shown for the previous set of examples, with an initial thermoelastic cooling giving place to dissipation-driven heating. Even though lower viscous strains are reached for higher imposed strain rates, the fact that higher viscous stresses are present dominates total dissipation, and results in higher temperature levels.

This can be seen in figure 5.7, where the entropy evolution profile is consistently higher for higher imposed strain rates.

The damage evolution profile predicted by the model is also presented in figure 5.7. Clearly, the brunt of damage evolution takes place during the relaxation phase of the test, instead of during the loading phase. For higher imposed strain rates, lower characteristic times are excited, and thus the initial higher slope in damage evolution. When high frequency effects have subsided, damage evolution is slower. On the other hand, for slower strain rates, it takes longer for excited modes to relax, and damage evolves longer.

Next, hysteresis curves for Maxwell and generalized Kelvin-Voigt/Maxwell rheological models are analyzed. The same material and loading parameters used in the previous chapter are kept here. Additionally, figures are presented in the same scales, in order to facilitate comparisons.

The rheological model with two Maxwell branches in parallel to a single spring is shown in figure 5.8. Once more, the hysteresis loop, representing energy loss due to irreversible viscous strains is evident. Now, due to damage evolution, however, stress levels obtained in the second traction phase are markedly lower.

In addition to viscous straining, damage evolution is an additional source of dissipation, which is reflected in higher temperature increase levels obtained throughout the cyclic test, as seen on the bottom of figure 5.8. The profile of predicted damage evolution is shown in figure 5.10.

For the full generalized Kelvin-Voigt/Maxwell model with damage, hysteresis loops are more pronounced, as shown in figure 5.9, because the Kelvin-Voigt dashpot is subjected to the full imposed strain rate instantly. In Maxwell elements, the spring in series with the dashpot acts as a buffer, and stresses change signs much closer to the original starting point. The effect of damage appears again in the lower stress levels obtained for the second traction step.

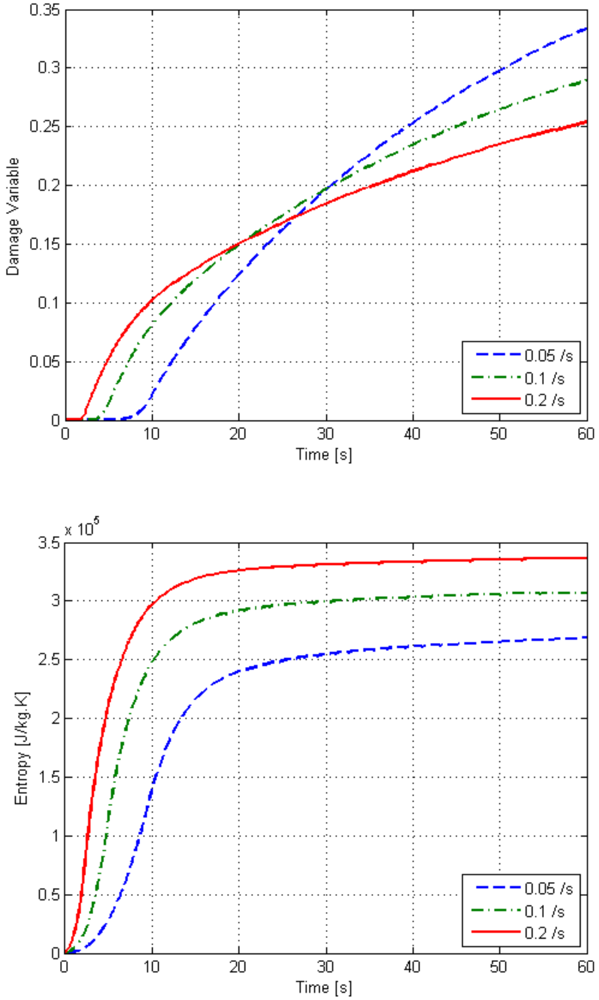

Figure 5.7 – Relaxation test of two Maxwell branches with damage at different strain rates: evolution of damage variable and entropy.

As expected, temperature levels are higher for the generalized model. This is also due to dissipation in the Kelvin-Voigt dashpot, which dominates temperature increase. The temperature profile on

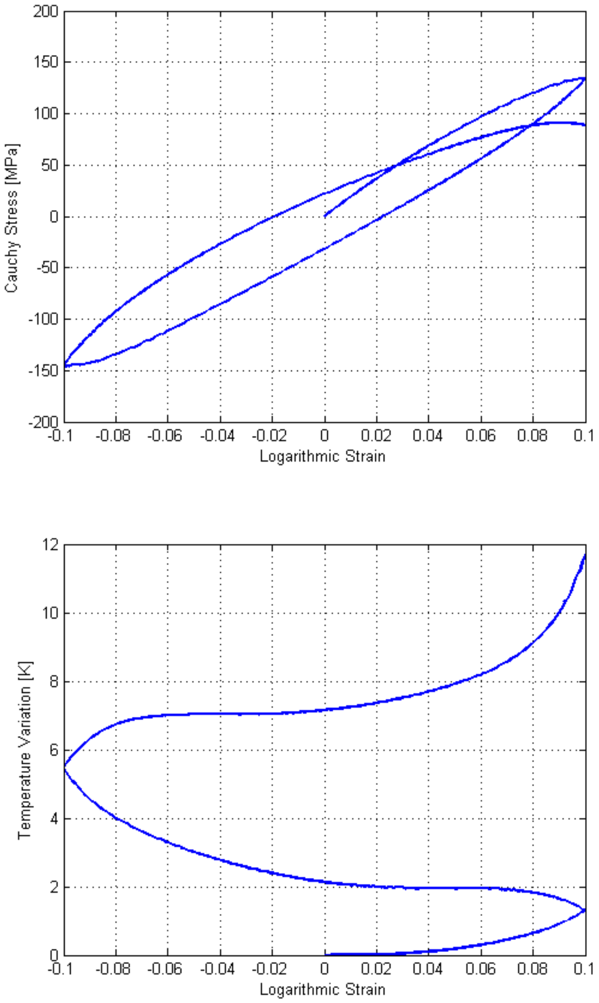

Figure 5.8 – Hysteresis loop in cyclic loading of Maxwell elements with damage: stress-strain and temperature-strain curves.

the bottom of figure 5.9 shows a strong linear component coming from the constant viscous stresses experienced by the dashpot in parallel, subjected to the total imposed strain, constant at every load step.

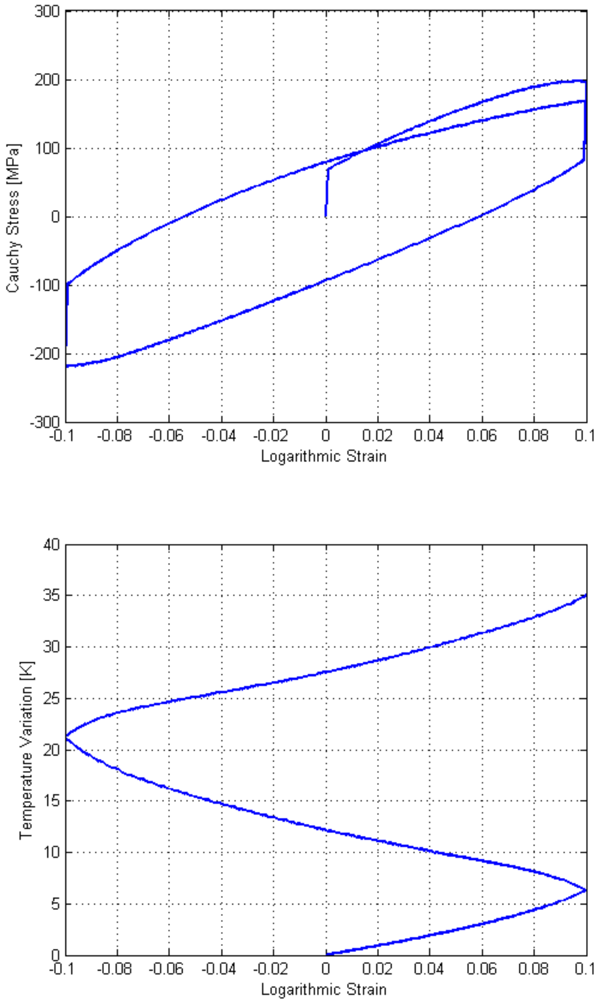

Figure 5.9 – Hysteresis loop in cyclic loading of a generalized Kelvin-Voigt/Maxwell rheological model with damage: stress-strain and temperature-strain curves.

The predicted damage evolution profile is represented in figure 5.10.

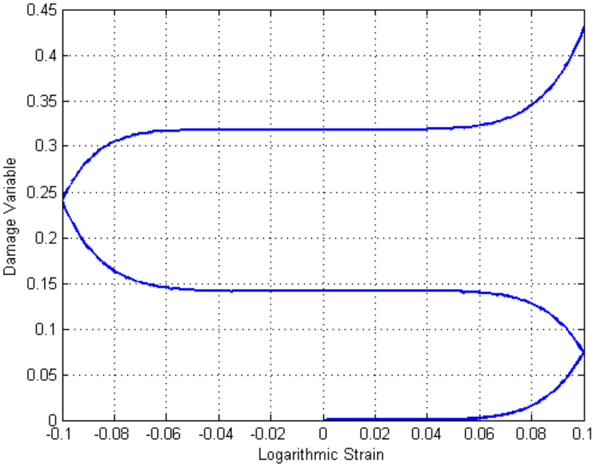

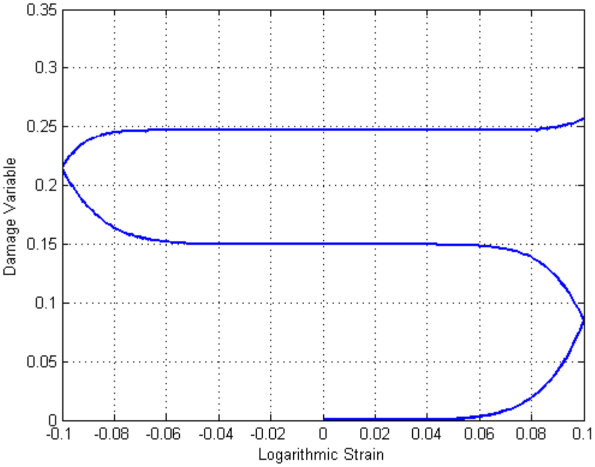

Figure 5.10 – Evolution of the damage variable during the cyclic loading of two Maxwell branches (on top) and of the generalized Kelvin-Voigt/Maxwell rheological model (on the bottom).

6 NONLOCAL TREATMENT OF THERMOVISCOELASTIC-DAMAGE THROUGH THE THICK LEVEL SET METHOD

> *Chapter overview: Purely local models of damage are limited by the known issue of spurious localization. Since material points do not communicate, damage (essentially a volume-depending measurement of the phenomenon of material degradation) can generate catastrophic failure in a vanishing volume, and thus with zero dissipation (the physically motivated model becomes strongly mesh dependent). This was the motivation for the development of all nonlocal damage models. A recent alternative, providing a bridge between damage and fracture using the level set toolbox, is the Thick Level Set method. In it, damage is associated to a characteristic length, which leads to the generation of fairly narrow regions of distributed damage around points where initiation was detected through the chosen criterion. In recently proposed enrichments to the original TLS model, it is shown that there must be restriction on the rate of damage evolution.*

6.1 INTRODUCTION: SPURIOUS LOCALIZATION AND NONLOCAL DAMAGE MODELS

All the previously presented damage models are essentially local, in that the evolution of internal variables is independent of their gradients. In other words, internal variables evaluated at every material point are oblivious to what happens in adjacent points, since there is no way for information exchange to take place. This is a feature shared by many classic damage models, giving rise to the thoroughly explored issue of spurious localization.

Since any material volume cannot share information with its neighbors in purely local models, it is possible for the damage initiation threshold to be attained in a single element while the rest of the material remains in its perfectly undamaged state. In turn, this may lead to typically brittle material behavior, with little to no dissipation taking place between damage initiation and evolution (since damage takes place in an arbitrarily small material volume, related to the level of refinement of the mesh - whereby spurious localization is often reflected in and referred to as pathological mesh dependence).

This problem was evident from the early papers on continuum damage mechanics onward, and has merited the attention of many researchers throughout the years. The field of nonlocal damage models is well established, and counts several different branches, depending on the proposed approach to circumvent the limitations of purely local models. A concise taxonomy of the more classical families of nonlocal damage models can be found in Peerlings et al. (2001), and is briefly reviewed below, along with other more recent approaches (such as those based on phase field theory, such as the one proposed by Miehe, Welschinger & Hofacker (2010), and variationally based formulations, as found in Bourdin, Francfort & Marigo (2008)). The more recent alternatives include the Thick Level Set method (originally proposed by Moës et al. (2011), and further developed by Bernard, Moës & Chevaugeon (2012) and Stolz & Moës (2012)), the chosen method used in conjunction with the proposed variational models in the following, which shall receive its own subsection and be explored in finer detail.

6.2 BRIEF OVERVIEW OF NONLOCAL DAMAGE MODELS

As previously mentioned, the main issue limiting the application of purely local damage models is their inability of transferring information between material points. This is the motivation behind the development of all types of nonlocal damage models. What differentiates them is the mechanism of information transfer between different parts of the body.

Before its application to damage problems, this sort of feature had already been incorporated into other constitutive models. Starting from the assumption that the free energy potentials should depend on gradients of some measure of deformation (appearing as additional independent variables in the set $\mathbf{Z}$) and then deriving the thermodynamic consequences of such a model by means of the Coleman-Noll procedure described in chapter 3, nonlocal constitutive models, such as nonlocal elasticity (due to Kröner (1967) and Eringen (1972)) and nonlocal plasticity (Eringen (1981, 1983), for a couple of early models), were successfully developed to deal with various issues, such as limiting localization around stress concentration regions.

The classical families of nonlocal damage models originated from the available tools for nonlocal constitutive models. Following a general classification used, for example, in Peerlings et al. (2001), Askes & Sluys (2002), Simone (2007), there are three main families of classical nonlocal damage models, according to the choices of variables to carry the nonlocal information. A very brief overview of the basis behind each family is given below.

The first nonlocal constitutive models dedicated to damage were the so called integral models, developed initially in Pijaudier-Cabot & Bazant (1987) and Bazant & Pijaudier-Cabot (1988). Though variations exist, in general the local (equivalent[6.1]) strain measure is replaced by a weighted average of strains in a neighborhood around each point (denoted with an overhead bar, $\bar{\epsilon}$), which then guides the evolution of damage. In small strains, this would translate to:

$$\bar{\epsilon}(\mathbf{x}) = \frac{\int_{\Omega_t} \omega(||\mathbf{x}-\boldsymbol{\xi}||)\epsilon(\boldsymbol{\xi})dV}{\int_{\Omega_t} \omega(||\mathbf{x}-\boldsymbol{\xi}||)dV} \tag{6.1}$$

In the above equation, a weighting function $\omega(||\mathbf{x}-\xi||)$ is used, with $\boldsymbol{\xi}$ denoting the neighborhood of the point $\mathbf{x}$. The size of the domain that is integrated can vary, from determined characteristic lengths (denoted from here on as l_c) to the full domain.

As discussed in Simone (2007), such integral models have some undesired numerical consequences, namely the significant reduction in matrix sparsity, as every element (in a finite element context) communicates with many others.

In order to circumvent the limitations to the application of nonlocal integral models of damage, gradient-based models were proposed. The central concept towards the development of gradient models is taking the Taylor expansion of the local (equivalent[6.2]) strains:

$$\epsilon(\boldsymbol{\xi}) = \epsilon(\mathbf{x}) + \frac{\partial \epsilon}{\partial x_i}[\xi_i - x_i] + \frac{1}{2!}\frac{\partial^2 \epsilon}{\partial x_i \partial x_j}[\xi_i - x_i][\xi_j - x_j] + ... \tag{6.2}$$

Depending on how the expanded expression of local (equivalent) strain is used, two families of gradient-enhanced damage models are commonly distinguished: explicit and implicit gradient models.

[6.1] As discussed in the previous chapter, in the present document the hypothesis of strain equivalence is considered, so that the distinction here is not necessary. Integral models, however, can be used in conjunction with any local model of damage. If the equivalent strain is defined differently, for instance when considering the hypothesis of strain energy equivalence, the nonlocal treatment is dispensed to the corresponding measure of strain.

[6.2] See discussion in footnote 6.1.

Taking this expansion back to the integral average of equation 6.1, and determining a cutoff to terms up to the second order, the averaged strain measure at point $\mathbf{x}$ now reads simply as follows, where $a(l_c)$ is a constant depending essentially on the determined size of the acting neighborhood, and therefore, of the introduced characteristic length l_c for damage phenomena:

$$\bar{\epsilon}(\mathbf{x}) = \epsilon(\mathbf{x}) + a(l_c)\nabla^2\epsilon \tag{6.3}$$

The equation above is the basis to the explicit gradient models, described in Askes & Sluys (2002) and used, among many other examples, in Frémond & Nedjar (1996). It is clear that the averaged measure guiding damage evolution takes into account a purely local contribution and some nonlocal information carried by the gradient of strains.

Explicit gradient damage models are easier to implement than integral models, and exhibit lower computational cost, as matrix sparsity is recovered (elements communicate only as far as determined to calculate gradients). However, as discussed in (ASKES; SLUYS, 2002), they may introduce spurious modes in some conditions, leading to non-physical results and reflecting some influence of the discretization (i.e., the damage model cannot be considered mesh independent).

Another alternative, for which these issues are no longer present, is the family of implicit gradient models. Developed in Peerlings et al. (1996), and used in many articles such as Peerlings, Massart & Geers (2004), the implicit gradient damage models assume that the local measure of strain is influenced by the gradient of the average strains, so that equation 6.3 becomes:

$$\epsilon(\mathbf{x}) = \bar{\epsilon}(\mathbf{x}) - a(l_c)\nabla^2\bar{\epsilon}(\mathbf{x}) \tag{6.4}$$

The average strains continue to be the driving force behind damage evolution. Now, two coupled sets of equations have to be solved, to enforce the definition of the local (equivalent) strains above.

This has several consequences on the mathematical structure of the nonlocal formulation. No extensive discussion is made here, as it falls outside the scope of the present document. However, it should be noted that implicit gradient formulations are equivalent to integral formulations, using Green's function as a weighting function, which attributes higher weights to material points $\boldsymbol{\xi}$ closer to the point $\mathbf{x}$ in question (PEERLINGS et al., 2001). The formulation can be shown to be fully mesh independent, and not to introduce non-physical response.

These classical models have deserved extensive attention in the literature in recent decades, being applied to various contexts. They still represent an increase on computational costs of damage modeling, however, and have thus remained short of completely solving the issues of nonlocal damage modeling in engineering applications, especially as damage increases to the point of demanding the inclusion of macroscopic cracks.

Recently, new alternatives based on other physical principles have been developed, in attempts to provide a different point of view to the problem, often straddling the conceptual gap between fracture mechanics (originated by Griffith (1921)) and continuum damage mechanics (this gap will be very briefly discussed in the following subsection).

One such effort is the phase-field approach to fracture, developed in Hakim & Karma (2005). Coming from a physics background, a model for the prediction of crack paths is proposed. A type of damage-like field is used to effectively diffuse the crack along some neighborhood. The evolution of the crack tip is then determined by the minimization of an energy-like function.

Another recent development is the variational approach to fracture presented in Bourdin, Francfort & Marigo (2008). The problems of crack initiation and evolution are respectively framed as global and local energy minimization problems. Once more, a type of smeared quantity around the crack (which can once more be interpreted as a measure of damage) is used in implementation, similarly to some models of cohesive forces.

Sharing some concepts with these recent alternatives to the nonlocal modeling of damage and fracture, but making use of a different set of numerical tools dedicated to more efficient implementations, the Thick Level Set approach proposed in Moës et al. (2011) is the nonlocal model of choice in the present document. It is described in detail in the following subsection.

6.3 THE THICK LEVEL SET APPROACH TO DAMAGE AND FRACTURE

One of the more recent alternatives to nonlocal damage modeling is the Thick Level Set (TLS) approach to damage and fracture. Originally proposed by Moës et al. (2011) and later developed by Bernard, Moës & Chevaugeon (2012) and Stolz & Moës (2012), the TLS model in fact constitutes a bridge between the classical fields of continuum damage mechanics and fracture mechanics. Although deeply steeped on and dependent of the mathematical toolbox of level sets, the TLS is not simply a numerical way of encompassing these two separate fields, but rather a theoretical foundation.

This theoretical foundation is related to the hypothesis that materials have an inherent property determining the minimum distance between fully sound and fully degraded regions of the material, a characteristic length (l_c) to the degradation of material properties. In chapter 2, the physical evidence of the existence of such a characteristic length in polymers was discussed, manifested through crazing in the wake of an evolving crack. As shown in further detail in the following paragraphs, the existence of such a property motivates the representation of damage variables in fields, where different regions are clearly distinguishable.

Instead of using only local variables to store damage information throughout the material domain, in the TLS approach, there are two clearly identified fronts. Using a single level set function, denoted ϕ, a damage initiation front is identified as the iso-zero contour of the level set (marked Γ_0, in figure 6.1 below). Next, a front of totally damaged material is identified as the "iso-l_c" contour (marked Γ_c in figure 6.1). In the wake of the "iso-zero" front, since the material is fully sound, no damage evolution model needs to be computed. No healing is considered, so that after the "iso-l_c", since the material has become completely degraded, no damage evolution model is necessary anymore. Hence, the computation of damage evolution, the nonlocal part of the model, only happens in a typically small region of the material domain Ω_t, a primer into one of the main advantages of the TLS over other nonlocal models of damage.

The level set ϕ has the property of being a signed-distance function, so that a constant distance between fronts Γ_0 and Γ_c can be kept at the constant value of the introduced characteristic length l_c. In order to remain a signed-distance function, the gradient of the level set ϕ must have unitary length:

$$||\nabla\phi|| = 1 \tag{6.5}$$

The damage variable then relates to the level-set function, as shown in equation 6.6 below. A representation of a possible damage field and its corresponding level-set is shown in figure 6.1.

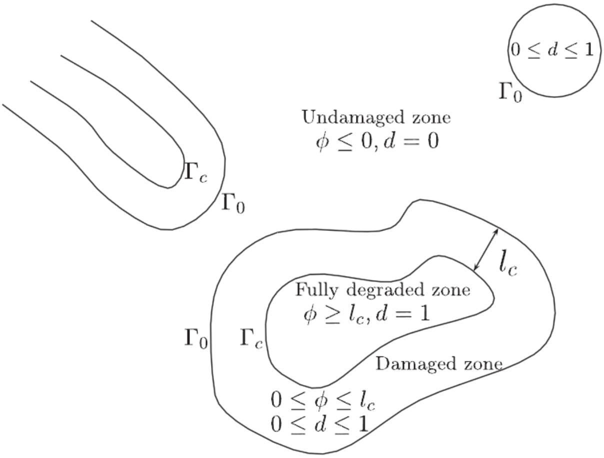
$0 \leq d \leq 1$
Γ_0
Undamaged zone
$\phi \leq 0, d = 0$
Γ_c
Γ_0
l_c
Fully degraded zone
$\phi \geq l_c, d = 1$
Γ_0
Γ_c
Damaged zone
$0 \leq \phi \leq l_c$
$0 \leq d \leq 1$

Figure 6.1 – Distribution of the damage variable as delimited by the Thick Level Set. [Source: (MOËS et al., 2011)]

$$\begin{aligned} &d(\phi) = 0, && \phi \leq 0 \\ &0 < d(\phi) < 1 \Leftrightarrow d'(\phi) \geq 0, && 0 \leq \phi \leq l_c \\ &d(\phi) = 1, && \phi \geq l_c \end{aligned} \tag{6.6}$$

Since the level-set is a signed-distance function, it can be shown that in parallel contours to the "iso-zero", the damage variable must be constant. This induces a natural change of variables, with the Cartesian coordinates in two dimensions giving place to the position along the front s and to the distance to the damage front (equal to the vale of the level-set itself, ϕ). This is represented in figure 6.2. All the damage evolution equations are formulated in these modified coordinates.

By construction, in addition to the characteristic length l_c, the second ingredient to the model is the damage profile along the level-set thickness ($d'(\phi) = \frac{\partial d}{\partial \phi}$). Smooth derivatives at $\phi = 0$ and $\phi = l_c$ are used for continuity of the model.

As usual, the level set evolution equation is given as follows, where the normal velocity of the damage front has magnitude v_n.

$$\frac{\partial \phi}{\partial t} + v_n \nabla \phi . \mathbf{n} = 0 \tag{6.7}$$

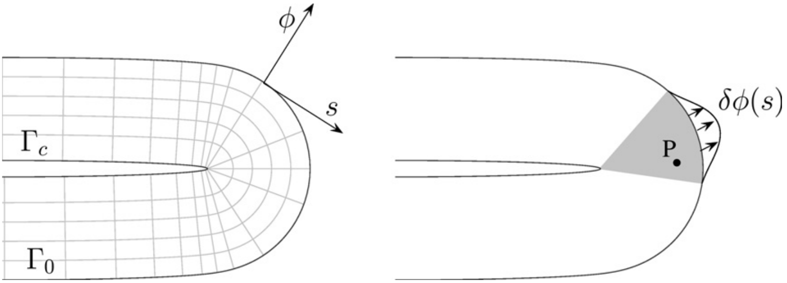

Figure 6.2 – Local coordinate system induced by the TLS: positions along the damage front s and normally along the level set thickness ϕ. [Source: (BERNARD; MOËS; CHEVAUGEON, 2012)]

Accordingly, the damage evolution equation is given by:

$$\dot{d} = \frac{\partial d}{\partial \phi}\frac{\partial \phi}{\partial t} = d' v_n \tag{6.8}$$

In order to verify thermodynamic consistency, a variational-like approach to damage modeling can be taken. Replacing the explicit dependence on the damage variable d by the level-set ϕ in the potential $\mathcal{H}_n$ representing the problem, the stationarity condition with respect to admissible variations $\delta\phi$ (which, for the proposed variational thermo-viscoelastic damage model, is of the specific form 5.24) of the level-set can be written as follows:

$$\frac{\partial \mathcal{H}_n}{\partial \phi}[\delta\phi] = \underbrace{-\int_\Omega Y^d d'(\phi)\delta\phi d\Omega}_{\text{I}} + \underbrace{\Delta t \int_\Omega \left\langle \frac{\partial \psi^d}{\partial (d'(\phi) v_n)} \right\rangle \delta\phi d\Omega}_{\text{II}} = 0 \tag{6.9}$$

The term marked I in the equation above can be interpreted as the necessary energy to make the level-set move by $\delta\phi$. Clearly, the integrals only need to be performed in the small region between Γ_0 and Γ_c, a typically small region denoted Ω_{0-c} in Moës et al. (2011), whose volume element after the change in variables can be shown to read as follows (where the curvature radius of the level-set at the "iso-zero" is denoted $\rho(s)$):

$$d\Omega = \left[1 - \frac{\phi}{\rho(s)}\right] d\phi ds \tag{6.10}$$

The incremental energy needed to make the level-set move by $\delta\phi$ can now be developed as follows, with the integral along the level-set thickness known *a priori* by the introduction of the damage profile $d'(\phi)$. A configurational force $g(s)$ is defined in equation 6.12:

$$\begin{aligned} -\int_{\Omega} Y^d d'(\phi)\delta\phi d\Omega &= -\int_{\Omega_{0-c}} Y^d d'(\phi)\delta\phi d\Omega \\ &= -\int_{\Gamma_0}\int_0^{l_c} Y^d(\phi, s) d'(\phi)\delta\phi(s)\left[1 - \frac{\phi}{\rho(s)}\right] d\phi ds \\ &= -\int_{\Gamma_0} g(s)\delta\phi(s) ds \end{aligned} \tag{6.11}$$

It can be seen that $g(s)$ is power conjugated to the velocity of the front (equation 6.13 brings the internal dissipation due to damage) and dependent on the imposed damage profile along the thickness of the level-set:

$$g(s) = \int_0^{l_c} Y^d(\phi, s) d'(\phi)\left[1 - \frac{\phi}{\rho(s)}\right] d\phi \tag{6.12}$$

$$\mathcal{D}^d_{int} = \int_{\Omega_{0-c}} Y^d d'(\phi) v_n d\Omega = \int_{\Gamma_0} g(s) v_n ds \tag{6.13}$$

Damage evolution equations can be derived by solving the non-linear equation 6.9. The correct admissible evolution of the level-set $\delta\phi$ is determined by the balance between terms I and II. This can be seen as a balance between the damage dissipation as estimated by the free energy (via the energy restitution rate Y^d) and by the damage dissipation pseudo-potential ψ^d. Following in the spirit of the change of variables, it is possible to write a new form for the dissipation pseudo-potential called $\bar{\psi}^d$, as a function of the front velocity v_n, which replaces the rate of the damage variable $\dot{d}$.

$$\int_{\Omega_{0-c}} \psi^d(d'(\phi) v_n) d\Omega = \int_{\Gamma_0} \bar{\psi}^d(v_n, s) ds \tag{6.14}$$

Since the damage profile along the level-set thickness is given, in Bernard, Moës & Chevaugeon (2012) an expression for the determination of an average value of the energy restitution rate along the level-set ($\bar{Y}^d$) is given as follows, and represented in figure 6.3. This can take all the necessary evaluations of functions in equation 6.8 to the damage initiation front, and render implementation more efficient:

$$\bar{Y}^d(s) = \frac{\int_0^{l_c} Y^d d'(\phi)\left[1 - \frac{\phi}{\rho(s)}\right] d\phi}{\int_0^{l_c} d'(\phi)\left[1 - \frac{\phi}{\rho(s)}\right] d\phi} \tag{6.15}$$

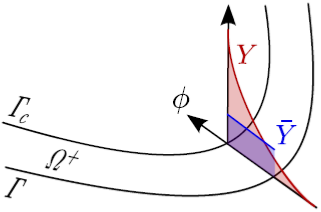

Figure 6.3 – View of the average energy restitution rate ($\bar{Y}^d$) along the thick level set. [Source: Kévin Moreau]

The original TLS model, in Moës et al. (2011), proposed the creation of small damage fronts around initiation points, as soon as a damage threshold (usually called Y^c in classical models) was reached. The nonlocal treatment of damage started from initiation. However, under certain conditions, the damage variable may be diffuse along the material domain. In other words, some loading conditions may lead to damage spread smoothly along the body. In those cases, no localization is occurring, and the chosen local damage model would be able to properly solve the problem.

In Bernard, Moës & Chevaugeon (2012), a different approach to the one in Moës et al. (2011) is proposed. Since the goal is to avoid localization, the TLS treatment need only be activated once the damage gradient reaches a certain value. In this diffused damage TLS model, damage evolution only starts to take into account nonlocal terms (such as $g(s)$) once the gradient of the level-set reaches $||\nabla\phi|| = 1$, the condition previously imposed so that it remains a signed-distance function. This leads to a new sectioning of the domain into areas of nonlocal modeling of damage (Ω^+, where it is imposed that $||\nabla\phi|| = 1$) and areas of local modeling of damage (Ω^-, where $||\nabla\phi|| < 1$), as seen in figure 6.4

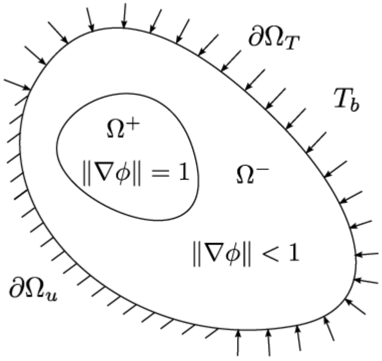

Figure 6.4 – Diffused damage TLS models: areas of nonlocal (Ω^+) and local damage modeling (Ω^-) as determined by the gradient of the level-set function. [Source: Kévin Moreau]

Two distinct terms now contribute to the internal dissipation due to damage evolution. In region Ω^-, the purely local damage model can be used in its original form. In region Ω^+, nonlocal contributions are taken into account in the determination of the average energy restitution rate $\bar{Y}^d$.

$$\mathcal{D}^d_{int} = \int_{\Omega^+} \bar{Y}^d d'(\phi) v_n d\Omega + \int_{\Omega^-} Y^d \dot{d} \quad d\Omega \tag{6.16}$$

In the final section of the present chapter, the diffused-damage version of the TLS is applied to a sample example of thermo-viscoelastic damage.

6.4 BRIEF OBSERVATIONS ON THE CONNECTION BETWEEN THE THICK LEVEL SET AND FRACTURE MECHANICS

Before moving on to the details of the coupling between the variational thermo-viscoelastic damage model proposed in chapter 5 and the TLS approach to damage described above, a brief aside must be made on the TLS as viewed from a fracture mechanics angle. One of the central reasons for the choice of the Thick Level Set approach to model polymer behavior in the full range of life, from fully sound to fully degraded materials, was its ability to include fracture and damage in a single framework. As mentioned of the phase-field and the variational approaches to fracture, the TLS also provides a bridge between fracture and damage mechanics, although founded upon different physical principles.

Developed by the same group that has extensively worked with the extended finite element method[6.3], the TLS lends itself well to the inclusion of material interfaces and discontinuities. The formalism of level sets is present, with its values stored at Gauss points allowing for elements to be cut and enriched, in X-FEM fashion (typically, Heaviside approximation functions are added to the regular FEM functions of choice, in the presence of a crack). Within the TLS formalism, the "iso-l_c" contours are clear delimiters of regions that have lost all their ability to bear loads. The inclusion of a crack at material regions where the damage variable has reached $d = 1$ is a natural way of proceeding in this context.

Much attention has been devoted to the numerical aspects of crack initiation, growth, coalescence and branching in the first publications on the Thick Level Set (MOËS et al., 2011; BERNARD; MOËS; CHEVAUGEON, 2012). Starting from fully sound material, the TLS model was applied to regularize damage behavior and determined when a macroscopic crack should be inserted in the domain. Once a crack is present and it necessary to evaluate if it will grow (the classical setting for Griffith-like fracture mechanics (GRIFFITH, 1921)), it is interesting to compare the typical quantities of TLS with those of fracture mechanics.

This was done in Moës et al. (2011), where a close relation between the configurational force $g(s)$ of TLS and the energy release rate G of fracture mechanics (roughly defined as the available energy for crack advancement) is drawn. Correspondingly, a parallel between the critical value for crack advancement G^c in fracture mechanics and the energy restitution rate threshold for damage Y^c is made. The direction of the crack is called $\mathbf{e}$, and the normal at each point of the level-set is named $\mathbf{n}(s)$.

$$G = \int_{\Gamma_0} g(s)\mathbf{e}.\mathbf{n}(s)ds \qquad G^c = \int_{\Gamma_0} \bar{Y}^c\mathbf{e}.\mathbf{n}(s)ds \tag{6.17}$$

Finally, depending on the chosen form of the damage dissipation potential, it is possible to calculate the stress intensity factor K around

---

[6.3] X-FEM for short; the interested reader is referred to a couple of the early articles on the method (MOËS; DOLBOW; BELYTSCHKO, 1999; SUKUMAR et al., 2000) the crack tip. Details are omitted here, as it falls outside the scope of the document. However, it should be clear that the TLS bridges the gap between damage and fracture mechanics. This is due to the inclusion of the characteristic length l_c, and not to the numerical tools used to deal with cracks, as demonstrated by the possibility of deriving closed form expressions relating TLS variables to fracture mechanics variables. In other words, the TLS is a unified theoretical model of damage and fracture, rather than a numerical framework with guidelines on how to change between two different models.

6.5 THICK LEVEL SET REGULARIZATION OF THE VARIATIONAL THERMO-VISCOELASTIC DAMAGE MODEL

One of the advantages of the Thick Level Set approach to damage is the ability of dealing with any local model of damage, as will be explored in the next paragraphs. In the founding articles (MOËS et al., 2011; BERNARD; MOËS; CHEVAUGEON, 2012), very classical local models of elastic damage (similar to the ones of Kachanov (1999), as decribed in equation 5.1) were used, as the objective was to demonstrate the nonlocal workings of TLS.

In the present text, instead of further developing and exploring the nonlocal tools, a converse goal can be stated. Throughout the previous chapters, extensive attention was dedicated to the development of a thermodynamically-consistent variational model of damage. In this chapter, the use of the tools of TLS in conjunction with the coupled model of thermo-viscoelastic damage is explored, in the final theoretical contribution of this document. So far, the combination of the TLS with other local models of damage had yet to be explored in the literature.

It is clear from the derived expression 6.9, for nonlocal damage evolution within the TLS framework, that there is no special restriction on the chosen forms for the Helmholtz free energy nor for the dissipation pseudo-potentials. Provided that the change of variables, from d to ϕ, and from Ω to Γ_0, are done correctly, any local model can be used to calculate the energy restitution rate Y^d and the corresponding dissipation term $\dfrac{\partial \psi^d}{\partial \dot{d}}$. In order to couple the TLS approach to a local damage model of choice, then, it suffices to define the appropriate expressions.

For the variational thermo-viscoelastic damage model of chapter 5, the energy restitution rate can be defined and expressed as follows, making use of the introduced separation between the equivalent problem of undamaged thermo-viscoelasticity (represented here in the Helmholtz free energy $\tilde{W}$):

$$Y^d = -\frac{\partial W}{\partial d} = -\frac{\partial f(d)}{\partial d}\tilde{W} \tag{6.18}$$

It suffices to change variables to have the appropriate expression of Y^d to plug into the TLS model. This can be done through the equation 6.15, where the average energy restitution rate along the level-set thickness is used, following Bernard, Moës & Chevaugeon (2012).

The definition of the power law form for damage dissipation of equation 5.15 is recalled here:

$$\psi^d\left(\frac{T_{n+1}}{T_n}\frac{\Delta d}{\Delta t}; d_{n+\alpha}, T_{n+\alpha}\right) = \\ \left\{\frac{m'}{m'+1} Y_0^d \dot{d}_0 \left[\frac{T_{n+1}}{T_n}\frac{\Delta d/\Delta t}{\dot{d}_0}\right]^{\frac{1}{m'}+1}\right\} \tag{6.19}$$

In the same spirit of what was done for the energy restitution rate, a change of variables needs to be performed, through equation 6.14. The new form of the damage dissipation potential $\bar{\psi}(v_n, s)$ can be shown to have a local expression for every point s along the damage front Γ_0:

$$\bar{\psi}(v_n) = \int_0^{l_c} \psi(d'(\phi)v_n)\left[1 - \frac{\phi}{\rho(s)}\right] d\phi \tag{6.20}$$

As indicated by the accolades in equation 6.9, since the proposed local model is thermomechanically-coupled and employs the parameterization of Yang, Stainier & Ortiz (2006), in order to keep thermodynamic consistency (energy conservation (STAINIER, 2011)) an appropriate average of the dissipation along the time step must be taken when evaluating derivatives in an incremental context.

Before moving on to the summary of operations needed to implement the TLS in conjunction with the thermo-viscoelastic damage model of the previous chapter, some previously discussed questions can be cast in new light; more specifically, the very need for nonlocal treatment of a thermo-mechanically coupled damage model.

A brief review of nonlocal damage modeling and the detailing of the TLS approach have made clear that including of some gradient measure into the damage evolution expressions is the main ingredient needed to circumvent spurious localization. This guarantees that every point takes into account information of some neighboring region into its damage computations.

In classical approaches, strain gradients are used to this effect. The TLS, on the other hand, can be seen to place restrictions on the damage gradient itself. Other options can also be envisioned, however.

In fully coupled thermomechanical contexts, in particular, other gradient measures are naturally involved in the formulations. When thermal effects both have an influence on and are influenced by mechanical effects, nonlocality can in theory be achieved through conduction modeling.

In the proposed variational model of thermo-viscoelastic damage, coupling mechanisms are manifold. Viscous effects, local heat generation, thermal softening and thermal dilatation are some of the first that come to mind. Focusing exclusively on the way damage is modeled, it is also possible to identify the sources of interplay. When considered as an additional dissipative mechanism, damage evolution clearly contributes to local heat generation. Conversely, since heat accumulation is considered a damage driving mechanism, together with all other volume-depending phenomena, temperature histories naturally influence damage histories.

Thus, as long as temperature modeling includes heat conduction, which is proportional to temperature gradients, it would appear that even the locally managed damage evolution would already include a fully developed nonlocal element.

However, counting on thermomechanical coupling to include the nonlocal element needed to prevent spurious localization can be risky, as will be shown for some examples in the next chapter. In short, it amounts to associating the level of damage concentration to that of temperature concentration. Domain geometry, loading and boundary conditions can all induce sharp temperature gradients, which would in turn be translated into sharp damage gradients and, consequently, into the spurious localization one had hoped to avoid through heat dissipation.

Nonlocality achieved by means of heat dissipation is heavily dependent on loading conditions. In other words, the relation between the time scales of load application and heat dissipation is one determining factor in quantifying the effectiveness of simply employing a model such as last chapter's. Additionally, stress concentration features of the domain geometry may induce severe concentration of heat along very small regions of the body. Thermal boundary conditions can also have a similar effect, in the case of a heat sink effect, for instance.

As previously discussed, there is ample rational and experimental evidence suggesting that a characteristic length for damage evolution is a property of materials, rather than simply being determined by loading conditions. Thus, having a tool such as the TLS is a necessity for various applications of the thermo-viscoelastic damage model presented previously.

6.6 AN ALGORITHMIC VIEW OF THE VARIATIONAL INCREMENTAL UPDATES FOR THE THERMO-VISCOELASTIC DAMAGE MODEL REGULARIZED THROUGH THE THICK LEVEL SET

The inclusion of the Thick Level Set approach to deal with localization issues has some consequences on the general structure of possible implementations of the thermo-viscoelastic damage problem. As for any nonlocal damage model, it is no longer possible to perform the optimization of the incremental functional with respect to damage at every material point independently. Therefore, the concept of effective incremental potential ($\mathcal{H}_n^{eff}$) needs to change, considering only the local optimization of viscous variables - something that can be done only because of the naturally separated structure of the free energy and dissipation potentials.

In order to give a better idea of the necessary effort in implementing the proposed nonlocal damage model, an algothmic view of operations is presented here. As for the previous chapters, a displacement and temperature-driven procedure is considered, and the full thermodynamic state of the material is assumed known at the start of the time step (instant t_n). Both the damage variable d_n and the values of the level-set function ϕ_n are available. Furthermore, the diffused-damage model is used.

1. From the imposed value of $\mathbf{C}_{n+1}$ and from the known value of $\mathbf{C}_n$, the predictor state $\mathbf{C}_{n+1}^{pr}$ is determined through equation 4.11. A spectral decomposition is performed, determining the eigenvectors shared by the Maxwell viscous strains tensor, as a consequence of the stationarity condition with respect to internal variables $\mathbf{M}_j^v$ (equation 4.49).

2. The internal variable update, no longer essentially local, is still

split into two parts because of the chosen form for the potentials (as demonstrated in equation 5.22). The update of viscous variables is performed exactly as before, by solving the nonlinear system of equations 4.52 and 4.55. A Newton-Raphson scheme is used, based on the construction of a tangent matrix to this system of equations. At this point, in addition to the imposed global variables, only the viscous internal variables are known. Damage remains to be determined.

3. With the values of viscous internal variables, an effective incremental potential is built through equation 4.57 (without damage), where a split between internal and external parts similar to the one in equation 4.57 can be done.

4. Damage update is now a nonlocal task. Nevertheless, a first trial is done with the purely local update through the usually nonlinear equation 5.24, with the known values of viscous strains in hand. This is used to update the values of the level-set ϕ. The gradient of the level set is calculated: if it is larger than 1 somewhere, the TLS model comes into action; otherwise, a condition of diffused-damage is present, and only the local damage update needs to be done.

5. For all regions identified as requiring nonlocal treatment (the previously described region Ω^+, either newly included in the current time step after reaching the damage gradient threshold, or in between the "iso-zero" and "iso-l_c" contours at the start of the time step), average quantities of the energy restitution rate $\bar{Y}^d$ and damage dissipation $\bar{\psi}^d$ are calculated. The final position of the level-set ϕ is determined through the nonlinear equation 6.9, corrected up to convergence. The value of the damage variable is updated.

6. Stresses at the end of the time step ($\mathbf{P}_{n+1}$) are updated in hyper-elastic-like fashion through equation 5.26, where the concept of effective stress ($\tilde{\mathbf{P}}_{n+1}$) is present. Iterations between stress and damage updates may be needed, as they are coupled and changes in either alters the stationarity with respect to the other.

7. Entropy is also updated from the stationarity of the effective incremental potential, through equation 5.28. Likewise, iterations may be necessary to achieve simultaneous convergence of stress, temperature and damage fields.

8. The evaluation of tangent moduli follows the formalism of the local model of thermo-viscoelastic damage. However, the cross-derivative terms $\frac{\partial d_{n+1}}{\partial \mathbf{C}_{n+1}}$ and $\frac{\partial d_{n+1}}{\partial T_{n+1}}$ are affected by nonlocal effects (the details are omitted here). Still, the necessary terms for the construction of the moduli are obtained from the same equations as before.

9. All the values of the independent variables, stress conjugates and stored energy are then stored, and the algorithm may continue to the next time step.

This algorithm was used in the implementation of some sample examples, presented in the next subsection.

6.7 SAMPLE NUMERICAL TESTS: TLS REGULARIZATION OF VARIATIONAL THERMO-VISCOELASTIC DAMAGE IN ONE-DIMENSIONAL DYNAMIC SIMULATION OF A BAR

Before moving on to show some simple examples of the connection between the Thick Level Set approach and the variational thermo-viscoelastic damage model (developed in chapter 5), the fundamental contribution of Kévin Moreau (a fellow doctoral student at the Ecole Centrale de Nantes, working with the TLS in dynamics) to their implementation is gratefully acknowledged.

After describing both the local variational model of damage and the nonlocal tools provided by the TLS approach, all the necessary theoretical ingredients are available to demonstrate the capabilities of the combined model.

It is now a nice place to recall the issue that led to the development of nonlocal models of damage. When the loads acting upon a single element (of the finite element mesh used to discretize the body of interest) go over the threshold for damage initiation, while all the neighboring elements remain in the undamaged state, there is a great chance that brittle-like failure phenomena will happen. Since the volume of the element is very small, the damage variable may go from 0 to 1 without dissipating energy. This goes against physical evidence for many materials, whence the name spurious localization. Oftentimes, refining the mesh only aggravates the issue, as failure continues to occur at a single element - whence the alternative name of pathological mesh dependence.

Hence, in order to test the capability of a nonlocal damage model, a possible idea is to induce concentration of loads in a single element of a sample domain. There are several ways to do so, be it via geometrical discontinuities, boundary effects or otherwise.

Another such way is to use the properties of wave propagation in a medium. By inducing constructive interference of colliding waves, a sudden increase in the loads felt by a single element is achieved. Of course, this means that inertia effects cannot be disregarded anymore. However, in simple one-dimensional cases of bars, this does not constitute a major issue.

”Elephant”, a Matlab code developed by Kévin Moreau for the simulation of dynamics applications of the TLS was used as a testing base for the variational thermo-viscoelastic damage model.

Initially designed for local elastic damage models in isothermal applications, the program required several modifications in the data structure, in order to properly deal with internal variables, temperature, entropy and stored energy. In addition, tangent moduli for the thermo-viscoelastic damage model (derived in chapter 5) had to be incorporated, as an imposed force problem is simulated, which requires iterations of the calculated strain field until convergence of mechanical equilibrium equation is achieved.

For simplicity, adiabatic conditions were assumed. Small displacements are considered. As discussed in previous chapters, by considering zero heat fluxes at the boundaries zero and heat generation in the bulk, this reflects a scenario where heat does not have enough time to dissipate, remaining ”trapped” at the point where it was generated by viscosity through thermomechanical coupling.

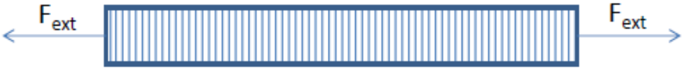

Figure 6.5 – Dynamic tensile loading of a one-dimensional bar divided into 500 elements.

A one-dimensional bar split into 500 elements of equal size and with a single Gauss point was the considered domain of the simulations. Tensile loads were applied at the extremities of the bar (see figure 6.5), following the exponential decay shown in figure 6.6.

As a basis for comparison, an elastic model of damage is simulated. Results for the evolution of the damage variable are shown in figure 6.7, it is clear that, up to time $t = 250s$, when the elastic

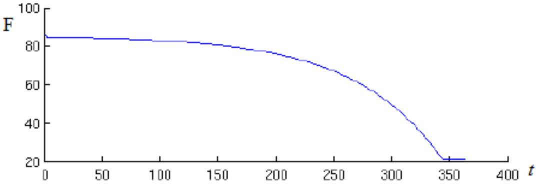

Figure 6.6 – Exponentially decaying applied forces at the extremities of the bar(measured in [N]) through time (in [s]) for all the examples of TLS use.

waves coming from the extremities meet in the central element of the bar ($\mathbf{x} = 250mm$) and constructively interfere, no damage appears in the domain. As the damage threshold Y^c is reached, damage tends to localize, and would lead to almost immediate failure (understood as reaching $d = 1$), had no nonlocal tools been used. Since the TLS is used, a damage evolution profile appears, spread around the central elements of the bar. It should be noted that, unlike many other nonlocal damage models, the damage variable is allowed to reach the value 1; the rest of the bar remains loaded while the waves travel back towards the extremities. Explicit integration of the evolution equations is used.

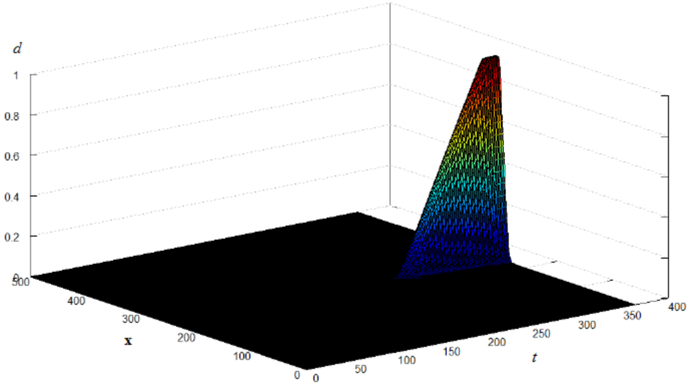

Figure 6.7 – Application of the TLS to an elastic local model of damage: development of a damage profile spread around the middle of the bar, instead of localized failure only at the central element of the bar.

The first thermo-viscoelastic damage example was run with a single Kelvin-Voigt branch. A Hencky-type viscous dissipation pseudo-potential is used, with viscous parameter $\mu^v = 5.10^{-2} MPa$. Figure 6.8 shows the evolution of the damage variable through the domain in time. Since viscosity is low, the calculated damage profile closely resembles that of the elastic damage model. However, it is possible to observe a slightly broader damage profile at the center of the bar. This is an indication that viscosity effects act in the sense of diffusing the localization. The increase in stress levels makes the damage threshold be attained earlier.

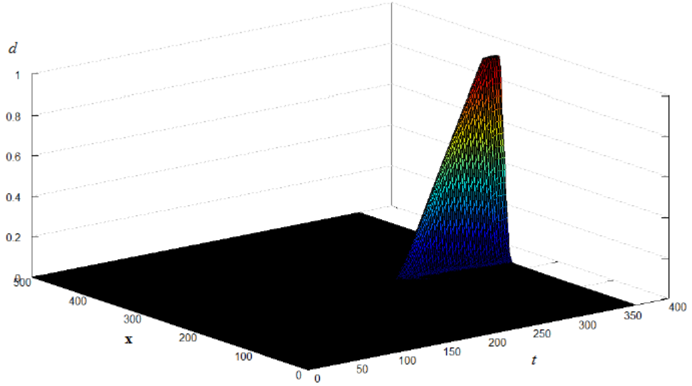

Figure 6.8 – Application of the TLS to a thermo-viscoelastic damage model: one single Kelvin-Voigt branch with low viscosity. Development of a slightly broader damage profile

Dissipation drives heat generation, which in adiabatic conditions stays trapped at the material point where it was generated. The calculated temperature increase profile for the low viscosity Kelvin-Voigt model is shown in figure 6.9. It is clear that a spike of temperature appears in the region of higher concentrated damage. This evidences that damage dissipation is the main driving force of heat generation.

However, viscosity also drives some heat generation. It is possible to isolate the two contributions to internal dissipation, in order to demonstrate how the Kelvin-Voigt dashpot leads to temperature increase through thermomechanical coupling. The profile of temperature increase due to viscosity effects is shown in figure 6.10. It can be seen that the extremities of the bar, having been submitted to loading for a

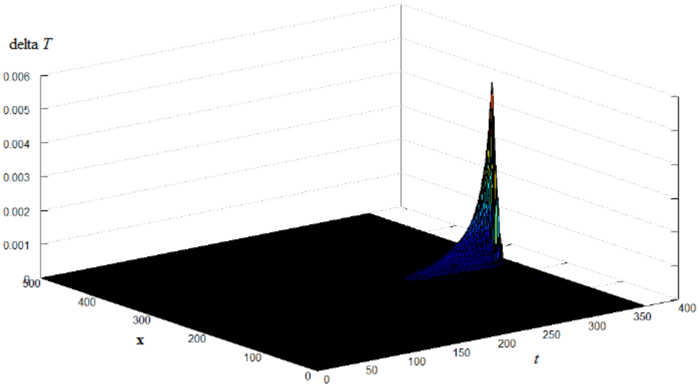

Figure 6.9 – Predicted temperature profile for the TLS applied to a thermo-viscoelastic damage model: one single Kelvin-Voigt branch with low viscosity. Damage dissipation dominating heat generation.

longer time than other regions, dissipate more heat than the center of the bar. Small perturbations are apparent at the point of constructive interference between elastic waves. At the final time step, it is also possible to distinguish a discontinuity on the viscous temperature profile, indicating the point where the TLS introduces nonlocal effects and constrains the evolution of viscous strains.

The same single Kelvin-Voigt branch is now simulated with a higher viscosity parameter $\mu^v = 5MPa$. Figure 6.11 shows the new calculated damage profile, much broader around the center of the bar. The advancement of the elastic waves can be followed by a small "step" going from the extremities towards the center. This reflects the attainment of the damage initiation threshold at the extremities of the bar - this happens due to increased stress levels due to viscous effects.

The estimated temperature evolution profile for the higher viscosity Kelvin-Voigt model is represented in figure 6.12. It is now apparent that dissipation due to viscosity (predominantly at the extremities of the bar) and due to damage evolution (predominantly in the center, where the elastic waves meet and localization is induced, as indicated by the peak) are of comparable magnitude. The jagged profile of temperature evolution can be explained by the explicit integration procedure employed.

Pure Kelvin-Voigt problems do not involve internal variables,

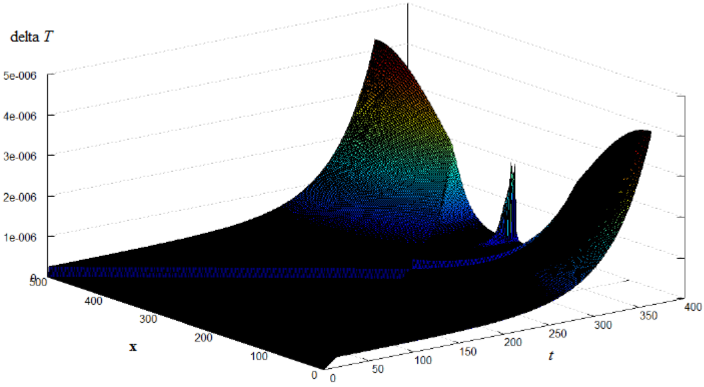

Figure 6.10 – Profile of temperature increase due to viscous effects only, in the application of the TLS to a thermo-viscoelastic damage model: one single Kelvin-Voigt branch with low viscosity.

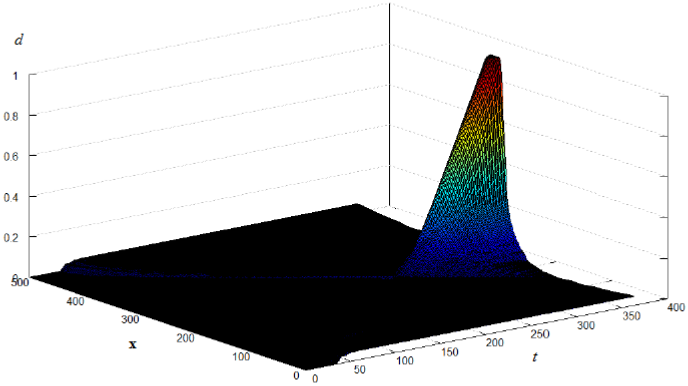

Figure 6.11 – Damage profile predicted by the application of the TLS to a thermo-viscoelastic damage model: one single Kelvin-Voigt branch with higher viscosity.

as the dashpot is subjected to total strains. In order to show the fundamental difference in the behavior of internal variable models, a single Maxwell branch is simulated. Hencky-type viscous dissipation pseudo-potentials are used with the higher viscosity parameter $\mu^v =$

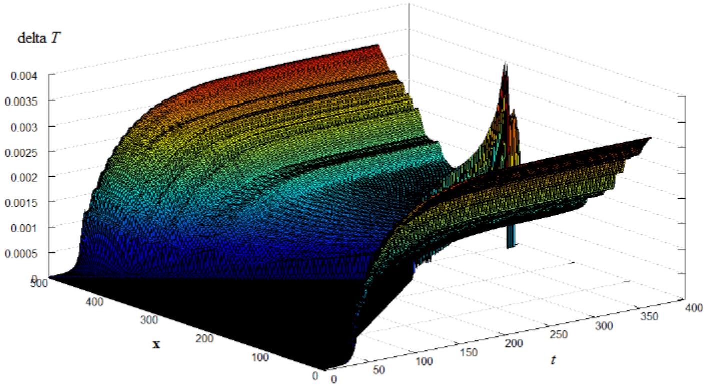

Figure 6.12 – Predicted profile of temperature increase (in $[K]$) for the TLS applied to a thermo-viscoelastic damage model: one single Kelvin-Voigt branch with higher viscosity. Comparable viscous and damage dissipation.

$5MPa$. In Maxwell rheological elements, suddenly imposed stresses are instantaneously felt by the spring. Only through time do viscous strains evolve. The damage profile of the Maxwell branch is shown in figure 6.13. The predicted damage profile is now even broader than for the last example. The internal variable model seems to further diffuse damage localization. For the first time, even at the end the simulation no point of the domain has reached full degradation.

The predicted temperature profile of the Maxwell thermo-viscoelastic damage model is shown in figure 6.14. Once more, due to the choice of material parameters, viscous and damage dissipation are of similar magnitudes. Deep qualitative differences between the aspect of the Kelvin-Voigt and Maxwell temperature and damage profiles can be observed.

Having demonstrated the differences between both types of behaviors, different applications combining various characteristic times (using an arbitrary number of Maxwell branches) can be envisioned.

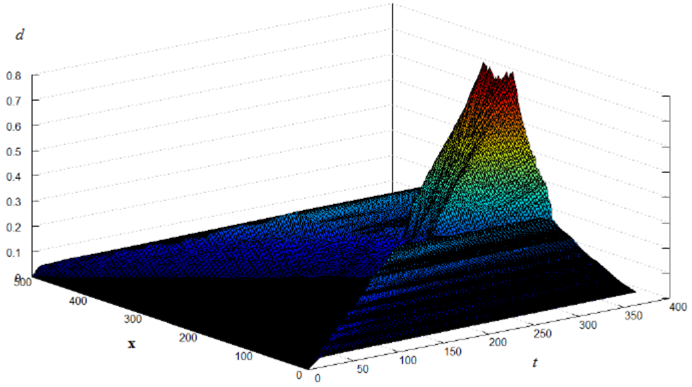

Figure 6.13 – Damage profile for the TLS applied to a thermo-viscoelastic damage model: one single Maxwell branch with higher viscosity. Broader damage profile.

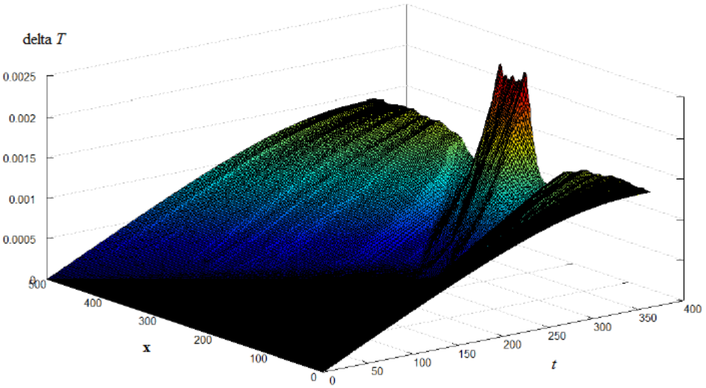

Figure 6.14 – Predicted temperature profile for the TLS applied to a thermo-viscoelastic damage model: one single Maxwell branch with low viscosity. Comparable viscous and damage dissipation.

7 APPLICATIONS OF THE PROPOSED MODELS

> *Chapter overview: After developing constitutive models suited to the description of polymer-like material behavior and evidencing their capabilities in sample examples, the present chapter focuses on larger scale applications. In order to do so, a brief presentation of the multiphysics simulation software Matlib is given. The finite element structure used for the finite strains thermomechanically-coupled problems is explored. Examples were chosen to highlight couplings between different phenomena. A classic case of a plate with a central hole is explored for different material parameters. Next, tests inspired by some of the most common polymer characterization tests are presented. The alternated loading of a standardized specimen that occurs during Dynamic Thermomechanical Analysis of polymers are tested. Necking in a tensile test is likewise demonstrated to fall within the predictive capabilities of the proposed model.*

7.1 IMPLEMENTATION DETAILS: ZORGLIB/MATLIB

A full development of a family of material models designed with the challenges posed by polymer behavior was presented in the previous chapters. Built in a variational framework, these models are able to account for a variety of effects. Large strains are properly treated, as well as strain rate and temperature dependence. Damage modeling takes into account both thermal and viscous effects, following the micromechanical description of the behavior of polymers, presented in chapter 2.

The basic features of the proposed models was evidenced in sample numerical results presented at the end of the previous chapters. By doing computations in a single Gauss point, in what are often called 0-D conditions, it was possible to demonstrate how the different physics interact and that generated curves follow polymer-like material behavior. These simple examples can be run in toy problems, in relatively concise Matlab/Octave routines, for instance, by following the previously proposed algorithms.

In order to run more realistic problems, though, it is usually advisable to move towards more general purpose simulation software, equipped with Finite Element or similar technology. Throughout the development of the present work, the proposed material models were implemented in a multiphysics simulation package called Zorglib, developed in house at the Ecole Centrale de Nantes.

Capable of dealing with general nonlinear systems through various numerical techniques, ranging from classical Finite Elements to Meshless methods, and specializing in the treatment of coupled problems, Zorglib works closely with a constitutive model library called Matlib, where the local models proposed in this document have been implemented.

Originally a part of Zorglib, Matlib can currently be used independently, to run consistency tests and other 0-D problems, or in conjunction with other Finite Element software. The routines programmed in Matlib are responsible for calculations performed at Gauss points, including internal variable updates, updates of fluxes (stresses and entropy, in thermomechanical contexts) and of tangent operators - essentially, the operations summarized in the algorithms presented at the end of chapters 4 and 5. Discretization-related operations, such as element and global matrix assemblies, time stepping schemes and numerical integration are delegated to the software of choice.

It should be noted that, for the time being, the connection between Matlib and XLibris, another package developed in house at the Ecole Centrale de Nantes and specializing in level sets and Extended Finite Element (X-FEM) applications, including most of the available code on the Thick Level Set method, has yet to be done. The task is envisioned for the near future, and shall bring interesting results in future works. Meanwhile, the connection of the local variational models to the TLS was only performed in simpler problems, in Matlab codes developed with the gracious help of Kévin Moreau and the TLS team, as mentioned in chapter 6.

Before moving on to the actual examples, a short presentation of some Finite Element aspects employed by Zorglib in dealing with coupled problems is necessary.

7.2 FINITE ELEMENT ASPECTS: DATA STRUCTURE, VOLUMETRIC LOCKING AND THERMOMECHANICAL COUPLING

The focus of this work laid squarely on the development of constitutive models applicable to polymer-like material behavior, and not in the numerical techniques associated to the solution of full-scale problems. As evidenced in Thick Level Set applications presented in chapter 6, the central goal is in sketching an understanding of numerical techniques that go hand in hand with the proposed models, rather than developing novel techniques. A similar approach is taken for the applications presented in this chapter. A brief overview of the Finite Element treatment chosen for the following examples is now given.

In previous chapters, extensive attention was given to the internal variable update, both of the viscous variables and of the damage variable. In fact, most of the presented operations were related to the determination of effective incremental potentials, for which the optimization operations (of essential local nature) with respect to set of internal variables had been performed. The resulting $\mathcal{H}_n^{eff}$ was then said to be subjected to global optimization procedures with respect to external independent variables measuring displacements and temperatures. Within the variational framework, these global operations yield expressions for the update of stresses and entropy in hyperelastic-like fashion, which show up in mechanical and thermal balance equations.

No significant attention has been lent to the specifics of this boundary-value problem so far in this document. Extensive details on the Finite element formulation of thermomechanical coupling in the present variational context can be found in Stainier (2013). The next few paragraphs only bring a general idea of the Finite Element strategy used to solve this global problem, starting with the classical concepts and notations and reinserting them into the global optimality conditions of the thermo-viscoelasticity problem.

The optimization operations with respect to displacements (or some strain measure) and temperatures are constrained to admissible spaces of functions, respecting imposed boundary conditions. Values of displacements or temperatures imposed respectively on regions $\partial_{\mathbf{x}}\Omega$ and $\partial_T\Omega$ of the boundary (Dirichlet boundary conditions), as well as forces or heat fluxes imposed respectively on regions $\partial_{\boldsymbol{\sigma}}\Omega$ and $\partial_{\mathbf{q}}\Omega$ (Neumann boundary conditions) have to be respected.

Such a space can be approximated using a set of an arbitrary number P of compact support shape functions $N_a(\mathbf{X})$, associated to nodes a in a mesh associated to the material domain of interest. A possible option is using the same mesh and set of shape functions (which constitute a discretization denoted by letter h) to describe both temperature and displacement functions. Displacement and temperature fields are built from the product of nodal values by the shape functions as:

$$\chi \cong \chi_h = \sum_{a=1}^{P} N_a(\mathbf{X})\mathbf{x}_a \qquad T \cong T_h = \sum_{a=1}^{P} N_a(\mathbf{X})T_a \tag{7.1}$$

It can be shown that in such a classical Finite Element approach, displacements and temperatures exactly match values at the nodes, in other words, that $\chi(\mathbf{X}_a) = \chi_h(\mathbf{X}_a)$ and $T(\mathbf{X}_a) = T_h(\mathbf{X}_a)$. Fluxes are equally determined by the product of nodal values by gradients of shape functions, which can be computed *a priori*. Thus, the deformation and temperature gradients are evaluated by:

$$\mathbf{F}(\mathbf{X}) \cong \mathbf{F}_h(\mathbf{X}) = \sum_{a=1}^{P} \mathbf{x}_a \otimes \nabla N_a(\mathbf{X}) \tag{7.2a}$$

$$\nabla T(\mathbf{X}) = \mathbf{G}(\mathbf{X}) \cong \mathbf{G}_h(\mathbf{X}) = \frac{\sum_{a=1}^{P} T_a \nabla N_a(\mathbf{X})}{\sum_{a=1}^{P} T_a N_a(\mathbf{X})} \tag{7.2b}$$

In this context, the optimality conditions of the thermo-viscoelastic potential with respect to strains and temperatures (corresponding to equation 4.56, for mechanical equilibrium, using definitions 4.57, 4.58 and 4.59; equations 4.68 and 4.67, for thermal equilibrium) are now approximated by the following expressions:

$$D_{\mathbf{x}_{n+1}}[\mathcal{H}_n^{eff}](\delta\mathbf{x}_{n+1}) \cong \sum_{a=1}^{P} \left\{ \int_{\Omega} \left[\mathbf{P}_h . \nabla N_a - \rho \mathbf{b}_R N_a\right] dV - \int_{\partial_{\boldsymbol{\sigma}}\Omega} \mathbf{t}_R N_a d\Gamma \right\} . \delta\mathbf{x}_a = 0, \forall adm \delta\mathbf{x}_a \tag{7.3a}$$

$$D_{T_{n+1}}[\mathcal{H}_n^{eff}](\delta T_{n+1}) \cong \sum_{a=1}^{P} \left\{ \int_{\Omega} \left[-(\eta_h - \eta_n)N_a + \frac{\Delta t}{T_n}\mathrm{r}_R N_a + \frac{\Delta t}{T_n}\mathbf{q}_h . (\nabla N_a + \mathbf{G}_h N_a)\right] dV - \int_{\partial_{\mathbf{q}}\Omega} \Delta t \overline{\mathbf{q}}_R \frac{N_a}{T_n} d\Gamma \right\} . \delta T_a = 0, \forall adm \delta T_a \tag{7.3b}$$

Where elastic and viscous contributions are present in the terms ($\mathcal{D}_{int}^{\dot{\mathbf{Z}}}$ denotes the internal dissipation due to the evolution of internal variables, previously discussed in detail):

$$\mathbf{P}_h = 2\mathbf{F}_h \frac{\partial \mathcal{H}_n^{eff}}{\partial \mathbf{C}_h}(\mathbf{C}_h, \dot{\mathbf{C}}_h, T_h) = 2\mathbf{F}_h \left[\frac{\partial W}{\partial T_h} + \frac{T_h}{T_n} \left\langle \frac{\partial \psi}{\partial \dot{\mathbf{C}}_h} \right\rangle \right] \tag{7.4a}$$

$$\eta_h = -\frac{\partial \mathcal{H}_n^{eff}}{\partial T_h}(\mathbf{C}_h, \dot{\mathbf{C}}_h, T_h) = -\frac{\partial W}{\partial T_h} - \frac{\Delta t}{T_n} \dot{\mathbf{C}}_h : \left\langle \frac{\partial \psi}{\partial \dot{\mathbf{C}}_h} \right\rangle - \mathcal{D}_{int}^{\dot{\mathbf{Z}}} \tag{7.4b}$$

It is clear that all gradients are performed over the previously known shape functions, and can be efficiently stored and reused. Additionally, since shape functions have compact support, integrals can be done element by element and later assembled in a global matrix. At every time step, the goal is then to determine the vector of nodal values of displacements and temperatures. This is done by balancing internal and external terms present in the nonlinear equations above.

Internal variables, such as viscous strains at Maxwell branches and damage variables, are usually stored in Gauss points, used to perform numerical integration within elements, rather than at the nodes of the mesh. All computations pertaining to the evolution of internal variables are local, and can be performed at the integration point level. By determining the effective incremental potentials, the necessary information for the determination of stiffness and thermal properties in the global optimization is made available.

These very standard Finite Element Method staples are used in all the examples that follow. Some non-standard choices are used, though.

As evidenced by the structure of all proposed incremental potentials, no inertia terms are considered. All computations performed throughout this work are in fact quasi-static in nature, even though different strain rates are important for viscous terms. In other words, the loading rate matters, but an underlying hypothesis is that mass effects are negligible in comparison to viscosity and elasticity. Quasi-static problems are then solved using fully-implicit time stepping schemes recast in a variational context[7.1].

The quasi-static formulation is also used for the thermal part of the problem, although heat capacity is in fact considered. This is done by introducing the heat capacity contribution along the time step Δt

---

[7.1] Examples coupling the proposed constitutive models to the Thick Level Set nonlocal approach work somewhat differently, and were not implemented in a fully variational context. See the final section of this chapter for a longer discussion on the subject.

into the entropy term highlighted above (through term $\frac{\partial W^{th}}{\partial T_{n+1}}$).

The thermomechanical problem is thus solved using the same time and space discretizations, with the same time integration strategy.

The well-known issue of volumetric locking, intrinsic to the standard use of linear shape functions for a variety of elements for the case of quasi-incompressible behavior, such as is assumed for viscous terms in the previously proposed constitutive models, can be overcome using extensively studied mixed formulations (for a comparative review of some mixed formulations of nearly incompressible elasticity, the reader is referred to Brink & Stein (1996)).

Initially proposed by Simo & Taylor (1991) for quasi-incompressible elasticity and detailed in Stainier (2013) in the thermomechanical context, the mixed formulation used for all the examples throughout this document is based on the introduction of two new variables that store volumetric strains and corresponding pressure, both constant in each element (hence the index $\overline{el}$ and the sum over the number of elements nel).

$$\Theta_h = \sum^{nel} \Theta_h^{\overline{el}} \qquad p_h = \sum^{nel} p_h^{\overline{el}} \tag{7.5}$$

The new variables are included as a penalty term into a reformulated incremental potential $\hat{\mathcal{H}}_n^{eff}$, enforcing the adequate volumetric relations while allowing for a properly approximated stiffness in the presence of isochoric material behaviors. Pressure serve as a Lagrange multiplier enforcing the consistency of the element-constant volumetric strains with the deformation gradient (where $J_h = \det \mathbf{F}_h$):

$$\begin{aligned}&\hat{\mathcal{H}}_n^{eff}(\mathbf{C}_h, \dot{\mathbf{C}}_h, T_h, \Theta_h, p_h) = \\ &\qquad \int_\Omega \left\{ \mathcal{H}_n^{eff}(\mathbf{C}_h, \dot{\mathbf{C}}_h, T_h) + p_h \left[J_h - \Theta_h \right] + \Delta t \frac{1}{T_n} \mathbf{q}_h \mathbf{G}_h \right\} dV\end{aligned} \tag{7.6}$$

The solution of the redefined problem remains in a variational framework. It is possible to show that the underlying variational principle now reads:

$$\inf_{\mathbf{C}_h, \Theta_h} \sup_{T_h, p_h} \hat{\mathcal{H}}_n^{eff}(\mathbf{C}_h, \dot{\mathbf{C}}_h, T_h, \Theta_h, p_h) \tag{7.7}$$

Closed form expressions for the calculation of these volumetric strains and for the pressures can be derived variationally, from the stationarity conditions with respect to each of the two new variables.

Unless stated otherwise, all finite element meshes used in the following examples were generated using Gmsh, an open source mesh generating software. For details on the software, the interested reader is referred to Geuzaine & Remacle (2009).

7.3 PLATE WITH A CENTRAL HOLE

A classical example used in the literature of viscoelasticity is a plate with a central hole. In the small strains regime and for infinite plates, analytic solutions are available, leading to the determination of stress concentration factors, for instance. This example has served as a standard basis of comparison for the numerical implementation of constitutive models.

Analytic solutions are not readily available to the models developed throughout this document, however. Nonlinear phenomena arising from the consideration of large strains, multiple rheological elements, thermomechanical coupling and damage render the task of obtaining closed form solutions daunting.

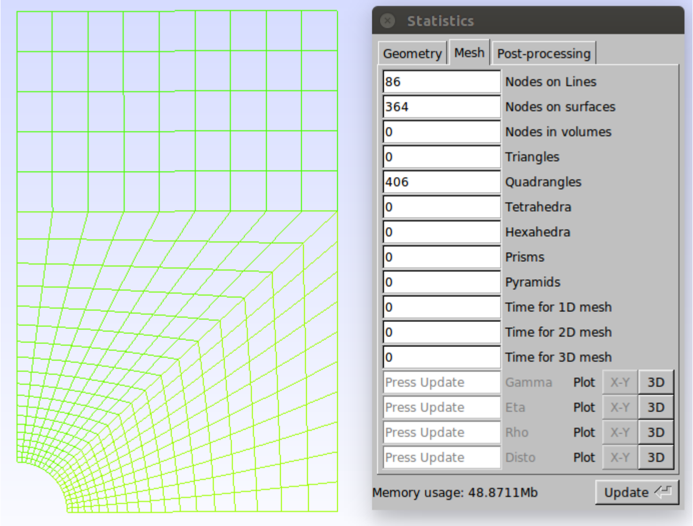

86 Nodes on Lines
364 Nodes on surfaces
0 Nodes in volumes
0 Triangles
406 Quadrangles
0 Tetrahedra
0 Hexahedra
0 Prisms
0 Pyramids
0 Time for 1D mesh
0 Time for 2D mesh
0 Time for 3D mesh
Press Update Gamma
Press Update Eta
Press Update Rho
Press Update Disto
Memory usage: 48.8711Mb

Figure 7.1 – Mesh used for the simulation of a plate with a central circular hole and mesh information.

Still, the simulation of a plate with central hole remains a hallmark for any proposed model of viscoelasticity. Its comparison to more standard models highlights the effects of large strain phenomena, thermomechanical coupling and damage.

Additionally, the stress concentration effect around the central hole induces damage localization and constitutes an interesting testing ground for the influence of several parameters of the proposed models. Of particular interest is the interplay between geometry-induced stress concentration and viscous dissipation and heat conduction, which introduces a gradient-dependent component into the model and could act as a regularizing factor.

Both the thermo-viscoelasticity model of chapter 4 and the thermo-viscoelastic damage model of chapter 5 are simulated in the following. Material parameters used for the simulations can be found in the appendix[7.2].

The mesh used in all simulations is represented in figure 7.1. Unlike the classical approach to a plate with a central hole, the dimensions of the plate (a square of $32mm$ side) are in the same order of magnitude of the central hole (radius $15mm$). This is done in order to explore boundary effects, such as convection, as well as to more clearly observe deformations of the test specimen when subjected to large imposed displacements.

The problem is simulated in two dimensions. Symmetries are used and the mesh represents only one quarter of the specimen. Positive displacements along the y-axis are imposed upon the top border. When allowed, convection with the environment can occur along the border of the hole, along the right vertical border and along the top border. Both the material and the environment are assumed to be at an equilibrium temperature of $293K$ at the start of the tests.

The first series of examples presented in the following is intended to draw comparisons between adiabatic and conduction-convection formulations for some loading conditions.

Several mentions to adiabatic formulations have been made throughout the text, most notably during the derivation of tangent moduli. More than merely a theoretical exercise, adiabatic conditions are often present in contexts where thermomechanical coupling is of importance. When loads are quickly imposed, such as in impact applications, there is not enough time for locally generated heat to dissipate either through

---

[7.2] As elsewhere in the present document, no specific polymer species is being simulated. Material parameters are merely chosen to qualitatively represent some features present in polymer-like behavior.

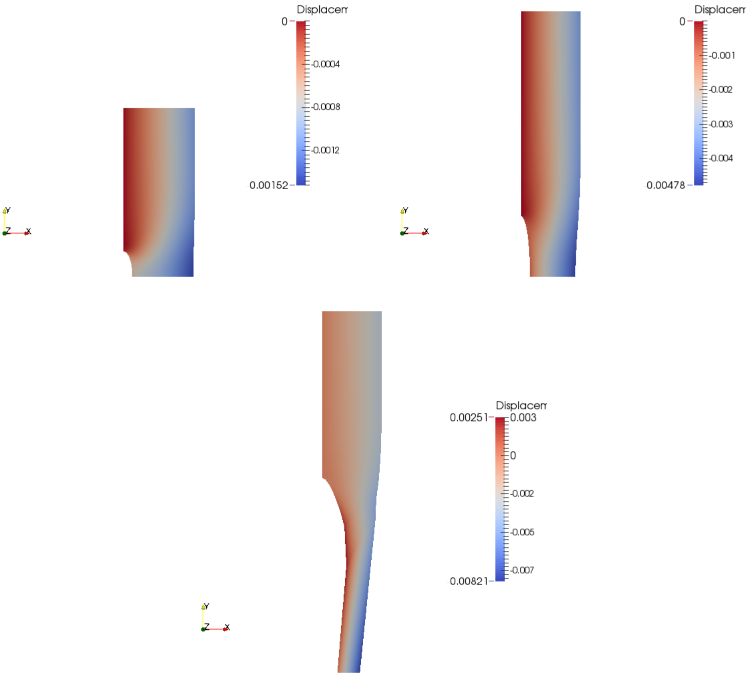
Displacem
0
-0.0004
-0.0008
-0.0012
0.00152
Y
Z
X
Displacem
0
-0.001
-0.002
-0.003
-0.004
0.00478
Y
Z
X
Displacem
0.00251
0.003
0
-0.002
-0.005
-0.007
0.00821
Y
Z
X

Figure 7.2 – Deformation of the plate with a central hole at three different time steps. Color scale shows the displacements along the x-axis, indicating localization of deformation next to the hole.

the material or to its environs.

The hypothesis of adiabatic conditions can have deep implications upon the formulation itself. As discussed earlier, temperature then becomes an additional internal variable whose evolution is in many ways a measure of local dissipation, be it through viscous strains or damage, in the present context.

A single Kelvin-Voigt element (one spring in parallel to a dashpot) is used for the first set of comparisons. The thermo-viscoelasticity model of chapter 4 is initially simulated. No temperature dependence of material parameters is assumed. Variables are observed for imposed displacements of $10mm$, $30mm$ and $50mm$. The imposed velocity on the border is $10mm/s$, so that the full simulated test takes place in only $5s$. The aspect of the deformed plate can be observed in figure 7.2.

Imposing $50mm$ displacement can seem extreme, and is certainly treated as a rather academic simulation, but polymer test specimens can sometimes exhibit very large straining before rupture. The intent of reaching such extremes is to show the deep thermomechanical coupling effects that appear once localization conditions are present.

Side by side comparisons of adiabatic and conduction-convection formulations are presented. Temperature levels for the three frames, $10mm$, $30mm$ and $50mm$ are shown in figure 7.3. As expected, since it is impossible for heat to dissipate, temperature is consistently higher at the border of the hole in adiabatic conditions, where the stress concentration is strongest. High exchange coefficients were employed in the convection model, so that, for the non-adiabatic case, the hottest spot is slightly distanced from the border of the hole. Not shown on the figures is the difference in the maximum temperature estimated, close to $400K$ higher in the adiabatic case.

An interesting feature to notice is the direction of the line of highest temperatures. Whereas temperatures are highest along the horizontal symmetry line for the adiabatic case, there is a slightly slanted line for the conduction case. Such a line is generated by the diffusive effect introduced by conduction.

Heat flux for each of the time steps is shown in figure 7.4. There, it is possible how heat flows diagonally from the border of the hole, the driving force behind the slanting of the temperature line mentioned above. Also, as the process evolves, heat flux along the right border increases, before dropping precipitously when the extreme localization of the third frame is reached.

Stress levels are essentially the same for both cases, since there is no temperature dependence of material parameters. One noticeable difference comes for the final frame, $50mm$, where heat conduction is responsible for higher temperatures close to the right border, which are in turn responsible for stresses generated by thermal dilatation, as shown in figure 7.5.

Next, the thermo-viscoelastic damage model of chapter 5 is tested. A generalized Kelvin-Voigt/Maxwell rheological model is employed, with two Maxwell branches. Testing conditions (imposed displacements, strain rate and initial temperature) are the same as for the first series of examples. No temperature dependence of the material parameters is considered, in order to isolate the effects of interest at each set of comparisons.

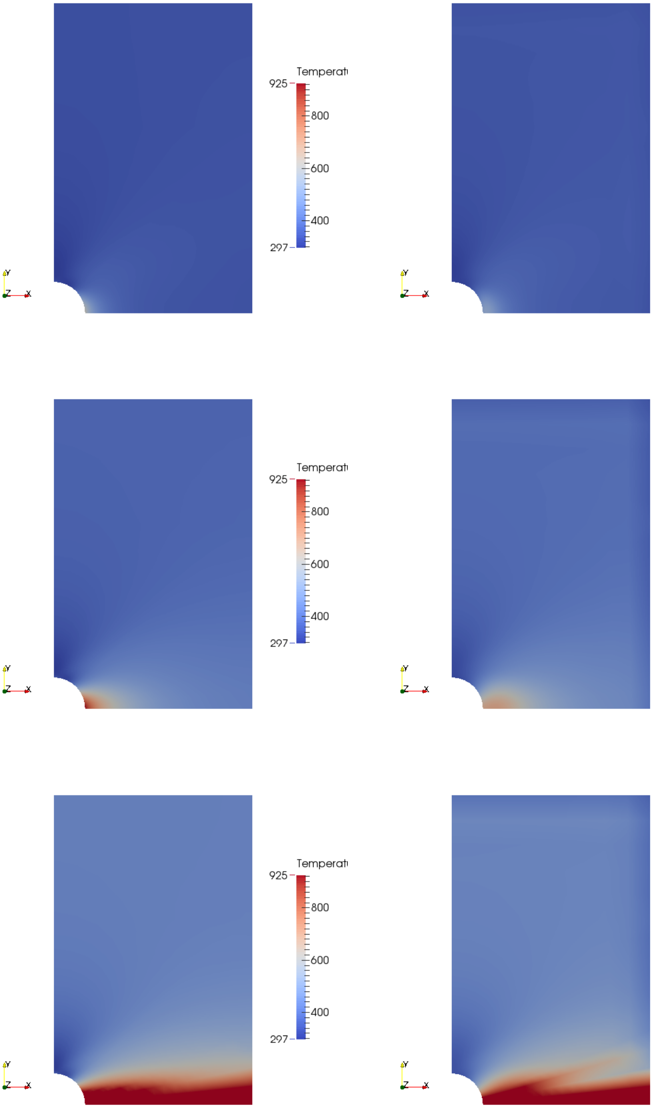

Figure 7.3 – Temperature profile for three different time steps. Adiabatic conditions on the left, convection-conduction on the right.

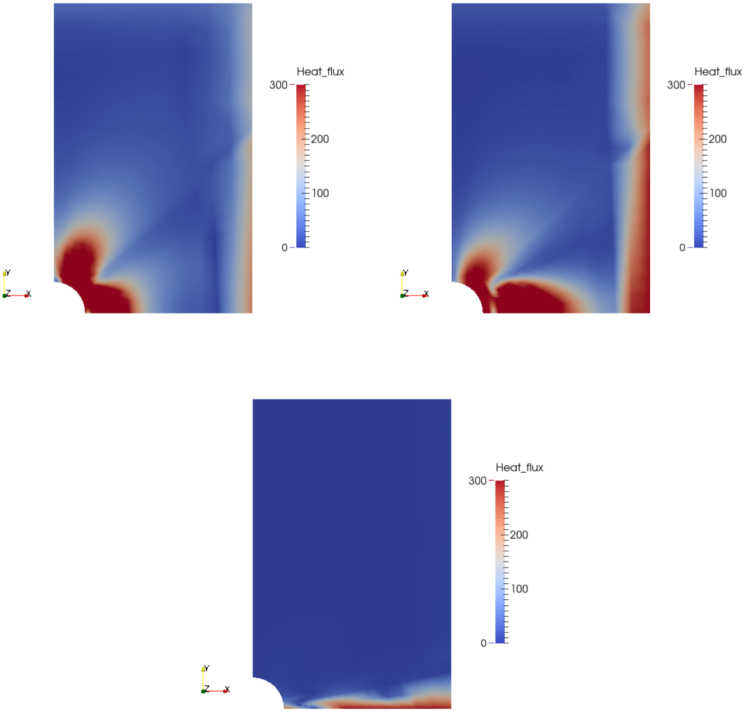

Figure 7.4 – Heat flux at three different time steps for the Kelvin-Voigt thermo-viscoelasticity model.

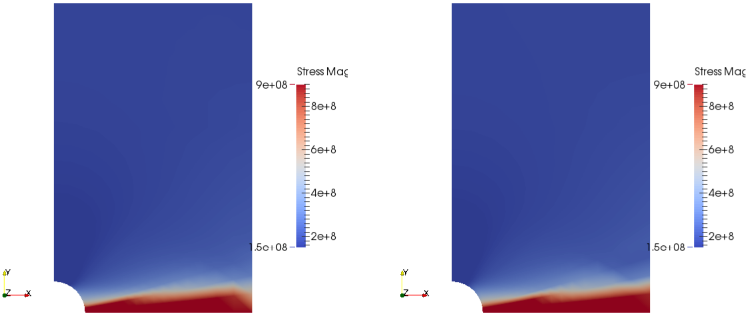

Figure 7.5 – Stresses at the final time step. Higher levels of stress closer to the right boundary for the convection/conduction case: thermal dilatation effect.

The influence of thermal boundary conditions is investigated first. Using the convection/conduction formulation, two different convection exchange coefficients along the boundaries are simulated: $25W/m$ and $250W/m$[7.3].

The temperature profile of both cases is shown in figure 7.6. Differences are subtle, but it is possible to see that higher convection exchanges make the hotter point in the material go farther from the border of the hole, however regions with higher temperature are slightly smaller. In the last frame, the maximum estimated temperatures are shown: around $4500K$ for the case with lower convection coefficient, around $2800K$ for the other.

Once again, this is an extreme case. Still, it is clear that for extreme localization even increases of an order of magnitude in heat exchanges would only slightly soften its effects. In impact conditions, for instance, such sudden spikes in temperature around stress concentration features is to be expected.

The conduction coefficient within the material is the same for both cases. What changes is only the convection coefficient. Thus, in the higher convection case, the boundary of the hole acts as a heat sink that keeps conduction in the material from having such an important.

[7.3] It is important to keep in mind that the simulation is performed in two dimensions, thus the unusual units of the convection exchange coefficients. Heat can only be exchanged with the environment along the non-symmetry boundaries of the mesh, as detailed earlier.

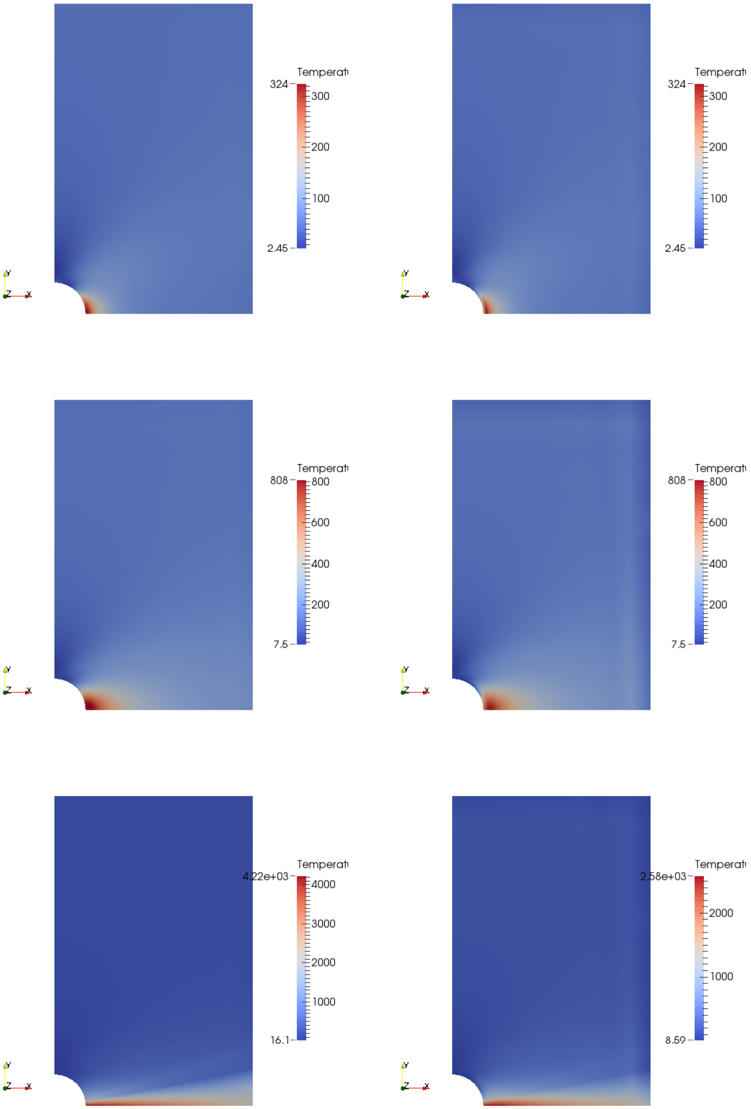

Figure 7.6 – Temperature increase profile for the thermo-viscoelastic damage model at three different time steps. Lower convection coefficient on the left, higher on the right.

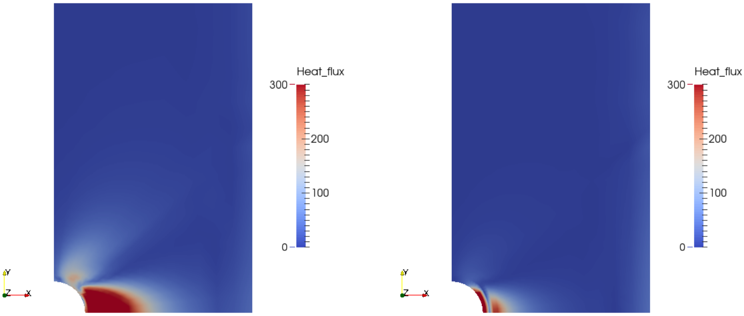

Figure 7.7 – Heat flux at the intermediate time step. Higher convection coefficient working as a heat sink.

The comparison between the heat flux at the intermediate time step ($30mm$ imposed on the top boundary) of figure 7.7 clearly shows this.

With the influence of convection in mind, damage profiles for the same test case paint an interesting picture, seen in figure 7.8. Different scales are used for each frame. Clearly, the lower convection case less damage concentration consistently; its damage profiles are much more smeared, i.e., larger portions of the domain exhibit some level of damage.

For the higher convection case, the hole boundary acts as a heat sink. Conduction is unable to spread out the concentration effect of the hole. Here it is important to keep in mind that heat accumulation has also been associated to damage in the proposed model. The damaging factor $(1-d)$ also multiplies W^{th} in the equations, and in turn, thermal accumulation is a component of the energy restitution rate. Therefore, the smaller regions close to the hole, where higher temperatures are concentrated in the higher convection case, are more vulnerable to this mechanism of damage evolution than its neighboring regions.

This explains the development of higher damage gradients for the case of higher convection. The heat sink avoids neighboring regions to become warmer (temperature gradients are also higher), so that thermal accumulation plays a smaller role in their locally calculated energy restitution rate. They thus remain more structurally sound and damage is more strongly localized closer to the hole.

In other words, even if a higher convection exchange coefficient

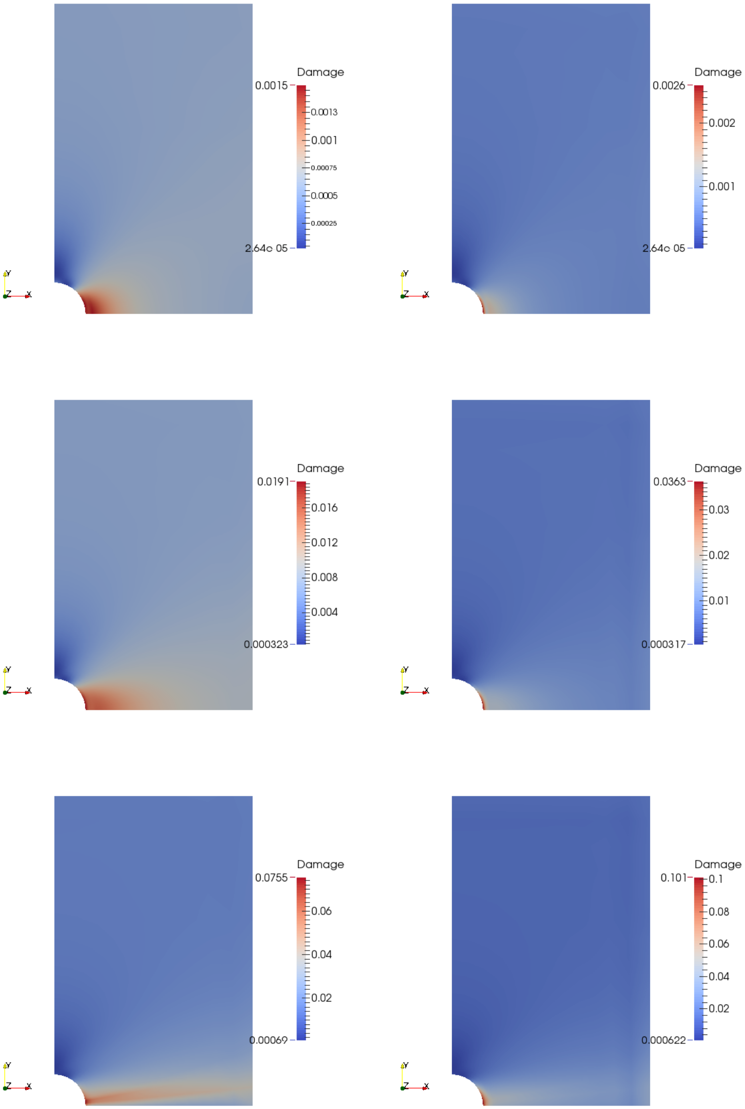

Figure 7.8 – Damage profile for the thermo-viscoelastic damage model at three different time steps. Lower convection coefficient on the left, higher on the right. Different scales for each figure.

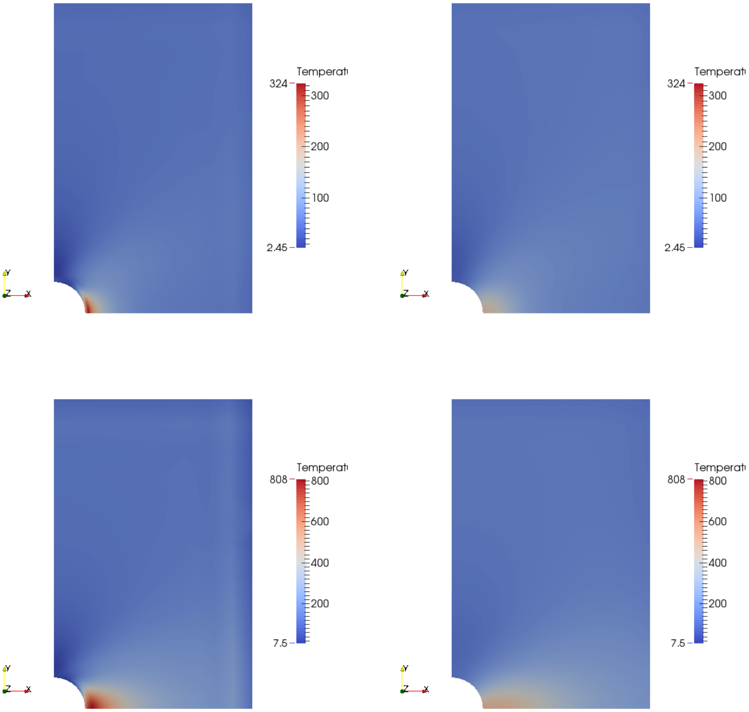

Figure 7.9 – Temperature increase profile for the thermo-viscoelastic damage model at two different time steps. Lower conduction coefficient on the left, higher on the right.

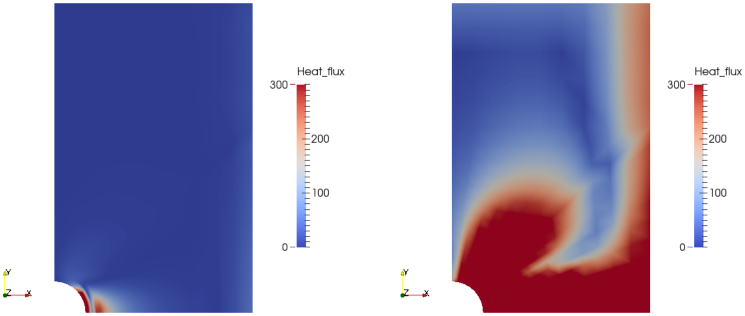

Figure 7.10 – Temperature increase profile for the thermo-viscoelastic damage model at the intermediate time step. Higher conduction counterbalances the heat sink effect of convection along the hole boundary.

avoids the development of the highest temperatures, its effect as a heat sink contributes to damage localization in a model where heat accumulation influences damage evolution. This happens because the gradient effect of heat conduction within the material domain is curtailed, and a smaller region is constantly subjected to higher temperature concentration.

As such an effect grows, i.e. if exchange coefficients along thermal boundaries increase, the localization effect follows suit. Also, as imposed strain rates grow, or when extreme localization onsets (as for when the imposed displacements reach $50mm$ in the current examples), heat generation tends to localize around the stress concentration geometric feature. Clearly, the duration of the loading process has to be compared with the time needed for heat to dissipate along the boundary and for conduction to take place, in order to determine the expected level of damage localization, as measured by the damage gradient. Equivalently, mesh refinement or coarsening should also take these factors into account.

These are some of the issues that must be assessed when resorting to a nonlocal modeling of damage, something that entails some computational and coding resources.

Another way of exploring the diffusive effect that conduction has upon the damage profile is by comparing two different conduction coefficients, for the same boundary conditions. This is done in the third

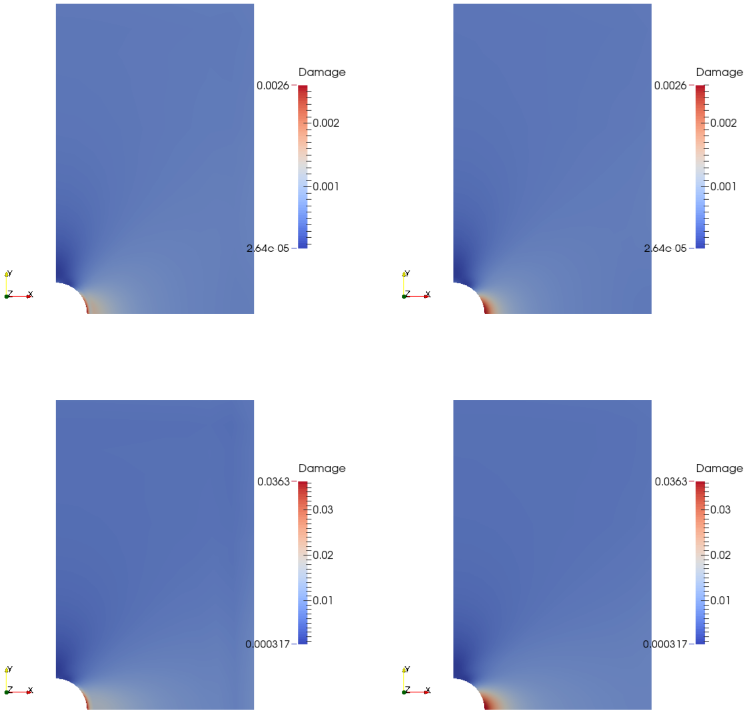

Figure 7.11 – Damage profile for the thermo-viscoelastic damage model at two different time steps. Lower conduction coefficient on the left, higher on the right. Same scale for each time step.

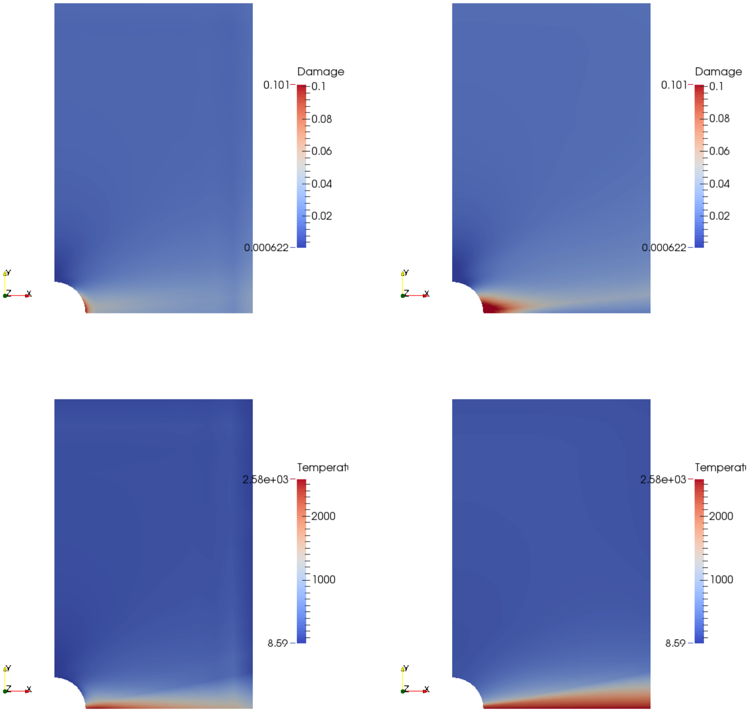

Figure 7.12 – Damage and temperature increase profiles for the thermo-viscoelastic damage model at the final time step. Higher temperatures reached even for higher conduction: damage dissipation.

set of comparisons. The generalized Kelvin-Voigt/Maxwell model is used again. Two different conduction coefficients are used, $0.01 W/m.K$ and $1.9 W/m.K$. Convection exchange coefficients are kept at the higher level used in the previous example, $250 W/m$.

Temperature levels are compared in figure 7.9. For higher conduction, highest temperatures and temperature gradients are clearly lower in the first two time steps, $10mm$ and $30mm$. Heat fluxes are much more spread out through the domain for the higher conduction case, as seen in figure 7.10 for the second time step.

Damage evolution profiles show lower localization closer to the hole in the higher conduction case, as seen in figure 7.11 for the first two time frames. The maximum damage levels are essentially the same for both cases, but the damaged region spreads out further for the higher conduction case.

Once extreme loading conditions are present (by imposing $50mm$ in the current examples), the geometry of the test specimen becomes severely compromised. Not even higher conduction can then prevent localization from taking place. The scenario is exposed in figure 7.12.

In the final time frame, higher temperatures extend much further from the hole, up to the right boundary, in a clear sign that the heat sink effect is less pronounced when conduction is increased. However, it is also clear that higher temperatures are reached, something that is explained by the higher damage levels reached at the extreme localization condition. Since a larger region was consistently affected by damage through the first two time steps for the higher conduction case, once the almost critical conditions are reached, the regions surrounding the hole boundary can no longer bear so much load. Damage again concentrates around the stress concentration feature and evolves much faster in the higher conduction case. This is reflected in the temperature evolution profile, exhibiting higher temperatures despite the higher conduction coefficient, due to the increased damage dissipation.

Therefore, while heat conduction does play a role in spreading out damage profiles and reducing the possibility of localization around stress concentration geometrical features, once loading conditions reach extreme levels the scenario can quickly change. Localization can then be in fact boosted by the damage history in neighboring regions.

Once again, the entire context has to be evaluated in order to determine whether a strictly local damage model will predict localization or not. The interplay between loading history, boundary conditions and material parameters is at the core of this discussion. Conduction itself cannot always be taken as a solution for localization in thermomechanically coupled problems. Its diffusive effect is limited to certain application conditions that may not always be present.

Given the previously discussed rational and experimental arguments toward the consideration of a characteristic length in polymer damage modeling, it appears that nonlocal tools remain necessary and powerful for a myriad of contexts, including applications involving impact loads and other high strain rates, heat sink effects (high exchange coefficients along thermal boundaries) and high distortion of original geometries when approaching necking conditions (as for the case when $50mm$ were imposed along the top boundary of the plate), among others.

7.4 REPRODUCTION OF ALTERNATED LOADING CONDITIONS OF THE DYNAMIC THERMOMECHANICAL ANALYSIS

A very common characterization procedure of polymer species is known as Dynamic Thermomechanical Analysis (DTMA), a family of tests encompassing various types of loading in order to identify different facets of thermomechanical coupling.

In the most commonly used DTMA test, standard specimens are subjected to cyclic loading under controlled increasing temperature. Low excitation frequencies (usually larger than $1 Hz$) are used in order for inertia to be small enough compared to viscoelastic effects. As temperatures evolve, material properties change and increased inelastic straining is observed.

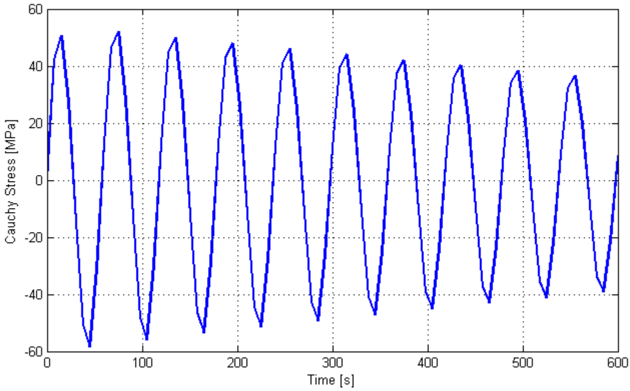

Figure 7.13 – Stress evolution through time during a temperature scan of a thermo-viscoelasticity model: thermal softening is responsible for the decreasing amplitude of stress.

A Kelvin-Voigt rheological model, with a single elastic (storage) modulus and a single viscous (loss) modulus, is used to generate the usual DTMA curves, such as the one on the bottom of figure 2.6. From the relation between the fitted storage and loss moduli, sharper peaks appear around transition areas. Glass transition temperatures are usually identified from the tan δ curve.

However, using a single Kelvin-Voigt element to generate the fitted curves is somewhat limiting. It is well known that nonlinearities

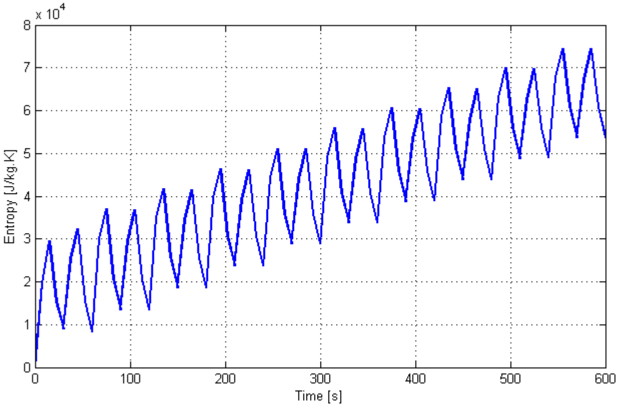

Figure 7.14 – Entropy evolution through time during a temperature scan of a thermo-viscoelasticity model: thermoelastic effects and viscous dissipation.

appear both in the elastic and inelastic phases of polymer behavior. As a consequence, DTMA curves can often be lacking in complexity to accurately reproduce features across various loading conditions. In fact, DTMA tests are run with different test specimens according to the type of loading. Different setups for bending, shearing, compression and tension tests can be seen in the top right of figure 2.6. The use of the resulting curves is advised for similar loading conditions only.

In the present section, the conditions present for several DTMA tests are reproduced. The most common characterization tests are simulated: temperature scans, frequency scans, long duration tension-compression tests and dynamic stress strain tests. For every one of them, a single material point is considered.

Once again, simulation parameters follow in the spirit of standard testing conditions defined by the ASTM in standard D7028 (ASTM, 2007).

All tests are performed for a generalized Kelvin-Voigt/Maxwell rheological model including a Kelvin-Voigt branch and two Maxwell branches. Material parameters employed in the simulation of all the curves can be found in the appendix.

The first test simulated, and the most commonly used in polymer characterization, is a temperature sweep (or temperature scan).

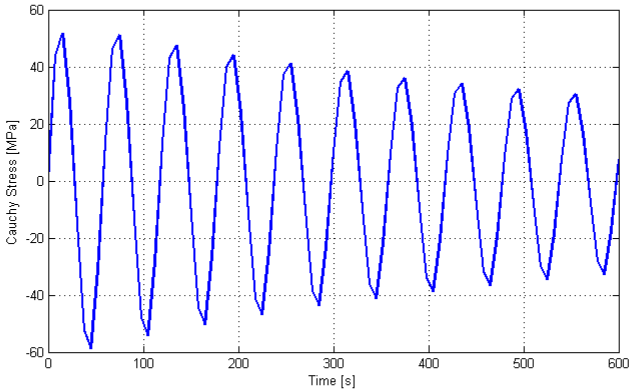

Figure 7.15 – Stress evolution through time during a temperature scan of a thermo-viscoelastic damage model: thermal softening and damage evolution are responsible for the decreasing amplitude of stress.

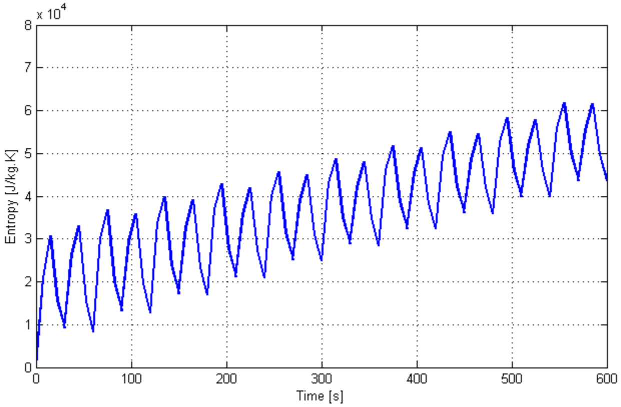

Figure 7.16 – Entropy evolution through time during a temperature scan of a thermo-viscoelastic damage model: lower dissipation levels than for the undamaged model.

A sinusoidal profile is used to impose logarithmic strains ranging from -0.04 (compression) to 0.04 (tension), with a period of $60s$. Temper-

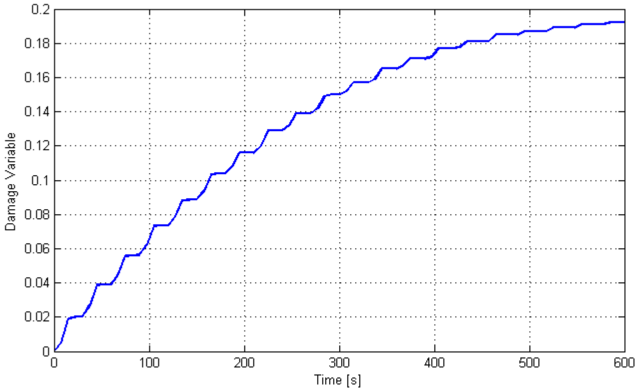

Figure 7.17 – Damage variable evolution during a temperature scan of a thermo-viscoelastic damage model: decreasing slope caused by stress softening.

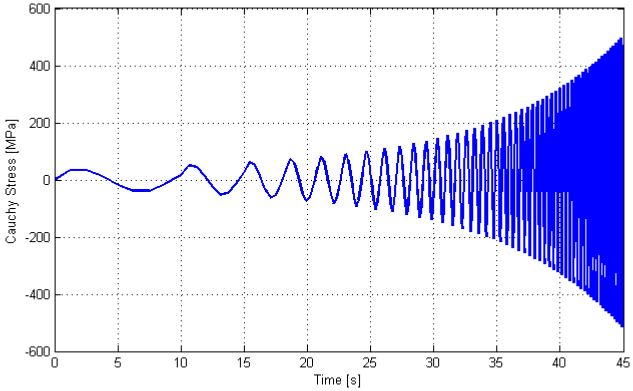

Figure 7.18 – Stress evolution through time during a frequency sweep of a thermo-viscoelasticity model: amplitude increase due to viscous effects.

ature rises at the rate of $1K/min$. Linear temperature dependence is assumed in all viscous and elastic moduli. Hencky-type potentials are used for all potentials.

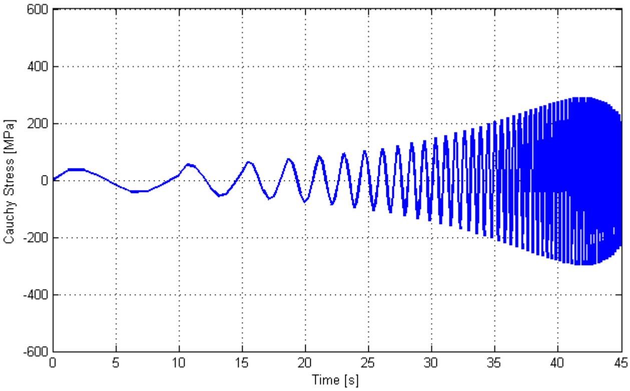

Figure 7.19 – Stress evolution through time during a frequency sweep of a thermo-viscoelastic damage model.

The results obtained for the thermo-viscoelastic model are presented in figures 7.13 and 7.14. Clearly, thermal softening is responsible for the stress amplitude to decrease by about 30% throughout the test. At every load direction reversal, a sudden drop in entropy can be perceived. This is due to thermoelastic effects. The trend line, though, is continuously growing, owing to viscous dissipation.

The same test is now run for a thermo-viscoelastic damage model. Figures 7.15, 7.16 and 7.17 show the results. Damage evolution clearly influences the stress profile along the test, further reducing its amplitude. The evolution of entropy shows lower levels of dissipation when compared to the undamaged model, despite there being a new source of dissipation in the problem. This shows that, for this particular choice of parameters, the reduced stress levels caused by damage evolution (viscous dissipation being proportional to the product of viscous strains and viscous stresses, as in equation 3.43c) dominate over the added dissipation related to damage evolution. The evolution of the damage variable shows a decreasing slope, a result of stress softening with the imposed temperature increase, which affects the energy restitution rate.

Next, a frequency sweep test is simulated. The material is subjected to a range of frequencies from $0.1Hz$ to $5Hz$, at a rate of $0.1Hz$ per cycle. Temperature is kept constant throughout the test, as is the

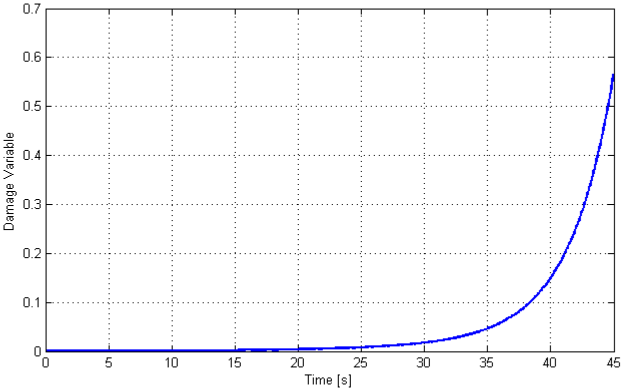

Figure 7.20 – Damage variable evolution during a frequency sweep of a thermo-viscoelastic damage model: sharp spike in higher loading frequencies.

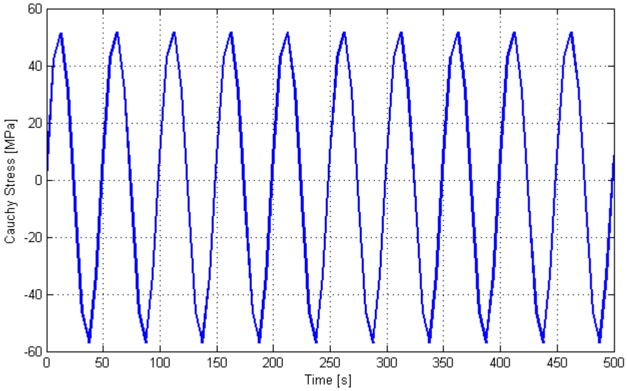

Figure 7.21 – Stress evolution in a long duration tensile/compressive test of a thermo-viscoelasticity model: no temperature dependence of parameters results in constant amplitude.

amplitude of imposed logarithmic strains (from −0.025 to 0.025). This type of test can be used to explore material response in a range of characteristic times.

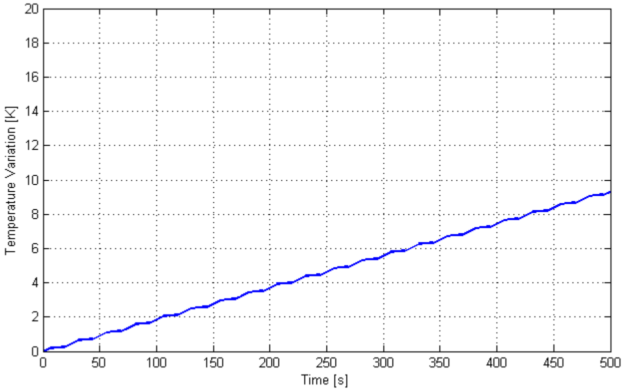

Figure 7.22 – Temperature evolution in a long duration tensile/compressive test of a thermo-viscoelasticity model.

Once more, a comparison between undamaged and damaged thermo-viscoelasticity models allows for some interesting observations. Figure 7.18 shows the evolution of stress for the thermo-viscoelastic model. Viscous effects dominate, and the amplitude of stress increases continuously with the increase in frequency. For the corresponding damaged model, shown in figure 7.19, as viscous stresses increase, so does damage's driving mechanism, the energy restitution rate. This translates into a reduction in stress amplitude and an explosion of the damage variable. This can be clearly seen in figure 7.20.

Long duration tensile/compressive cyclic tests are often also included in the category of DTMA. Unlike frequency sweeps, temperature is allowed to vary freely. As for temperature sweeps, low frequencies are used in order to keep inertia effects in check.

The same undamaged and damaged thermo-viscoelasticity models are tested under these conditions. Sinusoidal logarithmic strains are imposed, between -0.05 and 0.05 with a period of $50s$.

Since no temperature dependence of the material parameters is considered, the thermo-viscoelasticity model yields constant stress amplitude, as seen in figure 7.21. Temperature does evolve, however, due to thermomechanical coupling effects.

The thermo-viscoelastic damage model yields decreasing stress

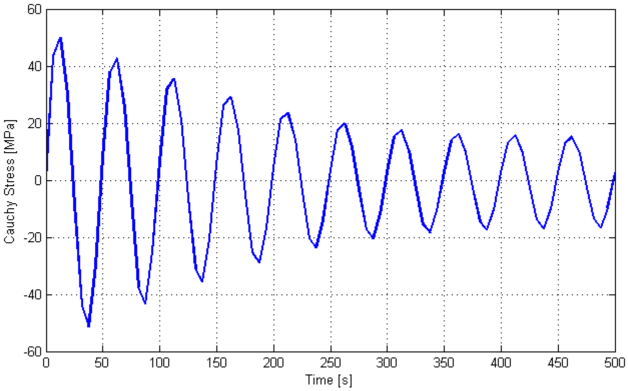

Figure 7.23 – Stress evolution in a long duration tensile/compressive test of a thermo-viscoelastic damage model.

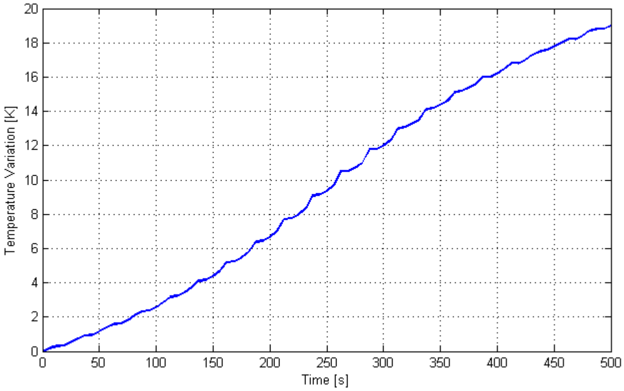

Figure 7.24 – Temperature evolution in a long duration tensile/compressive test of a thermo-viscoelastic damage model.

amplitudes, as seen in figure 7.23. The damage variable evolves as in figure 7.25, with some type of saturation as higher levels of degradation are attained. The temperature evolution profile of figure 7.24 shows a combination of the quasi-linear evolution of the equivalent undamaged

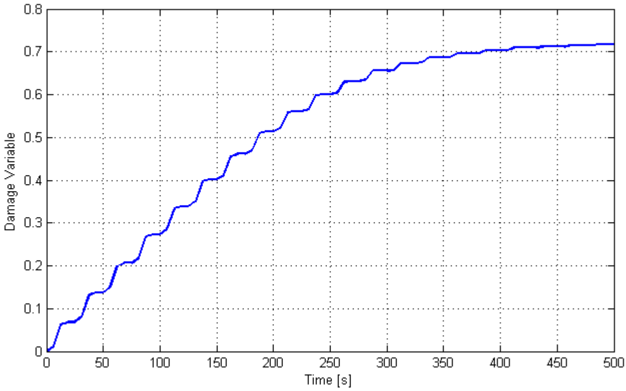

Figure 7.25 – Damage variable evolution in a long duration tensile/-compressive test of a thermo-viscoelastic damage model.

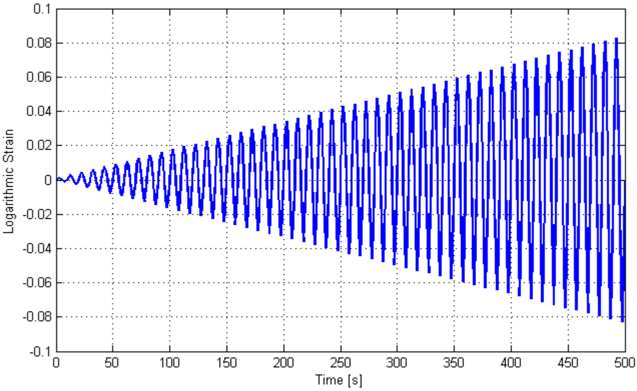

Figure 7.26 – Profile of imposed logarithmic strains in the dynamic stress-strain tests.

model (portrayed in figure 7.22) and an evolving contribution following damage evolution.

Finally, a dynamic stress-strain test is simulated. For a fixed imposed excitation frequency, strain amplitudes are constantly increased, as in figure 7.27. Strain rates thus vary along the test, and higher

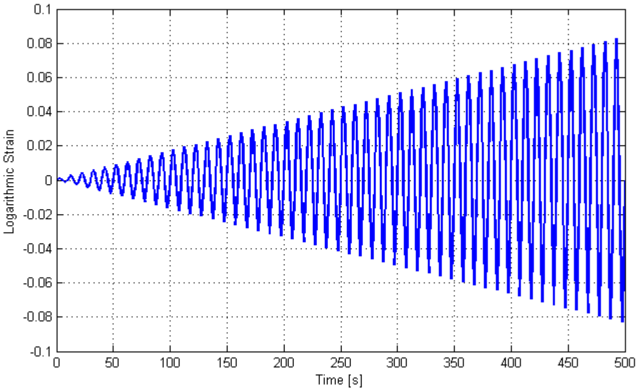

Figure 7.27 – Profile of imposed logarithmic strains in the dynamic stress-strain tests.

viscous stresses are to be expected.

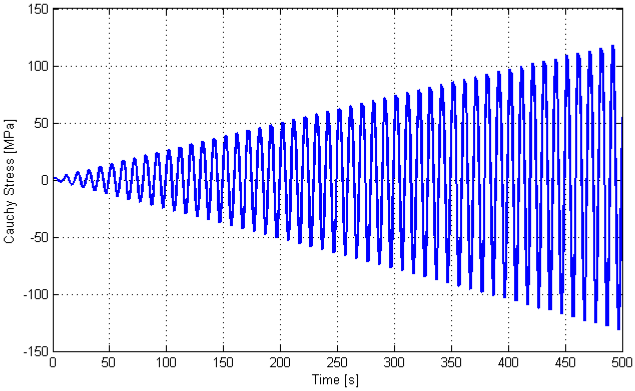

Figure 7.28 – Stress evolution in the dynamic stress-strain test of a thermo-viscoelasticity model: linear amplitude growth due to fixed temperature.

A period of excitation of $10s$ is imposed. Logarithmic strain amplitudes start from 0.001 and grow linearly to 0.08. As for the frequency sweep, temperatures are kept constant throughout the tests.

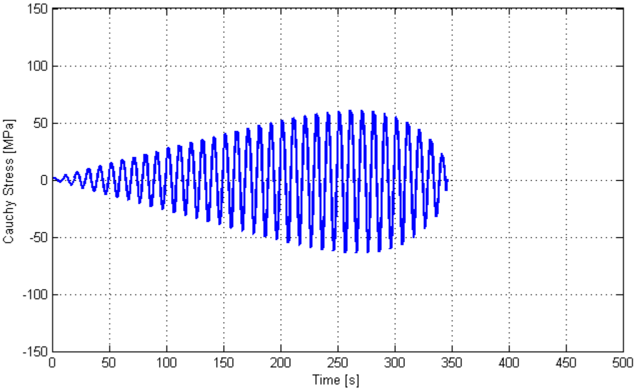

Figure 7.29 – Stress evolution in the dynamic stress-strain test of a thermo-viscoelastic damage model: damage reaches 1 and the material can no longer bear loads.

The undamaged thermo-viscoelasticity model then yields a linearly increasing stress amplitude as expected, as seen in figure 7.28.

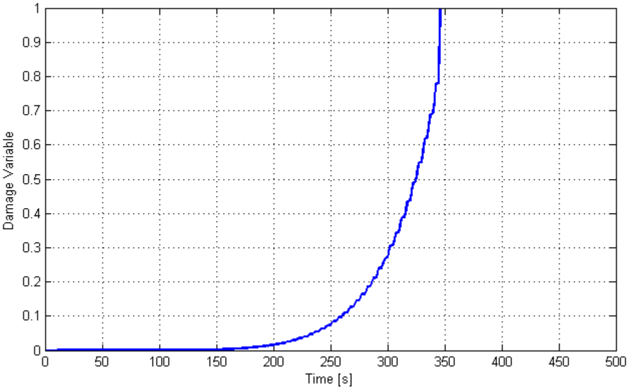

Figure 7.30 – Damage variable evolution in the dynamic stress-strain test of a thermo-viscoelastic damage model: sharp spike and failure.

The damaged model, on the other hand, is unable to reach the same imposed strain levels before failing. Increasing viscous dissipation take the damage variable to its maximum value of 1, as seen in figure 7.30, and the material can no longer bear any loads, as seen in figure 7.29.

A possible application of the proposed models could be based on using the geometries of test specimens for cyclic compression, shearing, bending and tensile tests[7.4]. An evaluation of the uniformity of loads in the process zone could be carried out. Thermal influence of the loading grips could also be investigated.

[7.4] It should be noted that no standard geometries are defined for each loading conditions. Each manufacturer of DTMA test machines follows has the liberty of defining test specimens suited to their set up.

7.5 STRAIN LOCALIZATION AND DAMAGE-INDUCED STRAIN SOFTENING IN TENSILE TESTS

Perhaps the most widely spread characterization procedure of polymers and other classes of materials are tensile tests. Requiring simpler and less expensive testing machines than those used for HDT and DTMA, for example, tensile testing is usually the method of choice in order to determine a material's mechanical properties, from elastic modulus to yield stress, ultimate strength, tenacity, plasticity, viscosity and damage parameters.

In most tensile testing machines, no temperature control is available, so that results are assumed to be valid for isothermal applications only. As strain rates grow (generating adiabatic-like conditions), though, and for materials sensitive to small temperature variations, thermal effects become more important and can trigger interesting phenomena such as strain localization and necking.

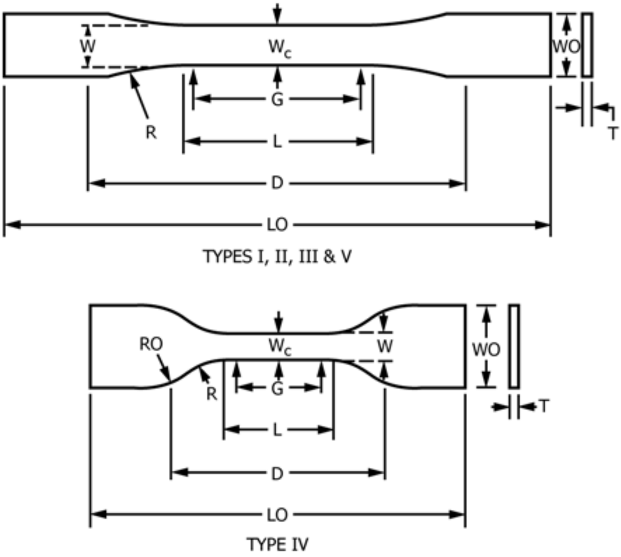

Figure 7.31 – Standard geometry for tensile plate test specimens according to ASTM D638. Types I, II and V indicated for plates with low thickness. Type III for plates of higher thickness. Type IV for special comparisons between rigid and nonrigid materials.

Variational models of viscoplasticity including thermal dependence have shown to exhibit necking in Selke (2009), for example. Even for models proposed in previous chapters, where no plasticity is considered, similar phenomena can be observed, as shown in the examples below.

Temperature dependence of material parameters is considered. Standard polymer test specimen geometries are used, and a model allowing for heat fluxes, both in the form of convection along the thermal boundaries and conduction within the material domain, is employed.

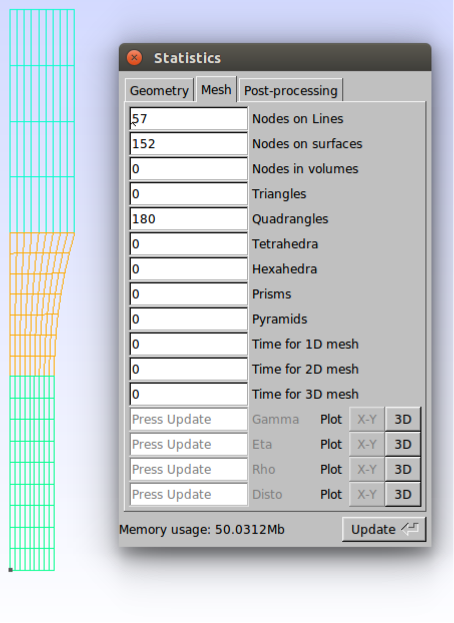

57 Nodes on Lines
152 Nodes on surfaces
0 Nodes in volumes
0 Triangles
180 Quadrangles
0 Tetrahedra
0 Hexahedra
0 Prisms
0 Pyramids
0 Time for 1D mesh
0 Time for 2D mesh
0 Time for 3D mesh
Press Update Gamma
Press Update Eta
Press Update Rho
Press Update Disto
Memory usage: 50.0312Mb

Figure 7.32 – Mesh used for the simulation of polymer tensile tests.

Simulated testing conditions are inspired by those defined by the ASTM as the standard for tensile testing of polymers in norm D638 (ASTM, 2014). Test specimens follow the standard dimensions for plates, as shown in figure 7.31. Dimensions for type I specimens are used: length of the process zone $G = 57mm$; radius $R = 76mm$; minimum length between grips $D = 115mm$; total length of test specimen $LO = 165mm$; width of the process zone $W_c = 13mm$; and total width of the test specimen $WO = 19mm$. Simulations were performed in two dimensions, so the standard thickness of $5mm$ is not considered in the mesh.

Symmetries are used, in order to simulate one quarter of a test specimen, as shown in figure 7.32. For all examples, tensile conditions are obtained by imposing positive displacements of the top horizontal line at a rate of $10mm/s$.

First, a thermo-viscoelasticity model with no damage is tested. Initially, no temperature dependence of material parameters is considered.

In this case, no unstable localization phenomenon appears even for very large imposed displacements. In figure 7.33, the final aspect of the deformed specimen is represented. Stress levels remain uniform and along the central process zone throughout the test, which explains the use of such test specimens for material characterization. Their geometries induce the development of uniform stress levels in the central process zone. This allows for accurate measurements of displacement and generation of reliable stress X strain relations. As loads increase, stress levels rise, indicating no softening.

In the undamaged case with no temperature dependence of material parameters, thermomechanical coupling still exists, but the influence on mechanical effects over thermal quantities is much greater than the opposite. The proposed model predicts temperature evolution represented in figure 7.34. Viscous dissipation is concentrated in the process zone, where stress levels are higher. Temperature profiles reflect this. Heat fluxes are mostly concentrated along the convection thermal boundary on the right, but as temperature gradients between coldest and hottest regions increases, there is some longitudinal conduction exchange between the process zone and the broader load application region as well (this can be clearly seen in the second frame of figure 7.34).

When temperature dependence of material parameters is considered, the well known effect of thermal softening takes place. However, the problem becomes less stable. Three frames of observation are chosen before thermal instabilities take place: $1mm$, $10mm$ and $20mm$ imposed along the top boundary.

Figure 7.35 shows the decreasing stress levels obtained, despite the higher imposed displacements. Clearly, convection along the boundary is not high enough to act as a heat sink, which would create transverse temperature gradients that might trigger localization. Under these conditions, stresses remain largely uniform along the process zone. As for the previous example, the process zone is uniformly af-

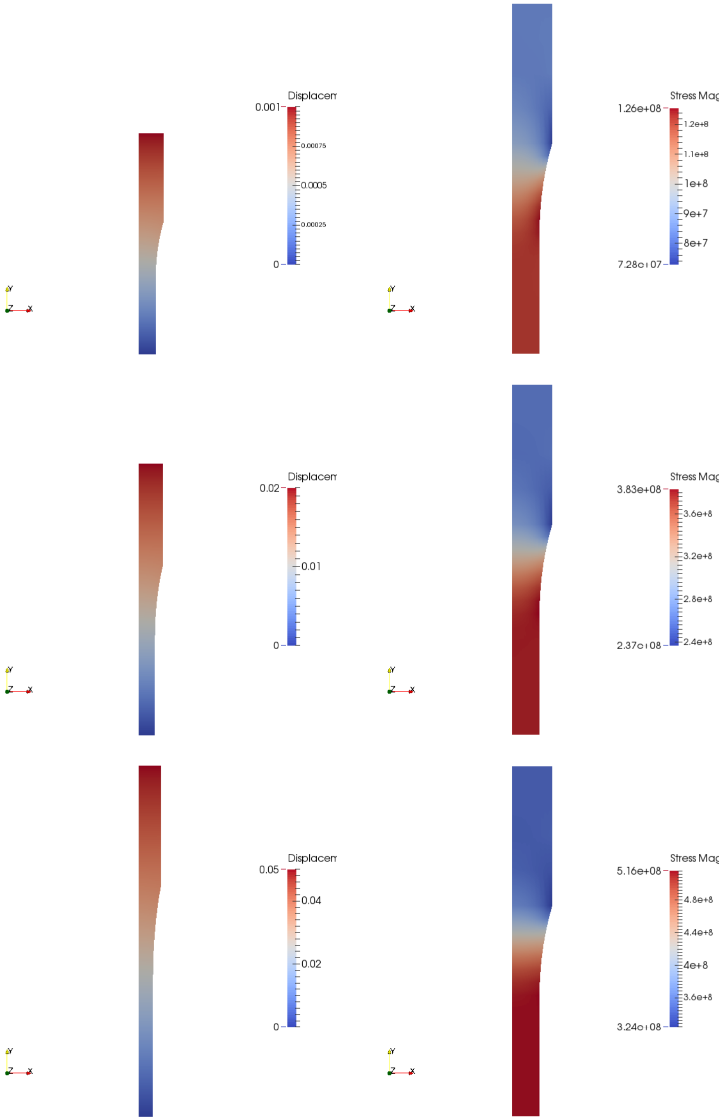

Figure 7.33 – Distributed necking of a standard tensile test specimen. Geometries at three different imposed displacements $1mm$, $20mm$ and $50mm$. Uniform stress along the central process zone, no softening.

fected by the imposed loads, and distributed necking is expected. This is a common occurrence in polymer testing, even for large imposed displacements, under certain loading conditions.

Figure 7.36 shows the predicted temperature profile and the evolution of heat fluxes during the test. Once again, temperature levels remain constant in the process zone. Unlike the previous case, fluxes are much higher and concentrate in the interior of the material, between coldest and hottest regions. Thermal softening effects seem to change the panorama of heat dissipation within the domain.

In addition to stress and temperature localization in the process zone, as test specimens are taken closer to their breaking point, damage phenomena become more and more important. In a controlled displacement tensile test, it is common to eventually observe diminishing stresses for increasing strains. This is often called the Mullins effect and, since it signals compromised material properties, is modeled through damage mechanics models.

Once again, no parameter fitting to a given polymer species is done in the following example, but a qualitative picture can be drawn to show the ability of the proposed models to reproduce the damage softening effect.

Figure 7.37 shows the necking effect. Transverse displacements are first evenly distributed along all the test specimen (first observed frame, when $10mm$ is imposed on the top border), then begin to concentrate just along the central process zone (second observation frame, for $20mm$ imposed). Later, just before the onset of unstable behavior related to higher values of damage (for imposed displacements of $22mm$), fluctuations indicate concentration of straining in smaller regions, precursors to localized failure.

Stress levels of figure 7.37 for the same frames show damage-induced softening and the beginning of localization upon very small regions of the material domain. The most damage spot is already clear in the second frame, marked by the blue spot in the process zone. The final frame shows great levels of stress relaxation around the most damaged point, which just before the onset of unstable behavior is led to bear a much higher load than its environs. Damage evolution is then clearly localized in a very small region.

This extreme localization is also evident in figure 7.38. At first, thermoelastic cooling dominates the specimen. As viscous strains (and consequently damage levels) begin to concentrate on the central process zone, the material begins to heat. When localization conditions are reached, damage dissipation dominates and high temperature gradients develop.

The profile of damage evolution shown in figure 7.38 exhibits much of the same behavior. Initially, damage is slightly higher along the top of the process zone, at the rounding radius, but mostly uniform along the central process zone. At the second frame, damage is concentrated almost exclusively on the process zone, still with no clear signs of localization at one single point. Finally, for the final time frame, fluctuations in the damage field become apparent, with the highest damage levels coinciding with the point of higher temperature and stress.

It is possible to conclude that, even when no temperature dependence of parameters is considered, the inclusion of damage into the model brings an ingredient capable of strongly localizing strains. While the undamaged model of figures 7.33 and 7.34 shows uniform stress and temperature levels along the process zone, its damaged counterpart accounts for additional thermomechanical coupling mechanisms.

For the undamaged case with no temperature dependence of the parameters, thermal quantities are strongly influenced by mechanical phenomena. The converse effect is much less pronounced. On the other hand, as temperature accumulation strongly influences damage evolution, mechanical quantities such as stresses become much more strongly affected by thermal phenomena. These thermal phenomena include gradient information through heat conduction, and thus not every point of the process zone experiences the same effects.

It is evident that, in this example, conduction-induced nonlocality is responsible for strain, stress and temperature localization. Once again, the extent to which the predicted damage localization has physical meaning or violates intrinsic material properties is a question to be assessed case by case, depending on the interplay between loading and boundary conditions and conduction properties.

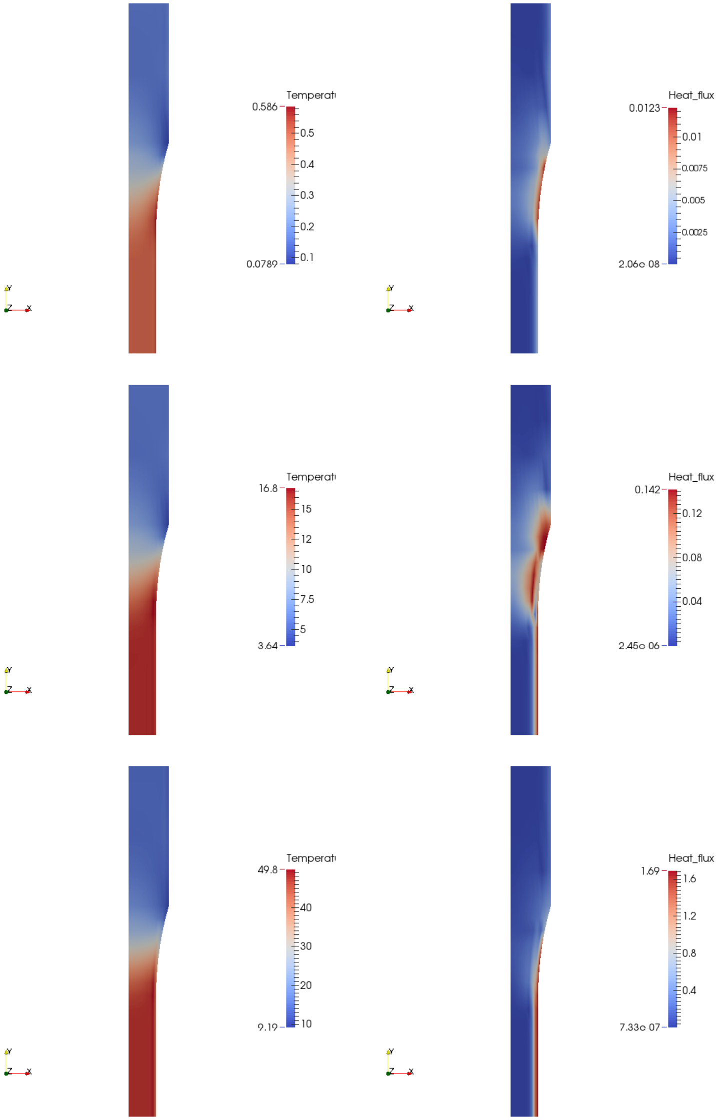

Figure 7.34 – Distributed necking of a standard tensile test specimen. Uniform temperature levels in the process zone (left column). Heat fluxes (right column) concentrated along the thermal boundary on the right.

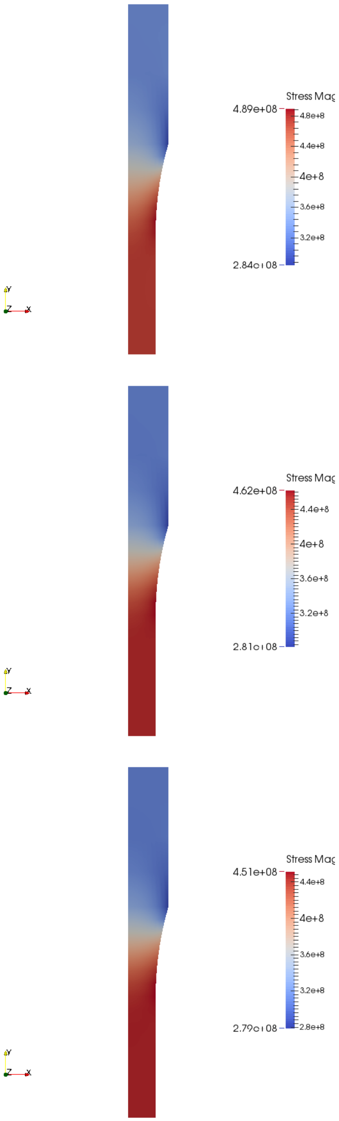

Figure 7.35 – Temperature softening of a standard tensile test specimen. Decreasing stresses for increasing imposed displacements. Viscous dissipation causes temperature increase, which then reduces elastic and viscous properties. Uniform stress along the central process zone.

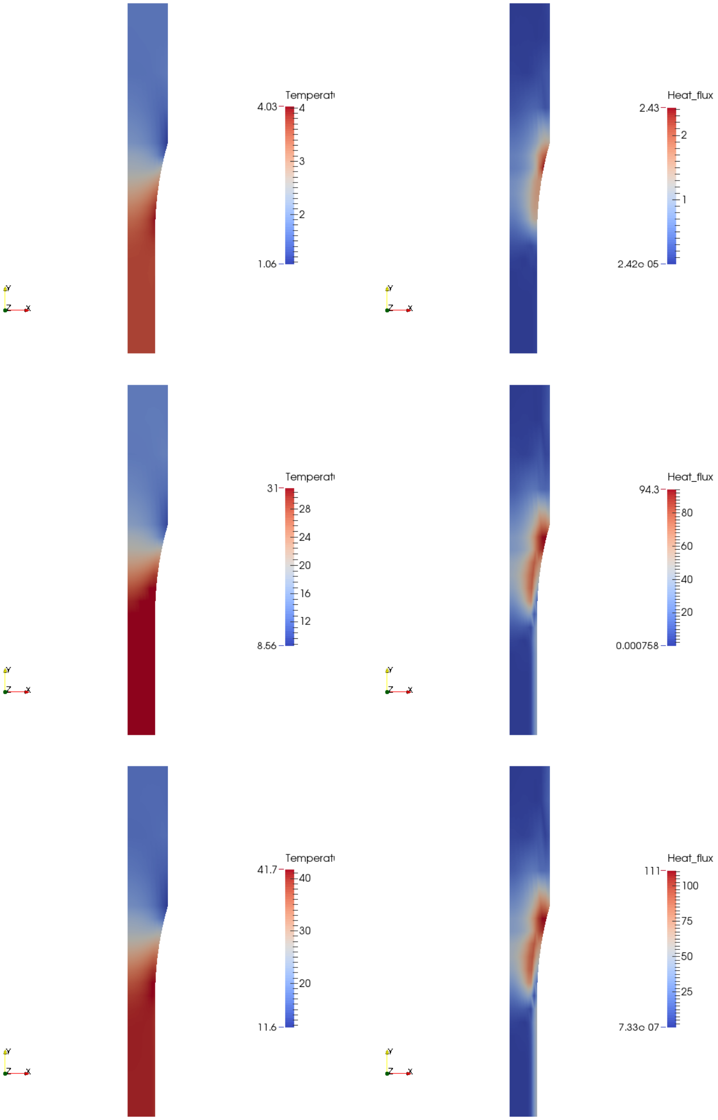

Figure 7.36 – Temperature softening of a standard tensile test specimen. Uniform temperature levels in the process zone (left column). Heat fluxes (right column) constantly concentrated between the same coldest and hottest regions.

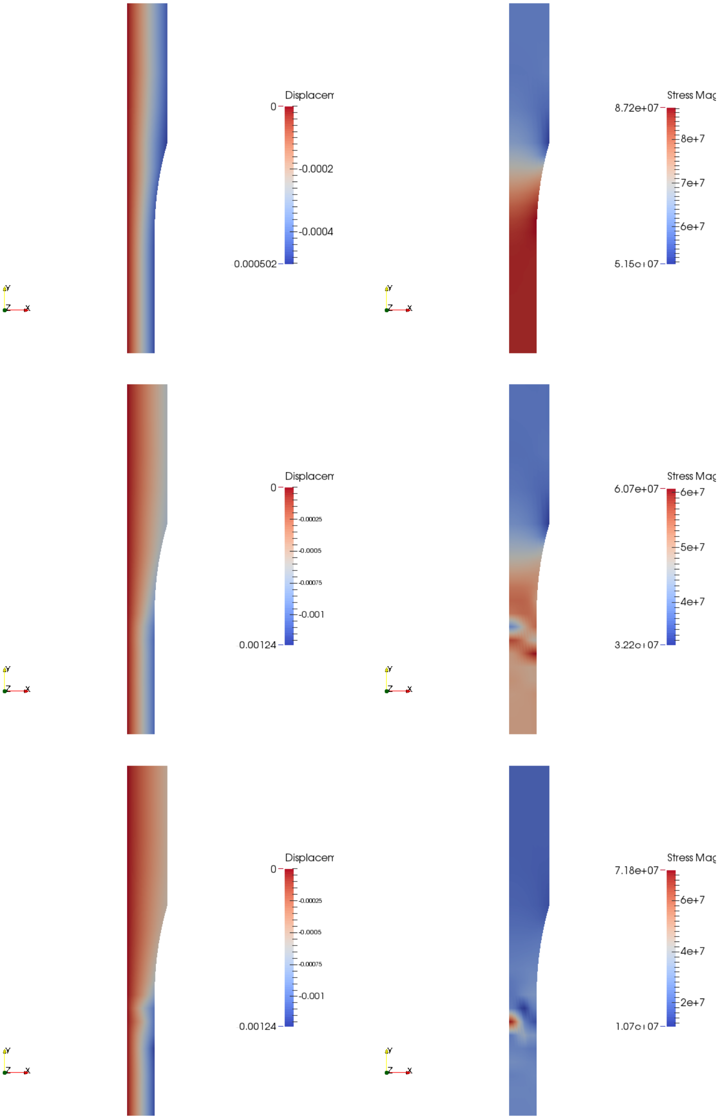

Figure 7.37 – Damage-induced softening of a standard tensile test specimen. Stress levels (right column) decreasing as imposed strains increase. Transverse displacement (left column) concentrating in the narrower process zone as damage increases at first, then showing signs of localization in a single spot.

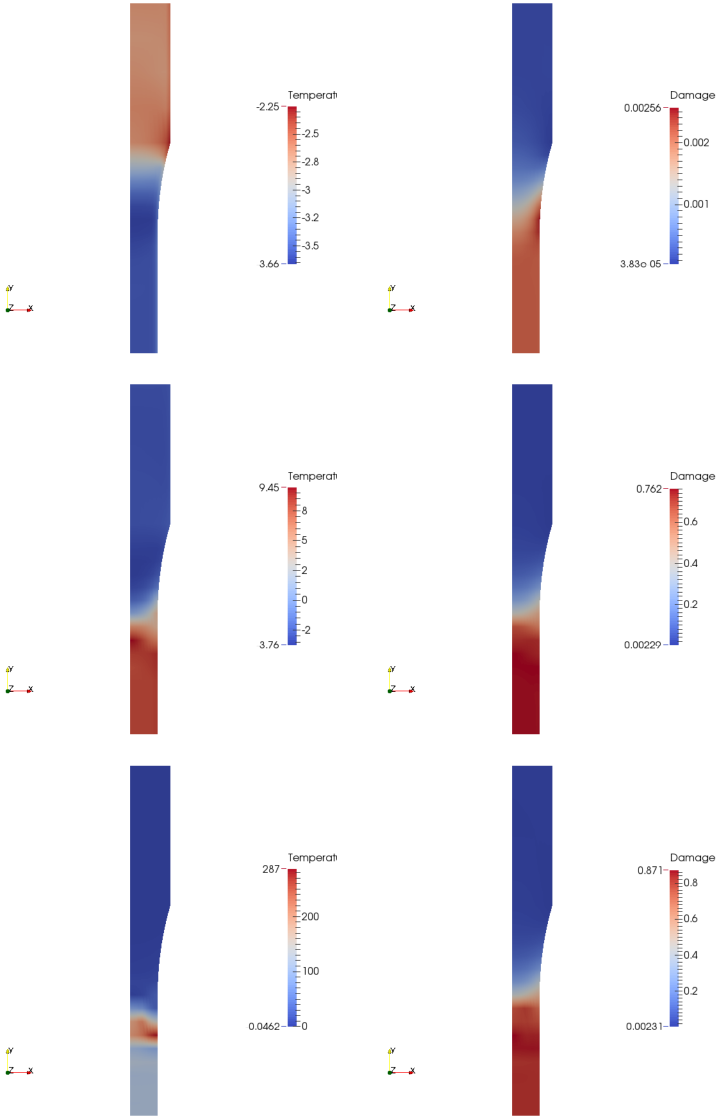

Figure 7.38 – Damage-induced softening of a standard tensile test specimen. Temperature levels (left column) go from thermoelastic cooling to extremely localized heating due to damage dissipation. Damage (right column) spreads through the process zone before beginning to localize in a narrow band.

8 CONCLUDING REMARKS AND FUTURE PERSPECTIVES

Motivated by the challenges related to the constitutive modeling of polymers in the full range of life, from fully sound material properties to full degradation and failure, this document presented a series of material models tailored to fit some of the main features in thermoplastic behavior.

In chapter 2, a micromechanical view of the thermal and mechanical loading of polymers based on specialized materials science literature led to the identification of a couple of key phenomena that had to be present in the developed constitutive models, namely viscoelasticity and thermomechanical coupling. Ruled by the relative motion between long polymer chains and by the breaking and forming of secondary bonds between them, these phenomena are essentially dissipative and required adequate thermodynamic models. Also dissipative in nature, the phenomenon of damage is responsible for the degradation of material properties throughout the volume of the considered domain. Arguments were presented for the coupling of damage to other dissipation sources in polymers. Finally, the issue of failure in polymers was discussed based on microscopy analysis of ruptured specimens. Features such as shear banding and stress crazing were shown to characterize the lead up to fracture in polymer specimens.

A fully coupled thermo-viscoelasticity model was presented in chapter 4. Drawn from the variational approach to dissipative problems known as variational constitutive updates, proposed in Ortiz & Stainier (1999) for mechanical problems and extended in Yang, Stainier & Ortiz (2006) for thermomechanics (a framework revised in detail in chapter 3), the novel model was shown to yield all the necessary balance and evolution equations from the stationarity condition of a single unified pseudo-potential function, which is built at every time step. All the steps towards the implementation of the model were discussed, especially the updates of internal variables and the construction of tangent moduli. Some of the capabilities of the model were demonstrated in sample examples, reproducing several features found in polymer behavior: strain rate dependence, temperature influence upon material parameters, stress relaxation, highly nonlinear behavior in stress X strain curves, large strain phenomena, thermomechanical coupling and hysteresis effects.

Next, in chapter 5, the variational formulation was extended to include damage effects, following the work done in Kintzel & Mosler (2011). Placed in the context of continuum damage mechanics (CDM), the proposed model was based on choices of special forms of potentials and on the principle of strain equivalence. A naturally separable structure between the updates of viscous and damage internal variables was achieved, rendering implementation of damage fairly modular in nature. Still, damage evolution remains coupled to thermal and viscous dissipation mechanisms, the other dissipative behaviors considered throughout the volume of the material. The influence of damage was explored in the routines for updating internal variables and in the derivation of tangent moduli. A few examples were used to show viscous strains as the main driving force behind damage evolution, instead of imposed stress. Additionally, some of the same examples used in the previous chapter were reproduced in order to determine the impacts of damage.

In order to overcome the issue of spurious localization, intrinsic to local models of damage such as the one proposed in chapter 5, whereby damage evolution can lead to failure with little to no dissipation and non-physical brittleness, a recent nonlocal approach was applied, in chapter 6. The Thick Level Set model (TLS) was revised and shown to provide a bridge between damage and fracture mechanics, allowing failure mechanisms to be seamlessly included into the constitutive model. In the TLS model, level-set functions are used to impose the existence of a damage front of a fixed characteristic length between regions of fully sound and fully degraded material. This is in apparent agreement to the observed crazing phenomena around cracks in polymers. Discussions on the coupling of the TLS to various local models of damage were provided, something that had yet be done in the literature, as well as a revised algorithmic view of the now nonlocal procedure for updating internal variables of damage. A discussion on the regularizing effect of heat conduction in a thermomechanically coupled damage model was also presented. It was made clear that such an effect is limited to certain loading and boundary conditions. If a characteristic length of damage gradients is considered a property of the material, as suggested by experimental and rational arguments, and the central hypothesis behind the TLS, then some nonlocal tool remains necessary even when the damage model includes temperature gradients. As sample applications, a comparison between an elastic damage model and the proposed thermo-viscoelastic damage model in dynamics was presented.

Implementations of all the proposed variational models in a finite element code dedicated to multiphysics problems are currently available. Developed in house at the Ecole Centrale de Nantes, Zorglib/-Matlib is a C++ based platform specialized in the simulation of complex constitutive models. So far, the TLS approach and the necessary level-set tools are not readily available in Zorglib. Further code development is still necessary to allow for a complete coupling between the proposed variational constitutive models and the TLS in larger scale problems.

In chapter 7, several applications of the proposed variational models were presented, with a focus on coupling mechanisms and the possibility of strong localization. For the classical case of a plate with a central hole, a first comparison was drawn between adiabatic and conduction formulations. Heat conduction was shown to indeed present a regularizing effect upon the damage profile. Next, though, it was shown that boundary conditions can strongly influence this phenomenon. By employing high convection coefficients along the boundaries, it was possible to show that a heat sink effect can greatly curtail the effect of conduction upon damage localization. Finally, different conduction coefficients were tested for the same boundary conditions. It was shown that damage profiles present lower gradients for higher conduction. However, as heat accumulation also drives damage evolution, higher levels of damage can appear and, for extreme loading conditions, damage localization can not be completely avoided.

Next, in the second set of applications, the conditions present for the very common Dynamic Thermomechanical Analysis tests were reproduced. Four different types of cyclic tests were simulated, in conditions inspired by industry standards. Several mechanisms of thermomechanical coupling were put in focus, together with the central driving forces behind damage evolution.

Finally, tensile tests for standard polymer test species were simulated. For the undamaged thermo-viscoelasticity model, both with and without temperature dependence of material parameters, stresses and temperatures were shown to develop uniformly along the central process zone. As higher imposed displacement levels were reached, the feature of distributed necking along all of the process zone was demonstrated. In the case with temperature dependence of material parameters, however, as temperature levels increased, unstable conditions were reached due to thermal softening. Next, the same test was performed for the proposed damage formulation. Even with no temperature dependence of material parameters, distributed necking was followed by predicted localization for small material regions. This shows that coupling thermal accumulation with damage introduced a new mechanism of thermomechanical coupling, with strong influence of thermal phenomena upon mechanical quantities such as strains and stresses.

A series of perspective works derived from the current document is envisioned.

One interesting issue to investigate (related essentially to mathematical and numerical aspects) would be the influence of heat diffusion in the stabilization of the damage behavior in conjunction with Thick Level Set nonlocal tools. Diffusive effects are known to introduce stabilization into localization problems. This was demonstrated in some examples of chapter 7. However, what was also shown is that, when load application happens at a time scale much shorter than the that of heat conduction (equivalently, for the assumed adiabatic conditions or for heat sink effects in the examples of chapter 7), the material can be expected to exhibit localization. The investigation of such a limit between load application and viscous and heat conduction time scales, after which nonlocal effects are naturally introduced by the coupling in the local damage model, would be interesting to explore especially in conjunction with the diffuse damage version of the TLS. By varying loading and boundary conditions, and checking when the localization triggers were activated in the TLS, a more precise notion of the regularizing effect of heat conduction could be achieved.

Another potential investigation topic (this time in the field of applications to specific materials) is the use of different damaging functions or of various damage variables related to each energy-storing or energy-dissipation mechanism. This would introduce more complex damage behavior, which could in turn help describe polymers in a broader range of applications. Of course, any such models would translate into a higher number of material parameters and into challenges of identification. However, given the favorable mathematical structure of the proposed variational models and the versatility of the generalized Kelvin-Voigt/Maxwell rheological model, parameter identification routines could be more easily run to fit the observed behavior of specific species of polymers in applications of interest.

In fact, parameter identification for specific polymer species could also be an interesting future research topic on its own (pertaining to material science). Variational formulations allow for easy determination of sensitivity factors, which can be used as the a base for material characterization. The recent development of measuring techniques could be an asset in fully characterizing thermomechanical coupling, something that, while not unusual, is still not readily available for many types of materials. Given the characteristics of polymers, such a characterization is of the utmost importance for many applications.

The coupling of the proposed models to plasticity-driven damage models also seems to be a promising line of work (in the field of variational constitutive modeling). Polymers often exhibit permanent strains, with rate dependent hardening and dissipation phenomena. The inclusion of Lemaître-type damage models into the variational framework is possible, as demonstrated in Kintzel & Mosler (2011), but their coupling to viscoelastic damage models has yet to be done. The competition between different driving forces (viscosity and plasticity) should yield interesting damage evolution behaviors.

The possibilities offered by the TLS approach of delimiting clear narrow damage bands in a domain can also be explored in dealing with the formation of shear bands. A typical thermomechanical problem, adiabatic shear banding characterizes failure in thermoplastics under certain loading conditions. The very framework of combining a thermomechanically-coupled damage model with the TLS would seem to be very well suited to applications of shear banding.

As material models grow in complexity, with the incorporation and coupling of various mechanisms, computational costs are bound to grow. In this context, the investigation of efficient solution algorithms for fully coupled problems, including staggered or fractional step methods (discussed, for instance, in Armero & Simo (1992) and Ramabathiran & Stainier (2013)), modified schemes for the solution of nonlinear systems (as in Bouery (2012)) or even different strategies based on domain decomposition (such as the Large Time Increment, LATIN, discussed in Cognard & Ladevèze (1993), or the more recent Proper Generalized Decomposition, PGD, discussed in Chinesta, Ladeveze & Cueto (2011)) can be of interest.

REFERENCES

ARMERO, F.; SIMO, J. A priori stability estimates and unconditionally stable product formula algorithms for nonlinear coupled thermoplasticity. **International Journal of Plasticity**, v. 9, n. 6, p. 749 – 782, 1993.

ARMERO, F.; SIMO, J. C. A new unconditionally stable fractional step method for non-linear coupled thermomechanical problems. **International Journal for Numerical Methods in Engineering**, John Wiley & Sons, Ltd, v. 35, n. 4, p. 737–766, 1992.

ARORA, J. **Introduction to Optimum Design**. Elsevier Science, 2004.

ARRUDA, E. M.; BOYCE, M. C.; JAYACHANDRAN, R. Effects of strain rate, temperature and thermomechanical coupling on the finite strain deformation of glassy polymers. **Mechanics of Materials**, v. 19, n. 2-3, p. 193 – 212, 1995.

ASKES, H.; SLUYS, L. Explicit and implicit gradient series in damage mechanics. **European Journal of Mechanics - A/Solids**, v. 21, n. 3, p. 379 – 390, 2002.

ASTM. **D7028 - Standard Test Method for Glass Transition Temperature (DMA Tg) of Polymer Matrix Composites by Dynamic Mechanical Analysis (DMA)**. [S.l.], 2007.

ASTM. **D638 - Standard Test Method for Tensile Properties of Plastics**. [S.l.], 2014.

BAZANT, Z. P.; PIJAUDIER-CABOT, G. Nonlocal continuum damage, localization instability and convergence. **Journal of Applied Mechanics**, American Society of Mechanical Engineers, v. 55, n. 2, p. 287–293, 1988.

BERNARD, P.; MOËS, N.; CHEVAUGEON, N. Damage growth modeling using the thick level set (tls) approach: Efficient discretization for quasi-static loadings. **Computer Methods in Applied Mechanics and Engineering**, v. 233-236, n. 0, p. 11 – 27, 2012.

BILLMEYER, F. W. **Textbook of Polymer Science**. Wiley India Pvt. Limited, 2007.

BIOT, M. Linear thermodynamics and the mechanics of solids. In: **Proceedings of Third US National Congress of Applied Mechanics**. [S.l.]: ASME, 1958. p. 1–18.

BIRD, R. B.; CURTISS, C. Thermoviscoelasticity: continuum-molecular connections. **Journal of Non-Newtonian Fluid Mechanics**, v. 79, n. 2-3, p. 255 – 259, 1998.

BJERKE, T. W.; LAMBROS, J. Theoretical development and experimental validation of a thermally dissipative cohesive zone model for dynamic fracture of amorphous polymers. **Journal of the Mechanics and Physics of Solids**, v. 51, n. 6, p. 1147 – 1170, 2003.

BLEIER, N.; MOSLER, J. A hybrid variationally consistent homogenization approach based on ritz's method. **International Journal for Numerical Methods in Engineering**, v. 94, n. 7, p. 625–647, 2013.

BONET, J.; WOOD, R. **Nonlinear Continuum Mechanics for Finite Element Analysis**. Cambridge University Press, 2008.

BOUERY, C. **Contribution to algorithmic strategies for solving coupled thermo-mechanical problems by an energy-consistent variational approach**. Tese (Doutorado) — Ecole Centrale de Nantes, 2012.

BOURDIN, B.; FRANCFORT, G.; MARIGO, J.-J. The variational approach to fracture. **Journal of Elasticity**, Springer Netherlands, v. 91, n. 1-3, p. 5–148, 2008.

BOYCE, M. C.; PARKS, D. M.; ARGON, A. S. Large inelastic deformation of glassy polymers. part i: rate dependent constitutive model. **Mechanics of Materials**, v. 7, n. 1, p. 15 – 33, 1988.

BRASSART, L.; STAINIER, L. On convergence properties of variational constitutive updates for elasto-visco-plasticity. **GAMM-Mitteilungen**, WILEY-VCH Verlag, v. 35, n. 1, p. 26–42, 2012.

BRASSART, L. et al. Homogenization of elasto-(visco) plastic composites based on an incremental variational principle. **International Journal of Plasticity**, v. 36, n. 0, p. 86 – 112, 2012.

BRINK, U.; STEIN, E. On some mixed finite element methods for incompressible and nearly incompressible finite elasticity. **Computational Mechanics**, Springer-Verlag, v. 19, n. 1, p. 105–119, 1996.

CALLISTER, W. **Materials Science And Engineering: An Introduction**. John Wiley & Sons, 2007.

CANADIJA, M.; MOSLER, J. On the thermomechanical coupling in finite strain plasticity theory with non-linear kinematic hardening by means of incremental energy minimization. **International Journal of Solids and Structures**, v. 48, n. 7-8, p. 1120 – 1129, 2011.

CANADIJA, M.; MOSLER, J. Low cycle fatigue in metals - a thermodynamically and variationally consistent constitutive model based on energy minimization. In: **Proceedings of COMPLAS XII - International Conference on Computational Plasticity, Fundamentals and Applications**. [S.l.: s.n.], 2013.

CANEVAROLO, S. V. **Ciência dos Polímeros: um texto básico para tecnólogos e engenheiros**. [S.l.]: Artliber Editora, 2006.

CHEN, X.; NGUYEN, T. D. Influence of thermoviscoelastic properties and loading conditions on the recovery performance of shape memory polymers. **Mechanics of Materials**, v. 43, n. 3, p. 127 – 138, 2011.

CHENG, H.; WANG, J.; HUANG, Z. A thermo-viscoelastic constitutive model for compressible amorphous polymers. **Mechanics of Time-Dependent Materials**, Springer Netherlands, v. 14, n. 3, p. 261–275, 2010.

CHINESTA, F.; LADEVEZE, P.; CUETO, E. A short review on model order reduction based on proper generalized decomposition. **Archives of Computational Methods in Engineering**, Springer Netherlands, v. 18, n. 4, p. 395–404, 2011.

COGNARD, J.-Y.; LADEVèZE, P. A large time increment approach for cyclic viscoplasticity. **International Journal of Plasticity**, v. 9, n. 2, p. 141 – 157, 1993.

COLEMAN, B. D.; NOLL, W. The thermodynamics of elastic materials with heat conduction and viscosity. **Archive for Rational Mechanics and Analysis**, Springer-Verlag, v. 13, n. 1, p. 167–178, 1963.

CORDEBOIS, J.; SIDOROFF, F. Damage induced elastic anisotropy. In: BOEHLER, J.-P. (Ed.). **Mechanical Behavior of Anisotropic Solids / Comportment Méchanique des Solides Anisotropes**. Springer Netherlands, 1982. p. 761–774.

DAFERMOS, C. Global smooth solutions to the initial-boundary value problem for the equations of one-dimensional nonlinear thermoviscoelasticity. **SIAM Journal on Mathematical Analysis**, v. 13, n. 3, p. 397–408, 1982.

DODD, B.; BAI, Y. **Adiabatic Shear Localization: Frontiers and Advances**. Elsevier Science, 2012. (Elsevier insights).

DROZDOV, A. A constitutive model in thermoviscoelasticity. **Mechanics Research Communications**, v. 23, n. 5, p. 543 – 548, 1996.

DROZDOV, A.; CHRISTIANSEN, J. Thermo-viscoelastic and viscoplastic behavior of high-density polyethylene. **International Journal of Solids and Structures**, v. 45, n. 14-15, p. 4274 – 4288, 2008.

DROZDOV, A.; DORFMANN, A. The effect of temperature on the viscoelastic response of rubbery polymers at finite strains. **Acta Mechanica**, Springer-Verlag, v. 154, n. 1-4, p. 189–214, 2002.

DROZDOV, A. D. Chapter 2 - constitutive models in linear viscoelasticity. In: DROZDOV, A. D. (Ed.). **Viscoelastic Structures**. Burlington: Academic Press, 1998. p. 25 – 106.

ERINGEN, A. Linear theory of nonlocal elasticity and dispersion of plane waves. **International Journal of Engineering Science**, v. 10, n. 5, p. 425 – 435, 1972.

ERINGEN, A. On nonlocal plasticity. **International Journal of Engineering Science**, v. 19, n. 12, p. 1461 – 1474, 1981, dedicated to Prof. K. Kondo on the occassion of his seventieth birthday.

ERINGEN, A. Theories of nonlocal plasticity. **International Journal of Engineering Science**, v. 21, n. 7, p. 741 – 751, 1983.

FANCELLO, E. et al. Identification of the strain rate parameters for structural adhesives. **Journal of Adhesion Science and Technology**, v. 22, n. 13, p. 1523–1540, 2008.

FANCELLO, E. et al. A simple extension of lemaître's elastoplastic damage model to account for hydrolytic degradation. **Latin American Journal of Solids and Structures**, v. 11, n. 5, p. 884 – 906, 2014.

FANCELLO, E.; PONTHOT, J.; STAINIER, L. A variational framework for nonlinear viscoelastic models in finite deformation regime. **Journal of Computational and Applied Mathematics**, v. 215, n. 2, p. 400 – 408, 2008, proceedings of the Third International Conference on Advanced Computational Methods in Engineering (ACOMEN 2005).

FANCELLO, E.; PONTHOT, J.-P.; STAINIER, L. A variational formulation of constitutive models and updates in non-linear finite viscoelasticity. **International Journal for Numerical Methods in Engineering**, Wiley Online Library, v. 65, n. 11, p. 1831–1864, 2006.

FANCELLO, E.; VASSOLER, J. M.; STAINIER, L. A variational constitutive update algorithm for a set of isotropic hyperelastic–viscoplastic material models. **Computer Methods in Applied Mechanics and Engineering**, North-Holland, v. 197, n. 49, p. 4132–4148, 2008.

FRÉMOND, M.; NEDJAR, B. Damage, gradient of damage and principle of virtual power. **International Journal of Solids and Structures**, v. 33, n. 8, p. 1083 – 1103, 1996.

GEUZAINE, C.; REMACLE, J.-F. A 3-d finite element mesh generator with built-in pre- and post-processing facilities. **International Journal for Numerical Methods in Engineering**, John Wiley & Sons, Ltd., v. 79, n. 11, p. 1309–1331, 2009.

GOVINDJEE, S.; SIMO, J. C. Mullins effect and the strain amplitude dependence of the storage modulus. **International Journal of Solids and Structures**, v. 29, n. 14 - 15, p. 1737 – 1751, 1992.

GRAMMENOUDIS, P.; RECKWERTH, D.; TSAKMAKIS, C. Continuum damage models based on energy equivalence: Part i - isotropic material response. **International Journal of Damage Mechanics**, v. 18, n. 1, p. 31–63, 2009.

GRAMMENOUDIS, P.; RECKWERTH, D.; TSAKMAKIS, C. Continuum damage models based on energy equivalence: Part ii - anisotropic material response. **International Journal of Damage Mechanics**, v. 18, n. 1, p. 65–91, 2009.

GRIFFITH, A. A. The phenomena of rupture and flow in solids. **Philosophical Transactions of the Royal Society of London. Series A, Containing Papers of a Mathematical or Physical Character**, v. 221, n. 582-593, p. 163–198, 1921.

GURTIN, M.; FRIED, E.; ANAND, L. **The Mechanics and Thermodynamics of Continua**. Cambridge University Press, 2010.

GURTIN, M. E.; ANAND, L. The decomposition $f = f^e f^p$, material symmetry, and plastic irrotationality for solids that are isotropic-viscoplastic or amorphous. **International Journal of Plasticity**, v. 21, n. 9, p. 1686 – 1719, 2005.

HAKIM, V.; KARMA, A. Crack path prediction in anisotropic brittle materials. **Phys. Rev. Lett.**, American Physical Society, v. 95, p. 235501, Dec 2005.

HALPHEN, B.; NGUYEN, Q. S. Sur les matériaux standard généralisés. **Journal de Mécanique**, v. 14, p. 39–63, 1975.

HASLACH, H. W.; ZENG, N. Maximum dissipation evolution equations for non-linear thermoviscoelasticity. **International Journal of Non-Linear Mechanics**, v. 34, n. 2, p. 361 – 385, 1999.

HAUDIN, J.-M.; MONASSE, B. Section 4.9 - plasticity of polymers. In: LEMAITRE, J. (Ed.). **Handbook of Materials Behavior Models**. Burlington: Academic Press, 2001. p. 255 – 264.

HOLZAPFEL, G. **Nonlinear Solid Mechanics: A Continuum Approach for Engineering**. Wiley, 2000.

HOLZAPFEL, G. A.; SIMO, J. C. A new viscoelastic constitutive model for continuous media at finite thermomechanical changes. **International Journal of Solids and Structures**, v. 33, n. 20-22, p. 3019 – 3034, 1996.

HUANG, Z. A constitutive theory in thermo-viscoelasticity at finite deformation. **Mechanics Research Communications**, v. 26, n. 6, p. 679 – 686, 1999.

HUANG, Z.; DUI, G.; YANG, S. A new interpretation of internal-variable theory in finite thermo-viscoelasticity. **Science China Physics, Mechanics and Astronomy**, SP Science China Press, v. 56, n. 3, p. 610–616, 2013.

KACHANOV, L. Rupture time under creep conditions. **International Journal of Fracture**, Kluwer Academic Publishers, v. 97, n. 1-4, p. 11–18, 1999.

KAKANI, S. **Material Science**. New Age International (P) Limited, 2006.

KALISKE, M.; NASDALA, L.; ROTHERT, H. On damage modelling for elastic and viscoelastic materials at large strain. **Computers & Structures**, v. 79, n. 22-25, p. 2133 – 2141, 2001.

KINTZEL, O.; MOSLER, J. An incremental minimization principle suitable for the analysis of low cycle fatigue in metals: A coupled ductile-brittle damage model. **Computer Methods in Applied Mechanics and Engineering**, v. 200, n. 45-46, p. 3127 – 3138, 2011.

KRÖNER, E. Allgemeine kontinuumstheorie der versetzungen und eigenspannungen. **Archive for Rational Mechanics and Analysis**, Springer-Verlag, v. 4, n. 1, p. 273–334, 1959.

KRÖNER, E. Elasticity theory of materials with long range cohesive forces. **International Journal of Solids and Structures**, Elsevier, v. 3, n. 5, p. 731–742, 1967.

KUMAR, R. S.; TALREJA, R. A continuum damage model for linear viscoelastic composite materials. **Mechanics of Materials**, v. 35, n. 3-6, p. 463 – 480, 2003.

LEMAÎTRE, J. **A course on damage mechanics**. Springer, 1996.

LEE, E. H. Elastic-plastic deformations at finite strains. **Journal of Applied Mechanics**, ASME, v. 36, n. 1, p. 1–6, 1969.

LEMAÎTRE, J.; DESMORAT, R. **Engineering Damage Mechanics: Ductile, Creep, Fatigue and Brittle Failures**. Springer, 2005.

LUO, W. et al. Long-term creep assessment of viscoelastic polymer by time-temperature-stress superposition. **Acta Mechanica Solida Sinica**, v. 25, n. 6, p. 571 – 578, 2012.

MALVERN, L. **Introduction to the Mechanics of a Continuous Medium**. Prentice-Hall, 1969. (Prentice-Hall series in engineering of the physical sciences).

MIEHE, C. Strain-driven homogenization of inelastic microstructures and composites based on an incremental variational formulation. **International Journal for Numerical Methods in Engineering**, John Wiley & Sons, Ltd., v. 55, n. 11, p. 1285–1322, 2002.

MIEHE, C.; WELSCHINGER, F.; HOFACKER, M. Thermodynamically consistent phase-field models of fracture: Variational principles and multi-field fe implementations. **International Journal for Numerical Methods in Engineering**, John Wiley & Sons, Ltd., v. 83, n. 10, p. 1273–1311, 2010.

MOËS, N.; DOLBOW, J.; BELYTSCHKO, T. A finite element method for crack growth without remeshing. **Int. J. Numer. Meth. Engng**, v. 46, p. 131–150, 1999.

MOËS, N. et al. A level set based model for damage growth: The thick level set approach. **International Journal for Numerical Methods in Engineering**, John Wiley & Sons, Ltd., v. 86, n. 3, p. 358–380, 2011.

MOSLER, J. Variationally consistent modeling of finite strain plasticity theory with non-linear kinematic hardening. **Computer Methods in Applied Mechanics and Engineering**, v. 199, n. 45-48, p. 2753 – 2764, 2010.

MOSLER, J.; BRUHNS, O. Towards variational constitutive updates for non-associative plasticity models at finite strain: Models based on a volumetric-deviatoric split. **International Journal of Solids and Structures**, v. 46, n. 7-8, p. 1676 – 1684, 2009.

MOSLER, J.; ORTIZ, M. Variational h-adaption in finite deformation elasticity and plasticity. **International Journal for Numerical Methods in Engineering**, John Wiley & Sons, Ltd., v. 72, n. 5, p. 505–523, 2007.

MOSLER, J.; ORTIZ, M. An error-estimate-free and remapping-free variational mesh refinement and coarsening method for dissipative solids at finite strains. **International Journal for Numerical Methods in Engineering**, John Wiley & Sons, Ltd., v. 77, n. 3, p. 437–450, 2009.

MURAKAMI, S. **Continuum Damage Mechanics: A Continuum Mechanics Approach to the Analysis of Damage and Fracture**. Springer, 2012. (Solid Mechanics and Its Applications).

NGUYEN, T. D. et al. A thermoviscoelastic model for amorphous shape memory polymers: Incorporating structural and stress relaxation. **Journal of the Mechanics and Physics of Solids**, v. 56, n. 9, p. 2792 – 2814, 2008.

ODEN, J.; ARMSTRONG, W. Analysis of nonlinear, dynamic coupled thermoviscoelasticity problems by the finite element method. **Computers & Structures**, v. 1, n. 4, p. 603 – 621, 1971, special Issue on Structural Dynamics.

ORTIZ, M.; REPETTO, E. Nonconvex energy minimization and dislocation structures in ductile single crystals. **Journal of the Mechanics and Physics of Solids**, v. 47, n. 2, p. 397 – 462, 1999.

ORTIZ, M.; STAINIER, L. The variational formulation of viscoplastic constitutive updates. **Computer methods in applied mechanics and engineering**, Elsevier, v. 171, n. 3, p. 419–444, 1999.

PEERLINGS, R. et al. A critical comparison of nonlocal and gradient-enhanced softening continua. **International Journal of Solids and Structures**, v. 38, n. 44-45, p. 7723 – 7746, 2001.

PEERLINGS, R.; MASSART, T.; GEERS, M. A thermodynamically motivated implicit gradient damage framework and its application to brick masonry cracking. **Computer Methods in Applied Mechanics and Engineering**, v. 193, n. 30-32, p. 3403 – 3417, 2004, computational Failure Mechanics.

PEERLINGS, R. H. J. et al. Gradient enhanced damage for quasi-brittle materials. **International Journal for Numerical Methods in Engineering**, John Wiley & Sons, Ltd, v. 39, n. 19, p. 3391–3403, 1996.

PIJAUDIER-CABOT, G.; BAZANT, Z. Nonlocal damage theory. **Journal of Engineering Mechanics**, v. 113, n. 10, p. 1512–1533, 1987.

RABOTNOV, Y. Creep rupture. In: HETÉNYI, M.; VINCENTI, W. G. (Ed.). **Applied Mechanics**. Springer Berlin Heidelberg, 1969, (International Union of Theoretical and Applied Mechanics). p. 342–349.

RADOVITZKY, R.; ORTIZ, M. Error estimation and adaptive meshing in strongly nonlinear dynamic problems. **Computer**

Methods in Applied Mechanics and Engineering, North-Holland, v. 172, n. 1, p. 203–240, 1999.

RAMABATHIRAN, A.; STAINIER, L. Staggered schemes for strongly coupled thermoviscoelastic problems based on an energy-based variational formulation of thermomechanics. In: **Proceedings of COMPLAS XII - International Conference on Computational Plasticity, Fundamentals and Applications**. [S.l.: s.n.], 2013.

RIVARA, M.-C. New longest-edge algorithms for the refinement and/or improvement of unstructured triangulations. **International Journal for Numerical Methods in Engineering**, John Wiley & Sons, Ltd, v. 40, n. 18, p. 3313–3324, 1997.

SELKE, A. **Modelo Constitutivo Variacional de Viscoplasticidade em Regime de Grandes Deformaçoes para um Problema Adiabatico Termomecanicamente Acoplado**. Dissertação (Mestrado) — Universidade Federal de Santa Catarina, 2009.

SIMO, J. On a fully three-dimensional finite-strain viscoelastic damage model: Formulation and computational aspects. **Computer Methods in Applied Mechanics and Engineering**, v. 60, n. 2, p. 153 – 173, 1987.

SIMO, J. C.; TAYLOR, R. L. Quasi-incompressible finite elasticity in principal stretches. continuum basis and numerical algorithms. **Computer Methods in Applied Mechanics and Engineering**, v. 85, n. 3, p. 273 – 310, 1991.

SIMONE, A. **Explicit and implicit gradient-enhanced damage models**. 2007. ALERT Graduate School - Course notes.

SOUZA NETO, E. de; PERIC, D.; OWEN, D. **Computational Methods for Plasticity: Theory and Applications**. Wiley, 2011.

STAINIER, L. Consistent incremental approximation of dissipation pseudo-potentials in the variational formulation of thermo-mechanical constitutive updates. **Mechanics Research Communications**, v. 38, n. 4, p. 315 – 319, 2011.

STAINIER, L. Chapter two - a variational approach to modeling coupled thermo-mechanical nonlinear dissipative behaviors. In:

BORDAS, S. P. (Ed.). Elsevier, 2013, (Advances in Applied Mechanics, v. 46). p. 69 – 126.

STAINIER, L.; CUITIÑO, A. M.; ORTIZ, M. A micromechanical model of hardening, rate sensitivity and thermal softening in bcc single crystals. **Journal of the Mechanics and Physics of Solids**, Pergamon, v. 50, n. 7, p. 1511–1545, 2002.

STAINIER, L.; ORTIZ, M. Study and validation of a variational theory of thermo-mechanical coupling in finite visco-plasticity. **International Journal of Solids and Structures**, Elsevier, v. 47, n. 5, p. 705–715, 2010.

STOLZ, C.; MOËS, N. A new model of damage: a moving thick layer approach. **International Journal of Fracture**, Springer Netherlands, v. 174, n. 1, p. 49–60, 2012.

SU, S.; STAINIER, L.; MERCIER, S. Energy-based variational modeling of fully formed adiabatic shear bands. **European Journal of Mechanics - A/Solids**, v. 47, n. 0, p. 1 – 13, 2014.

SUKUMAR, N. et al. Extended finite element method for three-dimensional crack modelling. **International Journal for Numerical Methods in Engineering**, John Wiley & Sons, Ltd., v. 48, n. 11, p. 1549–1570, 2000.

SUN, S. et al. Thermoviscoelastic analysis for a polymeric composite plate with embedded shape memory alloy wires. **Composite Structures**, v. 58, n. 2, p. 295 – 302, 2002.

TAYLOR, R. L.; PISTER, K. S.; GOUDREAU, G. L. Thermomechanical analysis of viscoelastic solids. **International Journal for Numerical Methods in Engineering**, John Wiley & Sons, Ltd, v. 2, n. 1, p. 45–59, 1970.

VASSOLER, J. **A pressure sensitive constitutive model based on a variational framework for the elasto-viscoplastic behavior and its application to a metallic foam**. Tese (Doutorado) — Politecnico di Torino, 2009.

VOYIADJIS, G. Z.; YOUSEF, M. A.; KATTAN, P. I. New tensors for anisotropic damage in continuum damage mechanics. **Journal of Engineering Materials and Technology**, v. 134, n. 2, 2012.

WARD, I.; SWEENEY, J. **An Introduction to the Mechanical Properties of Solid Polymers**. 2nd. ed. [S.l.]: John Wiley & Sons, 2004.

WEBER, G.; ANAND, L. Finite deformation constitutive equations and a time integration procedure for isotropic, hyperelastic-viscoplastic solids. **Computer Methods in Applied Mechanics and Engineering**, v. 79, n. 2, p. 173 – 202, 1990.

WEINBERG, K.; MOTA, A.; ORTIZ, M. A variational constitutive model for porous metal plasticity. **Computational Mechanics**, Springer-Verlag, v. 37, n. 2, p. 142–152, 2006.

YANG, B.; KIM, B.; LEE, H. Micromechanics-based viscoelastic damage model for particle-reinforced polymeric composites. **Acta Mechanica**, Springer Vienna, v. 223, n. 6, p. 1307–1321, 2012.

YANG, Q.; STAINIER, L.; ORTIZ, M. A variational formulation of the coupled thermo-mechanical boundary-value problem for general dissipative solids. **Journal of the Mechanics and Physics of Solids**, Elsevier, v. 54, n. 2, p. 401–424, 2006.

ZREID, I.; FLEISCHHAUER, R.; KALISKE, M. A thermomechanically coupled viscoelastic cohesive zone model at large deformation. **International Journal of Solids and Structures**, v. 50, n. 25-26, p. 4279 – 4291, 2013.

APPENDIX A – Parametric dependence in general dissipation pseudo-potentials

From when variational approaches to dissipative problems are introduced (section 3.4) and throughout all the following mentions to dissipation pseudo-potentials, a possible parametric dependence on the value of internal and external variables is assumed. So as not to deviate from the main ideas behind the construction of variational formulations for the various considered problems, discussions on the handling of this parametric dependence were omitted from the main text. The goal of this appendix is to explore this issue for a general dissipation pseudo-potential.

Responsible for keeping track of the history of the independent variables, the parametric dependence is denoted after a semicolon ($\psi\left(\dot{\mathbf{C}}, \dot{\mathbf{Z}}; \mathbf{C}, \mathbf{Z}\right)$). In the incremental context, it is represented by variables evaluated at an intermediate point $n+\alpha$ in the time step between n and $n+1$. A simple finite difference scheme for approximating the derivatives of variables is considered ($\dot{\mathbf{Z}} = \frac{\mathbf{Z}_{n+1}-\mathbf{Z}_n}{\Delta t}$):

$$\psi\left(\frac{\Delta\mathbf{C}}{\Delta t}, \frac{\Delta\mathbf{Z}}{\Delta t}; \mathbf{C}_{n+\alpha}, \mathbf{Z}_{n+\alpha}\right) \tag{A.1}$$

A generalized midpoint rule of the following kind shall be adopted: $\mathbf{Z}_{n+\alpha} = \alpha\mathbf{Z}_{n+1} - (1-\alpha)\mathbf{Z}_n$. Clearly, then, when determining the stationarity condition of the general equation 3.37 with respect to variables at the end of the time step, terms dependent on the parametric $\mathbf{C}_{n+\alpha}$ and $\mathbf{Z}_{n+\alpha}$ appear, in addition to terms related to the rate of independent variables.

$$\begin{aligned}
&D_{\mathbf{x}_{n+1}}[\mathcal{H}_n](\delta\mathbf{x}_{n+1}) = \\
&\qquad \int_\Omega \left\{\rho_R \frac{\partial W}{\partial \mathbf{C}} + \left[\frac{\partial \psi}{\partial \dot{C}} + \alpha\Delta t \frac{\partial \psi}{\partial \mathbf{C}_{n+1}}\right]\right\} \nabla\delta\mathbf{x}_{n+1} dV \\
&\quad - \int_\Omega \mathbf{t}_R . \delta\mathbf{x}_{n+1} d\Gamma - \int_\Omega \mathbf{b}_R . \delta\mathbf{x}_{n+1} dV = 0, \quad \forall adm \delta\mathbf{x}_{n+1}
\end{aligned} \tag{A.2a}$$

$$D_{\mathbf{Z}_{n+1}}[\mathcal{H}_n](\delta\mathbf{Z}_{n+1}) =$$
$$\int_\Omega \left\{ \rho_R \frac{\partial W}{\partial \mathbf{Z}_{n+1}} + \left[\overbrace{\underbrace{\frac{\partial \psi}{\partial \dot{\mathbf{Z}}}}_{Y_{(\dot{\mathbf{Z}})}} + \underbrace{\alpha \Delta t \frac{\partial \psi}{\partial \mathbf{Z}_{n+1}}}_{Y_{(\mathbf{Z}_{n+1})}}}^{Y} \right] \right\} : \delta\mathbf{Z}_{n+1} dV = 0,$$
$$\forall adm \delta\mathbf{Z}_{n+1} \quad \text{(A.2b)}$$

The mechanical equilibrium equation actually includes dissipative stress terms originated from the parametric dependence on the history of $\mathbf{C}$. Equivalently, the equation for the evolution of internal variables also has to account for terms depending on their history.

It becomes evident that the notation adopted throughout the main text is lacking in this regard, starting from equations 3.43. In fact, all derivatives of the dissipation pseudo-potential with respect to the rate of independent variables ($\frac{\partial \psi}{\partial \dot{\mathbf{Z}}}$) should be interpreted as the terms in square brackets in the equations A.2 above, for a general case.

Only for chosen dissipation pseudo-potentials exhibiting no history dependence does the derivative reduce to the simpler expression adopted throughout. This is the case, in fact, for many of the examples presented, where it is made clear that the chosen dissipative potentials are history independent. For a rigorous notation, though, the equations A.2 above should be considered.

Evidently, the issue is also present in the derivatives performed in assembling the tangent operators. Second derivatives of general dissipation pseudo-potentials include three terms. $K_{(\dot{\mathbf{Z}})}$ marks the second derivative with respect to the rate of internal variables. $K_{(\dot{\mathbf{Z}},\mathbf{Z}_{n+1})}$ marks the cross derivative with respect to the rate of internal variables and the parametric dependence on their history. $K_{(\mathbf{Z}_{n+1})}$ marks the second derivative with respect to the parametric dependence on the history of internal variables.

$$\frac{\partial^2 \psi}{\partial \mathbf{Z}_{n+1}^2} = \overbrace{\frac{1}{\Delta t^2} \frac{\partial^2 \psi}{\partial \dot{\mathbf{Z}}^2}}^{K_{(\dot{\mathbf{Z}})}} + \overbrace{2\alpha \frac{1}{\Delta t} \frac{\partial^2 \psi}{\partial \dot{\mathbf{Z}} \partial \mathbf{Z}_{n+1}}}^{K_{(\dot{\mathbf{Z}},\mathbf{Z}_{n+1})}} + \overbrace{\alpha^2 \frac{\partial^2 \psi}{\partial \mathbf{Z}_{n+1}^2}}^{K_{(\mathbf{Z}_{n+1})}} \quad \text{(A.3)}$$

Extending the variational formulation to thermomechanical problems involves the use of a specific parameterization of all dissipative behaviors. Closely connected to the concept of internal and external temperatures, as discussed in section 3.5, the term $\frac{T_{n+1}}{T_n}$ is factored into all dissipation mechanisms, which are, in turn, dependent on the rate of independent variables. Additionally, possible parametric dependence on the temperature history is also considered. The general notation of the dissipation pseudo-potential then becomes:

$$\psi\left(\frac{T_{n+1}}{T_n}\frac{\Delta\mathbf{C}}{\Delta t},\frac{T_{n+1}}{T_n}\frac{\Delta\mathbf{Z}}{\Delta t};\mathbf{C}_{n+\alpha},\mathbf{Z}_{n+\alpha},T_{n+\alpha}\right) \tag{A.4}$$

In order to ensure thermodynamic consistency of the variational scheme, a proper average of the dissipation has to be taken along the time step. This is denoted through accolades throughout the text, and the definition of equation 3.47 is recalled below.

$$\begin{aligned}\left\langle\psi\left(\frac{T_{n+1}}{T_n}\frac{\Delta\mathbf{C}}{\Delta t},\frac{T_{n+1}}{T_n}\frac{\Delta\mathbf{Z}}{\Delta t};\mathbf{C}_{n+\alpha},\mathbf{Z}_{n+\alpha},T_{n+\alpha}\right)\right\rangle = \\ \frac{T_n}{T_{n+1}}\psi\left(\frac{T_{n+1}}{T_n}\frac{\Delta\mathbf{C}}{\Delta t},\frac{T_{n+1}}{T_n}\frac{\Delta\mathbf{Z}}{\Delta t};\mathbf{C}_{n+\alpha},\mathbf{Z}_{n+\alpha},T_n\right)+ \\ \frac{T_{n+1}-T_n}{T_{n+1}}\psi\left(\frac{T_{n+1}}{T_n}\frac{\Delta\mathbf{C}}{\Delta t},\frac{T_{n+1}}{T_n}\frac{\Delta\mathbf{Z}}{\Delta t};\mathbf{C}_{n+\alpha},\mathbf{Z}_{n+\alpha},T_{n+\alpha}\right)\end{aligned} \tag{A.5}$$

The dissipation pseudo-potential has to be evaluated at different temperatures T_n and $T_{n+\alpha}$. This brings out additional parametric dependence terms to the expressions of both the thermodynamic force conjugated to internal variables $Y = Y_{(\dot{\mathbf{Z}})} + Y_{(\mathbf{Z}_{n+1})}$, and to the second order derivative of the dissipation pseudo-potential $K = K_{(\dot{\mathbf{Z}})} + K_{(\dot{\mathbf{Z}},\mathbf{Z}_{n+1})} + K_{(\mathbf{Z}_{n+1})}$.

These operations are detailed in the following appendices, first in the discussion of the contribution to entropy evolution of each portion of dissipation, then for the specific case of damage dissipation, in assembling the corresponding material tensors.

APPENDIX B – Thermomechanical dissipation pseudo-potentials: contribution to entropy evolution

As discussed in previous appendix, the chosen notation for the dissipation pseudo-potential (and its derivatives) in the main text is somewhat too economical when it comes to properly treating both the parametric dependence on the history of independent variables and the temperature correction that ensures thermodynamic consistency of the thermomechanical formulation. This was done in the interest of a more concise and clear notation for the main equations, but must be addressed for a complete picture.

In the general incremental thermomechanical case, dissipation pseudo-potentials take on the following form (equation 3.47):

$$\begin{aligned} \left\langle \psi\left(\frac{T_{n+1}}{T_n}\frac{\Delta\mathbf{C}}{\Delta t}, \frac{T_{n+1}}{T_n}\frac{\Delta\mathbf{Z}}{\Delta t}; \mathbf{C}_{n+\alpha}, \mathbf{Z}_{n+\alpha}, T_{n+\alpha}\right)\right\rangle = \\ \frac{T_n}{T_{n+1}}\psi\left(\frac{T_{n+1}}{T_n}\frac{\Delta\mathbf{C}}{\Delta t}, \frac{T_{n+1}}{T_n}\frac{\Delta\mathbf{Z}}{\Delta t}; \mathbf{C}_{n+\alpha}, \mathbf{Z}_{n+\alpha}, T_n\right) + \\ \frac{T_{n+1}-T_n}{T_{n+1}}\psi\left(\frac{T_{n+1}}{T_n}\frac{\Delta\mathbf{C}}{\Delta t}, \frac{T_{n+1}}{T_n}\frac{\Delta\mathbf{Z}}{\Delta t}; \mathbf{C}_{n+\alpha}, \mathbf{Z}_{n+\alpha}, T_{n+\alpha}\right) \end{aligned} \tag{B.1}$$

The additive decomposition of different dissipation mechanisms is assumed, leading to the three main dissipation components of the most complete thermo-viscoelastic damage problem: Kelvin-Voigt viscoelasticity ψ^{KV}, Maxwell viscoelasticity ψ^{MX} and damage evolution ψ^{d}.

Equation 5.28, reproduced below in more appropriate form, brings the entropy update equation for the thermo-viscoelastic damage problem. The internal dissipation includes contributions from the evolution of viscous variables $\mathcal{D}^{v}_{int}$ and from the evolution of the damage variable $\mathcal{D}^{d}_{int}$.

$$
\begin{aligned}
\eta_{n+1} &= -f(d_{n+1})\left[\frac{\partial \tilde{W}^{e}}{\partial T_{n+1}} + \frac{\partial \tilde{W}^{vol}}{\partial T_{n+1}} + \frac{\partial \tilde{W}^{h}}{\partial T_{n+1}}\right] \\
&= \overbrace{f(d_{n+1})\left[\Delta t \frac{\partial\left\langle \tilde{\psi}^{KV}\right\rangle}{\partial T_{n+1}} + \Delta t \frac{\partial\left\langle \tilde{\psi}^{MX}\right\rangle}{\partial T_{n+1}}\right]}^{\mathcal{D}^{v}_{int}} \\
&\quad + \underbrace{\Delta t \frac{\partial\left\langle \tilde{\psi}^{d}\right\rangle}{\partial T_{n+1}}}_{\mathcal{D}^{d}_{int}} + \eta_n + \Delta t \operatorname{Div}\left(\frac{\mathbf{q}_R}{T_n}\right) + \Delta t \frac{\mathrm{r}_R}{T_n} \qquad \text{(B.2)}
\end{aligned}
$$

It is only when viscous dissipation pseudo-potentials exhibit no history dependence that their temperature derivative reduces to $\frac{\partial\langle\psi\rangle}{\partial T_{n+1}} = \frac{\dot{\mathbf{Z}}}{T_n}\left\langle \frac{\partial \psi}{\partial \dot{\mathbf{Z}}}\right\rangle$, as written in equation 5.28.

In the present appendix, a complete form of the entropy evolution due to each portion of dissipation is derived.

$$
\begin{aligned}
\frac{\partial\langle\psi\rangle}{\partial T_{n+1}} = \frac{\dot{\mathbf{Z}}}{T_n}\overbrace{\left\langle \frac{\partial \psi}{\partial \dot{\mathbf{Z}}}\right\rangle}^{Y_{(\dot{\mathbf{Z}})}} + \alpha \frac{T_{n+1}-T_n}{T_n}\overbrace{\frac{\partial \psi}{\partial T_{n+1}}(T_{n+\alpha})}^{Y_{(T_{n+1})}} \\
+ \frac{T_n}{T_{n+1}^2}\left(\psi(T_{n+1}) - \psi(T_{n+1})\right) \qquad \text{(B.3)}
\end{aligned}
$$

The portion $Y_{(T_{n+1})}$ corresponds to a thermodynamic force associated to the parametric dependence on temperature history. Due to the factorization of all dissipative behaviors through a temperature term, the temperature derivative commutes to the one related to the evolution of independent variables, yielding the term: $\frac{\dot{\mathbf{Z}}}{T_n}\left\langle \frac{\partial \psi}{\partial \dot{\mathbf{Z}}}\right\rangle$. What remains to explore is the influence of the thermodynamically consistent temperature average.

$$
Y_{(\dot{\mathbf{Z}})} = \left\langle \frac{\partial \psi}{\partial \dot{\mathbf{Z}}}\right\rangle = \frac{\partial \psi}{\partial \dot{\mathbf{Z}}}(T_n) + \frac{T_{n+1}-T_n}{T_n}\frac{\partial \psi}{\partial \dot{\mathbf{Z}}}(T_{n+1}) \qquad \text{(B.4)}
$$

Thus, for each of the three main sources of dissipation in the general thermo-viscoelastic damage problem, the contributions to entropy evolution (by means of internal dissipation) is given by the following expressions, instead of the simpler terms in equation 5.28:

$$\begin{aligned}
\mathcal{D}_{int}^{KV} &= f(d_{n+1})\Delta t \frac{\partial \left\langle \psi^{KV} \right\rangle}{\partial T_{n+1}} = \\
& f(d_{n+1}) \left\{ \frac{\Delta c_j}{T_n} \left\langle \frac{\partial \psi^{KV}}{\partial \dot{c}_j} \right\rangle + \alpha \Delta t \frac{T_{n+1} - T_n}{T_n} \frac{\partial \psi^{KV}}{\partial T_{n+1}} (T_{n+\alpha}) \right. \\
& \qquad \left. + \Delta t \frac{T_n}{T_{n+1}^2} \left(\psi^{KV}(T_{n+1}) - \psi^{KV}(T_{n+1}) \right) \right\} = \\
& f(d_{n+1}) \left\{ \frac{\Delta c_j}{T_n} \left[\frac{\partial \psi^{KV}}{\partial \dot{c}_j}(T_n) + \frac{T_{n+1} - T_n}{T_n} \frac{\partial \psi^{KV}}{\partial \dot{c}_j}(T_{n+1}) \right] \right. \\
& \qquad + \alpha \frac{T_{n+1} - T_n}{T_n} \frac{\partial \psi^{KV}}{\partial T_{n+1}} (T_{n+\alpha}) \\
& \qquad \left. + \frac{T_n}{T_{n+1}^2} \left[\psi^{KV}(T_{n+\alpha}) - \psi^{KV}(T_n) \right] \right\}
\end{aligned} \tag{B.5a}$$

$$\begin{aligned}
\mathcal{D}_{int}^{MX} &= f(d_{n+1})\Delta t \frac{\partial \left\langle \psi^{MX} \right\rangle}{\partial T_{n+1}} = \\
& f(d_{n+1}) \left\{ \frac{\Delta q_j}{T_n} \left\langle \frac{\partial \psi^{MX}}{\partial \dot{q}_j} \right\rangle + \alpha \Delta t \frac{T_{n+1} - T_n}{T_n} \frac{\partial \psi^{MX}}{\partial T_{n+1}} (T_{n+\alpha}) \right. \\
& \qquad \left. + \Delta t \frac{T_n}{T_{n+1}^2} \left(\psi^{MX}(T_{n+1}) - \psi^{MX}(T_{n+1}) \right) \right\} = \\
& f(d_{n+1}) \left\{ \frac{\Delta q_j}{T_n} \left[\frac{\partial \psi^{MX}}{\partial \dot{q}_j}(T_n) + \frac{T_{n+1} - T_n}{T_n} \frac{\partial \psi^{MX}}{\partial \dot{q}_j}(T_{n+1}) \right] \right. \\
& \qquad + \alpha \frac{T_{n+1} - T_n}{T_n} \frac{\partial \psi^{MX}}{\partial T_{n+1}} (T_{n+\alpha}) \\
& \qquad \left. + \frac{T_n}{T_{n+1}^2} \left[\psi^{MX}(T_{n+\alpha}) - \psi^{MX}(T_n) \right] \right\}
\end{aligned} \tag{B.5b}$$

$$\begin{aligned}
\mathcal{D}^d_{int} = \Delta t \frac{\partial \left\langle \psi^d \right\rangle}{\partial T_{n+1}} = \\
\frac{\Delta d}{T_n} \left\langle \frac{\partial \psi^d}{\partial \dot{d}} \right\rangle + \alpha \Delta t \frac{T_{n+1} - T_n}{T_n} \frac{\partial \psi^d}{\partial T_{n+1}} (T_{n+\alpha}) \\
+ \Delta t \frac{T_n}{T_{n+1}^2} \big(\psi^d(T_{n+1}) - \psi^d(T_{n+1}) \big) = \\
\frac{\Delta d}{T_n} \left[\frac{\partial \psi^d}{\partial \dot{d}} (T_n) + \frac{T_{n+1} - T_n}{T_n} \frac{\partial \psi^d}{\partial \dot{d}} (T_{n+1}) \right] \\
+ \alpha \frac{T_{n+1} - T_n}{T_n} \frac{\partial \psi^d}{\partial T_{n+1}} (T_{n+\alpha}) \\
+ \frac{T_n}{T_{n+1}^2} \big[\psi^d(T_{n+\alpha}) - \psi^d(T_n) \big]
\end{aligned} \tag{B.5c}$$

APPENDIX C – Thermo-viscoelasticity: derivatives with respect to eigenvalues of strain predictor

Section 4.5 consists of a detailed look into the determination of tensor moduli $\mathbb{C}$ and $\mathbb{D}$. Thermomechanical coupling terms $\mathbb{C}_{thm} = \mathbb{D}_{thm}$ are likewise discussed. Different terms corresponding to each portion of the free energy and dissipation potentials are identified. Throughout the section, the proposed predictor-corrector scheme is employed for evaluating the contribution of each Maxwell branch, so that many of the necessary derivatives are performed with respect to predictor quantities.

What remains to be done in order to complete final expressions for the tensor moduli is determining a couple of derivatives with respect to predictor strains. This appendix employs a similar procedure found in the appendices of Selke (2009) (where the focus was on thermo-viscoplasticity) to determine terms marked I and II, respectively in equations 4.90 and 4.91, namely: $\frac{\partial \epsilon_j^e}{\partial \epsilon_j^{pr}}$ and $\frac{\partial T}{\partial \epsilon_j^{pr}}$.

The starting point for the procedure are the stationarity conditions with respect to internal viscous variables, to their corresponding Lagrange multiplier and to temperature, recalled below (in the case of history independent dissipation pseudo-potentials) for reading convenience:

$$r_j = -\frac{\partial W^e}{\partial \epsilon_j^e} + \lambda_0 + \frac{T_{n+1}}{T_n}\left\langle \frac{\partial \psi^{MX}}{\partial \dot{q}_j} \right\rangle = 0 \tag{C.1a}$$

$$r_4 = \sum_{j=1}^{3} q_j = 0 \tag{C.1b}$$

$$r_T = \left[\frac{\partial W}{\partial T} + \eta_n\right] + \frac{\Delta t}{T_n}\left\langle \frac{\partial \psi^{KV}}{\partial \dot{c}_j} : \dot{c}_j + \frac{\partial \psi^{MX}}{\partial \dot{q}_j} : \dot{q}_j \right\rangle + \frac{\Delta t}{T_n}\operatorname{Div}(\mathbf{q}_R) - \frac{\Delta t}{T_n}\mathrm{r}_R = 0 \tag{C.1c}$$

From the definition of the predictor state, it is possible to write:

$$\epsilon_j^e = \epsilon_j^{pr} - \Delta q_j \Rightarrow \frac{\partial \epsilon_i^e}{\partial \epsilon_j^{pr}} = \delta_{ij} - \frac{\partial q_i}{\partial \epsilon_j^{pr}} \tag{C.2}$$

Next, derivatives of all equations above with respect to predictor strains are performed:

$$\frac{\partial r_i}{\partial \epsilon_j^{pr}} = -\left[\frac{\partial^2 W^e}{\partial \epsilon_i^{e2}} \frac{\partial \epsilon_i^e}{\partial \epsilon_j^{pr}} + \frac{\partial^2 W^e}{\partial \epsilon_i^e \partial T} \frac{\partial T}{\partial \epsilon_j^{pr}}\right] + \frac{\partial \lambda_0}{\partial \epsilon_j^{pr}}$$
$$+ \frac{1}{\Delta t} \frac{T_{n+1}}{T_n}^2 \left\langle \frac{\partial^2 \psi^{MX}}{\partial \dot{q}_i^2} \right\rangle \frac{\partial q_i}{\partial \epsilon_j^{pr}} +$$
$$\frac{1}{\Delta t} \frac{T_{n+1}}{T_n} \frac{\Delta q_j}{T_n} \left\langle \frac{\partial^2 \psi^{MX}}{\partial \dot{q}_i^2} \right\rangle \frac{\partial T}{\partial \epsilon_j^{pr}} = 0 \quad \text{(C.3a)}$$

$$\frac{\partial r_4}{\partial \epsilon_j^{pr}} = \frac{\partial q_i}{\partial \epsilon_j^{pr}} = 0 \quad \text{(C.3b)}$$

$$\frac{\partial r_T}{\partial \epsilon_j^{pr}} = \left[\frac{\partial^2 W}{\partial T^2} \frac{\partial T}{\partial \epsilon_j^{pr}} + \frac{\partial^2 W^e}{\partial T \partial \epsilon_i^e} \frac{\partial \epsilon_i^e}{\partial \epsilon_j^{pr}}\right]$$
$$+ \frac{1}{\Delta t}\left[\frac{\Delta c_i}{T_n}\right]^2 \left\langle \frac{\partial^2 \psi^{KV}}{\partial \dot{c}_i^2} \right\rangle \frac{\partial T}{\partial \epsilon_j^{pr}} + \frac{\Delta q_i}{T_n} \left[\frac{1}{\Delta t} \frac{T_{n+1}}{T_n} \left\langle \frac{\partial^2 \psi^{MX}}{\partial \dot{q}_i^2} \right\rangle \frac{\partial q_i}{\partial \epsilon_j^{pr}}\right.$$
$$\left. + \frac{\dot{q}_i}{T_n} \left\langle \frac{\partial^2 \psi^{MX}}{\partial \dot{q}_i^2} \right\rangle \frac{\partial T}{\partial \epsilon_j^{pr}}\right] = 0 \quad \text{(C.3c)}$$

Rearranging the system of equations above using relation C.2:

$$\frac{\partial r_i}{\partial \epsilon_j^{pr}} = \left[\frac{\partial^2 W^e}{\partial \epsilon_i^{e2}} + \frac{1}{\Delta t} \frac{T_{n+1}}{T_n}^2 \left\langle \frac{\partial^2 \psi^{MX}}{\partial \dot{q}_i^2} \right\rangle\right] \frac{\partial q_i}{\partial \epsilon_j^{pr}} + \frac{\partial \lambda_0}{\partial \epsilon_j^{pr}}$$
$$+ \left[-\frac{\partial^2 W^e}{\partial \epsilon_i^e \partial T} + \frac{1}{\Delta t} \frac{T_{n+1}}{T_n} \frac{\Delta q_j}{T_n} \left\langle \frac{\partial^2 \psi^{MX}}{\partial \dot{q}_i^2} \right\rangle\right] \frac{\partial T}{\partial \epsilon_j^{pr}}$$
$$- \delta_{ij} \frac{\partial^2 W^e}{\partial \epsilon_i^{e2}} = 0 \quad \text{(C.4a)}$$

$$\frac{\partial r_4}{\partial \epsilon_j^{pr}} = \frac{\partial q_i}{\partial \epsilon_j^{pr}} = 0 \quad \text{(C.4b)}$$

$$\begin{aligned}\frac{\partial r_T}{\partial \epsilon_j^{pr}} = &\left[-\frac{\partial^2 W^e}{\partial T \partial \epsilon_i^e} + \frac{1}{\Delta t}\frac{\Delta q_i}{T_n}\frac{T_{n+1}}{T_n}\left\langle \frac{\partial^2 \psi^{MX}}{\partial \dot{q}_i^2}\right\rangle\right]\frac{\partial q_i}{\partial \epsilon_j^{pr}} \\ &+ \left[\frac{\partial^2 W}{\partial T^2} + \frac{1}{\Delta t}\frac{\Delta c_i}{T_n}^2\left\langle \frac{\partial^2 \psi^{KV}}{\partial \dot{c}_i^2}\right\rangle\right. \\ &\left. + \frac{1}{\Delta t}\frac{\Delta q_i}{T_n}^2\left\langle \frac{\partial^2 \psi^{MX}}{\partial \dot{q}_i^2}\right\rangle\right]\frac{\partial T}{\partial \epsilon_j^{pr}} + \delta_{ij}\frac{\partial^2 W^e}{\partial T \partial \epsilon_i^e} = 0 \quad \text{(C.4c)}\end{aligned}$$

A nonlinear system of equations taken from the equations above can be used to fully determine the derivatives of elastic strains and temperatures with respect to predictor strains. Newton-Raphson schemes can be applied to a system of the type $\mathbf{K}\mathbf{a} = \mathbf{b}$, defined as follows to organize equations:

$$\mathbf{K} = \begin{bmatrix} K_{11} & 0 & 0 & 1 & K_{15} \\ 0 & K_{22} & 0 & 1 & K_{25} \\ 0 & 0 & K_{33} & 1 & K_{35} \\ 1 & 1 & 1 & 0 & 0 \\ K_{15} & K_{25} & K_{35} & 0 & K_{55} \end{bmatrix} \quad \text{(C.5)}$$

Where individual terms are given by:

$$K_{ii} = \frac{\partial^2 W^e}{\partial \epsilon_i^{e2}} + \frac{1}{\Delta t}\frac{T_{n+1}}{T_n}^2\left\langle \frac{\partial^2 \psi^{MX}}{\partial \dot{q}_i^2}\right\rangle, \quad i = 1,2,3 \quad \text{(C.6a)}$$

$$\begin{aligned}&K_{i5} = K_{5i} = \\ &\quad -\frac{\partial^2 W^e}{\partial \epsilon_i^e \partial T} + \frac{1}{\Delta t}\frac{T_{n+1}}{T_n}\frac{\Delta q_j}{T_n}\left\langle \frac{\partial^2 \psi^{MX}}{\partial \dot{q}_i^2}\right\rangle, \quad i = 1,2,3 \quad \text{(C.6b)}\end{aligned}$$

$$\begin{aligned}&K_{55} = \\ &\quad \rho_n\frac{\partial^2 W}{\partial T^2} + \frac{1}{\Delta t}\frac{\Delta c_i}{T_n}^2\left\langle \frac{\partial^2 \psi^{KV}}{\partial \dot{c}_i^2}\right\rangle + \frac{1}{\Delta t}\frac{\Delta q_i}{T_n}^2\left\langle \frac{\partial^2 \psi^{MX}}{\partial \dot{q}_i^2}\right\rangle \quad \text{(C.6c)}\end{aligned}$$

Vectors **a** and **b** are defined as follows:

$$\mathbf{a} = \begin{bmatrix} \frac{\partial q_1}{\partial \epsilon_1^{pr}} & \frac{\partial q_1}{\partial \epsilon_2^{pr}} & \frac{\partial q_1}{\partial \epsilon_3^{pr}} \\ \frac{\partial q_2}{\partial \epsilon_1^{pr}} & \frac{\partial q_2}{\partial \epsilon_2^{pr}} & \frac{\partial q_2}{\partial \epsilon_3^{pr}} \\ \frac{\partial q_3}{\partial \epsilon_1^{pr}} & \frac{\partial q_3}{\partial \epsilon_2^{pr}} & \frac{\partial q_3}{\partial \epsilon_3^{pr}} \\ \frac{\partial \lambda_0}{\partial \epsilon_1^{pr}} & \frac{\partial \lambda_0}{\partial \epsilon_2^{pr}} & \frac{\partial \lambda_0}{\partial \epsilon_3^{pr}} \\ \frac{\partial T}{\partial \epsilon_1^{pr}} & \frac{\partial T}{\partial \epsilon_2^{pr}} & \frac{\partial T}{\partial \epsilon_3^{pr}} \end{bmatrix}$$

$$\mathbf{b} = \begin{bmatrix} \frac{\partial^2 W^e}{\partial \epsilon_1^{e2}} & 0 & 0 \\ 0 & \frac{\partial^2 W^e}{\partial \epsilon_2^{e2}} & 0 \\ 0 & 0 & \frac{\partial^2 W^e}{\partial \epsilon_3^{e2}} \\ 0 & 0 & 0 \\ -\frac{\partial^2 W^e}{\partial \epsilon_1^e \partial T} & -\frac{\partial^2 W^e}{\partial \epsilon_2^e \partial T} & -\frac{\partial^2 W^e}{\partial \epsilon_3^e \partial T} \end{bmatrix} \tag{C.7}$$

APPENDIX D – Thermo-viscoelastic damage: aspects of the derivation of tangent moduli

The stationarity equation with respect to the damage variable at the end of the time step (which shall be denoted r_d throughout this appendix) can be a starting point for the derivation of the second derivative terms that comprise the material tensor of the full thermo-mechanically coupled problem. It reads as follows, in general form:

$$r_d = \frac{\partial f(d)}{\partial d} \left[\tilde{W}^{vol} + \tilde{W}^{e} + \tilde{W}^{th} + \Delta t \left\langle \tilde{\psi} \right\rangle \right] + \Delta t \frac{\partial \left\langle \psi^d \right\rangle}{\partial d} = 0 \qquad \text{(D.1)}$$

The factorization of all dissipative behaviors with the temperature term $\frac{T_{n+1}}{T_n}$ has been previously discussed. When the dissipation pseudo-potential has no parametric dependence on the value of the damage variable (the term denoted as $d_{n+\alpha}$ below), damage stationarity takes on the slightly simpler form below, presented in chapter 5:

$$\begin{aligned} r_d = \frac{\partial f(d)}{\partial d} & \left[\tilde{W}^{vol} + \tilde{W}^{e} + \tilde{W}^{th} + \Delta t \left\langle \tilde{\psi} \right\rangle \right] \\ & + \frac{T_{n+1}}{T_n} \left\langle \frac{\partial \psi^d}{\partial \dot{d}} \right\rangle = 0 \qquad \text{(D.2)} \end{aligned}$$

Using the most common damaging function ($f(d) = 1 - d$), the equation above reads as follows:

$$\frac{T_{n+1}}{T_n} \left\langle \frac{\partial \psi^d}{\partial \dot{d}} \right\rangle = \left[\tilde{W}^{vol} + \tilde{W}^{e} + \tilde{W}^{th} + \Delta t \left\langle \tilde{\psi} \right\rangle \right] = Y^d \qquad \text{(D.3)}$$

In the interest of completeness, however, in the present appendix the most general expressions are derived, encompassing different forms of dissipation pseudo-potentials not explored in the main part of the text.

These equations are developed in what follows. In order to do so, the form of the thermodynamically-consistent average (equation 3.47) of the dissipation potentials along the time step is recalled:

$$\left\langle \psi\left(\frac{T_{n+1}}{T_n}\frac{\Delta d}{\Delta t}; d_{n+\alpha}, T_{n+\alpha}\right)\right\rangle = \\ \frac{T_n}{T_{n+1}}\psi\left(\frac{T_{n+1}}{T_n}\frac{\Delta d}{\Delta t}; d_{n+\alpha}, T_n\right) \\ + \frac{T_{n+1}-T_n}{T_{n+1}}\psi\left(\frac{T_{n+1}}{T_n}\frac{\Delta d}{\Delta t}; d_{n+\alpha}, T_{n+\alpha}\right) \quad \text{(D.4)}$$

It should be observed that possible parametric dependence with respect to temperature and the current value of damage is considered. The proper derivatives of the equations above may then include various terms, as shown below.

Going back to the stationarity of the incremental potential with respect to the damage variable, the full derivative with respect to strains and temperature can be taken. This gives the necessary elements to calculate the derivative of damage with respect to variations of strains and temperature, correcting terms appearing in the expressions of the material tensor.

For strains:

$$\frac{d}{d\mathbf{C}}\left(-Y^d + \Delta t\frac{\partial\left\langle\psi^d\right\rangle}{\partial d}\right) = 0 \quad \text{(D.5)}$$

$$-\frac{\partial r_d}{\partial \mathbf{C}} + \Delta t\frac{\partial^2\left\langle\psi^d\right\rangle}{\partial d^2}\frac{\partial d}{\partial \mathbf{C}} = 0 \quad \text{(D.6)}$$

From the definition of the energy restitution rate, the first term can be shown to yield the equivalent stresses, including elastic, thermal and viscous components. A simple rearrangement of terms then yields an expression for the derivative of the damage variable with respect to variations of strains:

$$\frac{\partial d}{\partial \mathbf{C}} = \frac{\frac{\partial Y^d}{\partial \mathbf{C}}}{\Delta t\frac{\partial^2\left\langle\psi^d\right\rangle}{\partial d\partial d}} = \frac{\frac{\partial \tilde{\mathcal{H}}^{effInt}}{\partial \mathbf{C}}}{\Delta t\frac{\partial^2\left\langle\psi^d\right\rangle}{\partial d\partial d}} = \frac{\frac{1}{2}\mathbf{F}^{-1}\tilde{\mathbf{P}}}{\Delta t\frac{\partial^2\left\langle\psi^d\right\rangle}{\partial d^2}} \quad \text{(D.7)}$$

For temperature:

$$\frac{d}{dT}\left(-Y^d + \Delta t\frac{\partial\left\langle\psi^d\right\rangle}{\partial d}\right) = 0 \quad \text{(D.8)}$$

$$-\frac{\partial r_d}{\partial T}+\Delta t\frac{\partial^2\left\langle\psi^d\right\rangle}{\partial d^2}\frac{\partial d}{\partial T}=0 \tag{D.9}$$

Again, going back to the definition of the energy restitution rate, the first term takes on a character akin to the entropy at time step $n+1$ in the equivalent state. Rearranging terms, the derivative of damage with respect to variations of temperature reads:

$$\begin{aligned}\frac{\partial d}{\partial T}=\frac{\frac{\partial r_d}{\partial T}}{\Delta t\frac{\partial^2\left\langle\psi^d\right\rangle}{\partial d^2}}&=\frac{\frac{\partial Y^d}{\partial T}+\Delta t\frac{\partial^2\left\langle\psi^d\right\rangle}{\partial d\partial T}}{\Delta t\frac{\partial^2\left\langle\psi^d\right\rangle}{\partial d^2}}\\&=\frac{\frac{\partial\tilde{\mathcal{H}}^{effInt}}{\partial T}+\Delta t\frac{\partial^2\left\langle\psi^d\right\rangle}{\partial d\partial T}}{\Delta t\frac{\partial^2\left\langle\psi^d\right\rangle}{\partial d\partial d}}=\frac{\tilde{\eta}+\Delta t\frac{\partial^2\left\langle\psi^d\right\rangle}{\partial d\partial T}}{\Delta t\frac{\partial^2\left\langle\psi^d\right\rangle}{\partial d^2}}\end{aligned} \tag{D.10}$$

It should be clear that the quantity $\tilde{\eta}$ associated to entropy in the equivalent strain space in equation D.10 above does not include any contribution due to the presence of damage.

What remains is to explore all terms arising from the derivative of the dissipation pseudo-potential (terms $\frac{\partial\left\langle\psi^d\right\rangle}{\partial d}$, $\frac{\partial^2\left\langle\psi^d\right\rangle}{\partial d^2}$ and $\frac{\partial^2\left\langle\psi^d\right\rangle}{\partial d\partial T}$ in equations above), while accounting for all possible parametric dependencies on values of the damage variable and temperature (as evidenced by terms $d_{n+\alpha}$ and $T_{n+\alpha}$ in the general notation) and the thermodynamically-consistent average along the time step (denoted by the accolades $\left\langle\psi^d\right\rangle$).

The first order derivative with respect to the damage variable then yields the following terms:

$$\begin{aligned}\frac{\partial\left\langle\psi^d\right\rangle}{\partial d}=&\overbrace{\frac{\partial\psi^d}{\partial\dot{d}}(T_n)+\frac{T_{n+1}-T_n}{T_n}\frac{\partial\psi^d}{\partial\dot{d}}(T_{n+\alpha})}^{Y_{(\dot{d})}}\\&\underbrace{+\alpha\Delta t\left[\frac{T_n}{T_{n+1}}\frac{\partial\psi^d}{\partial d_{n+1}}(T_n)+\frac{T_{n+1}-T_n}{T_{n+1}}\frac{\partial\psi^d}{\partial d_{n+1}}(T_{n+\alpha})\right]}_{Y_{(d_{n+1})}}\end{aligned} \tag{D.11}$$

Two groups of terms are identified. $Y_{(\dot{d})}$ marks the terms coming from the derivative with respect to the damage evolution rate, while $Y_{(d_{n+1})}$ marks those coming from the possible parametric dependence on the current value of the damage variable. It should be noted that the dissipation pseudo-potentials proposed in the main part of the text do not consider this parametric dependence, so that their first derivative with respect to damage reduces to the terms $Y_{(\dot{d})}$ only.

The second order derivative with respect to the damage variable is given by the following expression:

$$\begin{aligned}
&\frac{\partial^2 \left\langle \psi^d \right\rangle}{\partial d^2} = \\
&\overbrace{\frac{1}{\Delta t}\frac{T_{n+1}}{T_n}\frac{\partial^2\psi^d}{\partial \dot{d}^2}(T_n) + \frac{1}{\Delta t}\frac{T_{n+1}}{T_n}\frac{T_{n+1}-T_n}{T_n}\frac{\partial^2\psi^d}{\partial\dot{d}^2}(T_{n+\alpha})}^{K_{(\dot{d})}} \\
&\quad + 2\alpha \overbrace{\Bigg([\frac{\partial^2\psi^d}{\partial\dot{d}\partial d_{n+1}}(T_n) + \frac{T_{n+1}-T_n}{T_n}\frac{\partial^2\psi^d}{\partial\dot{d}\partial d_{n+1}} \Bigg]}^{K_{(\dot{d},d_{n+1})}} \\
&\quad + \underbrace{\alpha^2\Delta t \left[\frac{T_n}{T_{n+1}}\frac{\partial^2\psi^d}{\partial d_{n+1}^2}(T_n) + \frac{T_{n+1}-T_n}{T_{n+1}}\frac{\partial^2\psi^d}{\partial d_{n+1}^2}(T_{n+\alpha})\right]}_{K_{(d_{n+1})}}
\end{aligned} \tag{D.12}$$

Three groups of terms are identified. $K_{(\dot{d})}$ marks the second derivative with respect to the damage evolution rate. $K_{(\dot{d},d_{n+1})}$ marks the cross derivative with respect to the damage evolution rate and the parametric dependence on the value of the damage variable. Finally, $K_{(d_{n+1})}$ marks the second derivative with respect to the parametric dependence on the value of the damage variable.

The cross derivative with respect to the damage variable and to temperature can be calculated as follows:

$$
\begin{aligned}
\frac{\partial^2 \left\langle \psi^d \right\rangle}{\partial d \partial T} = {} & \overbrace{\frac{1}{T_n}\dot{d}\left[\frac{\partial^2 \psi^d}{\partial \dot{d}^2}(T_n) + \frac{T_{n+1}-T_n}{T_n}\frac{\partial^2 \psi^d}{\partial \dot{d}^2}(T_{n+\alpha})\right]}^{\frac{\Delta d}{T_n}K_{(\dot{d})}} \\
& + \overbrace{\alpha \Delta t \frac{1}{T_n}\dot{d}\left[\frac{T_n}{T_{n+1}}\frac{\partial^2 \psi^d}{\partial d_{n+1}\partial \dot{d}}(T_n) + \frac{T_{n+1}-T_n}{T_{n+1}}\frac{\partial^2 \psi^d}{\partial d_{n+1}\partial \dot{d}}(T_{n+\alpha})\right]}^{\frac{\Delta d}{2T_n}K_{(\dot{d},d_{n+1})}} \\
& + \overbrace{\alpha \frac{T_{n+1}-T_n}{T_n}\left[\frac{\partial^2 \psi^d}{\partial \dot{d}\partial T_{n+1}}(T_{n+\alpha}) + \alpha \Delta t \frac{T_n}{T_{n+1}}\frac{\partial^2 \psi^d}{\partial d_{n+1}\partial T_{n+1}}(T_{n+\alpha})\right]}^{K_{(\dot{d},T_{n+1})}+K_{(d_{n+1},T_{n+1})}} \\
& + \alpha \Delta t \frac{T_n}{T_{n+1}^2}\left[\frac{\partial \psi^d}{\partial d_{n+1}}(T_{n+\alpha}) - \frac{\partial \psi^d}{\partial d_{n+1}}(T_n)\right] + \frac{1}{T_n}\frac{\partial \psi^d}{\partial \dot{d}}(T_{n+\alpha}) \qquad \text{(D.13)}
\end{aligned}
$$

In addition to previously identified second derivative terms (namely, $K_{(\dot{d})}$ and $K_{(\dot{d},d_{n+1})}$), new cross derivatives terms have now been identified: terms marked $K_{(d_{n+1},T_{n+1})}$ represent the cross derivative with respect to the damage evolution rate and the parametric dependence with respect to temperature, while terms marked $K_{(d_{n+1},T_{n+1})}$ represent the second parametric derivative with respect to the value of the damage variable and to temperature. Additional unmarked terms round out the consistent temperature derivation.

Other useful expressions in the construction of the material tensors are the first and second derivatives of the damage dissipation pseudo-potential with respect to temperature. Contributing to the thermal capacity portion, it is given by the following expression (where $\Delta T = T_{n+1} - T_n$, for short):

$$
\begin{aligned}
\frac{\partial^2 \left\langle \psi^d \right\rangle}{\partial T^2} = & \\
& \alpha \Delta t \frac{\Delta T}{T_{n+1}} \left[2 \frac{\dot{d}}{T_{n+1}} \frac{\partial^2 \psi^d}{\partial \dot{d} \partial T_{n+1}} (T_{n+\alpha}) + \alpha \frac{\partial^2 \psi^d}{\partial T_{n+1}^2} (T_{n+\alpha}) \right] \\
& \quad + \frac{\Delta d}{T_{n+1}^2} \left\{ \dot{d} \left[\frac{\partial^2 \psi^d}{\partial \dot{d}^2} (T_n) + \frac{\Delta T}{T_n} \frac{\partial^2 \psi^d}{\partial \dot{d}^2} (T_{n+\alpha}) \right] \right. \\
& \qquad \left. + 2 \left[\frac{\partial \psi^d}{\partial \dot{d}} (T_{n+\alpha}) - \frac{\partial \psi^d}{\partial \dot{d}} (T_n) \right] \right\} \\
& \quad + 2 \Delta t \left[\alpha \frac{\partial \psi^d}{\partial T_{n+1}} - \frac{\psi^d (T_{n+\alpha}) - \psi^d (T_n)}{T_{n+1}} \right] \frac{T_n}{T_{n+1}^2} \qquad \text{(D.14)}
\end{aligned}
$$

These expressions are then used in the assembly of the consistent material tensors for the problem.

Following definitions and notations used earlier in the text, the mechanical, cross derivative and thermal portions of the consistent material tensor now read as follows.

$$
\begin{aligned}
\mathbb{C}_{mech} &= f(d_{n+1}) \tilde{\mathbb{C}}_{mech} + \frac{\partial f(d_{n+1})}{\partial d_{n+1}} \frac{\partial d_{n+1}}{\partial \mathbf{C}_{n+1}} \frac{\partial \tilde{\mathcal{H}}_n^{effInt}}{\partial \mathbf{C}_{n+1}} \\
&= [1 - d_{n+1}] \tilde{\mathbb{C}}_{mech} - \frac{\partial d_{n+1}}{\partial \mathbf{C}_{n+1}} \otimes \left[\frac{1}{2} \mathbf{F}_{n+1} \tilde{\mathbf{P}}_{n+1} \right] \qquad \text{(D.15a)}
\end{aligned}
$$

$$
\begin{aligned}
\mathbb{C}_{thm} &= f(d_{n+1}) \tilde{\mathbb{C}}_{thm} + \frac{\partial f(d_{n+1})}{\partial d_{n+1}} \frac{\partial d_{n+1}}{\partial T_{n+1}} \frac{\partial \tilde{\mathcal{H}}_n^{effInt}}{\partial \mathbf{C}_{n+1}} \\
&= [1 - d_{n+1}] \tilde{\mathbb{C}}_{thm} - \frac{\partial d_{n+1}}{\partial T_{n+1}} \left[\frac{1}{2} \mathbf{F}_{n+1} \tilde{\mathbf{P}}_{n+1} \right] \qquad \text{(D.15b)}
\end{aligned}
$$

$$
\begin{aligned}
\mathbb{D} = f(d_{n+1})\tilde{\mathbb{D}} + \Delta t \frac{\partial^2 \left\langle \psi^d \right\rangle}{\partial T_{n+1}^2} + \frac{\partial f(d_{n+1})}{\partial d_{n+1}} \frac{\partial d_{n+1}}{\partial T_{n+1}} \frac{\partial \tilde{\mathcal{H}}^{effInt}}{\partial T_{n+1}} \\
= [1 - d_{n+1}]\tilde{\mathbb{D}} + \overbrace{\Delta d \frac{\dot{d}}{T_n^2} \frac{\partial^2 \left\langle \psi^d \right\rangle}{\partial \dot{d}^2}}^{eq\ \ D.12 : K_{(\dot{d})}} \\
+ \underbrace{\frac{\Delta d}{T_n} \frac{\partial^2 \left\langle \psi^d \right\rangle}{\partial \dot{d} \partial T_{n+1}}}_{eq\ \ D.13 : K_{(\dot{d}, T_{n+1})}} + \underbrace{\Delta t \frac{\partial^2 \left\langle \psi^d \right\rangle}{\partial T_{n+1}^2}}_{eq\ \ D.12 : K_{(T_{n+1})}} - \frac{\partial d_{n+1}}{\partial T_{n+1}} \frac{\partial \tilde{\mathcal{H}}^{effInt}}{\partial T_{n+1}} \qquad \text{(D.15c)}
\end{aligned}
$$

APPENDIX E – Material parameters used in the applications

Due to an implementation choice, all Hencky potentials are described by a Young's modulus (E) and a Poisson coefficient (ν), instead of the commonly used shear (μ) and bulk moduli (K). They are related by the following equations:

$$\mu = \frac{E}{2(1-2\nu)} \tag{E.1}$$

$$K = \frac{E}{3(I-2\nu)} \tag{E.2}$$

The following tables contain the parameter sets used in several of the examples presented throughout this document.

Table E.1 – Material 1: standard material properties used for most examples of chapter 7 (1 Kelvin-Voigt element, 2 Maxwell elements)

Elastic properties (1 KV + 2 MX; Hencky model)			
E_0^{KV}	$1.0GPa$	ν	0.3
dE_1^{KV}	$1.6MPa/K$		
E_0^{MX1}	$1.0GPa$	E_0^{MX2}	$100MPa$
ν^{MX1}	0.3	ν^{MX2}	0.35
α	$6.0\times10^{-5}K^{-1}$		
Thermal properties and mass density			
$\mathcal{C}$	$1048J/m^3.K$	κ	$1.0\times10^{-2}J/K$
ρ_R	$1450kg/m^3$		or $1.9J/K$
Viscous properties (1 KV + 2 MX; Hencky model)			
E^{vKV}	$1.0GPa$	ν^{vKV}	0.45
dE^{vKV}	$0.3MPa/K$		
E^{vMX1}	$1.0GPa$	ν^{vMX1}	0.45
E^{vMX2}	$100MPa$	ν^{vMX2}	0.45
Damage properties (power law)			
Y_0^d	50×10^6J	$\dot{d}_0$	1.0×10^{-3}
m'	1.0		

Table E.2 – Material 2: properties for thermo-viscoelasticity model used in figure 4.4 (1 Kelvin-Voigt element, Ogden viscous potential)

Elastic properties (1 KV; Hencky model)			
E_0^{KV}	$100.0MPa$	ν	0.4
α	$6.0\times10^{-5}K^{-1}$		
Thermal properties and mass density			
$\mathcal{C}$	$500J/m^3.K$	κ	$5.0\times10^{-1}J/K$
ρ_R	$3000kg/m^3$		
Viscous properties (1 KV; Ogden model)			
μ_1^{vKV}	$6.0GPa$	μ_2^{vKV}	$150.0MPa$
α_1^{KV}	1.5	α_2^{KV}	0.3
μ_3^{vKV}	$0.4MPa$		
α_3^{KV}	2.0		

Table E.3 – Material 3: material properties used for the final example of tensile testing in section 7.5 (1 Kelvin-Voigt element, 2 Maxwell elements)

Elastic properties (1 KV + 2 MX; Hencky model)			
E_0^{KV}	$0.4GPa$	ν	0.4
E_0^{MX1}	$0.1GPa$	E_0^{MX2}	$1MPa$
ν^{MX1}	0.4	ν^{MX2}	0.4
α	$2.0\times10^{-4}K^{-1}$		
Thermal properties and mass density			
$\mathcal{C}$	$1048J/m^3.K$	κ	$0.48J/K$
ρ_R	$1450kg/m^3$		
Viscous properties (1 KV + 2 MX; Hencky model)			
E^{vKV}	$100MPa$	ν^{vKV}	0.5
E^{vMX1}	$500GPa$	ν^{vMX1}	0.5
E^{vMX2}	$40MPa$	ν^{vMX2}	0.5
Damage properties (power law)			
Y_0^d	9.75×10^6J	$\dot{d}_0$	1.5×10^{-1}
m'	3.5		